N° d'ordre 45 /2021

THESE DE DOCTORAT

Présentée par

Mme : ZINEB MOUMEN

Discipline : Géologie

Spécialité : Eau et Environnement

Sujet de la thèse:

Application des outils de la modélisation spatiale, et de la Géo-informatique pour la gestion intégrée des ressources en eau appliquée au bassin d'Innaouène.

Formation Doctorale : Sciences et Génie de la matière, de la Terre et de la Vie.

Thèse présentée et soutenue le samedi 19 juin 2021 à 10h au Centre des conférences devant le jury composé de :

Nom Prénom	Titre	Etablissement	
Lahcen BENAABIDATE	PES	Faculté des Sciences et Techniques de Fès	Président
Carlos HAFFMANN SAMPAIO	PES	Université Polytechniques de Catalogne Espagne	Rapporteur
E-l Mostafa MILI	PES	Faculté des Sciences de Meknès	Rapporteur
Abdelkader EL GAROUANI	PES	Faculté des Sciences et Techniques de Fès	Rapporteur
Alae-Eddine BARKAOUI	PH	Faculté des Sciences Oujda	Examinateur
Hinde CHERKAOUI DEKKAKI	PH	Faculté des Sciences et Techniques El Hocaima	Examinateur
Abderrahim LAHRACH Abdel-Ali CHAOUNI	PES PES	Ecole Nationale des Sciences Appliquées de Fès Faculté des Sciences et Techniques de Fès	Directeurs de thèse

Laboratoire d'accueil : Ecologie Fonctionnelle et Génie de l'Environnement.

Etablissement : Faculté des Sciences et Techniques de Fès.

Dedication

*I dedicate this thesis to my mother **SERHROUCHNI YOUSSEFI Maria**, who drunk my two lives, mine, and yours, without her I would never be the person who I am.*

*To my father-in-law **BAADIE Mohammed** for all his support.*

Acknowledgement

Before starting, I would like first to thank the dean of the science and technology faculty of Fez and the director of the doctoral study center for their support for scientific research at the faculty of sciences and technologies of Fez.

I would like to express my deep gratitude and sincere thanks to ***Mr. Abderrahim LAHRACH****, professor at the Faculty of Science and Technologies of Fez, and Director of the National School of Applied Sciences (ENSA-Fez) who gave me the honor of supervising me during my research project, and throughout my all-scientific career. You have always welcomed me with your kindness and simplicity, and you have guided me with your precious advice during the realization of this research. May this work be for me the moment to express my gratitude and my great consideration.*

I warmly thank ***Mr. Abdel-Ali CHAOUNI****, professor at the Faculty of Sciences and Technologies of Fez, for his enormous help and his availability, flexibility, and his support during critical moments.*

My sincere thanks for ***Mr. Lachen BENABIDATE*** *professor at the faculty of science and technologies of Fez, for his collaboration kindness, seriousness, sympathy, and generosity.*

I address my sincere considerations to Madame ***Najiba AMRANI****, for her effort in terms of international collaboration and for the opportunities she has granted me to make mobilities within the framework of my research project.*

I would like to thank ***Mr. Carlos Hoffmann Sampaio****, professor at the Polytechnic University of Catalonia for reviewing this work.*

With all my heart, I will take this opportunity to dedicate a special thanks to my second family; ***Abdessamad JALOUNI, Fatima DAID*** *and* ***Soumaya NABIH*** *for being my strength in my sickness and my weakness, for supporting me, and for all what they have done. To express my humble gratitude, I will borrow some word from Washintong Irving, "They are not the mark of weakness, but of power, they are the messenger of overwhelming grief, of deep contrition and my unspeakable love"*

I also address my sincere thanks to ***Dr. Ismail EL HASSNOAUI*** *for serving this thesis.*

I acknowledge and thank the tribunal members and the reviewers for agreeing to examinate this research study.

I would also like to thank all the professors of the Geo-resources and Environment department of the Faculty of Sciences and Technologies for their help and supports

Finally, I give all my respect and gratitude to all my friends who have encouraged and supported me during my studies.

Acronyms

AET	Actual evapotranspiration
AIC	Akaike information criterion
AR5	The fifth assessment report of IPCC
COP	Conference of the Parties
CFSR	Climate Forecast System Reanalysis
CORDEX	Coordinate Regional Climate Downscaling Experiment
DEM	Digital elevation model
ET	Evapotranspiration
FAO	The Food and Agriculture Organization of the United Nations
GA	Geeffective ic Algorithm
GCM	The Global Climate Models
GDA	Geographical Differential Analysis
GDP	Gross Domestic Product
GHG	Greenhouse Gas
GIS	Geographic Information System
GIWR	Gross irrigation water requirement
GPCC	Global Precipitation Climatology Centre
GPM	Global Precipitation Measurement
GWP	Global Water Partnership
INRA	National Institute of Agronomic Research (INRA)
ISRIC	International Soil Reference and Information Centre
IWR	Irrigation water crop requirement
IWRM	Integrated Water Resources Managament
MAE	Mean absolute error
MAPM	Ministry of Agriculture and Maritime Fisheries
MDG	Millennium Development Goals
MGP	Moroccan Green Plan
MODIS	Moderate Resolution Imaging Spectroradiometer
MSE	Mean squared error
NASA	National Aeronautics and Space Administration
NDVI	Normalized difference vegetation index
NDWI	Normalized difference water index
NIR	Near-Infrared
NSE	Nash-Sutcliffe Efficiency
OLI	Operational Land Imager
PDR	Partial drying of the roots
QDM	Quantile delta mapping
RCP	Representative Concentration Pathway
RDI	Regulated deficit irrigation

RMSE	Root Mean Square Error
SCS	Soil conservation curve number
SDGs	Sustainable Development Goals
SDSM	Statistical DownScaling Model
SPAW	Soil-Plant-Air-Water
STRM	Shuttle Radar Topography Mission
SUFI-2	Sequential Fitting method
SWAT CUP	Soil and Water Assessment Tools Calibration and Uncertanity Program
SWAT	Soil & Water Assessment Tool
SWR	Stepwise regression
TIS	Thermal Infrared Sensor
TMPA	Multi-satellite Precipitation Analysis
TRMM	Tropical Rainfall Measuring Mission
TSAVI	Transformed Soil Adjusted Vegetation Index
UNCED	UN Conference on Environment and Development
UNFCCC	United Nations Framework Convention on Climate Change
WWC	World Water Council

Tables of Contents

Résumé xv

General Introduction 1

Main Objectif 1

Specific Objectifs 1

Part I 3

Chapter I: Literature review 4

1. Downscaling 5

1.1. Climat data 5

1.2. Biais correction 6

1.1. Temporal downscaling 7

1.3. Spatial downscaling 10

2. Hydrological modeling : 10

2.1. Hydrological cycle 11

2.2. Watersheds, hydrologic response, and Flood hydrographs 12

2.4. Flood forecast 14

2.5. Classification of hydrological models 15

3. Deficit Irrigation 22

Chapter II: Study area 26

1. Choice of study area 26

2. Geographic location 26

2.1. Inaouen watershed 26

3. Geological context 32

3.1. The meseto atlas domain 33

3.2. The pre-Rif domain: 35

4. Soil context of the Inaouen Basin 37

5. Hydro-climatology of the Inaouen watershed 38

5.1. Data control 38

5.2. Precipitation 39

5.3. Temperatures 41

5.4. Evapotranspiration 42

5.4. The water balance 44

5.5. Flow study 45

5.6. Gumbel's law 46

6. Statistical analysis 48

6.1. Temporal variation 50

6.2. Spatial variation 53

6.3. Kurtosis test 55
6.4. Description of graphs 56
Part II 61
1. Introduction 62
2. The hydrological framework for water security 62
3. Water Security 64
5. Morocco between water insecurity and management strategies 67
5.1. Morocco and the policy of dams 68
6. Green Morocco Plan (PMV) 69
6.1. Pillar I 70
6.2. Pillar II 70
7. Partial conclusions 71
Chapter II: Downscaling Global Precipitation Data Using a Machine Learning Algorithm. 73
1. Introduction 73
2. Methodology 74
2.1. Study zone 74
2.2. Collection of data 75
2.3. Method 77
2.4. Calibration and validation of precipitation 81
3. Partial conclusion 82
Chapter III: Hydrological modeling 83
1. Introduction 83
2. The SWAT model 83
2.1. Spatial discretization of the SWAT model 84
2.2. The hydrological components of the SWAT models 85
2.2.1. Atmospheric part : 86
2.2.2. Land part 87
2.2.3. Sub-lateral flow 93
2.2.4. Underground part: 95
2.3. Routing the model 96
2.4. SWAT CUP 97
2.4.1. The GLUE method (generalized likelihood uncertainty estimation): 97
2.4.2. The SUFI-2 method (sequential uncertainty fitting) 98
3. Methodology 100
3.1. Definition of sub-watershed 100
3.2. Hydrological response units (HRU) 101
3.2.1. The slope map 101

3.2.2. The soil map 101
3.2.3. Land use 105
3.3. Hydro-climatic stations 106
3.3.1. Climatic station 106
3.4. Model calibration 109
3.4.1. Calibration 110
3.5. Evaluation criteria 111
3.5.1. Nash stucliffe 111
3.5.2. The mean absolute error (MAE) 111
3.5.3. The root of the mean squared error (RMSE) 111
3.5.4. The coefficient of determination R^2 111
3.5.5. Percent bias (PBIAS) 112
4. Partial conclusion 112
1. Crop data : 113
2. Olive yield 114
3. Water use efficiency and water productivity 115
4. Partial conclusion 116
Part III: Results and discussions 117
1. Reduction of spatial scale 118
1.1. Bare ground line 118
1.2. Correlation between TRMM 3B43 and TSAVI 120
1.3. Correlation between TRMM 3B43 and predictors using machine learning 121
1.1. Calibration and Validation 123
2. Hydrological modeling 128
2.1. Sensitivity analysis 130
2.2. CFSR database 132
2.3. Simulation using observed data 134
2.4. Simulation results with observed data 135
2.5. Sensitivity analysis 135
2.6. Calibration 138
2.7. Model validation 139
2.8. Discussion 139
3. Deficit Irrigation 141
3.1. Evapotranspiration : 141
3.2. Irrigation deficit: 142
3.3. Water use efficiency and water productivity 145
General conclusion 148

Futures perspectives. 151
References 152
Annexes 167
Annex 1: Descriptive statistics of Bab Merzouka station 167
Annex2: Descrptive statistics of Idriss first station 169

List of figures

Figure 1: Principe of biais correction 6
Figure 2: Precipitation hydrograph for a rainy event 13
Figure 3: Schematic representation of a hydrological model 16
Figure 4: Classification of hydrological models 18
Figure 5: History of the development of hydrological models 21
Figure 6: Cost & gross revenue in function to the applied water. 23
Figure 7: Geographic location map of the Inaouen basin drived from STRM file 27
Figure 8: Hypsometric map of the watershed 28
Figure 9: Cumulative area in%, hypsometric curve. 29
Figure 10: The slope map. 29
Figure 11: Hydrographic effective work of the Inaouen watershed 31
Figure 12: Geological map of the Inaouen basin 32
Figure 13: Synthetic profile of the Meso-Cenozoic cover of the boutenière of Tazekka 34
Figure 14: Double cumulation test for the “Boured” and “Bab chhoub” stations. 38
Figure 15: Average annual precipitation of stations; "Bab merzouka ", "Bab chhoub", "Idriss first". 40
Figure 16: Maximum and minimum monthly average temperature variation, for the “Tissa” and “Bab Merzouka ” stations. 41
Figure 17: Ombrothermal diagram of the “Bab Merzouka ” and “Tissa” stations 42
Figure 18: Variation of the monthly potential evapotranspiration for the “Bab merzouka ” and “Tissa” stations. 42
Figure 19: Water balance of the Inaouen watershed for the “Tissa” and “Bab Merzouka ” stations. 44
Figure 20: Average annual flow for the stations of "Bab merzouka ", "Bab chhoub" ,. 46
Figure 21: Variation of average monthly flows for the stations of Bab Chhoub, bab merzouka , and Bni haitem 46
Figure 22: Adjustment of the max flow rates j by the graphic method of Gumbel's law 47
Figure 23: IDF curves for Bab merzouka station. 48
Figure 24: Plot of Frequency Distribution as a function of a random variable that shows the difference between Mesokurtic, Leptokurtic, Plakurtic Zone 50
Figure 25: bar graph and boxplot of variables; precipitation, relative humidity and temperature in station 1 during the decades from 1980 to 2010. 52
Figure 26: Bar chart and boxplot of variables; precipitation, relative humidity and temperature in station 2 during the decades from 1980 to 2010. 53
Figure 27: Boxplot of precipitation data for stations 1 and 2 during the 1980-2010 decades. 54
Figure 28: Frequency diagram of a set of data from the Bab Merzouka station and the first Idriss station for the period from 1979 to 2014. 55
Figure 29: Water security global indicators 66
Figure 30: Chronological order of the water law 69
Figure 31: Map of Moroccan sub-basins and bioclimatic stages 75
Figure 32: General methodology of the downscaling algorithm 78
Figure 33:Representation of the hydrological model in the SWAT model 86
Figure 34: Cumulative runoff curve as a function of cumulative precipitation 89
Figure 35: The solution of the runoff equation 90
Figure 36: Distribution curve of the normal law 98

Figure 37: Relation between the uncertainty of the input parameters and the simulated parameters 99
Figure 38: Map of the delimitation of the sub-watersheds by ARC SWAT. 101
Figure 39: Soil type 105
Figure 40: Land use 106
Figure 41: Map of Oued Sebou stations and Global Weather Dtata measurement points. 107
Figure 42: Growth of young olive branches in irrigation scenarios (INRA, 2019) 114
Figure 43: Effect of the irrigation scenario on the height of olive trees (INRA, 2019) 115
Figure 44: Effect of the irrigation scenario on the conductance of the somatic leaves of olive trees (IN, 2019) 115
Figure 45: Bare soil line extracted for all Moroccan watersheds, from Landsat 8 OLI images, based on NIR versus red point cloud; using the quantile regression method 119
Figure 46: Correlation between TRMM 3B43 and TSAVI precipitation over the period 1999-2004 121
Figure 47: R^2 of the comparison between TRMM versus TSAVI and TRMM versus TSAVI, DEM and distance from the sea, over the period 1999-2014 122
Figure 48: R^2 of the correlation between TRMM precipitation and the independent variables (TSAVI, DEM and distance from the sea; over the period 1999-2014. 122
Figure 49: Statistical model precision metrics: R^2, adjusted R^2, Cp and AIC; for TRMM vs TSAVI, DEM and sea distance. 123
Figure 50: Precipitation estimated using TSAVI, DEM and distance from the sea in a spatial resolution of 0.25 ° × 0.25 °, over the reference period 1999-2004 124
Figure 51: Spatial distribution of the regression residue at a spatial resolution of 1 km × 1 km, over the reference period 1999-2004 125
Figure 52: Precipitation reduced and calibrated to a spatial resolution of 1 km * 1 km, over the reference period 1999-2004 125
Figure 53: TRMM vs reduced and calibrated precipitation over the reference period 1999-2004 126
Figure 54: Water balance obtained by the SWAT model using the CFSR database 132
Figure 55: graph of a comparison between the observed average monthly flows and that obtained by the different iterations using the CFSR database 134
Figure 56: Location of stations in the CFSR database and data observed in the Sebou watershed 134
Figure 57: The initial water balance of the Inaouen watershed 135
Figure 58: Results of the sensitivity analysis 136
Figure 59: Comparison between observed and simulated flow rates for the 1999-2007 calibration period 138
Figure 60: Comparison between observed and simulated flows for the 2008-2014 validation period 139
Figure 61: Monthly evapotranspiration derived from MODISA16 over the period 2008-2019 142
Figure 62: Gross water requirements (mm) per ha, over the period 2008-2019 144
Figure 63:Irrigation water requirements (mm) per ha, over the period 2008-2019 144
Figure 64: Variation in irrigation water requirements in the event of complete irrigation and irrigation deficit, over the period 2008-2019 145
Figure 65: Water saved thanks to the deficit irrigation applied over the period 2008-2019.. 145

Figure 66: Water use efficiency under full irrigation supply and deficit irrigation, over the period 2008-2019 146
Figure 67: Water productivity under full irrigation supply and deficit irrigation, over the period 2008-2019 147

List of Tables

Table 1: Table of references for the different bias adjustment methods 7
Table 2: References of the weather generator model 8
Table 3: Global water distribution..... 12
Table 4:Morphometric characteristics of the Inaouen basin. 27
Table 5: Average altitude of the watershed..... 28
Table 6: Table of altitude ranges in % 28
Table 7: Average slope and overall slope of the Inaouen basin 30
Table 8: Characteristic of the hydrographic effective work of the Inaouen basin. 30
Table 9: Table of the percentage of surface areas of each lithologic type 37
Table 10: Table of percentages for each type of soil 37
Table 11: Estimation of the total annual water volume by the three methods. 40
Table 12: The Thermal index and the alpha coefficient for the “Tissa” and “Bab merzouka ” stations:..... 42
Table 13: Calculation of evapotranspiration by Turc method for the “Bab merzouka ” and “Tissa” stations..... 43
Table 14: Calculation of the monthly ETR by the Thornthwaite method for the “Tissa” station. 43
Table 15: Calculation of the monthly ETR by the Thornthwaite method for the “Bab merzouka ” station..... 43
Table 16: Results of the calculation of the monthly ETR by the Thornthwaite balance method for the “Tissa” and “Bab merzouka ” stations..... 43
Table 17: Flow corresponding to different return periods by the graphic method..... 47
Table 18: Flow corresponding to different return periods by the method of moments. 47
Table 19: Rain intensity according to the return periods and duration of precipitation..... 48
Table 20: Asymmetry and kurtosis coefficient for two stations 1 and 2..... 55
Table 21: Economic, Social, Environmental dimension of water security 64
Table 22: Economic, Social, Environmental dimension of water security 65
Table 23: Data sets 77
Table 24: The formula for calculating the TSAVI 80
Table 25: Characteristics of the digital elevation model 100
Table 26: Physico-chemical parameters of the soil and their references 103
Table 27: Physico-chemical characteristics of the soils in the study area 104
Table 28: Coordinates of hydromoetric and pluviometric stations 108
Table 29: Monthly harvest coefficient for olive trees (Masmoudi et al., 2004)..... 113
Table 30: The values of the reduction coefficients corresponding to the vegetation cover (Conseil Oleicole International, 1997) 114
Table 31: Average production costs and average margins of olive trees irrigated by drip irrigation in the Saiss region (Source: Regional Directorate of Agriculture of Fès-Meknes) 115
Table 32: Slope and intersection of the line of bare soil extracted from all the watersheds of Morocco, using the quantile regression method..... 119
Table 33: Spatial statistical measurements calculated reduced precipitation and validated against in situ measurements of precipitation from rainfall stations..... 127

Table 34: Correlation between TRMM 3B43 and TSAVI, for the five bioclimatic stages over the period 1999-2004 127
Table 35: Parameter values obtained by the different iterations of the AAT approach 136
Table 36: Evaluation criteria of the simulation 139

Abstract

In the realm of Climate change, population growth, industrialization, water is resources are under high pressure. To help manager and decision makers to adopt the appropriate land management strategies, the grasping of the hydrological behavior and quantification of water yield are paramount. In this cradle the main objective of the presented thesis is to provides an integrated approach to tackle water drawbacks.

The methodology adopted consists of improving downscaling models by reducing soil brightness noise using the Transformed Soil Adjusted Vegetation Index, TSAVI, DEM, and distance from the sea. The second part aims to test the ability of the distributed model SWAT (Soil & water Assessment Tool) to simulate and reproduce the hydrological behavior of Inaouen watershed, SWAT was performed on a daily time step from 1999 to 2007 for calibration and 2008 to 2014 for validation. The model accuracy was evaluated by measuring the Nash-Sutcliffe coefficient and R^2, RMSE, MAE, et PBIAS. The last part aims to estimate the evapotranspiration using Modis Evapotranspiration Product and assess the productivity of 2500 ha of the olive crop under deficit irrigation condition.

The result exhibits that the Transformed Soil Adjusted Vegetation Index (TSAVI) enhanced the downscaling model over the Humid and Saharan bioclimatic stages due to its capacity to reduce the soil brightness with an R^2 ranging between 0.30 and 0.82. Concerning the hydrological modeling the obtained resulted when using the CFSR database are not satisfactory, the model is enhanced when using the observed climatic data for calibration but still need to be improved. This could be explained by the inadequacy of the parameters that represent the groundwater transfers (**REVAP, GWQMN**, **GW_REVAP**, **and REVAPMN**) to Inaouen basin. The last part result's shows that 0.75 of full irrigation could save water irrigation by 17% by reducing water irrigation supply by an average of 5Mm3.

This study highlights the importance of Geographic Information Systems, hydrological modeling, and remote sensing in addressing water issues. The methodology used could be transposed to other regions facing the same problems.

<u>Keywords:</u> ISRIC database, Distributed model, Hydrologic Response Unit, Spatial downscaling, TSAVI, Deficit irrigation, SWAT, CFSR, hydrologic modeling, Water security, Sustainable development, Water management.

Résumé

Le changement climatique, la croissance démographique, l'industrialisation ont des problèmes majeurs qui aboutissent à la détérioration des ressources en eau. Afin d'aider les gestionnaires et les décideurs à adopter les stratégies de gestion appropriées, la compréhension du comportement hydrologique et la quantification du rendement de l'eau sont primordiales. Dans ce contexte, l'objectif principal de la présente étude est de fournir une approche intégrée pour adresser ces embarras.

La méthodologie adoptée consiste à améliorer les modèles de réduction d'échelle en réduisant le bruit de la luminosité du sol à l'aide de l'indice de végétation ajusté au sol transformé, TSAVI, DEM, et la distance de la mer. La deuxième partie vise à tester la capacité du modèle distribué SWAT (Soil & water Assessment Tool) à simuler et reproduire le comportement hydrologique en amont du bassin versant d'Inaouen. Le modèle SWAT a été procédé sur un pas de temps quotidien de 1999 à 2007 pour la calibration et de 2008 à 2014 pour la validation. La précision du modèle a été évaluée en mesurant le coefficient de Nash-Sutcliffe et R^2, RMSE, MAE, et PBIAS. La dernière partie vise à estimer l'évapotranspiration en utilisant le produit d'évapotranspiration de Modis, et à évaluer la productivité de 2500 ha de la culture d'olives dans des conditions d'irrigation déficitaires.

Les résultats obtenus montrent que l'indice de végétation ajusté au sol transformé (TSAVI) a amélioré le modèle de réduction d'échelle sur les étages bioclimatiques humide et saharienne en raison de sa capacité à réduire la luminosité du sol. Le R^2 compris entre 0,30 et 0,82. En ce qui concerne la modélisation hydrologique, les résultats obtenus lors de l'utilisation de la base de données CFSR ne sont pas satisfaisants, le modèle est amélioré lors de l'utilisation des données climatiques observées pour l'étalonnage mais la qualité de simulation reste modeste. Cela pourrait s'expliquer par l'inadéquation des paramètres qui représentent les transferts d'eau souterraine (REVAP, GWQMN, GW_REVAP, et REVAPMN) au bassin d'Inaouen. Les résultats de la dernière partie montrent que 0,75 de l'irrigation complète pourrait permettre d'économiser 17% d'eau en réduisant l'approvisionnement en eau d'irrigation de 5Mm3.

La présente étude souligne l'importance du système d'information géographique, de la modélisation hydrologique et de la télédétection dans le traitement problématique relatif à l'eau. La méthodologie utilisée pourrait être transposée à d'autres régions qui sont confrontées aux mêmes problèmes.

<u>Mots-clés :</u> Base de données ISRIC, Modèle distribué, Unité de réponse hydrologique, Réduction d'échelle spatiale, TSAVI, Irrigation déficitaire, SWAT, CFSR, modélisation hydrologique, Sécurité de l'eau, Développement durable, Gestion de l'eau.

General Introduction

The consequences of climate change, scarcity, and pollution, increase the pressure on water resources. In 2017, the United Nations set a program of sustainable development goals in which water is the main concern, thus ensuring water security to maintain the balance of life for humans and ecosystems. As the world has different climatic contexts, the impact of change will be systematically different. If this factor is combined with the rate of development, the effect will be more severe for developing countries (DCs) and least developed countries (LDCs), especially those located in an arid and semi-arid climate context, such as African countries. The main problem to be solved is therefore to define the appropriate management toward the changes, starting with the understanding of the problems, studying historical trends of variations, and then defining the strategies.

As a developing country, Morocco's vulnerability to the impact of water scarcity takes on a critical dimension since its economy is mainly based on agriculture. The spatio-temporal imbalance in the distribution of water, and its contamination amplify the pressure. According to the intergovernmental panel on climate change, over Morocco, rainfall will decrease by 40% by 2071 (IPCC, 2019).

Based on the two main aspects noted, the following study provides a comprehensive approach for addressing water issues and exanimating the likelihood of improving irrigation efficiency at a pilot plot level by considering the hydrological conditions. It could be also used as a reference for future studies.

Main Objectif

The general objective of this study is to define an integral approach for the management of water resources, by providing data on rainfall, defining trends, and proposing an adaptation strategy applied to the agricultural sector.

Specific Objectifs

- Improve downscaling model by reducing brightness noise, introducing the Transformed Soil Adjusted vegetation index, TSAVI, DEM, and distance from sea level using stepwise regression, AIC, and the Cp criterion, to evaluate the error and performance of the model MSE, MAE, RMSE and R-Square parameters were used.
- The second part focuses on modelling with the SWAT (soil and water assessment tool), the model is used to simulate the hydrological behavior of the Inaouen catchment, test

the reliability of the ISRIC soil and CFSR climate databases, and its applicability to the catchment. The focus of the second part the hydrologic modeling using soil and water assessment tool SWAT, the model is used to simulate the hydrological behavior of the Inaouen watershed, test the reliability of the ISRIC soil databases and CFSR climate, and its applicability to the basin.

- In the last part, the AET evapotranspiration was estimated using the Modis evaporation product throughout the period 2007-2019 under Google Earth Engine Could-Computing. About 2,500 ha of olive crops were assessed with full drip irrigation and compared to irrigation at 75% of the total water used.

To proceed, 7 chapters have been treated, divided into three parts.

Part I: The first part defines the concepts of downscaling, hydrological modeling, and irrigation deficit, emphasizing the importance of the three concepts in terms of water resources management. It also presents a description of the study area, morphometry, geology, climatology, hydrology. The statistical analysis of the central tendency aims to define the variation in climate trends over the last 4 decades

- Chapter I : Littérature review
- Chapter II : Study area

Part II: The second part describes the methodology adopted. This part contains 4 chapters.

- Chapter I: Describes the water issues in Morocco as well as the measures taken to alleviate them.
- Chapter II: Downscaling of global precipitation data using a Machine Learning algorithm.
- Chapter III: Hydrological modeling
- Chapter IV: Deficit Irrigation

Part III: The third part is focused on the presentation and discussion of the results obtained as well as the future perspectives.

Part I

Chapter I: Literature review

Hydrological data are crucial for carrying out studies related to water resources issues, for example to assess the level of water scarcity on crop yields, precipitation and evapotranspiration are necessary.

These data could be extracted from several sources (eg observed climate data recorded by weather stations, or open access data gateways such as global weather data, IPCC, GMIP). The climatic variables vary in space (latitude, longitude, altitude) and in time scale (hours, day, month, etc.), the acquisition of a set of data in a defined area during a determined period defined by the spatio-temporal resolution.

However, the additional problems encountered are always their availability and even if they are available, the spatial and temporal resolution is low and does not cover the infinitesimal variations.

watersheds agencies do not always ensure wide and complete coverage, for example in the case of the Inaouen watershed, only four hydrometric stations are available in an area of approximately 3000 km² with a non-homogeneous time scale.

GCM global climate model data and the corresponding RCM scaled-down regional climate model data provide a wide range of large-scale climate and environmental data. But before being used, the data must first be bias-corrected and then reduced (spatially or temporally) depending on the purpose of the study.

1. Downscaling

Downscaling means reduction in scale, either temporal (e.g. daily to hourly) or spatial (e.g. 1Km to 1m), the two main approaches illustrated in the literature are dynamical downscaling and statistical downscaling; the first relies on the processing of a high-resolution climate model at regional scale using lower resolution of observed data.

1.1. Climat data

The Intergovernmental Panel on Climate Change provides a wide range of different climate data through global climate models and regional climate models, the results were used in the Intercomparisons Coupled Model project in the fifth AR5.

The climate model is a mathematical conceptualization and abstraction of the Earth's climate dynamics considering state variables such as temperature, precipitation, solar radiation, winds ... in fact, the climate process is impacted by physical, chemical, biological components and the interactions between them, the model is a codification and conceptualization of all this.

The complexity of these models varies depending on the number of components represented and which one needs to be exposed, for example, the coupled atmosphere-ocean general circulation models (AOGCMs) provide a representation of the climate system that is close to the fullest end of the currently available spectrum (AR5, 2014)

The AR5 has several global climate models provided by several meteorological centers around the world, for example the CMCC-CMS with a horizontal grid of 1.875 ° × 1.875 ° provided by the National Center for Meteorological Research / European Center for Research and Training Advances in Scientific Computing, a detailed summary of these models is presented in the book of statistical downscaling for hydrological and environmental application.

To process a climate change study, such as impact assessment, the global climate model data is too large, regional climate data (RCM) is its spatially reduced form. The Coordinated Regional Climate Downscaling Experiment (CORDEX) separates the Earth into domains, such as South America, Central America, North America, Europe, Africa, South Asia, East Asia, Central Asia, Australasia, Antarctica, Arctic, Mediterranean and Southeast Asia, for which a regional downscaling takes place (Taesam, 2019)

More details on the regional climate model are found in the following websites.

• CORDEX East Asia: https://cordex-ea.climate.go.kr/

• CORDEX North America: https://na-cordex.org/

• CORDEX Europe : www.euro-cordex.effective /

1.2. Biais correction

Data derived from climate models cannot be used directly because they reveal systematic errors, in other words they are biased. Some phenomena and parameters could not be conceptualized in a mathematical equation, so a calibration with real observations had to be done, there are parameters embedded in the models that were not meaningful. The problem with spatial resolution is that global climate models could not cover infinitesimal changes. Bias correction consists of fixing and correcting GCM data by calculating the difference and coefficient of variation between the observed data and the GCM data.

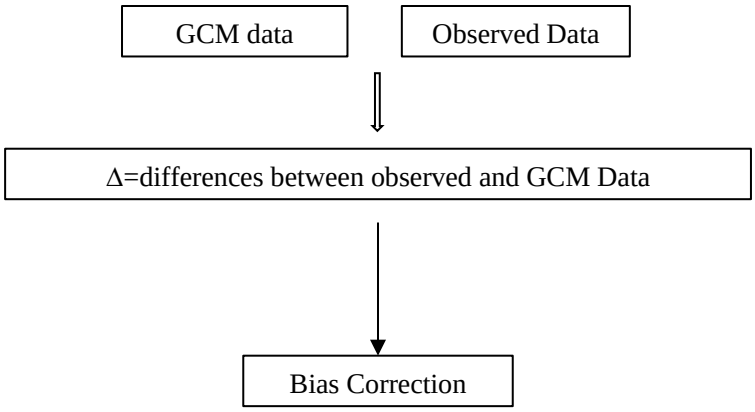


Figure 1: Principe of biais correction

The literature highlights different bias correction methodologies with a different level of complexity, this more is done by transformation adjustment algorithms, the adjustment of the correction could be transposable to future climatic conditions. Some methods are based on correction for the mean, others focus on more advanced statistical parameters (e.g. coefficient of variation, standard deviation, and quantile values) (Smitha et al. 2018). Teutschbein et al. A review of the literature on bias correction methods (Tab. 1) explaining the advantages and limitations of each through an application on 11 different temperature and precipitation series simulated by RCM for five watersheds in Sweden (Teutschbein and Seibert 2012). for example, the linear correction adjusts the average precipitation does not influence the coefficient of variation, precipitation and temperature intensity during the day is not considered. Piani et al. Propose an improved bias correction method based on an adjusted histogram equalization function, applied to daily precipitation and mean, maximum and minimum temperatures derived from the global climate model, to be used for hydrological modeling, over a 30-year

data set, later successfully fit the data by improving the mean and standard deviation, (Piani et al. 2010), other studies overcome unrealistic seasonal fluctuations by adding factors of correction to the existing method, however,

Table 1: Table of references for the different bias adjustment methods

Method	Principle	Reference
Linear scaling	**Precipitation is corrected with a factor based on the ratio of long-term monthly mean observed and control run data.**	**Lenderink et al., 2007**
Local intensity scaling	**adjusts the mean as well as both wet-day frequencies and wet-day intensities of precipitation time series separately**	**Schmidli et al. (2006)**
Power transformation Precipitation	**While linear scaling accounts for bias in the mean, it does not** **allow differences in the variance to be corrected. Therefore, a non-linear correction in an exponential form, a * Pb.** **This is done with a root-finding algorithm using Brent's method (Brent, 1971).**	**(Leander and Buishand, 2007; Leander et al., 2008)**
Variance scaling	**The above described power transformation is an effective meth-** **od to correct both the mean and the variance, but is limited to precipitation time series due to the use of a power function**	**Chen et al. (2011a, b)**
Distribution transfer	**The idea of distribution mapping is to correct the distribution** **function of RCM-simulated climate values to agree with the ob- served distribution function.** **The equation is expressed in term of cumulated function (Gmubel for precipitation and Gaussien for the temperature)**	**(Sennikovs and Bethers, 2009), (Block et al., 2009; Ines and Hansen, 2006), (Boe et al., 2007; Déqué et al., 2007; Johnson and Sharma, 2011; Sun et al., 2011), (Piani et al., 2010), (Rojas et al., 2011; Sennikovs and Bethers, 2009)**
Delta-change approach	**to use the RCM-simulated future change (anomalies) for a perturbation of observed data rather than to use the RCM- simulations of future conditions directly**	**(Andréasson et al., 2004; Bosshard et al., 2011; Gellens and Roulin, 1998; Graham et al., 2007a, 2007b; Lettenmaier et al., 1999; Middelkoop et al., 2001; Moore et al., 2008 ; Shabalova et al., 2003**

Source: the methods presented are derived from the literature review of (TEUTSCHBEIN, C. et al 2012)

1.1. Temporal downscaling

The temporal statistical dowscaling is first based on the development of statistical relationships between climatic variables or what is called the predictor (such as precipitation, relative

humidity, wind speed, etc.), and large predictors. ladder. To go into more detail, three main methods are illustrated:

- **Transfer function**: which is the ratio of the Laplace transform of the input variable to the Laplace transform of the output variable with an initial condition of 0. Amongst these are the Delta method which determines the projected or Delta changes of a climate variable from which the global climate model is applied to the observations, and the regression-based technique which includes a predictor and a predictand

- ***Weather typing***: or model classification technique, used a set of atmospheric models of a GCM to build a relationship with observations, e.g. collecting 50 years of daily weather maps of a certain region covering different varieties (dry days, wet days or below normal), the observed data of the target area are mandatory, each weather map has to be linked to the corresponding information during the historical period, once matched, the historical maps are collected on the GCM maps, to elaborate the statistical relationship between the variables

- ***Weather generator***: uses the change in statistical climate project produced by GCM to influence historical observation statistics to define how they will vary in the future.

The *weather generator* is the most used method, the literature highlights various applications of this method to generate a daily hydrometeorological data set, (Tab 2.)

Table 2: References of the weather generator model

Models	References
WGEN	(Richardson & Wright 1984)
SIMMETEO	(Geng & Auburn 1986, Geng et al. 1986, 1988)
LARS-WG	(Semenov & Barrow 1997, Semenov et al. 1998)
TAMSIM	(McCaskill 1990)
MARKSIM	(Jones & Thornton 2000)

Source: LEE, T. and JEONG, C., 2014. Nonparametric statistical temporal downscaling of daily precipitation to hourly precipitation and implications for climate change scenarios. JOURNAL OF HYDROLOGY [en línea], vol. 510, pp. 182–196. ISSN 0022-1694. DOI 10.1016/j.jhydrol.2013.12.027. Disponible en: http://dx.doi.org/10.1016/j.jhydrol.2013.12.027.

WGEN have been applied in a number of previous studies (e.g. Meinke et al.1995, Semenov et al.1998, Puche & Silva 2001), Soltani et al. 2003 evaluate the performance of the two stochastic

weather generator models WGEN and SIMMETEO and investigate the impact of the parameter estimated by each method on the quality of the generated data. Statistical indices, such as t-and F-, were used to evaluate the difference between observed and simulated data and between the two models. The WGEN reproduces well the maximum and minimum temperature and the number of frost days (Soltani and Hoogenboom 2003).

In order to assess the hydrological effects of climate variations at small spatial scales and to capture daily variations in runoff, hydrometeorological data at sub-daily temporal scales are needed, several approaches have been used. Koutsoyanis et al, 2001 developed a point process model for desegregation of daily precipitation into hourly precipitation based on the Bartlett-Lewis process, (Koutsoyiannis and Onof 2001), machine learning and neural effective work method was also used to downscale to hourly data (Kumara et al.2011)

Random distribution, sinusoidal distribution method and normal distribution were all used for hourly temporal downscaling, but they underestimate the maximum intensity of precipitation, based on this discrepancy Chen & al. (2011) applied a proportional method, but the problem was that the daily precipitation is divided proportionally into four parts and the statistical dispersion parameters are not well reproduced (Chen et al. 2011)

The key factor for the development of this type of model is the diurnal cycle, the distribution of precipitation during the day depends essentially on it, which is linked to the synoptic scale of thermal conditions, and atmospheric dynamics, Previous studies have shown that convective and summer rains generally tend to occur in the afternoon or early evening inland, and occur at midnight or early in the morning downstream from high elevation areas (Wallace, 1975), also the seasonal variations in the diurnal cycle, during the winter the rain fall in the early morning unlike the summer season where it takes place in the late afternoon and this is due to the strong instability of solar heat.

Therefore, capturing and representing this cycle is a key parameter to predict climate variation, however, some previous models did not take it into account. The GA geeffective ic algorithm and k-nearest neighbor resampling (KNNR) are now widely used for stochastic simulation. (Lee et al., 2007).

Taesam Lee et al., 2014 applied a non-parametric statistical time scale reduction of daily precipitation to produce hourly precipitation at Jinju station in South Korea, the results obtained showed that the reproduced data model preserves the statistical variation. (Lee and Jeong 2014), (Lee and Park 2017)

1.3. Spatial downscaling

Machine learning algorithms provide a strong steppingstone for the evolution of the downscaling model. In fact, the reduction process consists of four main stages;

- The storage of the data
- Abstraction
- Generalisation
- Evaluation

Therefore, global data could be downscaled using appropriate algorithms, a study was carried out by Qiang Zhang et al., (2016) to downscale rainfall data from the mission of measurement of tropical precipitation 3B43 (TRMM 3B43), taking into account the normalized vegetation index, in order to reduce errors due to the influence of vegetation. The methodology consists first of processing a regression model based on a power function, then the analysis of geographic differences was applied for the calibration, in three steps; quantifying the difference between the downscaled data and the observed data for regions that have a gauging station, then interpolated this error into a grid of 8 km * 8 km, the error is then added to the uncalibrated rainfall. The correlation coefficient was around 0.7, but at the same time is a convincing improvement in spatial resolution. C. Folberth et al. (2019), also applied an extreme gradient increase and random forests to simulate the global mesh crop model data at the final scale, the obtained results show a correlation coefficient of 0.96 (Folberth et al. 2019).

From a mathematical point of view, the main methodology used for spatial downscaling is; Bilinear interpolation and nearest neighbor interpolation, the difference between the two is that the former considers that the unknown value of the value z for ap and bp [i.e. z (ap, bp)] must be found with the known values at the four points like z (a1, b1), z (a1, b2), z (a2, b1) and z (a2, b2), and the second Nearest neighbor interpolation simply selects the value of the nearest location (Singh 2019), more details of the mathematical proof are based in the cited reference.

2. Hydrological modeling :

Water is the most important natural resources on Earth, 97% of water supply is salty, the reminding 3% is frozen in ices or glaciers or stored in underground, that leaves only 1% of surface water which is useful to meet everyone needs. From cellular metabolism to big industry water is the basic element of human life, indeed, on microscopic level water molecule is

required to carry on nutrients and oxygen to body cells, and transform the food to energy, water is also required to maintain a good life quality and for economic and industrial development. Hydrologic cycle is the movement of water among the atmosphere, hydrosphere, and lithosphere. There are two sub systems in the water cycle the first one is the precipitation and evaporation between the atmosphere and the ocean, the second is the evapotranspiration between the atmosphere and land surface, the subsystems are interconnected by horizontal water movement in the atmosphere called advection, and the runoff in the surfaces (Miller. E & all, 1992)

2.1. Hydrological cycle

Hydrology deals with the circulation, distribution, dynamics, and properties of water through the study of the components of the water cycle; precipitation, evaporation, transpiration, interception, infiltration, runoff, transport of dissolved substances (PERRIN, 2000).

Precipitation is the process by which water falls directly to the surface of the ground, under several forms, liquid (rain), frost (snow or hail) or vapor (fog and fog), the part that directly fall om the oceans, rivers and streams constitutes the flow, and the part that falls to the ground and vegetation forms the intercepted rain (PERRIN, 2000). the interception is the temporary storage of water by vegetation, three categories are distinguished; the throughfall is the water directly evaporated or dripped by vegetation, steam flow is water that flows along twigs and three branches, interception loss is the precipitation that is retained by plant absorbed and evapo-transpirated. (ward, 1990). The spatial distribution of precipitation varies depending on the properties of the soil, land use and vegetation cover, during precipitation events, water drains from rivers and slope surfaces, if the soil is permeable (sandy or gravelly) water seeps in, the force of gravity pulls the water down, and through cracks, fractures and pores it seeps into the deep underground aquifer, the water continues to flow move laterally towards rivers, lakes, and oceans. (USGS, 2016).

Evaporation is the transformation of liquid water into water vapor, the process is powered by heat from solar energy, the latent heat of water evaporation increases with water temperature and breaks intermolecular bonds (Likens, 1981). water evaporates from wetlands; the roots of plants absorb groundwater and release it by evapotranspiration (USGS, 2016), the density of water vapor is low, mixing with particles suspended in the atmosphere, water condenses into clouds, and after reaching the dew point temperature, water vapor again falls into the surface of the Earth.

Table 3: Global water distribution

Water	Global volume of water in (Km3)
Oceans	1348x106
Ice Cream Poles	2782x104
Groundwater and soil moisture	8062x103
Lakes and rivers	2250x102

Sources: Baumgartner and E. Reichel, the World Water Balance (Munich: Elsevier, 1975), P.179

Around 30 percent of the total mass of Earth is covered by land, then the continental area receive just 1/3 of the total precipitation, Due to climatic and geographic characteristics the total income water is unequally distributed over the world, some regions have a water excess when others suffer from water scarcity, according to the world water development fourth report, saharien and sub saharien regions are more exposed to water scarcity stress, a 700 million people in 43 different countries suffer today from water shortage. for example, in the in south-western America, there are years in which they may receive no rain, and when it rains the precipitation total amount does not exceed 508 millimeters (Miller. E & all, 1992)

2.2. Watersheds, hydrologic response, and Flood hydrographs

Watershed is the topographic area drained by the principal stream effective work and its tributaries, from the upstream to downstream, all the hydrologic process take places in this section, those later are impacted by the climate, vegetation, topography, pedology, and geology (Yonaba, 2009), watershed's sizes may vary from some fraction of meter square to kilometer squares, its limits are defined from topographic crest line, its hydrogeologic limits are determinate by the expansion of water in deep aquifer. The hydrologic response is the way watersheds behave regarding solicitations, during a precipitation event, before reaching the land surface, most of this water is lost to evaporation, transpiration, an interception. The remained portion constitute runoff when the soil moisture reaches a maximum value, the water or infiltrate into the deep aquifer or flows to the outlet.

The flow of a river at determinate point is defined as the variation of the volume of water per time unit, this change is measured in m3/s, the change of this discharge in time unit define the flood hydrograph, they take the shape of a dissymmetric bell, and they have three main components (Maria A, & all, 2015);

Surface runoff: water flowing over the ground surfaces,

Intermediate runoff or interflow: water which moves laterally beneath the ground surface in the unsaturated zone, and returns directly to the ground surface or stream banks,

Baseflow: water drained from saturated zone to the river flow.

Figure 2 shows a hydrograph for a flood event with hyetograph, which is the intensity of precipitation over time, presented in the top of the graph.

t0: The rain started, the water loses are firstly extracted from the total amount,

t0-t1: The rest of rainfall is converted to direct runoff; the discharge rises progressively (rising limb) until the peak flow, which is the maximum streamflow of a rain event. The lag time is the difference between the peak of rainfall and the peak of flow.

t1-t2: The decrease of flow discharge is known as a falling limb and the water return to the baseflow conditions. (Maria A, & all, 2015)

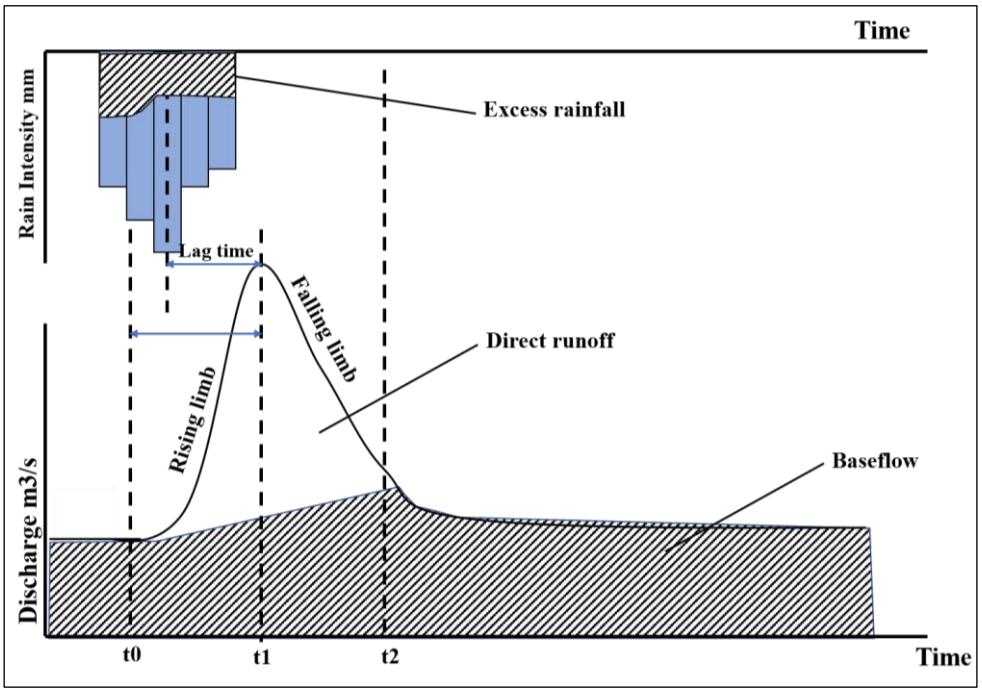


Figure 2: Precipitation hydrograph for a rainy event

Source: Maria A., Evangelos A., Vassilios A. (2015). Hydrology and Water Resource Systems Analysis

The above figure shows a hydrograph for a hyetograph flood event, which is the intensity of precipitation over time, shown at the top of the graph.

t0: The rain has started, the water losses are first extracted from the total amount,

t0-t1: The rest of the precipitation is converted into direct runoff; the flow gradually rises (rising branch) to the peak flow, which is the maximum flow of a rain event. Latency time is the difference between peak precipitation and peak flow,

t1-t2: The decrease in discharge flow is known as the downward branch and the water returns to basal flow conditions. (Maria A, and all, 2015)

Flooding occurs when water covers an area that is normally dry (Australian government), it's amplified by human activities, deforestation and urbanization. In deforested areas, during heavy precipitation, water is not intercepted either absorbed by vegetation, the flow is rapidly vehiculated to the downstream, through the drainage way it erodes soils. The paved roads and the urban areas prevent water from infiltration. The water may overflow rivers also when the rainfall intensity exceeds the infiltration capacity of the ground. (Horton & Robert E.1933)

2.3. Flood risks

The water availability is the pylon of development, the distribution of this source over the world goes hand by hand with the rate of countries' development. For example, Egyptian civilization was developed near the Nile River, which floods and fertilize the lands. However, the water excess may destroy humanity, if it exceeds the needed rate, a heavily unexpected rain may cause human and economic damages. For instance, in 1993 the Mississippi River and its tributaries overflew and inundated more than 9.3 million of hectares, 50 were dead and the materials damages were estimated by 12 million dollars (Raven & all, 1992). According to Munich Re's natural catastrophe database (NatCatService), in Europe during the last 15 years, flash floods and storms have caused economic damages between 1 and 18 billion US dollars per incident. The Elbe and Danube floods in Germany and other parts of Eastern Europe in 2002 and 2013, caused more than 10 billion US dollars of damages (Munich, 2014), and according to a recent estimate by (Jia et al. 2016), the risk of inundation in China is eight times higher than the global average. The economic damages can be split into tangible and intangible damage (Smith &Ward,1998), the difference whether the two types is that the first one could be estimated in moeffective ary terms, when the second is not measurable, for example, environmental impacts, health impacts, heritage cultural impact (Meyer & Schwarze, 2019). Such damages place the vulnerable area for inundation under a critical risk, in order to protect humankind, and the environment the foreseeing of floods is mandatory.

2.4. Flood forecast

Forecasting is the estimation of the future conditions at a certain period, to warn the extreme events such as floods, there are two types of flood forecasting methods the short term and the long term (David R.1992). The first one is based on channel routing and rainfall-runoff modeling.

The Channel routing forecast method is a one-dimension simulation of the river represented by St. Venant equation, the models that use this equation, computes the water surface expansion

into rivers, and stream from the data flow. HEC RAS model is an example of a dynamic wave model, it was created by the American army in order to simulate and map the overflows, this model was applied in various study for forecasting floods, sediment, and nutrient yield (Khaddor, 2016) (Pierre, & Moussa.02009)(Base Modelisation, & Et, 2013)(Abdulrazzak & al., 2019)(Berterreche & al, 2008). The rainfall-runoff modeling or hydrologic models simulate the flow in watershed's downstream, using rain and soils characteristics as an input.

Long term forecasting method groups three methods; index-variable, storage accounting and conceptual simulation, the first one relate the forecast period runoff to one or more variable index that is likely to affect stream flow, like soil moisture, the second estimate the quantity of water stored in the catchment which may contribute in the future in the surface run-off, the latest one uses a rain-flow simulation gathered from observed data, from which the forecasting period variable is estimated, which is the study case presented in this chapter. (David R.1992)

2.5. Classification of hydrological models

The introduction and development of digital tools and approaches, combined with geographical information system advance, allowed to progress in hydrological/hydraulic models and made the process of understanding the hydrological system better.

Model is a representation of a physical phenomenon to understand the mechanisms which control the system, this simulation may be physic, analogic or mathematics.

Hydrologic model is the total or partial representation of the hydrologic cycle (Marchandise, 2007), it describes the system and allows to predict how it may behave in the future if one of its parameters (rain, temperature, pollutants…) is modified. This representation is realized by a set of the mathematic equation which reproduces the system, in general, hydrologic models, presents six types of variables (Boudahiraa,2007)

- **Input variable:** The set of parameters required by the models, which depend on the time and space (evaporation, precipitation, hydrodynamic characteristics of the study area)

  Output variable: Variables by which the model responds (flow, pollutants concentration…)
- **Stats variable**: Characterize the state of the simulated systems and could vary according to the time (soil depth, rate of soil saturation, slopes, relative humidity…)
- **Mathematics equations**: Links Input variables, Output variables, and State variables in order to represent the process implied in the watershed dynamic

- **Parameters:** Related to the model's equation, serve to adapt the relation which regulates the model to the real observed functionality
- **Calibration parameters:** Certain parameters could not be directly measurable from the field, the calibration has as scoop the determination of the value of this variable, in order to find the best fit between the observed and the simulated results.

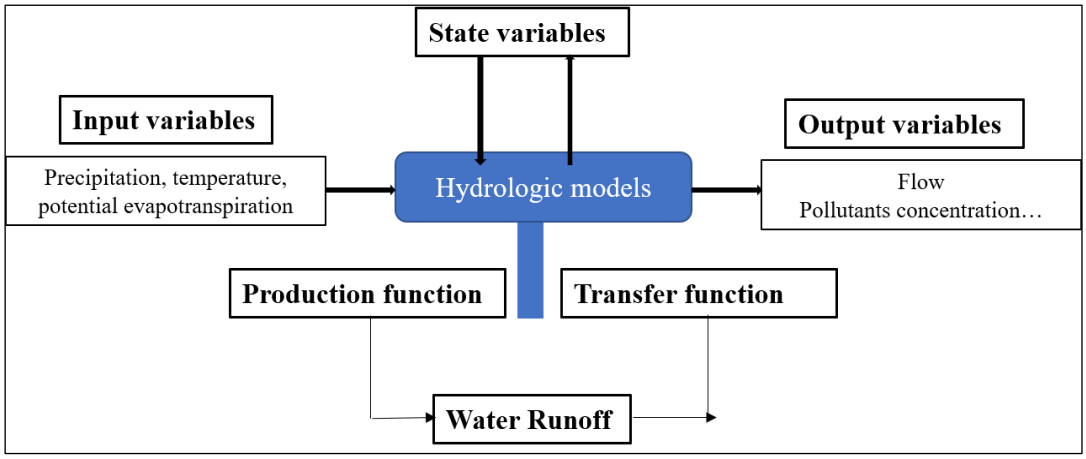


Figure 3: Schematic representation of a hydrological model

Source: the representation was reproduced from (PERRIN, SAMI, & HENDRICKX, 2009) Scheme

Figure 3 is a simplification of the hydrological simulation process; the latter is subdivided into two main parts transfer and production.

- The production is the estimation of water runoff quantity from the total incoming water,
- The transfer is the function which assures the transformation of water runoff already determined by the production function to flood hydrograph.

The modeling of the rain-flow transformation integrates the various elements of the hydrological cycle in its context. Certain types of models allowing to go through the modeling of each element before building the final rainfall-runoff model. The unit of study is generally the topographically limited watershed, except in the case where geological features drain excluded areas outside the topographic boundaries of the basin. Rainfall-runoff modeling can provide the answer to many water-related questions focused on resource and risk management (CHACHOUA, 2010):

- Reconstruction of the flow series by filling in the gaps in the historical series in order to allow statistical processing used in particular in the feasibility studies of the structures and the determination of the values of the projects.
- Frequency forecasts with extreme flows (floods and low water) may take place.

- The predetermination of the hydrological response of a watershed with a time step, to allow the development of a prevention and alarm system.

2.5.1. Simulation approach

The literature describes two simulation approaches (Grayson, 2000):

- **Ascendant approach**: The diversity of the whole system is considered in this approach. The rain-flow relation is determined by physics laws, a part of the parameters derived from these laws are not directly measurable, then, in order to estimate their value, the model should be calibrated,
- **Descendant approach:** The watershed is considered as a functional unit, the system's outputs are defined by its inputs (rain and state variables), the parameters of rain-flow relation do not have a physical significance.

2.5.2. General classification

The equivocation of interaction between the components of the hydrologic cycle and the complexity of the studied systems, lead to the elaboration of a wide range of hydrologic models. (SINGH,1995), (BEVEN, 1989), (ASCE, 2000), (AMBROISE B., 1998) suggest different classification.

(REFSGAAED, 1997) categorize hydrologic models according to the description of physical processes, as a conceptual or physic, and according to spatial discretization as a lumped or distributed. According to Singh, a model is characterized by five elements: the geometry of the systems, Inputs, formalization laws of processes, the initial state and boundary condition of the system and then Outputs. To class hydrological models Sigh proposes three criteria, the processes description, spatial and temporal scales and the methods used to resolve the equations of systems (Figure 4).

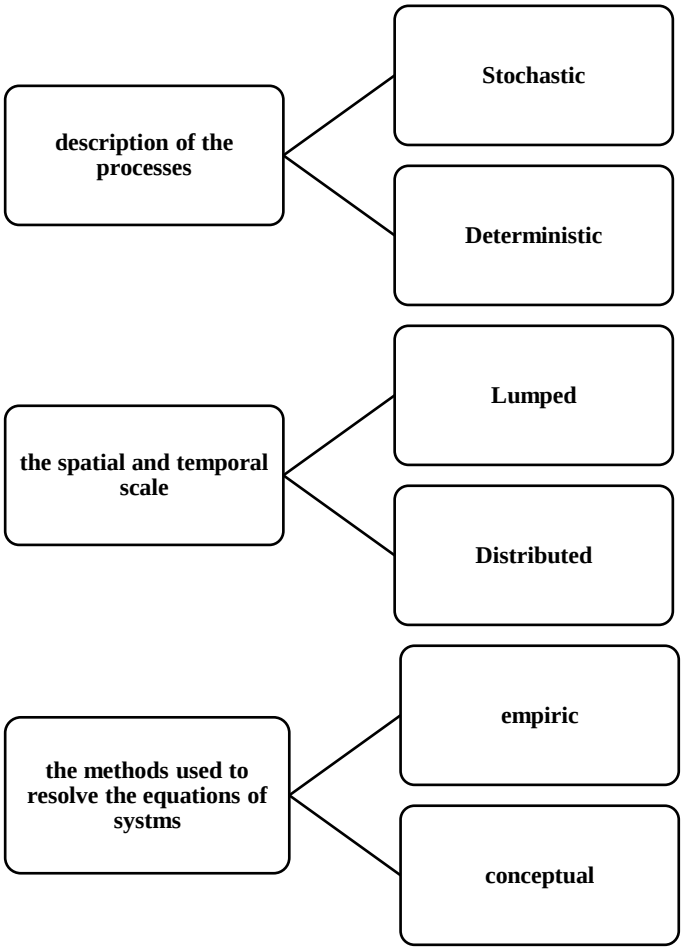


Figure 4: Classification of hydrological models

Source: The scheme was derived from the hydrologic model classification proposed by Singh, 1995

2.5.3. Classification according to the abstraction degree

Physical models: are the representation of systems on a reduced scale, the equation used is derived from the laws of physics (mass conservation, energy quantity…), the final simplified form has a physical meaning.

Mathematical models: Describe the hydrological process with mathematical equations that relate the input variables to the output variables.

2.5.4. Classification according to the type of variable

Deterministic models: the relationship between inputs and outputs is phenomenological, a determined input always produces the same output.

Stochastic or probabilistic models: these models randomly generate the output using statistical distribution laws

2.5.5. Classification according to spatial discretization

Lumped models: this model considers the whole watershed as one homogeneous unit, all the characteristics parameters of the basin are described by their mean value. (MAISON, 2000)

Distributed models: consider the spatial variability and the heterogeneity of watershed, if the system component is not completely spatialized the models is semi-distributed.

According to the description of the processes involved in the hydrologic cycle (precipitation, infiltration, interception)

Conceptual models: are vertical interconnection between humidity reservoirs, every reservoir presents a level of water storage, this model is based on the determination of physical phenomena which impact Inputs and then Outputs. (AMBROISE, 1991)

Empirical models: used to reproduce the global system behavior without a description of elementary processes, they are called black box models when the $Flow = f(rain)$, the function f is determinate by statistical regression from the rain-flow data series. (AMBROISE, 1991)

2.5.6. Classification according to temporal discretization

This classification is based on the temporal resolution.

Continuous models: The continuous model deals with the rain-runoff transfer over a long period, usually more than 5 years, the hydrological process such as evapotranspiration, water percolation, infiltration must be considered, to run these models, a wide range of input data must be fed into the model to reduce uncertainties.

Event-based models: these models simulate the watershed response to a short, infradaily, or daily rainfall event (could range from 1 hour to 24 hours), typically the model requires the definition of the previous climate state of the basin (eg base flow value, relative humidity, soil saturation…).

There are numerous typologies of these models that are widely used (Philip B. &al 2012), such as single-event models that are used to simulate or calculate the resulting storm hydrograph, from a well-defined watershed area, for a given pattern of rainfall intensity (ex; HEC-HMS), continuous models (ex; SWMM and SWAT, presented in this chapter) that take in consideration soil moisture storage, evapotranspiration and antecedent rainfall over long time periods, statistical models that generates time series of rainfall, and finally distributed models (ex; MIKE) that can handle input, output and data manipulation at the watershed level (Figure 5).

The soil and water assessment tool (SWAT) which is semi-distributed physical based hydrologic model was used in this research, it is a widely applied model in the world for the

study of the watershed hydrologic behaviors, the impact of land use, urbanization and climate change on water resource (Kannan & al., 2019), (Zhou & al., 2013), (Wang & al. , 2014), (Luzio & all., 2003), and in Morocco in particular, it is even considered better performing hydrological model in Moroccan context (Brirhet, 2016), its popularity is attributed to the fact that the model is open source and relies on GIS-based interfaces to collect, create, visualize, analyze and manipulate its inputs and provides sensitivity, calibration, and uncertainty analysis tools (Srinivasan and Arnold; 1994). Thus, not only hydrological modelers can use it by modifying its source code but also hydrological model users.

The study presented in this chapter was carried on the upstream part of Inaouen watershed. The pilot zone is facing plenty of environmental drawbacks, related to pollution, erosion and flood risks (Jamal & al., 2012). Those problems are mainly a consequence of geology and climatic factors. Different models have been used to forecast the floods runoff, like HEC RAS for hydraulic modeling and HEC HMS for hydrological modeling. Swat model was applied on Bab Merzouka (Bouslihim and al.,2016) watershed, however, to date no actualized research has been reported, furthermore the last cited study used a climatic data from the global weather website, and a soil database from the FAO, which subdivide to basin to only three pedologic types.

.

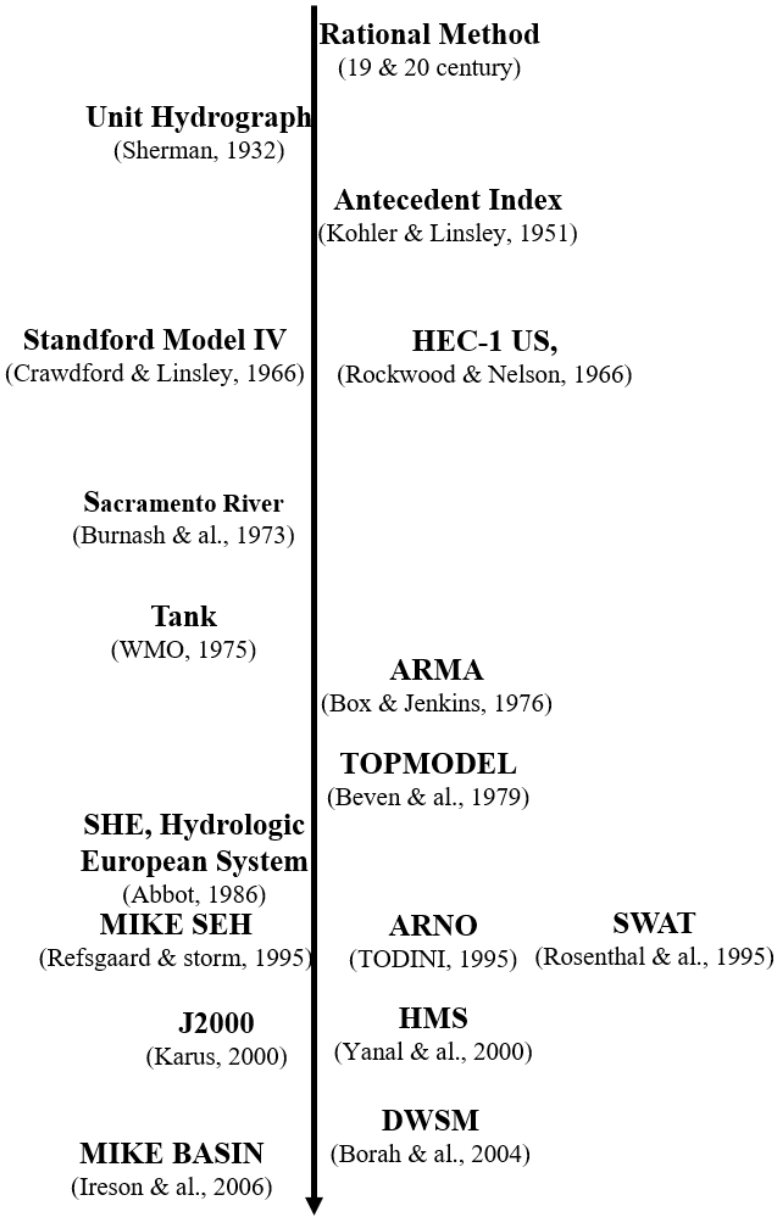


Figure 5: History of the development of hydrological models

Source: Zemzami, 2013. Applied hydrology

The hydrological modeling involves the following steps:

- Model identification: Identification and study of the target studied system then define the appropriate model to simulate it.
- Calibration: by estimating the parameters of the model, which cannot be measured, according to deductive criteria or observations of inputs and outputs. There are two ways of estimating the parameters from a sample: the passive method (we take all the available input-output pairs, and by statistical methods, we evaluate the coefficients of the equations) and the active method (by giving a higher specific weight for certain

observations or group of observations). It could be manual or automatic. (BOUDAHRAA, 2007)

- Evaluation: by comparing the simulated response to the observed data using different evaluation criteria and formulas
- Validation: Running other simulation using new data range and estimate the error percentage. (AMBROISE B., 1998)

3. Deficit Irrigation

The concept of deficit irrigation goes back to the 1970s, and for 20 years it was only a theoretical concept. An almost comprehensive approach to deficit irrigation emerged in the 1990s, with the publication of the first manual on deficit irrigation systems, it addresses all the operations to provide optimal water in a deficit situation and achieve maximum yield.

However, the paradigm shift has come up against obstacles due to the risk of crop failure and ignorance of the optimal amount of water needed for each type of crop.

Charmles, 1981, defines deficit irrigation as "the reduction in irrigation quantities during certain phases of the plant cycle" (Chalmers et al., 1981) and according to (English, 1990), "deficit irrigation is irrigation below full evapotranspiration ET in order to maximize the profit from water use", the paradigm has recently branched out into two subsystems.

• Regulated deficit irrigation: RDI

• Partial drying of the roots: RDI

According to (Chalmers et al., 1981), RDI "is an irrigation strategy based solely on reducing irrigation quantities during certain phases of the plant cycle". The literature shows the positive results of using this technique, it was previously applied to sugar beet, cotton and tomatoes, and the results of all these studies revealed a good increase in the effectiveness of the water (Miller and Hang, 1980), (Snyder, 1992) and (Hsiao, 1993).

PDR is the use of water stress to control vegetative and reproductive growth, such an application requires a good knowledge and understanding of the physiological process and the length of the culture cycle of each phonological type, this could be possible by prior analysis of the yield under drip irrigation and micro-irrigation conditions (Souza et al., 2005), PRD allows part of the root system to be in constant contact with moist soil (Capra, Consoli and Scicolone 2008).

Reducing the amount of water used for irrigation has a double positive effect; the first on the preservation of water resources and the second on economic gain.

3.1. Efficiency

(Hsiao et al., 2007; Sepaskhah et al., 2004) define efficiency, as "the proportion of biomass in the harvested product", the irrigation deficit increases water conservation. Normally, the amount of water applied for irrigation stays in the root and accumulates with the percolating water during rain period, the ratio of the amount of water evapotranspired to the amount of water in the area root can increase because crops are forced to extract more water. Ground levels (Capra, Consoli and Scicolone 2008)

The relationship between irrigation water (w) and crop yield (y) is expressed by the following equation

$$y(w) = a + bw + c\,w^2 \quad (1)$$

The corresponding parabola of this quadratic equation presented the variation of the culture according to the available water. Crop yield increases with rising water applied, after a short stability, decreases slightly.

The cost of irrigation

Irrigation income is estimated by multiplying the production function by the price of the crop, according to the below equation.

$$R(w) = Pc \cdot y(w) \quad (2)$$

Where R (w) is the income per hectare, y (w) is the crop production function, w is the depth of water applied and Pc is the price per unit weight paid for the crop.

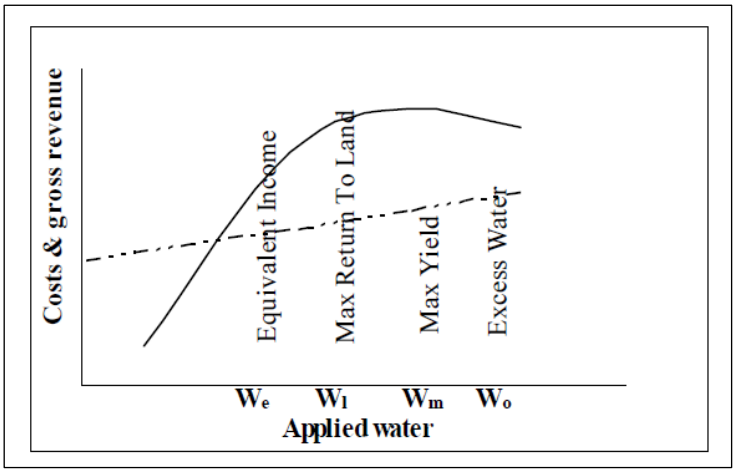


Figure 6: Cost & gross revenue in function to the applied water.

Source: CAPRA, A., CONSOLI, S. and SCICOLONE, B., 2008. Deficit irrigation: Theory and practice. Sl: sn ISBN 9781604565799.

The curves take the form of a bell, it could be subdivided into four parts; the start of the increase represents the equivalent income We, the Max returns to the earth when the applied water W1 reaches the maximum value, the maximum efficiency Wm, at this level the water use efficiency is zero and adding additional water does not increase crop yield and finally excess water W0.

Profit reaches a maximum level when the water applied is in W1, so if additional land can be irrigated, it should be under W1 (Capra, Consoli and Scicolone 2008)

The part where the amount of water applied is constant could relate the total production cost to the water applied in a linear relationship as follows;

$$\mathbf{C\ (w) = a + b\ (w)\ (3)}$$

So generally, the linear curve has an intersection and a slope, according to (Cortés and Gil 2007), the intersection represents the capital costs, taxes, insurance, fixed costs of tillage, planting, land use. chemicals and harvesting, while the slope represent the marginal variable costs of production which include the variable costs of irrigation water, pumping costs… (Capra, Consoli and Scicolone 2008), so since water depth had an impact on crop yield, the cost function could become nonlinear.

3.2. Optimal water

According to (English 1990), the optimum water depth is the water that allows the maximum profit per unit of land, the 5 optimum levels of water applied are:

- Level at which crop yield per unit of land is maximized, Wm
- Level at which effective income per unit of land is maximized, Wl
- Level at which effective income per unit of water is maximized, Ww
- Level at which effective income is equal to that of full irrigation when land is limited, Wel
- Level at which effective income is equal to that of full irrigation when water is limited, Wew

(Capra, Consoli and Scicolone 2008) analyzed several articles that deal with the DI paradigm, applied in different fields all over the world, the result has an overall tendency towards a total fresh mass and a reduction in the total production, the effects on dry matter and product quality are positive.

For example, Fabeiro Cortés et al., 2003 apply RDI on garlic cultivation in Spain, the results have shown negative effects at the blurbification and ripening stages. Dorji et al., 2005 applied

the PDR on a pepper crop in New Zealand, the results show no effect on the total dry mass, and a significant result in water savings. The rest of the studies developed vary between the decrease and the increase of the yield according to the type of culture, for example the PRD + RDI, carried out by Spreer & al., 2006, leads to a decrease in the yield, increase in the size of the fruit and the edible fraction, where the RDI applied by Zhang et al, 2006 in China on spring wheat leads to an increase in yield, biomass, crop index and WUE.

Likewise, an integrated agro-economic approach to deficit irrigation on lettuce crops was carried out in Sicily (Italy), the study consisted of evaluating the impact of four different levels of irrigation on the economic income of lettuce, estimating the optimum water applied. level proposed in the English literature cited (1990), the results have shown that obtaining water savings is approximately 49% in 2005 and 10% in 2006 The review of the case studies carried out here has shown, in general, positive effects

The deficit irrigation paradigm was recently applied in the region of Fès Meknes, in the north-west of Morocco, the study aims to assess the agro-physiological behavior of potatoes under full irrigation and two conditions of water restriction 25%, and 50%, compared to full irrigation (100%), the application of 25% water restriction did not affect the performance parameters, while the severe 50% condition could result in loss of significant yield, under such conditions yield parameters were impacted (reduction in size, weight, tuber diameters, decrease in chlorophyll and increase in leaf temperature)(El Bergui et al. 2020)

This implies that the use of such a system requires a good understanding of the agro-physiology of the crop, and an optimization of water saving, as strict water saving could damage the whole crop and, in this case, the loss will be high (water loss and crop yield).

Chapter II: Study area

1. Choice of study area

This study includes three main study areas; downscaling part is carried out over the whole Morocco since this type of study requires a large scale, the second and third part were carried out on the Inaouen watershed, this region is faced with critical water problems.

Floods: The flood events the region faced in the late decades, considerably affected the economic and social sectors, since the stormwater is channeled through rivers to the urban areas like Taza and Oued Amlil. (INGEMA, 2011)

Erosion: Rainfall and excessive water runoff on agricultural land can cause hydric erosion of soils, this issue has significant ecological and financial consequences.

Pollution: In 2011 a qualitative study was carried out on this region. The results reveal that the concentrations of COD and BOD5are high and this is due to waste generated by uncontrolled discharges. Also, the content of heavy metals such as Fe, Mn and Ni exceeds the defined standards. Bacteriological analyzes are marked by the presence of Escherichia Coli. (Naoura, J). To conclude that quality of the Inaouen is deteriorated.

2. Geographic location

2.1. Inaouen watershed

The Inaouen watershed is located between Fez and Taza (region known geographically as the Fez-Taza corridor). It covers an area of 3996 km² and a perimeter of 268 km. in the outlet there is Idriss first reservoir which is 20 Km far from the Fez. The basin is limited to the east by the middle Moulouya to the north-west by the Ouergha and to the south-west by the upper Sebou.

The area of this study will concern the upstream part of the watershed, the considered outlet is the entry of Idriss first dam. The Inaouen basin is in a mountainous area (between PreRif and Middle Atlas) with a maximum altitude of 1970 m mostly concentrated in the northern part, and 57 m when moving towards the outlet. The basin has a semi-arid to Mediterranean climate, marked by strong seasonal contrasts and very remarkable irregularities in rainfall.

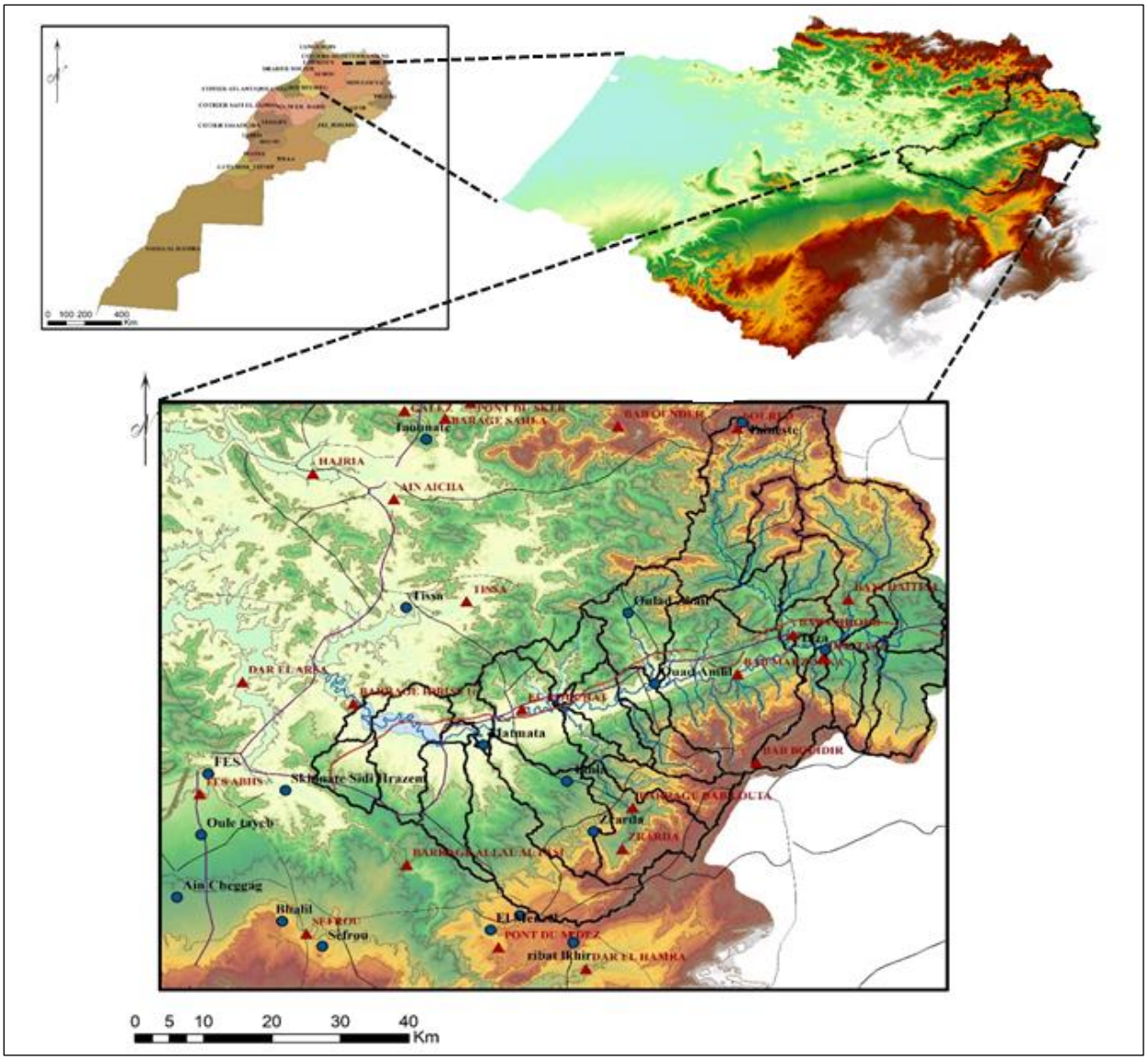


Figure 7: Geographic location map of the Inaouen basin drived from STRM file

2.1.1. Morphometric characteristics

Table 4:Morphometric characteristics of the Inaouen basin.

Area (km²)	Perimeter (km)	Gravilus coefficient	Equivalent rectangle	
			Width (km)	Length (km)
3669	**483**	**2.23**	**16.86**	**226.63**

2.1.2. Watershed hypsometry

The characteristics of the altitudes of the watershed are based on the analysis of the digital elevation model.

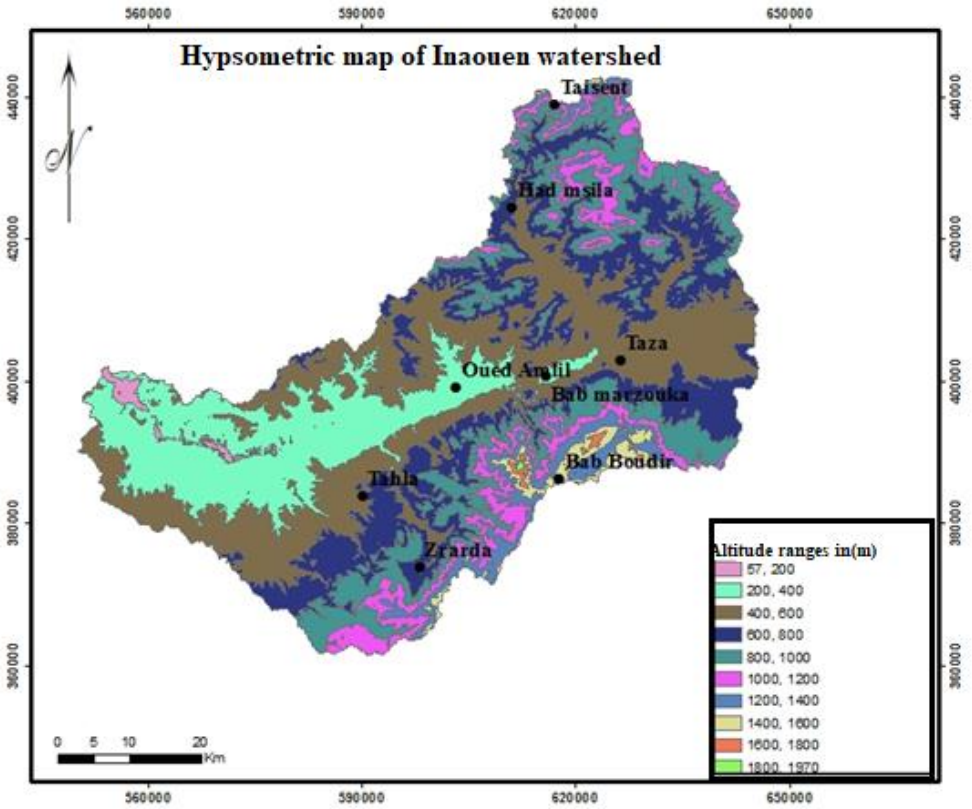


Figure 8: Hypsometric map of the watershed

The hypsometry of the watershed decreases from upstream to downstream.

2.1.3. Average altitude of the watershed

Table 5: Average altitude of the watershed.

Maximum altitude (m)	Minimum altitude (m)	Average altitude (m)	Elevation in (m)
1970	**57**	**1013.5**	**1913**

2.1.4. Hypsometric curve

Table 6: Table of altitude ranges in %

Altitude in (m)	Area in%	cumulative area in%
57-200	0.75	0.75
200-400	17.7	18.45
400-600	28.36	46.81
600-800	23.36	70.17
800-1000	15.65	85.82
1000-1200	7.89	93.71

1200-1400	4.16	97.87
1400-1600	1.82	99.69
1600-1800	0.29	99.98
1800-1970	0.03	100

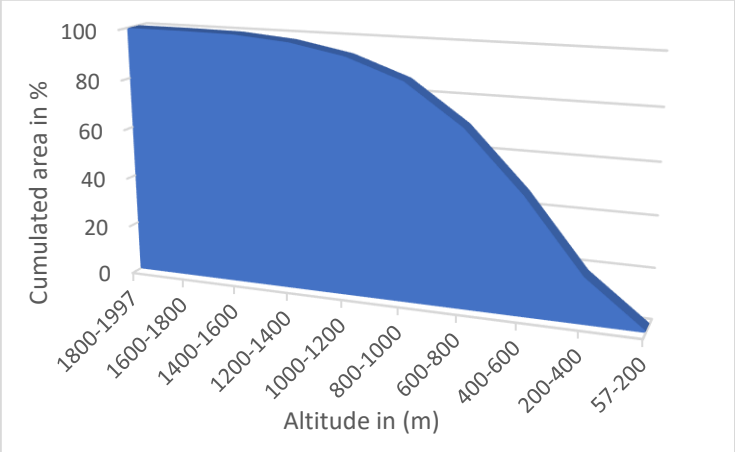


Figure 9: Cumulative area in%, hypsometric curve.

From 1997m to 1200m the surface varies slightly, it gradually decreases from 1000m to 57m.

2.2.5. Slope

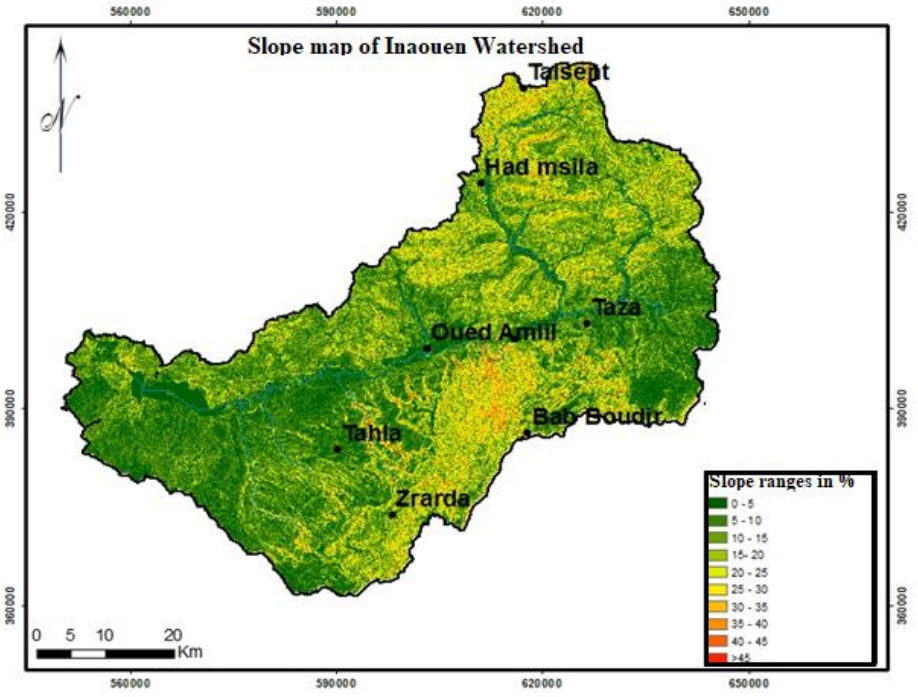


Figure 10: The slope map.

The steep slopes (greater than 45%) are concentrated in the north-east and south-east part of the watershed, this slope gradually decreases towards the central part of the basin where it becomes moderated (between 10 and 20%).

Table 7: Average slope and overall slope of the Inaouen basin

Average slope (m / Km)	Global slope index (m / Km)
12.09	**7.35**

According to the OSTROM classification, the Inaouen basin has a very strong relief.

2.1.5. Characteristics of the hydrographic effective work

The hydrographic effective work of a watershed can take many forms, and this depends on several factors (geology, vegetation cover, anthropogenic factors, etc.).

Oued Inaouen receives water from several tributaries, like Larbaa, Lahdar and Amlil (Figure 9). These tributaries collect the runoff from the Preifian hills. On the left bank, it is supplied in part by the primary massif of Tazzeka and by the limestones of the Middle Atlas, which are often karstic. The main tributaries of the left bank are Bou Hellou, Zireg, Matmata and Ahmar (El Mizani, 2006).

2.1.6. Drainage density

Table 8: Characteristic of the hydrographic effective work of the Inaouen basin.

Drainage density (km-1)	Stability constant (Km)
0.76	**1.31**

In the case of Inaouen the drainage density is 0.76 / km, the stability constant of the water effective work is equal to 1.31km.

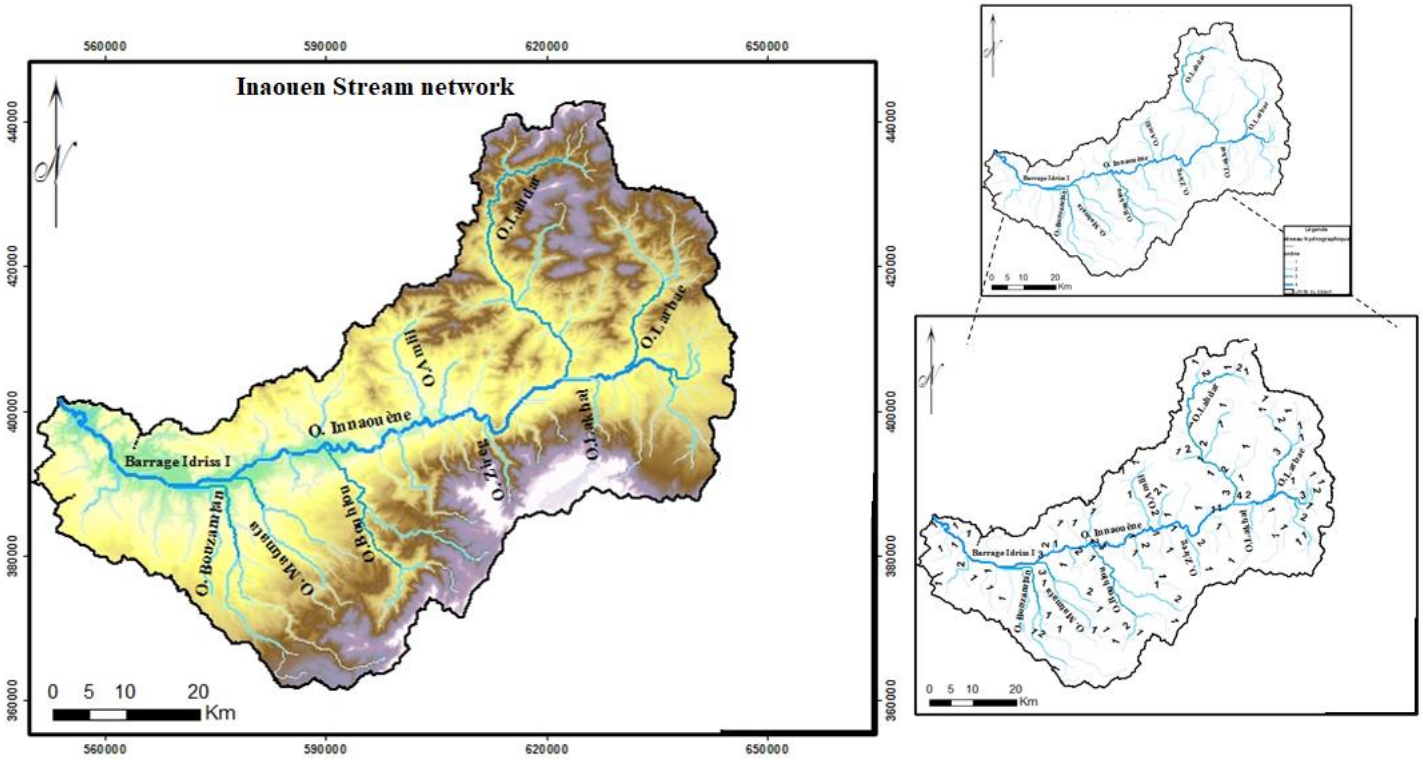


Figure 11: Hydrographic effective work of the Inaouen watershed

According to Strahler's classification, the Inaouen stream effective work has an order of 4.

3. Geological context

The basin is spread over two major structural Moroccan areas, southern part of the Rif, the northern part of the Meseto-Atlas domain. These two domains are separated by the Southern Rifian Trench, which takes the form of an elongated corridor following the East-West direction to close at the Touahar Pass and which extends from the Atlantic to the Mediterranean between the Rif chain to the north and the Hercynian moles of the meseta and the Middle Atlas to the south (Colo G, 1961).

Despite the diversity of outcrops, they can be grouped according to the permeability into two categories; the outcrops which have a high permeability, they are in the Middle Atlas region and characterized by essentially carbonate formations with a developed karstic system. The second category is found in the pre-Rif part, it takes the form of a flank with a marly substratum and therefore impermeable. These two types of permeable and impermeable formations will largely influence the hydrological behavior and the response of the watershed to rain events **(Naoura J, 2011).**

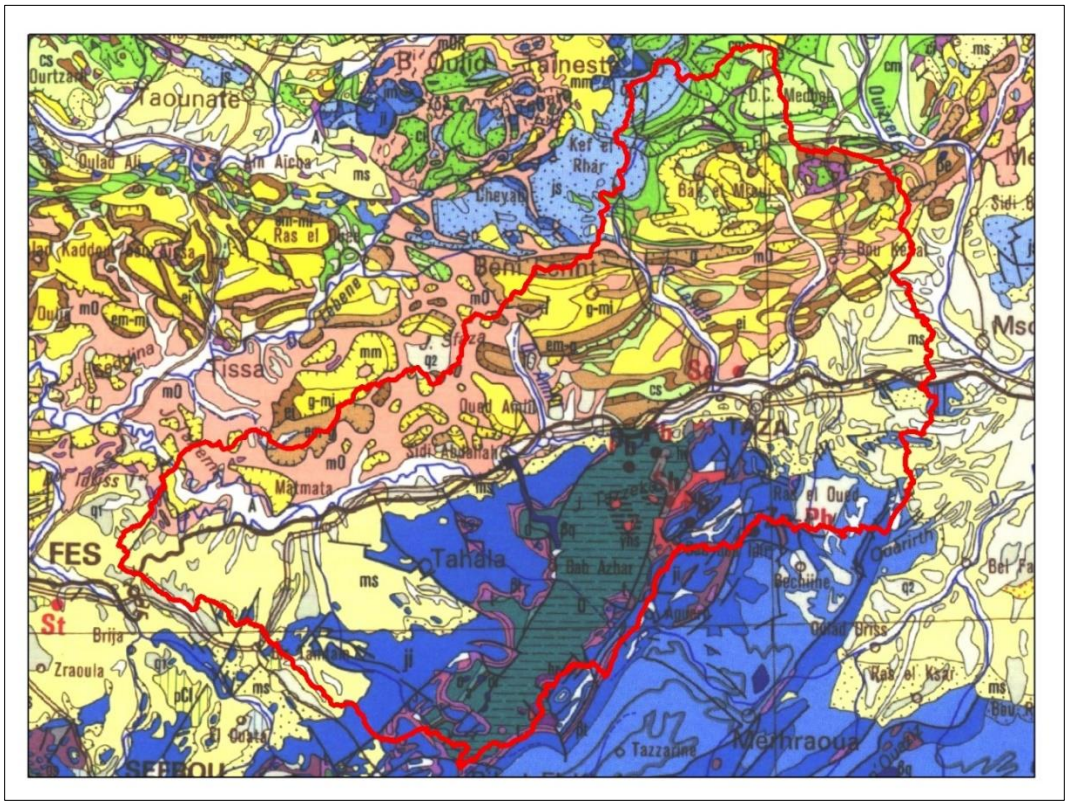


Figure 12: Geological map of the Inaouen basin

Source: Geological map of Morocco 1/1000000 (1985)

3.1. The meseto atlas domain

3.1.1. Primary

It is formed by shales and sandstones, which clearly outcrop in the Tazekka buttonholes, these terrains date from the Ordovician period and constitute a major part of the outcrops according to Hoepffner, 1989 the Tazekka massif is subdivided into three structural domains

- The western sandstone-pelitic domain of Lower Ordovician to Devonian age.
- The central domain, consisting of greenish-grey shales, with rare small quartzite banks, which are Ordovician in age.
- The eastern area is formed by olive-green schistose pelites, or so-called Tazekka shales. It dates from the Lower Ordovician and is overlain by a volcano-sedimentary complex of Upper Visian-Namurian age.
- The Silurian age outcrops in the western Tazekka, at the level of Oued Bou-Ayach.

3.1.2. The secondary

The Mesozoic terrains date from the Triassic to the Lower Aalenian-Bajocian.

The major characterization of the Atlas domain is the replay of the Hercynian accident which led to the formation of the Subsidiary Basins, the Atlas Triassic is formed by clay-sandstone structures, discordant on the Primary, often accompanied by tholeitic basalt flows and evaporitic levels (Laville et al., 2004)

The Jurassic Lias is formed by dolomitic facies which gradually becomes calcareous and marly as it moves towards the southern Rift valley where it is concealed under the marl and limestone of the Miocene.

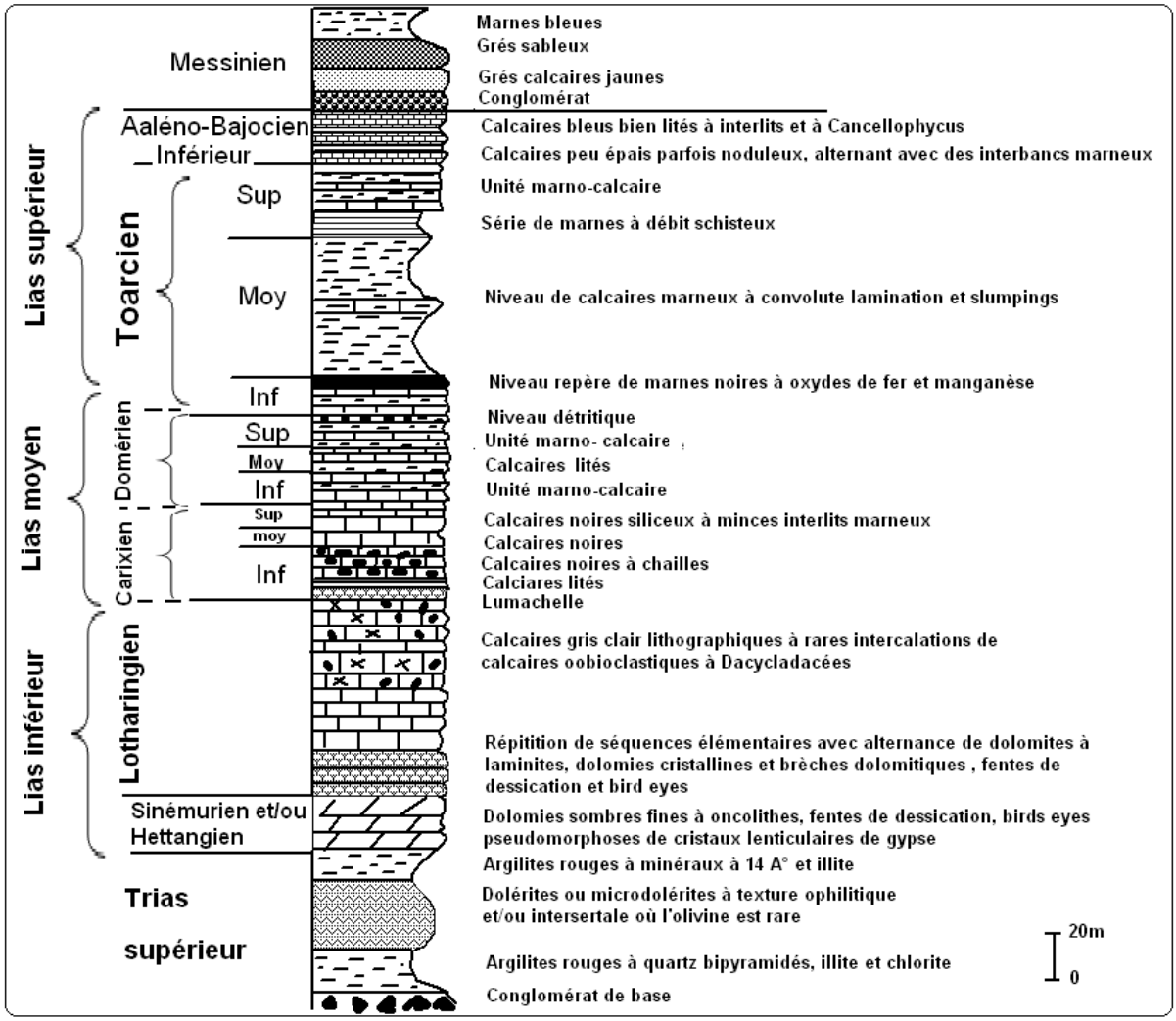


Figure 13: Synthetic profile of the Meso-Cenozoic cover of the boutenière of Tazekka

Source: (Auajjar and Boulegue, 1999, modified by Naoura Jamal).

3.1.3. Liasic formations:

3.1.3.1. The lower lias

The lower Lias is characterized by a calcaro-dolomitic series (Sabaoui, 1998;Auajjar). This formation is well developed at the level of the Middle Atlas Causse, moving towards the East they appear in the buttonhole of Tazzeka.

3.1.3.2. The Middle Lias (Carixian -Domerian)

The sedimentary phase of the middle Lias is essentially characterized by the presence of Cephalopod and Ammonite limestones which mark the transition between the lower Lias and middle Lias. The presence of the dendrites of the Upper Demonian is an indication of the instability phase experienced by the Middle Atlas during this phase, the lower Lias was dislocated by synchronous normal faults which resulted in the formation of the Jurassic Atlas basins.

The detrital levels of the Upper Domerien testify to a phase of instability in the Middle atlas, in addition, south of Taza the thickness of the formations is very important to the east than in the west; this proves the dislocation of the lower Lias platform by faults

3.1.3.3. Upper lias

The upper Lias is characterized by the presence of marly levels, their formation is due to invasion of the Toracian Sea, the formations of this level are arranged in the form of synclinal series.

3.1.3.4. Bajocian (Middle Jurassic)

During the Aalenian - Bajocien, the marly sedimentation which began in the Toarcian continues with the appearance of limestones, which bear traces of Zoophycos.

3.1.3. The Tertiary

According to Sabaoui and viallard (1998), two main levels are distinguished

- The detrital Helvetian (sandstone and marl-limestone),
- The marly Tortonian
- The Pliocene is based on the Tortonian is characterized by basic conglomerates on which rests tuffous limestones

3.1.4. The Quaternary

The quaternary presents two types of deposit:

- Lake limestones: North of Ras Chedaya located in the southern part of dayat Chikker (Naoura, 2011)
- Travertines: Travertine formations or limestone tuffs are well developed. The most striking outcrop is that of the Oued Haddar waterfalls fed by the Ras Elma resurgence.

3.2. The pre-Rif domain:

The Rif domain has several structural zones, moving from the north-east to the south-west, there is the internal Rif, the flysch zone and the external Rif. In the study area, the Rif domain is only represented by the outer domain. (Piqué et al, 2007, Faure-Muret). It is essentially characterized by a sandstone-schist bedrock, the external domains are in the form of a marly bedrock which comprises three parts; the intra-Rif, the meso-Rif and the pre-Rif.

The nappes of the Rifian domains are nappes with mesoRifarian affinities, dominated by Upper Jurassic flysch, lithonic limestones, Neocomian marlstones, Middle Cretaceous flysch and flysch and marlstone from the Senomian to the base of the Eocene.

They may be rooted, as in the case of the Tainest nappes, or allochthonous, emplaced by sliding, as in the case of the Tsoul nappe. Lithostratigraphically, these nappes are characterized by series ranging from the Upper Cretaceous to the Middle Miocene (Piqué et al, 200)

Table 9: Table of the percentage of surface areas of each lithologic type

Lithological surface	**Lithological nature**	**area in%**
Tender substratum	Marl-schists	26.0
Resistant substratum	Schist; marl-limestone; sandstone and pelites	24.9
Very tender substratum	marls	12.8
Very resistant substratum	Limestone; sandstone; granite; silt, michaschist	36.3

4. Soil context of the Inaouen Basin

Table 10: Table of percentages for each type of soil

Soil type	**% of the surface**
Little evolved soil	18.43
Iron sesquidox soil	11.68
Browned soil	0.36
Slightly evolved brown soil	1.20
Calcimagnesium soil	21.89
Cacimagnesic to isohumic soil	2.40
Slightly evolved cacimagnesic soil	4.21
Isohumic soil	7.68
Poorly evolved soil calcimagnesium sesquidoxes of iron	0.21
Vertisol ground	11.11
Little evolved iron sequidox soil	20.79

The cartography of the soil cover made by Wladimir Cavallar (1950); Heush (1962), Duran (1970), Mardare-Seg (1983) allow us to distinguish the following soils:

- Slightly evolved brown soils and less evolved soils located upstream of the Inaouen basin.
- The vertisols encountered on the marly hills of the pre-Rif, their proportion is about 11.11% compared to the whole soil cover of the basin.
- The calcimagnesic soils cover some part of the valley of Oued Inaouen.

- Isohumic soils, presented by two types; the chestnut soils frequent in the east of Oued Bouhlou, and the Mediterranean red soils characterized by a high rate of iron oxides cover only a small area of the basin 0.21%.

We can conclude that the pedological distribution of the Inaouen basin is directly linked to the nature of the lithological substratum thus, the less evolved soils extend over the pre-Rif while the thick soils mark out the lowlands of the fluvial terraces of Oued Inaouen.

5. Hydro-climatology of the Inaouen watershed

5.1. Data control

In order to characterize the climatology of the Inaouen basin, an analysis of hydrometric and rainfall data was carried out. The data is provided by the watershed hydraulic agency of Sebou. The metadata of the hydrometric and rainfall stations used, and the map of their geographical locations are detailed in Part II, Chapter 3.

To highlight the representativeness of the data, and to fill in missing values, we will apply a double accumulation test on the stations "Bni haitem", "Zrarda", "Bab chhoub", the base station is "Bab merzouka " because it covers a larger period.

$$Y_{(t)} = Y_i = \sum_{j=1}^{i} Y_j \quad et \; X_{(t)} = X = \sum_{j=1}^{i} X_j \quad (4)$$

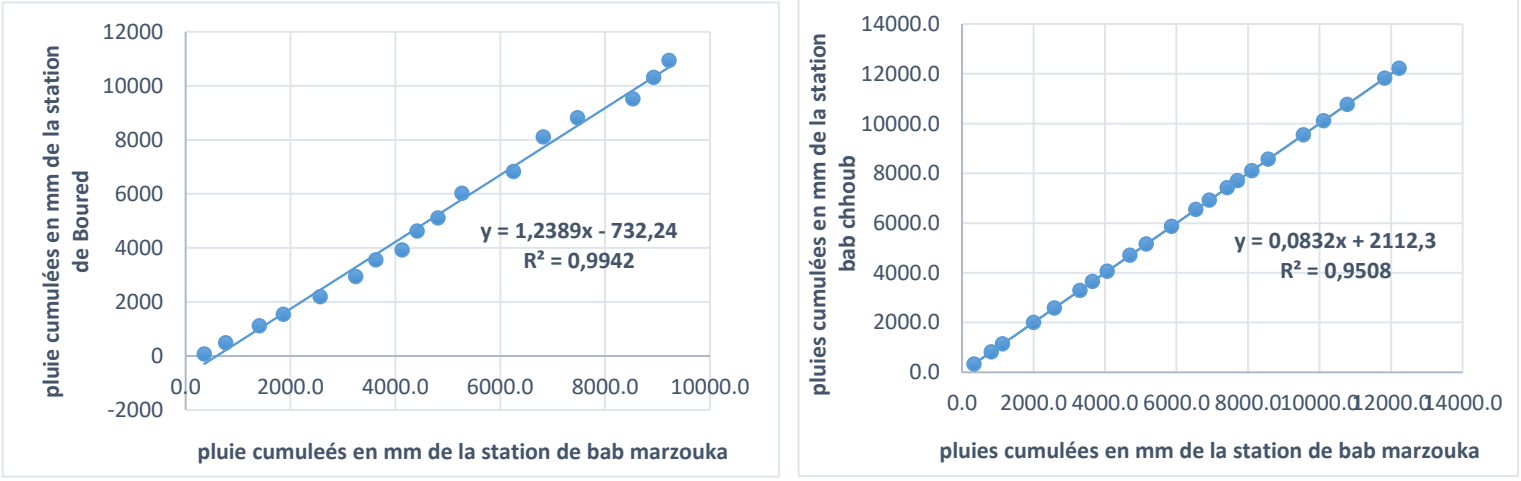
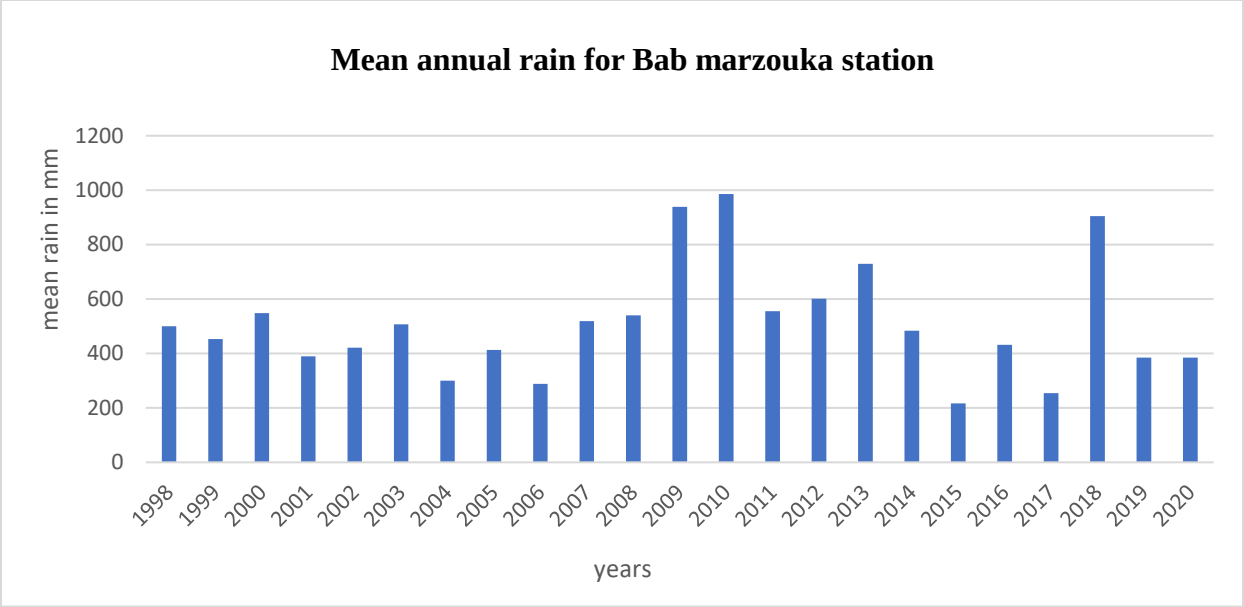


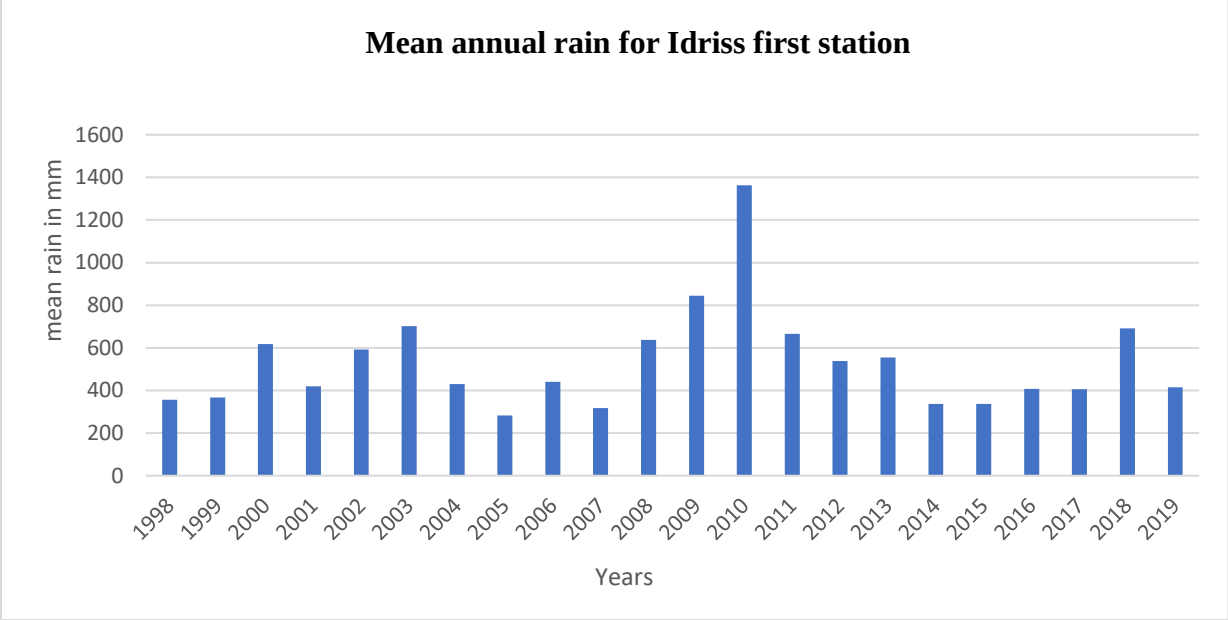
Figure 14: Double cumulation test for the "Boured" and "Bab chhoub" stations.

The points obtained are distributed harmoniously around the line, the homogeneity test is therefore confirmed.

5.2. Precipitation

5.2.1. Annual precipitation





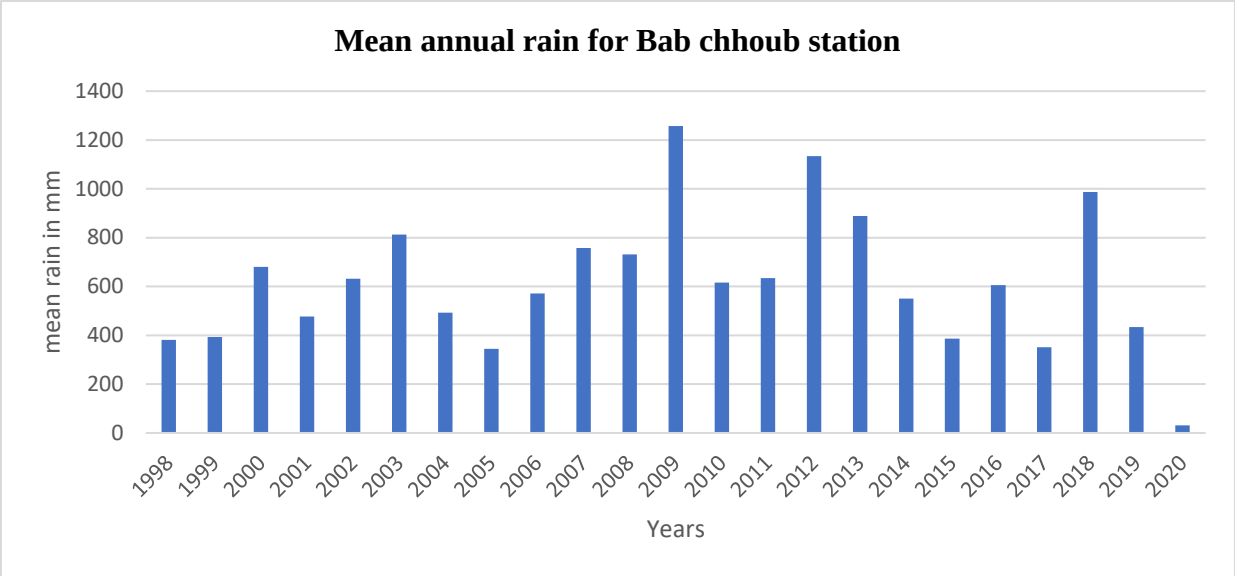


Figure 15: Average annual precipitation of stations; "Bab merzouka ", "Bab chhoub", "Idriss first".

For the Bab Merzouka station, the rainfall analysis of the series (1998-2020) shows that 2010 is the wettest hydrological year with an average of about 1300mm, we also notice that the station records very high rainfall with a cyclicity of approximately 10 years. Similarly, 2010 is the wettest year for the other two stations.

5.2.3. Estimation of the annual mean water depth

5.2.3.1. Arithmetic method

$$Pmoy = 626.025mm$$

5.2.3.2. Isohyet method

In the upstream of the catchment area, the average precipitation is significant (> 1150mm), it gradually decreases going towards the center of the basin downstream. This distribution is linked to the hypsometry of the watershed, as well as to the lithological nature of the substratum.

5.2.3.3. Average precipitation by the three methods

To estimate the mean water depth, we take the arithmetic mean calculated by the three methods

Table 11: Estimation of the total annual water volume by the three methods.

Method	**Arithmetic**	**Theissen**	**isohyets**	**Medium**
P avg in mm	626,025	597.03	570.93	597.99

5.2.3.5. Estimation of annual water volume

$$V = Pmoy.ST \rightarrow V = 3320.106 * 597.99.10\text{-}3$$

$$V = 1959.98.106\ m3 / s$$

Part of this volume will be subject to evapotranspiration and infiltration (cracked limestone from the middle atlas), so direct runoff can only take place after the saturation of the water tables.

5.3. Temperatures

5.3.1. Monthly average temperatures

Temperature data is only available at Tissa and Bab Merzouka stations.

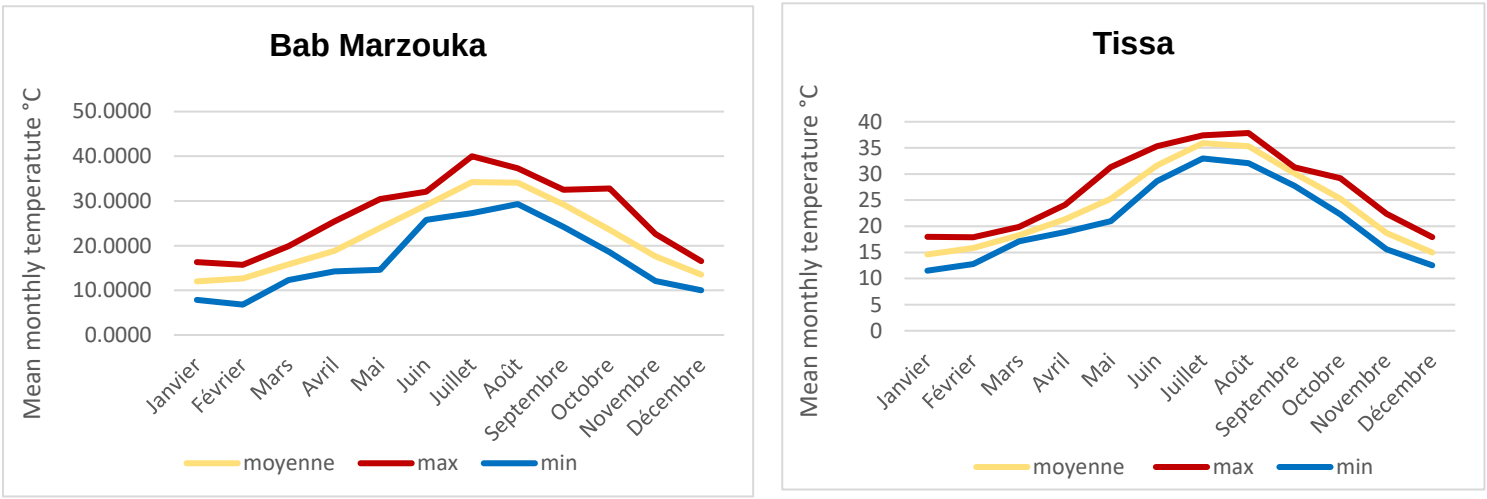
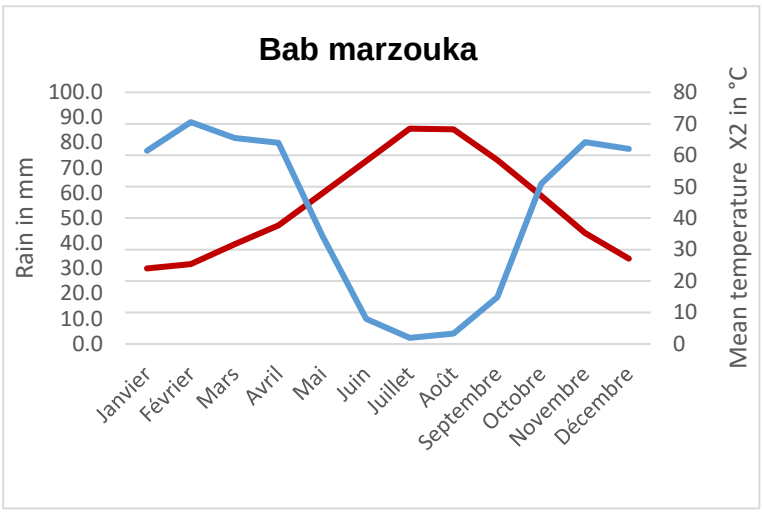


Figure 16: Maximum and minimum monthly average temperature variation, for the "Tissa" and "Bab Merzouka " stations.

We can distinguish two contrasting seasons, a wet one spread over eight months from September to May, the dry season is spread over four months, the maxima are marked in July with an average temperature of 40°C for the Bab Merzouka station and 37.41°C for the Tissa station, the coldest months are December and January, the average temperature reaches extreme values (7.8°C for the Bab Merzouka station and 11.5°C for the Tissa station)

5.3.2. Ombrothermal diagram



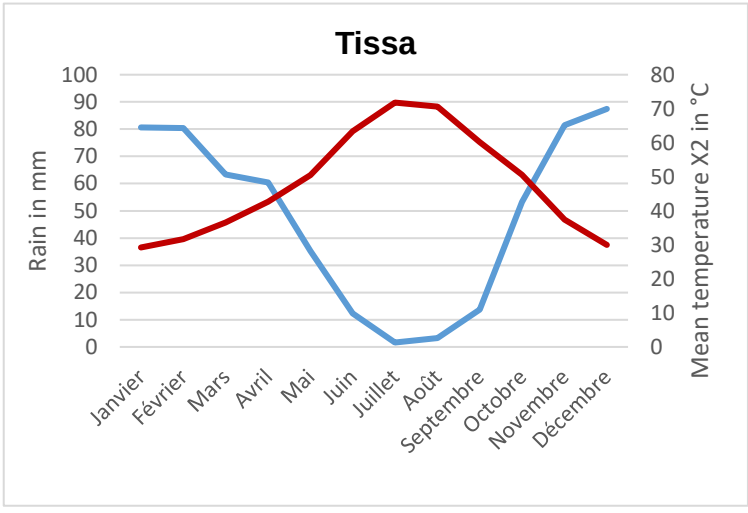


Figure 17: Ombrothermal diagram of the "Bab Merzouka " and "Tissa" stations

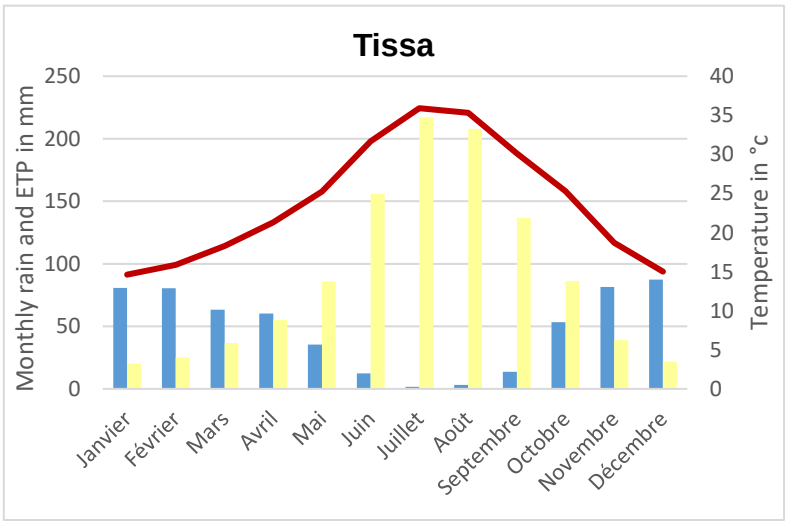
The diagrams show that the wet period lasts six months, it extends from October to May, thereafter the dry season takes over and lasts six months (from April until the month of May). month of September).

5.4. Evapotranspiration

5.4.1. Estimation of potential evapotranspiration by the Thornthwaite method

Table 12: The Thermal index and the alpha coefficient for the "Tissa" and "Bab merzouka " stations:

Stations	Thermal index I in ° C	Coefficient ∝
Tissa	133.38	2.63
Bab merzouka	124.26	2.48



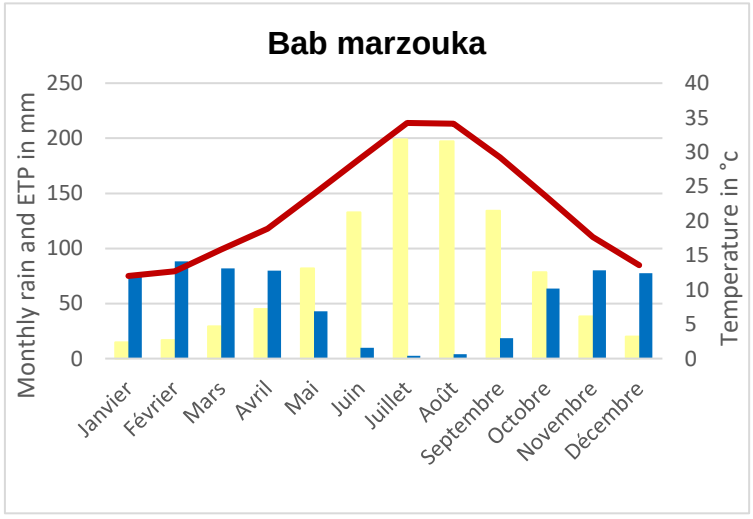


Figure 18: Variation of the monthly potential evapotranspiration for the "Bab merzouka " and "Tissa" stations.

5.4.2. Estimation of actual evapotranspiration by the Method of Turc.

Table 13: Calculation of evapotranspiration by Turc method for the "Bab merzouka " and "Tissa" stations.

Stations	Coefficient L	P in mm	T in ° C	ETR in (mm)
Bab merzouka	1392.19	590	22.1	567.83
Tissa	1580,095	523.11	23.9	520.61

The real evapotranspiration value is very close to the precipitation value that can be explained by the semi-arid climate of the Inaouen basin.

5.4.3. Thornthwaite method for water balance estimation

Table 14: Calculation of the monthly ETR by the Thornthwaite method for the "Tissa" station.

Month	S	O	NOT	D	J	F	M	AT	M	J	JU	TO
precipitation	13.75	53.29	81.44	87.44	80.67	80.45	63.35	60.36	35.3	12.34	1.62	3.21
AND P	136.66	86.35	38.99	21.77	20.35	25.20	36.62	55.04	85.95	156.05	217.26	207.95
ETR	13.75	53.29	38.99	21.77	20.35	25.20	36.62	55.04	85.3	12.34	1.62	3.21
RFU	0.00	0.00	42.45	50.00	50.00	50.00	50.00	50.00	0.00	0.00	0.00	0.00
Deficit	122.91	33.06	0.00	0.00	0.00	0.00	0.00	0.00	0.65	143.71	215.64	204.74
Excess	0.00	0.00	0.00	58.11	60.32	55.25	26.73	5.32	0.00	0.00	0.00	0.00

Table 15: Calculation of the monthly ETR by the Thornthwaite method for the "Bab merzouka " station.

Month	S	O	NOT	D	J	F	M	AT	M	J	JU	TO
precipitation	18.61	63.64	80.20	77.50	76.71	88.14	81.33	79.91	43.05	9.92	2.41	4.08
AND P	134.24	78.30	38.23	19.85	14.68	16.83	29.29	45.11	81.85	132.64	198.99	197.22
ETR	18.61	63.64	38.23	19.85	14.68	16.83	29.29	45.11	81.85	21.12	2.41	4.08
RFU	0.00	0.00	41.98	50.00	50.00	50.00	50.00	50.00	11.2	0.00	0.00	0.00
Deficit	115.64	14.66	0.00	0.00	0.00	0.00	0.00	0.00	0.00	116.41	196.58	193.14
Excess	0.00	0.00	0.00	49.63	62.04	71.31	52.04	34.80	0.00	0.00	0.00	0.00

Table 16: Results of the calculation of the monthly ETR by the Thornthwaite balance method for the "Tissa" and "Bab merzouka " stations.

Station	ETR value in mm
Tissa	367.50
Bab merzouka	350.79

The variation of evapotranspiration is closely linked to that of rainfall, the agronomic deficit reaches its maximum in July (215.64mm for the station of Tissa and 196.58 for the station of Bab Merzouka), the maximum of excess is reached in January with a value of about 60 mm, this is due to the strong rainfall.

5.4. The water balance

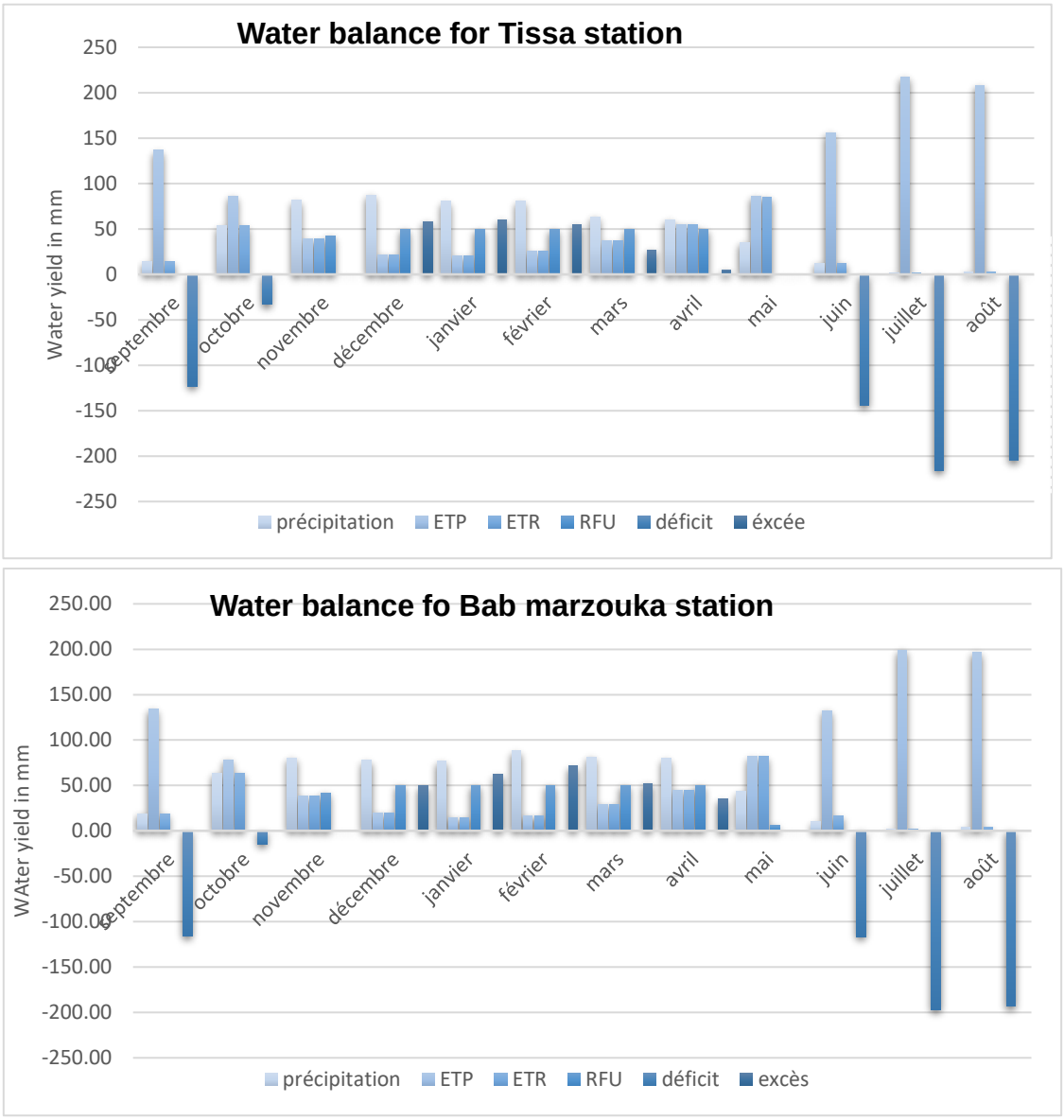


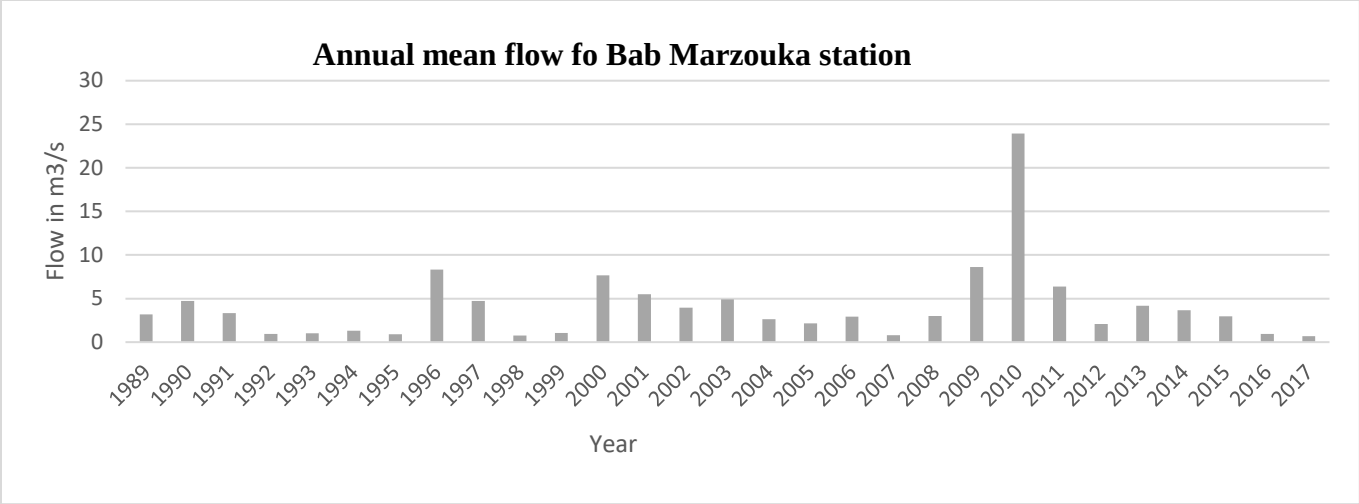
Figure 19: Water balance of the Inaouen watershed for the "Tissa" and "Bab Merzouka " stations.

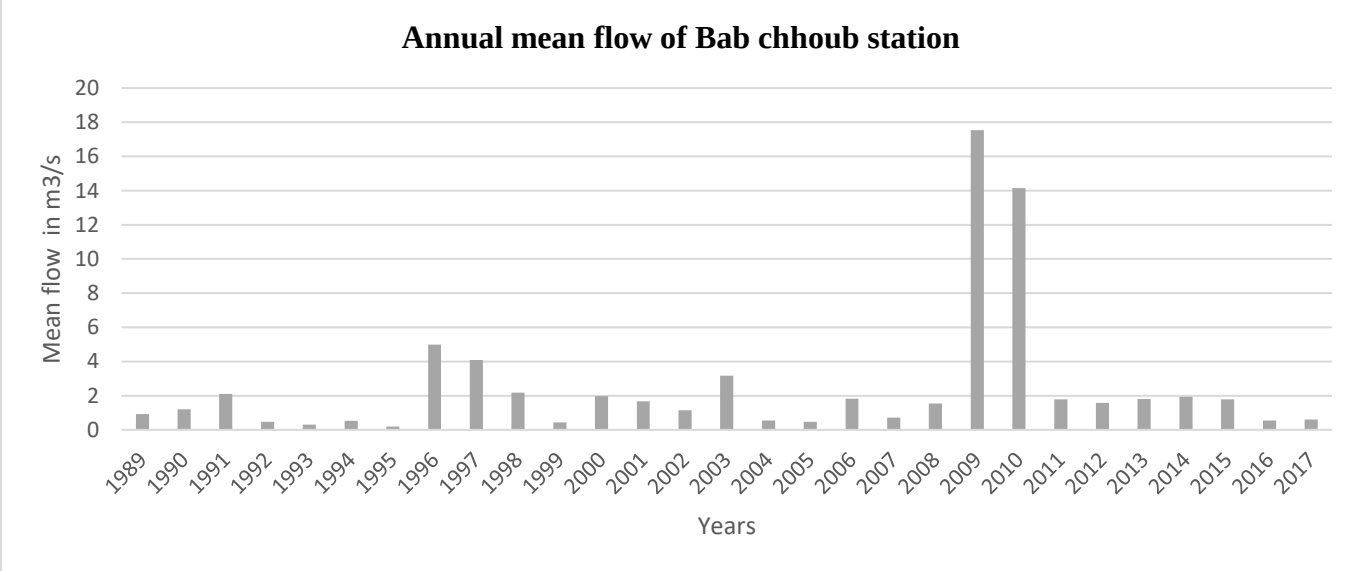
According to the graphs, two main phases can be distinguished:

- The deficit phase: which extends from July to October when the available water capacity is totally withdrawn, so there is no runoff.
- The surplus phase: extends from November to May, this phase can be subdivided into two sub-phases: one of reconstitution of the available water capacity of the soil used in the deficit phase, (November and December), and a phase of excess where precipitation largely exceeds evapotranspiration, in this case direct runoff is important.

5.5. Flow study

5.5.1. Average annual flow





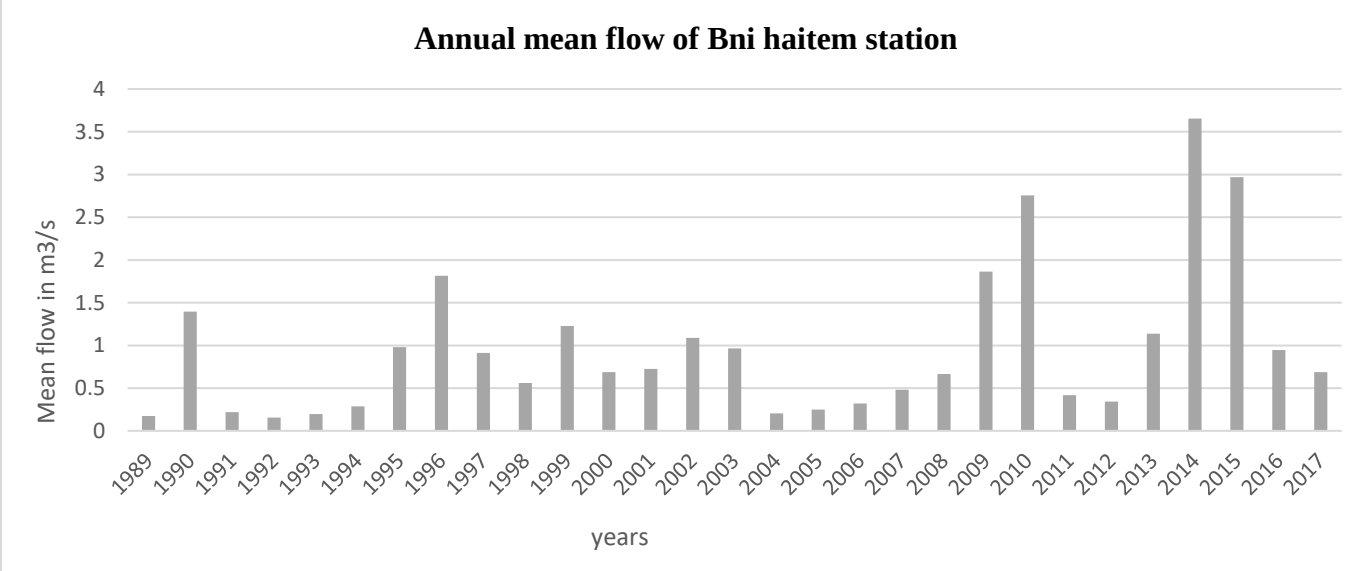


Figure 20: Average annual flow for the stations of "Bab merzouka ", "Bab chhoub" ,.

The variation in the average annual flows reflects temporal irregularities and highlight a succession of wet and dry periods.

5.5.2. Monthly average flow

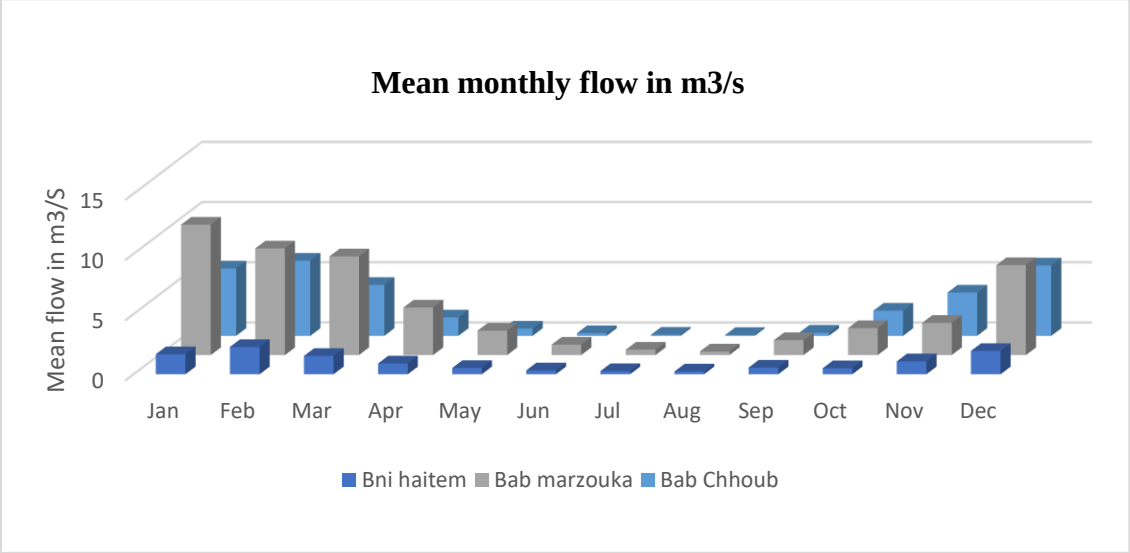


Figure 21: Variation of average monthly flows for the stations of Bab Chhoub, bab merzouka , and Bni haitem

The monthly variation in the flow rates recorded by the three stations goes with the seasonal variations in precipitation, the Bab Merzouka station records high flows compared to the other two stations, this spatial variation may be due to their geographical position.

5.6. Gumbel's law

The frequency analysis of a long series of maximum values makes it possible to estimate the return period of a particular rain event. This prediction is based on the definition and the implementation of a frequency model which is an equation describing (modeling) the statistical behavior of a process. The purpose of Gumbel's law analysis is to determine peak flow rates at different return periods. In the literature different method exists, the Gumbel method is adapted to the Inaouen watershed; it has already been applied in the study of Naoura, 2011 and produced satisfactory results. For the current study the analysis will be carried out on a series of maximum daily flows (1989-2019) from the Bab Merzouka station.

5.6.1. Gradex method

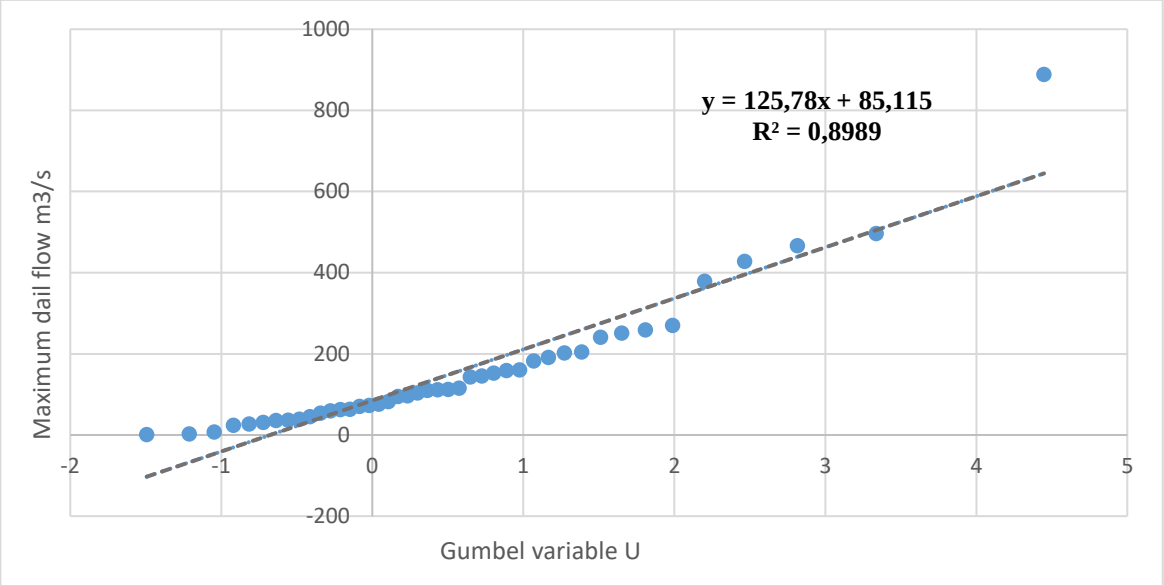


Figure 22: Adjustment of the max flow rates j by the graphic method of Gumbel's law

Table 17: Flow corresponding to different return periods by the graphic method.

Return periods	2	5	10	20	50	100
Probability of not exceeding QP	0.5	0.8	0.9	0.95	0.98	0.99
Gumbel's reduced variable	0.37	1.50	2.25	2.97	3.90	4.60
Qp for return period in m3 / s	131.11	273.67	368.06	458.60	575.80	663.62

5.6.2. Method of moments

Table 18: Flow corresponding to different return periods by the method of moments.

Return periods	2	5	10	20	50	100
P of not exceeding	0.5	0.8	0.9	0.95	0.98	0.99
Reduced variable of Gumbel	0.36651292	1.49993999	2.25036733	2.97019525	3.90193866	4.60014923
Qp for return period in m3 / s	129.506291	277.567342	375.59664	469.628697	591.34355	682.551704

5.6.3. Intensity-duration-frequency (IDF) curves

The IDF curves give the maximum intensity as a function of the duration t, for a return period T. the construction of these curves will refer to the maximum daily precipitation data from the Bab Merzouka station.

Table 19: Rain intensity according to the return periods and duration of precipitation

	Rain intensity in (mm)					
rain duration (h)	I (T = 2)	I (T = 5)	I (T = 10)	I (T = 20)	I (T = 50)	I (T = 100)
5	0.020376748	0.015817132	0.014416499	0.013546796	0.01278782	0.012811459
10	0.004114604	0.002738082	0.002365135	0.002145081	0.00196024	0.001965901
15	0.001613957	0.000981503	0.000821595	0.000729867	0.00065443	0.00065672
20	0.000830847	0.000473986	0.000388018	0.000339665	0.00030049	0.000301665
30	0.000325901	0.000169907	0.000134789	0.000115572	0.00010032	0.000100773
60	6.58079E-05	2.94123E-05	2.21131E-05	1.83003E-05	1.5378E-05	1.54634E-05
90	2.58132E-05	1.05432E-05	7.68161E-06	6.22671E-06	5.1339E-06	5.16565E-06
120	1.32884E-05	5.09152E-06	3.62782E-06	2.89778E-06	2.3573E-06	2.37285E-06

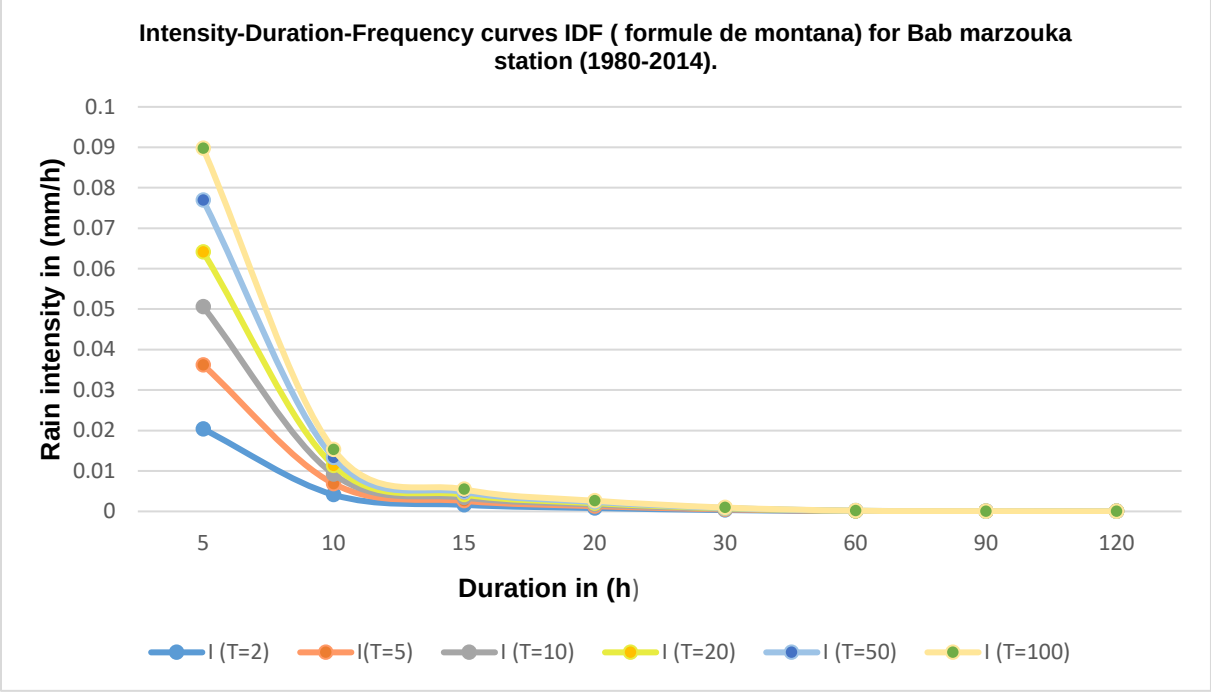


Figure 23: IDF curves for Bab merzouka station.

6. Statistical analysis

The statistic descriptive is usually used to describe the form of the distribution of the data range with some common parameters such as central tendency, skewness, and taildness.

The central tendency is measured using three parameters, the mean, the mode, and the median, this later correspond to the value of the studied variable at which the values on both sides are

equal, considering a data series with n observation arranged in ascending order the median is the observation that half the values on two, the dispersion is then concluded by measuring how closely the random variables are distributed, clustered or spread out around the central value.

The symmetry of data describes the data distribution in respect to the mean, the data may be tailed to the left or the right, differently said skewed to the left or the right, depending on if the skewness coefficient is positive or negative, it is expressed by the following equation

$$Cs = \frac{n\sum_{i=1}^{n}(x_i - \overline{x})^3}{(n-1)(n-2)S^3}\ ^1 \quad (6)$$

- The skewed right data or positive skewness has Cs>0
- The skewed left data or the negative skewness has Cs<0

Concerning the tailedness, this parameter is referred to the coefficient of Kurtosis value, this later points out the effect of existing outliers and measure the taildness of distribution, it is expressed by the following equation

$$K = \frac{n\sum_{i=1}^{n}(x_i - \overline{x})^4}{(n-1)(n-2)(n-3)S^4} \quad (7)$$

Based on this measurement, the distribution could be:

- Mesokurtic: k = 3 the distribution is qualified as normal
- Leptokurtic: k> 3 the distribution is more concentrated near the mean

[1]Source: MAITY, R., [sin fecha]. Springer Transactions in Civil and Environmental Engineering Statistical Methods in Hydrology and Hydroclimatology [en línea]. Sl: sn ISBN 9789811087783. Available in: http://www.springer.com/series/13593

- Platykurtic: k <3, a smaller concentration of probability near the mean

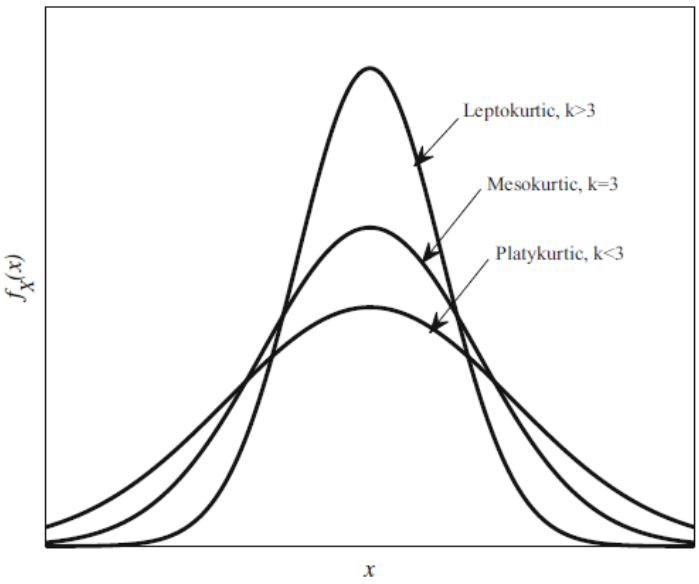


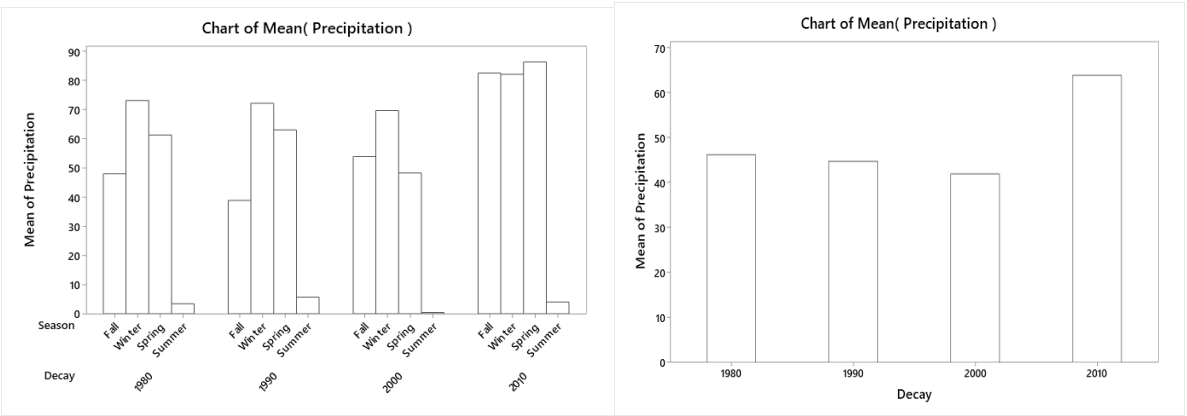
Figure 24: Plot of Frequency Distribution as a function of a random variable that shows the difference between Mesokurtic, Leptokurtic, Plakurtic Zone

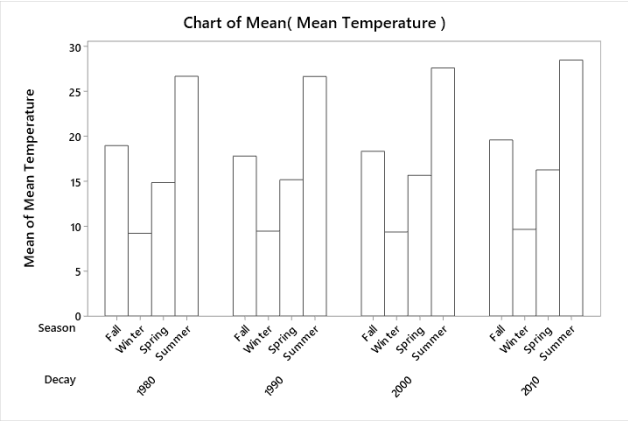
Source: MAITY, R., [sin fecha]. Springer Transactions in Civil and Environmental Engineering Statistical Methods in Hydrology and Hydroclimatology [en línea]. Sl: sn ISBN 9789811087783. Available in: http://www.springer.com/series/13593.

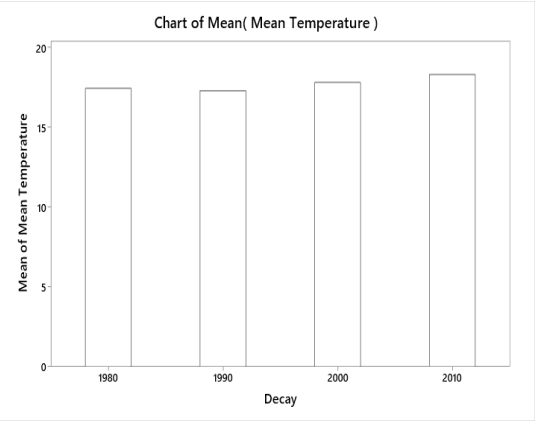
In this case study, the descriptive statistics were carried out under Minitab, central tendency parameters were defined and described for three climatic variables (precipitation, temperature, and relative humidity) for the two stations; Bab Merzouka (Sation 01) and Idriss first (Station 02) to define the variation and fluctuation trends. The precipitation is provided by the watershed hydraulic agency of Sebou, the other two variables are derived from the database of Global weather data CFSR, more details on the data are described in chapter 3 of part II.

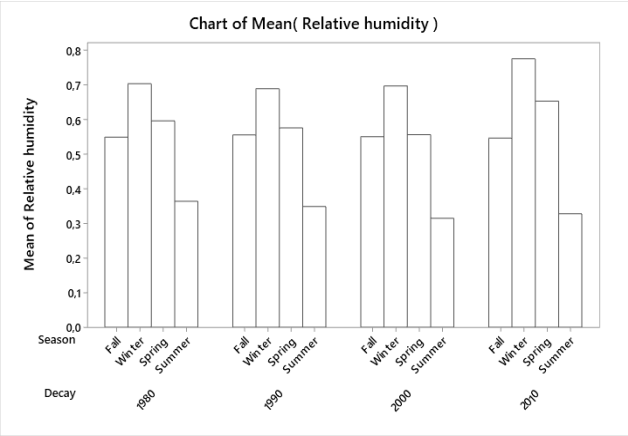
6.1. Temporal variation

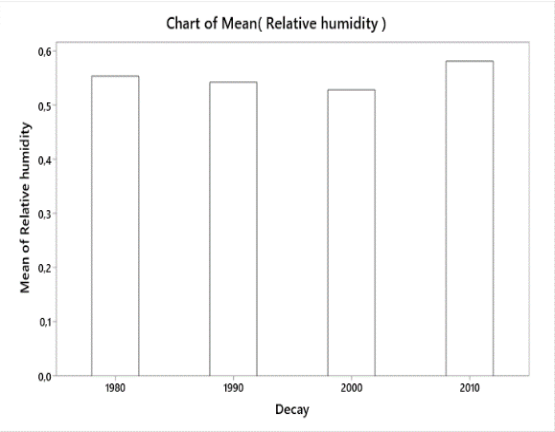
6.1.1. Bab Merzouka station

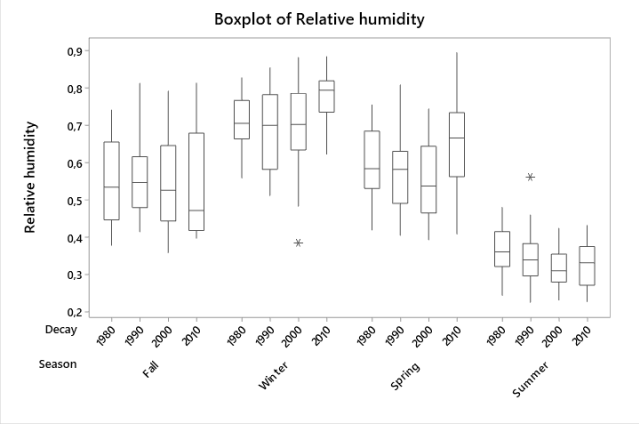


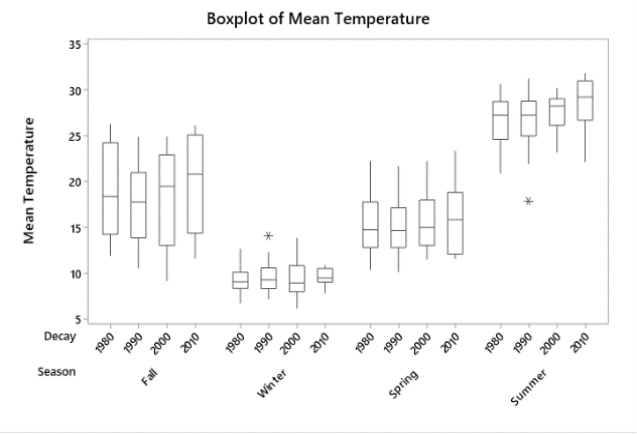

Chart of Mean(Mean Temperature)
Mean of Mean Temperature
Season
Fall
Winter
Spring
Summer
Decay
1980
1990
2000
2010


Chart of Mean(Mean Temperature)
Mean of Mean Temperature
Decay
1980
1990
2000
2010


Chart of Mean(Relative humidity)
Mean of Relative humidity
Season
Fall
Winter
Spring
Summer
Decay
1980
1990
2000
2010


Chart of Mean(Relative humidity)
Mean of Relative humidity
Decay
1980
1990
2000
2010


Boxplot of Relative humidity
Relative humidity
Decay
Season
Fall
Winter
Spring
Summer


Boxplot of Mean Temperature
Mean Temperature
Decay
Season
Fall
Winter
Spring
Summer

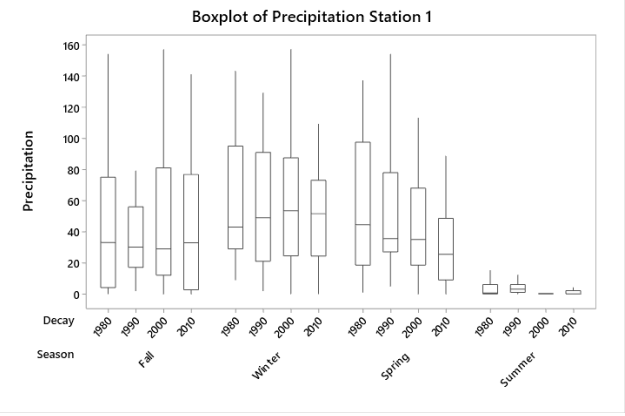
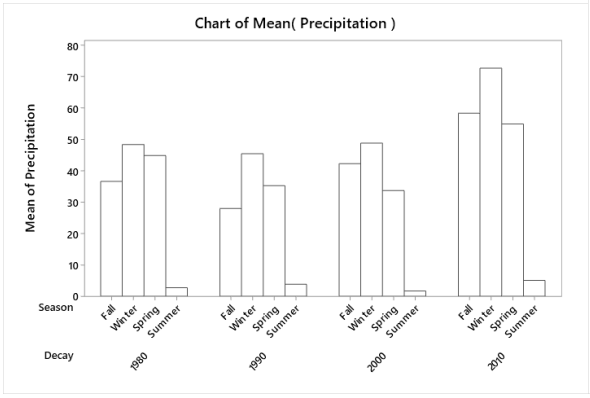
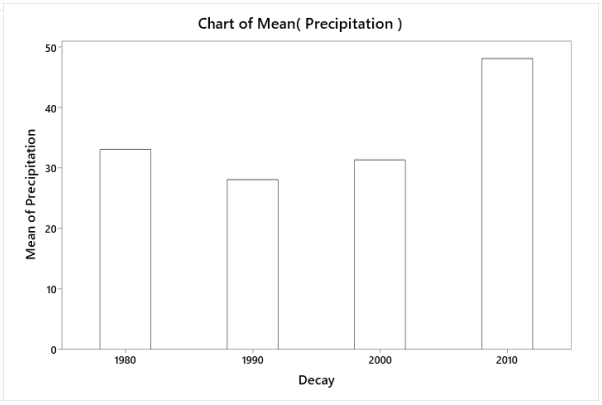
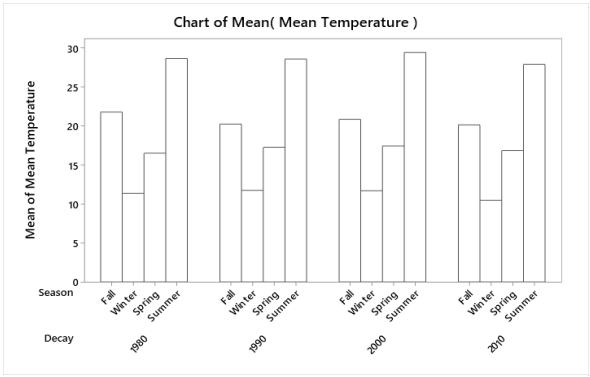

Boxplot of Precipitation Station 1
Precipitation
Decay
Season
Fall
Winter
Spring
Summer

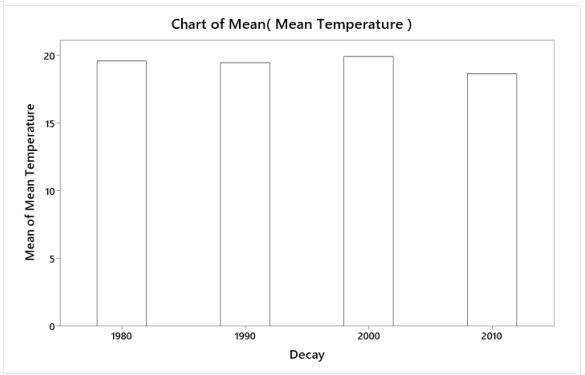
Figure 25: bar graph and boxplot of variables; precipitation, relative humidity and temperature in station 1 during the decades from 1980 to 2010.

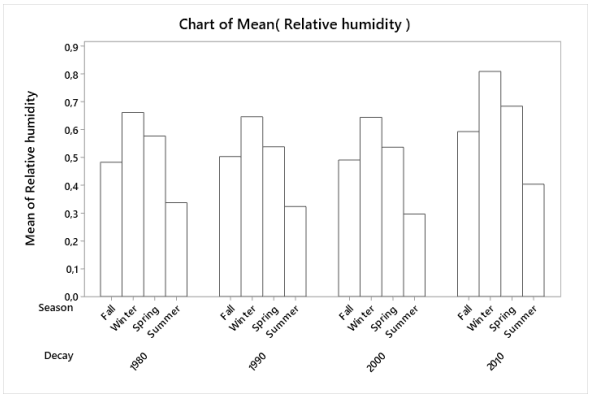
6.1.2. Idriss first station

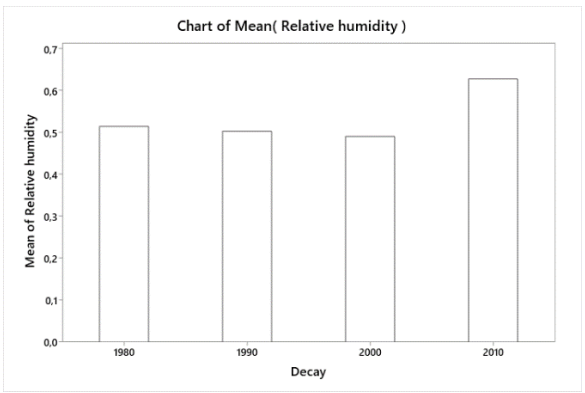


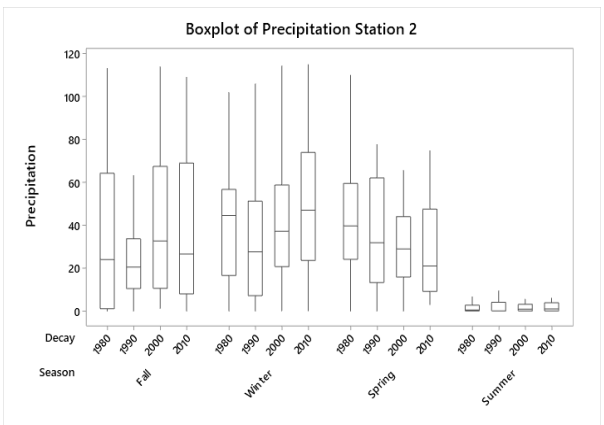


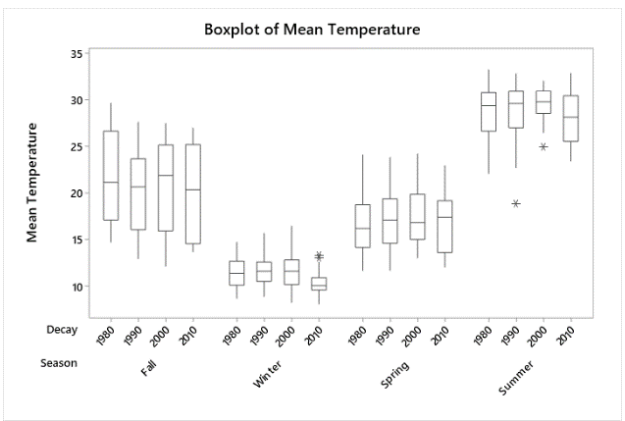












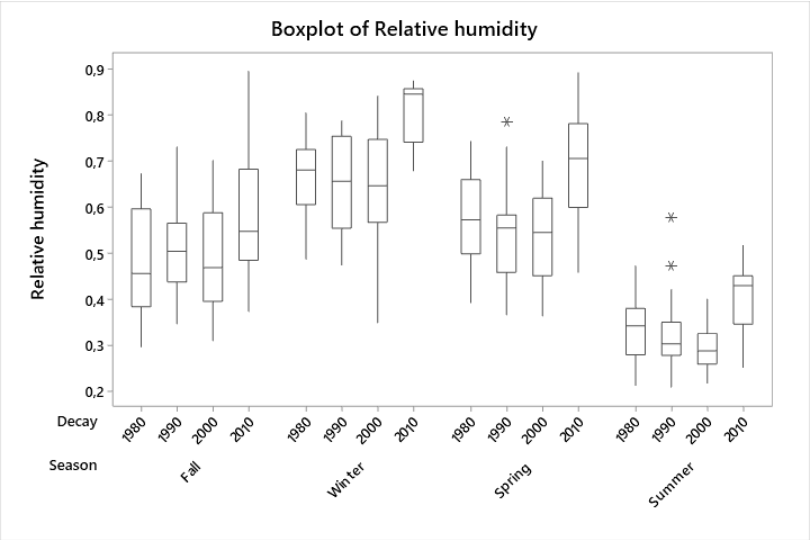
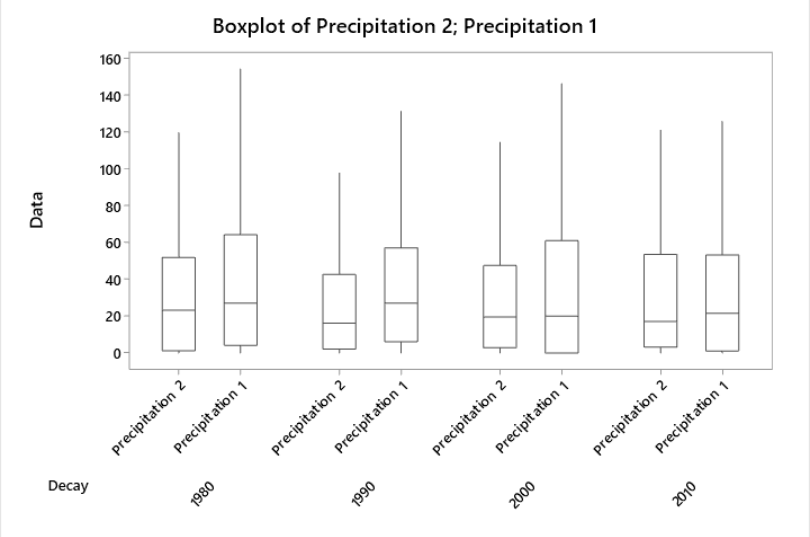


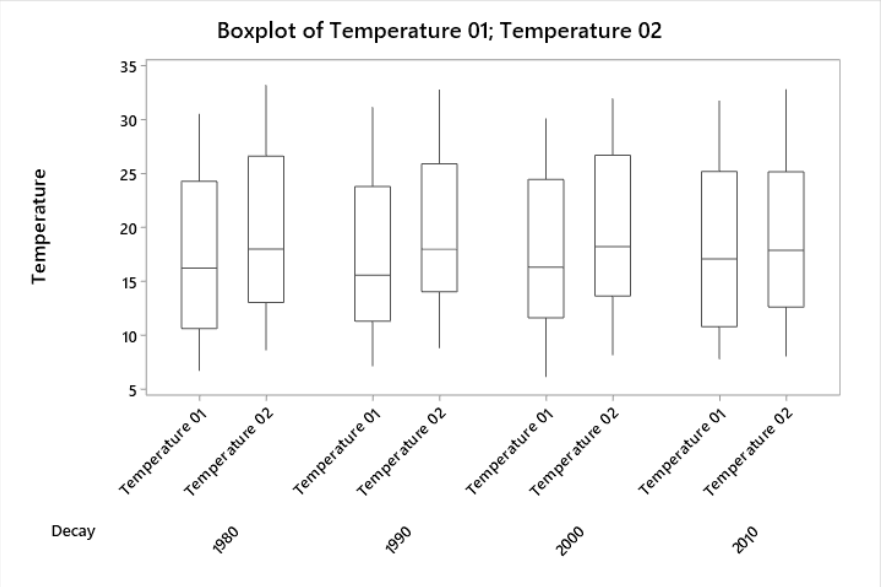
Figure 26: Bar chart and boxplot of variables; precipitation, relative humidity and temperature in station 2 during the decades from 1980 to 2010.

6.2. Spatial variation

6.2.1. Precipitation



6.2.2. Temperature



6.2.3. Relative humidity

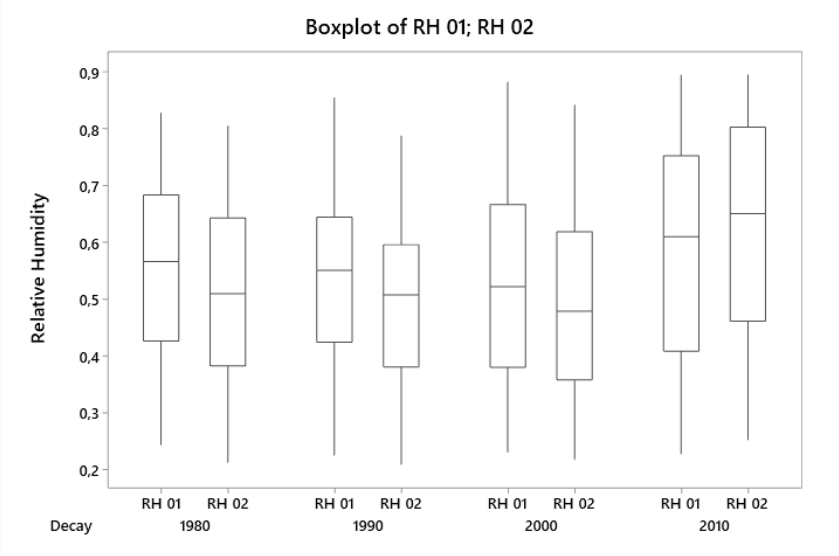


Figure 27: Boxplot of precipitation data for stations 1 and 2 during the 1980-2010 decades.

6.3. Kurtosis test

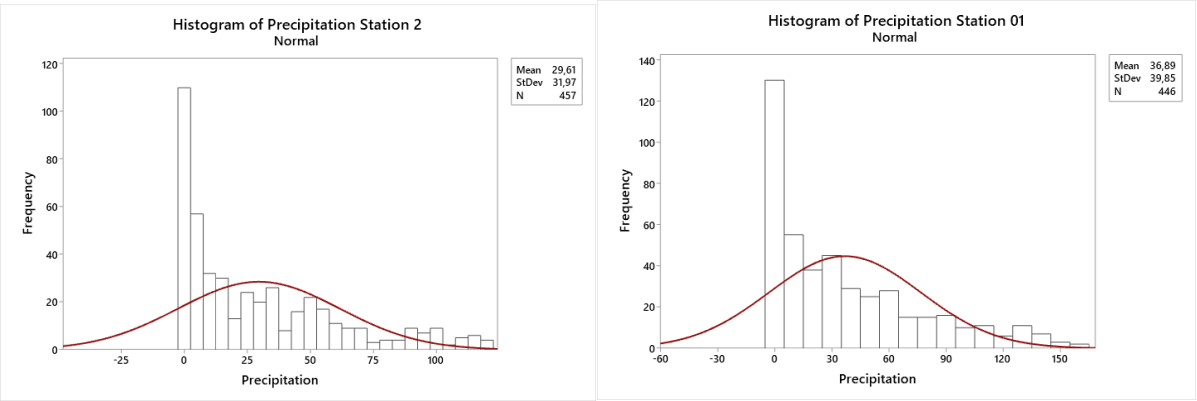


Figure 28: Frequency diagram of a set of data from the Bab Merzouka station and the first Idriss station for the period from 1979 to 2014.

Kurtosis illustrates how the distribution tails differ from the normal distribution. In general, normally distributed data sets the benchmark for kurtosis.

Table 20: Asymmetry and kurtosis coefficient for two stations 1 and 2

Variable	Decade	Skewness	Kurtosis
Precipitation 2	1980	0.95	-0.11
	1990	1.22	0.69
	2000	1.19	0.65
	2010	1.02	0.00
Precipitation 1	1980	0.98	-0.17
	1990	1.13	0.44
	2000	1.23	0.75
	2010	1.12	0.49

Positive kurtosis

A distribution with a positive kurtosis value implies that the distribution has heavier tails than the normal distribution.

Negative kurtosis

A distribution with a negative kurtosis value indicates that the distribution has lighter tails than the normal distribution.

6.4. Description of graphs

6.4.1. Bab Merzouka station

Starting by relative humidity, for the station 01 bab merzouka the mean value is in the order of 0.55% in autumn, 0.7 in winter, 0.59 in spring and around 0.3 in summer, in decades 2010 a slight increase is marked by 0.1 % for spring, the minimum value is recorded in summer and the maximum in winter. The standard deviation benchmark how data are spread to their mean value, the high the value is the bigger the data span, for the relative humidity this value is in the order of 0.006 more or less 0.04 for the whole season, with a slight rise for the last two decades. The variance corresponds to the standard deviation squared, a low variance traduces a high precision and a low marge of defects, its value range in the round of the 0.01, the maximum value corresponds to the fall of the decades 2010.

The median is barely similar to the mean for example for the fall of the 1980 decades it equals 0.53 when the mean takes a value of 0.54, which implies that the data distribution is symmetric.

The temperature has mean values closes to the median with a slight difference of plus or – 2 °C, contrarily to the relative humidity the temperature data has shown a high variance for all the recorded decades, the interquartile interval is high, and the max is recorded in the summer with a value of around 28°C. The large variance could be explained by the error linked to the data generated while the high interquartile is due to the nature of the climate and diurnal cycle.

The precipitation records different value during the four seasons, the maximum value is recorded in the winter, for instance for the decades of 1980 the mean precipitation value during the winter has reached 72.1 mm, and 5.68 in the summer, moving through the year this value increase remarkably, in decades 2000 no precipitation was recorded in the summer, for all the decades the median differ to the mean, In 1980 the mean value of the winter is 73.1mm, and it is greater than the median that takes a value of 49 mm, that implies that the data are asymmetric and 50 % of the values are positioned under the mean, from where the presence of extreme value and outliers. The interquartile interval is high, especially in the winter season.

6.4.2. Idriss first station

Comparing to the first station the second one is characterized by a slight increase in the temperature recorded value, for instance for the decades 1980 the average temperature for fall, spring summer winter are successively 19.6°C,16.26°C, 28.473°C, 9.64°C; versus 18.96°C, 14.85°C, 26.66°C, 9.19°C.

The relative humidity shows a slight variance for the four decades during the four seasons, the lowest value is recorded during the summer, where the humidity is low, also during the summer, the lowest interquartile interval is recorded for example in the summer of the decades 1980 the value is 0.07554, not to mention that during 2010 relative humidity marks a slight increase, the maximum value is recorded during the winter with 0.7754.

As mentioned in the first station the precipitation varies widely from summer to the winter in which the maximum value is recorded the standard deviation and the variance is very high, this could be explained first by the presence of outlier that maybe due to the uncertainties and also the occurrence of an extreme event and sudden precipitation that increase the difference.

The upper graphs show the total average precipitation, average temperature, relative humidity according to four decades; 1980, 1990, 200 and 2010, the lefts graphs, the seasonal variation of the three mentioned variables according to the decades. The graphs have been established for the studied stations.

Station 01

An overall rising trend is noted from 1980 to 1990, during the last four decades the temperature has increased from around 17 °C to 19 °C, the maximum mean is recorded in the summer of decades 2010. The seasonal variation exposes a noticeable variation, the lowest value is recorded during the winter with an average of around 9°C, followed by spring fall and the summer.

The temperature also scores a hike over the decades from an average of 45 mm in 1980 to 65 mm in 1990. The seasonal variation of the precipitation goes contrarily to the temperature, the high value is recorded in the winter where in the summer the precipitation is barely null.

The relative humidity displays a slight rising in the last decades by around 0.05%, the variation goes with the precipitation variation, increase in the winter when high rainfall is recorded and decrease in the summer when the temperature increase.

Sation2

The average temperature records a slight decrease in the decades 201 (around 2°C), contrarily to the rainfall and relative humidity that display in noticeable increase, the intra-seasonal variation goes in concordance with the station 01.

The box plot underlines the dispersion of the dataset, the length of the whiskers measures the outer range from 10 to 25 percentile, and from 75 to 90 percentile, how noticeably different the extremes are. The IQR is small compared to the whiskers, the middle clustering of data about the median represents a large dispersion of the outlie. The study of the skewness shows whether the deflection from the median is negative or positive. In upward skewness, the median is shifted toward the lower position with a wider range of data in the upper quartiles compared to the lower, the opposite shows a downward skewness

The plots display the dispersion of the variables; precipitation, temperature and relative humidity, data in both station bab Merzouka and Idriss First, throughout four decades

For the precipitation data, the upper whiskers are large, for fall, winter, and spring. The data are spanning in the first middle

50% of the total rainfall is varying from 0mm to around 62 mm, the maximum recorded value is in the round of 120 mm, for most of the decades in the four seasons the median is skewed left or right, for example during the winter of the decades 1980 the medial is skewed left which mean that 50% of the precipitation varies between 50 mm and 60 mm, moreover, the fill weights of the plots in the summer is smaller than the rest of the seasons, a large dispersion is also recorded ducting the spring of the decades 2010, the temperature shows a high inter-seasonal variation, during the maximum value are recorded during the summer, in 1980 50% of the temperature vary between 30 and 34 °C, in 2000 the median is barley situated in the middle of the box, less dispersion is marked compared to the fall. Some outlier appears in the winter of 2010, the summer of 1990 and 2000.

The relative humidity varies according to the precipitation rate, most of the ranges have an asymmetric distribution since the median is not in the middle, in the winter of 2010 the relative humidity is too close to the limit of the box, which mean that 50% is close to the value of Q75%, the station 2 marks the same variation trend as the first station with slight variability in the value.

6.4. Spatial variation

The plot underlines the average temperature, the average relative humidity, and the total precipitation for the two stations: bab merzouka and Idriss First throughout four decades.

The Station 2 marks a high value regarding the station 1, the appearance of the boxes shapes is almost similar, in term of fill weight and whiskers length, the difference is noted in the positioning of the values, and the median,

The box dispersion is high, and this indicates that there is a variation in the data set, the median is quietly skewed. For the temperature, most of the value varies between the minimal value (in the order of 6 °C) and the median which vary in the surrounding of 17°C. The relative humidity rises slightly over the decades.

The difference recorded between the two stations could be due to the geographic position, the Idriss First Station where the value of temperature is high and the precipitation and the relative humidity is higher is located near Saiss lowland, the bab merzouka station is in higher altitude.

7. Partial conclusion

This part aimed to develop the general framework of the study. In the first chapter a literature review on the three main features was carried out. The methodology of downscaling for the extraction of hydro-climatic data, hydrological modelling, deficit irrigation and its economic interest.

The second chapter is related to the study area. The Inaouen watershed is a sub-basin of Sebou, limited to the East by the basin of the average Moulouya, to the North-West by the high Ouergha and to the South by that of the high Sebou, it extends over a surface of 3996km2, according to the coefficient of Gravilus the basin is elongated, which will cause a delay of the routing of the water towards the outlet, the relief is very strong. From a geological point of view, two types of formation can be observed: marl and limestone.

The study of the climatic data of the Inaouen reveals that:

The examination of the annual rainfall measurements shows the succession of dry years interspersed with very wet years, the most marked maximum is in 2010, the monthly rainfall is very variable. The rainy season extends from November to April, while the driest months are July and August.

From the temperature analysis, January is the coldest month with an average of 11°C, while August is the warmest. The study of these two parameters shows that the Inaouen basin has a semi-arid climate. The variation of evapotranspiration follows that of precipitation and temperature, the calculation of potential evapotranspiration by the Turkish method and the

Thornthwaite balance gives an average value of 451.68 mm, which is less than the total precipitation of the basin, the excess will contribute to the recharge of underground reserves and in areas with impermeable substratum to direct runoff. The hydrological balance reveals the different paths that water can take, in fact we can distinguish two main phases: a surplus phase where evapotranspiration reaches its minimum, so part of the excess water runs off the surface and part recharge the groundwater, the maximum evapotranspiration is reached in the deficit period, where all the useful reserve is exhausted. The evolution of the flows has allowed us to highlight the spatio-temporal variation of the flow. The runoff coefficient takes a value of 0.3, which can be explained by the presence of marl.

The descriptive statistics support the results obtained by the hydrological study; in fact the basin is characterized by four seasons. According to the kurtosis test the distribution of the precipitation series for both stations is Platykurtic. For the spatial variation of the studied parameters, a slight increase in temperature with a decrease in precipitation and relative humidity is observed moving toward the downstream of the basin.

Part II

Chapter I: Morocco between water security and sustainable development

1. Introduction

From the starting of civilization evolving, water was not only a source of life but also a root of conflict and annihilation, because of extreme flood and drought. Through history, water trigger several wars, back to the World War II, the U.S bombard the North Vietnamese irrigation canals in the 1960s (Jerome 2015), in 1999s, the people protest the privatization of water in Cochabamba, Bolivia (Card 2005), and the disobedience in Cape Town, because of insufficient water supply in 2012s (Jerome 2015). In the other hand, the water excess may destroy humanity, a heavily unexpected rain may cause human and economic damages. For instance, in 1993s the Mississippi River overflew and inundated more than 9.3 million hectares, (Julie Bosman n.d.). According to Munich Re's natural catastrophe database (NatCatService), in Europe during the last 15 years, flash floods and storms have caused economic damages between 1 and 18 billion US dollars per incident. The Elbe and Danube floods in Germany and other parts of Eastern Europe in 2002 and 2013, caused more than 10 billion US dollars of damages (Kottasova et al. n.d.), and according to a recent estimation, the risk of inundation in China is eight times higher than the global average (Feng et al. 2018).

According to the sixth report of intergovernmental panel on climate change (IPCC, 2014), a decrease of up to 20% in rainfall is predicted by the end of this century, and the increase in temperature is expected to reach 2.5 °C to 5.5 °C under the same scenario.

This chapter introduces a broad definition of water security and sustainable development, the interaction between them, in the purpose of providing clear grasping of the concept. The second part is focused on Morocco as one of the countries in development that convoy sustainable development goals. It describes the legal framework of water, the role of the dam's policy and emphasizes the green Morocco plan (PMV). The last section points out the gaps in the cited strategies and provide a recommendation that could be transposable to every country in development.

2. The hydrological framework for water security

Only 2.5% of the total amount of water available of Earth is fresh water, 45 000Km3/year flow annually through the stream effective work to the sea (Oki 2006).

Hydrological cycle assures the conservation of the water stock, the rainfall flows perennial and intermittent rivers, and supply Groundwaters, the part that falls on the overland and vegetation forms the intercepted rain (Perrin et al. 2009), the heat of sun energy, raises the water temperature, breaks the intermolecular links, and transform it into a gas form (Likens 2013).

The spatial distribution of precipitation is up to the geography and climate dynamics, there are regions with high water cyclicity, where extremes flood and droughts evoke risks of inundation and water scarcity.

The flow is the variation of water volume measured in cubic meter through the time, in another term, it is the circulation speed multiplied by the flowing area, this measure is relevant for the estimation of resident time of water molecule in a specific reservoir, by dividing its volume by the mean flux (Oki 2006), in zones unaffected by anthropogenic activities, the residential time in water stream is around two and a half weeks (Institute of Industrial Science, Japan). In contrast, the recharge rate of groundwater is very slow according to the human time scale, the excessive uses lead to the exhausting of the resource (Oki 2006).

Countries located in areas of high climate contrast (unpredictable floods and extensive drought) suffer from water insecurity. Grey and Sadoff (2007) emphasize the relation between hydrologic legacy and poverty rate, the study claims that countries which have an “easy” hydrologic legacy reach water security and have a high economic growth, in contrast, those with “difficult” hydrologic legacy are considered poor. This assumption is supported by Brown & Lall (2006), who claim that high rainfall variability is statistically associated with lower capita incomes.

Certain aquifers or rivers could be shared between two or more countries, the world counts 263 transboundary rivers and 300 transboundary aquifers. For instance, Nile River is shared between Burundi, Central African, Republic, Egypt, Hala’ib triangle, Eritrea, Ethiopia, Kenya, Rwanda, Sudan, Abyei, South Sudan, United Republic of Tanzania, Uganda, Dem, and Republic of the Congo (Ntem and Melvin n.d.). The excessive use, the depletion, the pollution, the growing demand for water supply, imperil these shared resources and cause political and social conflict. 1948 Know 37 warfare about water (Thematic et al. n.d.), in the endeavor of resolving this encompassing issue, 295 international water agreement was signed (UNECE water convention, the legal framework for transboundary water cooperation ..).

3. Water Security

Depending on the context and disciplinary perspectives on water use, the definition of "water security" that first emerged in the 1990s differs (Cook and Bakker 2012), it is a coupled human-water system (Srinivasan et al. 2017) and a concept that provides a common language for all parties and components involved in water management (Arriens 2014), In the framework of UNESCO's International Hydrological Program's (IHP) Strategic Plan, Water Security was globally defined as the capacity of a population to safeguard sustainable access to adequate quantities of acceptable quality water for sustaining livelihoods, human well-being, and socio-economic development, for ensuring protection against water-borne pollution and water-related disasters, and for preserving ecosystems in a climate of peace and political stability(Shrestha S, Aihara Y 2018). This implies that water security is a cycle with the implication of multiple interconnected and interdependent sectors or dimensions (hydrologic, geographic, economic, environmental, social, political, legal, financial…etc.) at local, national, regional, and global scales.

Water security concept is multidimensional, according to Van Beek and Arriens (2016), Falkenmark (2001) in his paper claRify the importance of bridging water security, with food and environmental security, as a major key to reach the sustainable development. Three key ones are to be considered – social equity, environmental sustainability, and economic efficiency (Table 12, Table 13).

Table 21: Economic, Social, Environmental dimension of water security

Economic dimension	**Social dimension**	**Environmental dimension**
• increasing water productivity and conservation in all water-using sectors • sharing economic, social, and environmental benefits in managing transboundary rivers, lakes, and aquifers.	• ensuring equitable access to water services and resources for all through robust policies and legal frameworks at all levels • building resilience in communities in the face of extreme water events through both hard and soft measures.	• managing water sustainably as part of a green economy • restoring ecosystem services in river basins to improve river health

Source: Thematic, Waters et al. (2013)

To assess water security at regional scale so many indexes were developed, some of them can be described in the table below; while these indicators are helpful, they are limited and don't take in consideration a lot of important dimensions.

Table 22: Economic, Social, Environmental dimension of water security

Index	Meaning	Framework	developers
NWSI	the national water security index (NWSI)	a national framework of water security measure applied to compare nations' water security performance in Asia and the Pacific region, The NWSI has five key dimensions: household, economic, urban, and environmental security, and resilience to water-related disaster.	Asian development (ADB, 2016).
WII	water insecurity index	It was applied on a regional scale in India and consisted of six key dimensions: resource, access, consumption, capacity, environment, and climatic stress	Aggarwal, Punhani, and Kher (2014)

The concept of water shortage was quantifying first by Falkenmark in 1989, by developing the water crowding index, using a threshold value of water scarcity level, the critic limit occurs when the index is low to meet people's water needs (<1700 m3 cap−1 yr−1) (Falkenmark et al 1997). The crowding index was the steppingstone of the evolving of water stress indicators, (Raskin et al 1997), (Vörösmarty et al 2000), (Oki et al 2001), and (Alcamo et al 2003) develop other water stress indicator. The critical ratio compares the annual amount of available fresh water to withdrawal water (Alcamo et al 1997, 2000), (Klepper and van Drecht 1998) develop a "water satisfaction ratio', (Douglas et al 2006) worked on the 'relative water stress index". All the above index converges to the same result, water stress is high when the used ration is superior to 0.4.

However, these indicators did not include the interaction between human and ecosystem (Cook and Bakker 2012).

Water resource faces other pressures, such as mismanagement, depletion, population, economic growth, and climate change impact, thus, the evolving of indicators that express better the relation between human-water-ecosystem is crucial for a better grasp and then management (Gain et al. 2016).

(Vörösmarty & al 2010) work on biophysical indicators to assess water security, (Lautze and Manthrithilake 2012) add the human dimension and assess water security in 46 Asian countries, (Gain et al. 2016) figure out the gap in the listed studies by providing the first global-scale assessment of water

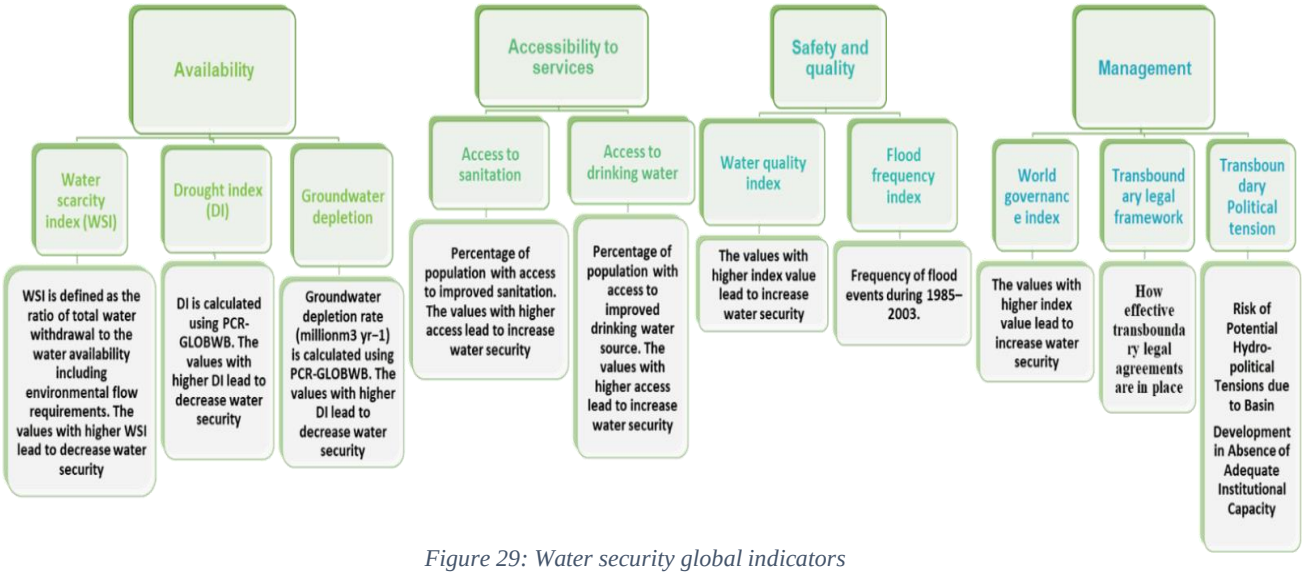


Figure 29: Water security global indicators

Source: Gain et al 2016

security, by the virtue of multi-criteria analysis, the study conceptualizes the security term in 4 majors' part, each one is assessed by specific index (Figure 29) and gather them into one normalized unique index.

4. Sustainable development

The concept of sustainable development was first introduced in 1987 in the Report of the World Commission on Environment and Development called "our common future" as a "development that meets the needs of the present without compromising the ability of future generations to meet their own needs" (UN 1987). Sustainable Development (SD) is usually described as a three-dimension concept; environmental, economic and social (Giddings, Hopwood, & O´Brien, 2002). For a world called "sustainable", this concept must be achieved in all these dimensions.

A sustainable environment can be attained by reserving, improving, and valuing the environment and natural resources in the long term, maintaining the major ecological balances, on the risks and on the environmental impacts. A sustainable society can be maintained if it satisfies human needs and meet a social goal, by encouraging the participation of all social groups in health, housing, consumption, education, employment, culture…. etc., and finally a sustainable economy that aims for a developing growth and economic efficiency through sustainable production and consumption patterns (UN 1987).

In 2000 the United Nations started the first steps by setting 8 original Millennium Development Goals (MDGs) to be achieved by 2015, to eradicate extreme poverty and hunger, achieve universal primary education, promote gender equality and empower women, reduce child mortality, improve maternal health, combat HIV/AIDS, malaria and other diseases, ensure environmental sustainability, and develop a global partnership for development. In September 2015 the Sustainable Development Goals (SDGs) were approved by the 193 UN Member States and are also known as Agenda 2030 (Transforming our World: the 2030 Agenda for Sustainable Development). The framework consists of 17 goals for environmental sustainability, social inclusion, economic development, peace, justice, good governance and partnership, the main issues for the world population in the 21st century. Each goal has several targets that better define its aims. While the MDGs aimed to reduce the existing issues mostly in under/developing countries by half, the new set of goals were set to eliminate them and has all countries as target (Sustainability Science 2018), and according to the agenda are "integrated and indivisible and balance the three dimensions of sustainable development: the economic, social and environmental (UN 2015).

Since water resources are embedded in all forms of development, Water is considered as one of the central focuses of Sustainable Development Goals, as it is at the heart of sustainable development and is critical for socio-economic development, energy and food production, healthy ecosystems and human survival (UN 2018), The UN entirely distinguishes the importance of managing water for sustainable development, and the need for the water and water-using sectors to collaborate and wisely use the world's limited water resources.

The SDG 6 namely sustainable water and sanitation for all, is allocated to water and comprises 11 global indicators, to track the progress.

5. Morocco between water insecurity and management strategies

Morocco is a northwest African country, cover an area of 710,850 km², the agricultural land represents 25 %, 80% of the total surface of the country receive less than 250 mm/year of rain (Africa et al. 2014), 80% evaporated and 0.6% is intercepted or infiltrated, the remained part is used for industry, irrigation and human consumption (AQUASTAT). According to 2017 census, the population is 35 M. The total yield of water is estimated by 22 Md m3 (Africa et al. 2014), world water problems are downscaled on Moroccan scale, the resource is rare especially

in the South and the South-eastern because of arid climate conditions, unequally distributed in space and time, facing a growing demand and climate change impact (Africa et al. 2014).

The historical analysis of the hydrologic series data showed that morocco recorded during the last decencies, more than 20 dry periods (Africa et al. 2014), between 1982-1983 the water deficit in Ziziguir watershed reach minus 80 mm, In 1995 the deficit was almost minus 100 mm in Loukous.

The frequency analysis of the chronologic data point out that the risk of drought is increasing from 5 years in 40 years (1940-1979) to 4 years over 10 (1996-2006) (Africa et al. 2014)

These droughts have a direct impact on water supply and water ued for irrigation, for instance, in Tangier, there was a restriction of nearly 50% between 1993 and 1995, the deficit in the water allocated for irrigation rise from 16% to 90% between 1994-1995 (Africa et al. 2014).

According to the UN Intergovernmental Panel on Climate Change (IPCC), Morocco is a "very vulnerable" country concerning climate change effect, the average temperatures are predicted to increase by 1 to 1,5°, respectively Annual precipitation will decrease (IPCC 2014), In the 2050s, people living in urbanized area will face problem with access to water and food (Global Nexus 2017). The three major sources of water pollution in Morocco are municipal wastewater discharge, industrial effluents, and agricultural activities, urban area generate around 500 m3/year of wastewater, and it may reach 900 m3 in 2020. The high salinity and nitrate concentration affect the underground water, streams are generally contaminated by phosphorus, ammonia, organic matters, and high coliform counts. This polluted water is directly discharged to a natural water body, for example, Sebou watershed which constitutes 29% of Moroccan water resources is heavily polluted by nitrates, phosphorus, and pesticide residues (World Bank group, 2012),

5.1. Morocco and the policy of dams

The water legislation framework in the country starts first with the Islamic laws, which incite rational management and the equitable sharing of the resource. During the French protectorate, the government put all the resources under the government authority, and in 1925, they adopt a law that defines the public ownership of water and defines the conditions of water use for irrigation and other purposes (A. Laamari, M. Boughlala, A. Herzenni n.d.). The independence era marks the green revolution when Morocco oriented the economic growth toward the evolvement of the agricultural sector, by adopting the revolutionary dam's policy. In the1995s the government passed the Water Law of 1995 (Law 10/95), which, integrate and coordinate

the allocation and management of all water sources, also create 6 river basin agencies in order to decentralize water institutional reforms (A. Laamari, M. Boughlala, A. Herzenni n.d.). The law 10-95 of 1995 was promulgated in October 2016 and become 36-15 this later has 12 chapter and 163 articles (Figure 30).

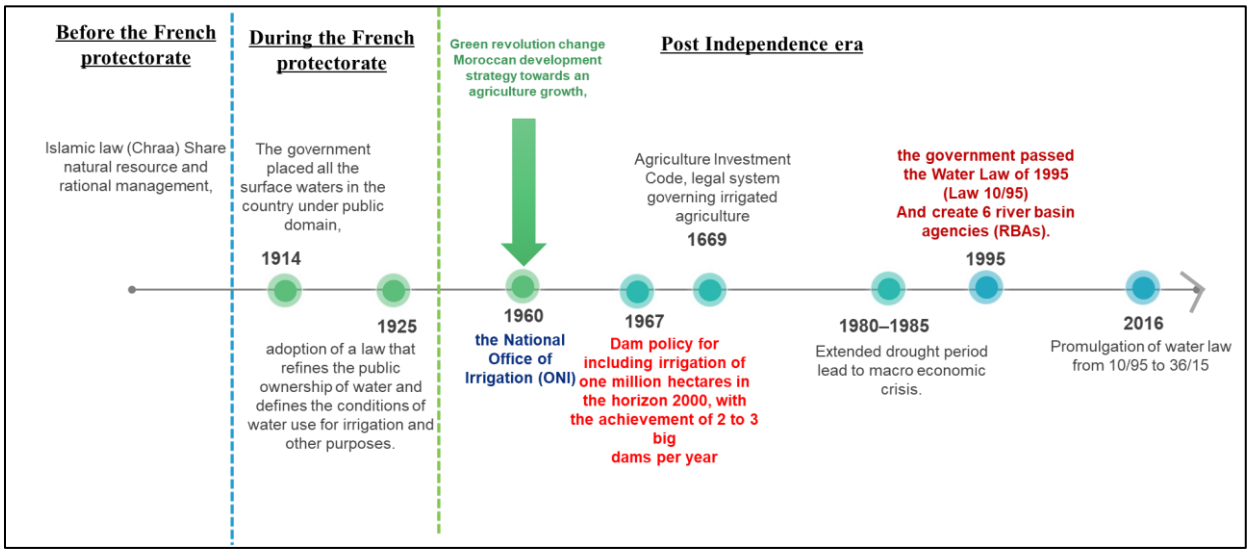


Figure 30: Chronological order of the water law

source: all the information in the scheme are in the following reference (A. Laamari, M. Boughlala, A. Herzenni [sin fecha]) &("Dahir n ° 1-16-113 of 6 kaada 1437 promulgating the law n ° 36-15 relating to water." 2016)

The law 36-15 includes cooperation between users and the public authorities, aims to protect human health through the regulation of exploitation, distribution and sale of drinkable waters, provision for sanctions and the regulation of activities that may pollute water resources (Dahir n°1-16-113 du 6 kaada 1437 portant promulgation de la Loi n°36-15 relative à l'eau. 2016).

In addition to water laws, the policy of dams is one of the most effective and decent management strategies that Morocco adopt, it includes solutions for a set of critical drawbacks, and gives strong support to the economic growth. Now, Morocco counts 140 large dams, with a global capacity higher than milliards cubic meters, 13 are used for water transfer with a capacity of 200m3 /s, length 1100 km and a volume of 2.5 billion m3 / year (El and Directeur 2016).

6. Green Morocco Plan (PMV)

The Green Morocco Plan (PMV) aims to accelerate growth, reduce poverty, and ensure the long-term sustainability of agriculture (Ministry of Agriculture and Maritime Fisheries 2016). The plan has two pillars (Ministry of Agriculture and Maritime Fisheries 2016):

6.1. Pillar I

Aims to develop modern agriculture, market-oriented, with strong competitiveness, develop a new market in the USA, Russia, Asia, and encourage private investment through aggregation. This latter form is based on a double contracting, the aggregators should sign a contract with Morocco and with operators, this strategies mobilize 75 billion dirhams3 of investments over ten years, and benefit 540.000 farmers (Aksebi 2012).

6.2. Pillar II

The objectives The targets of this approach are the elimination of poverty by improving the performance of smallholder farming (around 560,000 farmers), specifically those living in the marginalized area, and this through three social projects (Aksebi 2012);

- Reconversion projects that aim to switch from cereals to higher value products and less sensitive to water deficit, such as olive trees, almond trees, carob trees, cacti…
- Diversification project and augmentation of territory product.
- Intensification project is concentrated on the supervising of farmers and providing the decent to enhance the yield and raise the production rate.

The National Irrigation water saving program (PNEEI) aims to reduce water stress since it is the main limiting factor to the improvement of agricultural productivity. This program consists of conversion to localized irrigation over an area of nearly 550,000 hectares; an average equipment rate of nearly 55,000 ha/year (Ministry of Agriculture and Maritime Fisheries 2016).

In addition to drip irrigation, Morocco adopts other strategies for dealing with water stress issues, for example

- The rainwater harvesting method based on the collection of water rain using different technics (Hasnaoui 2011), this later is legally managed by the decrees number 2-97-224 of 24/10/1997.
- Soil composting help protecting the environment and especially water from the toxic substances impact, improving soil fertility and then agricultural productivity, reduce plant's pelt, the liquid extracted from the composting is used in drip irrigation (LABIDI 2016) and (Azin khalid, INRA d'agadir).

7. Partial conclusions

The water, food, energy, and ecosystems complex are a dynamic system in which there is plenty of interactions. Water is the source of life and energy, which are crucial for food production, the food is the basic element that maintains the ecosystem equilibrium. In contemporary society, energy is used for the water treatment process, groundwater extraction, and food production…

Regarding the environmental problems that the world face, the United Nation define 17 sustainable. Water is included in all forms of development, since it is the central focuses of Sustainable Development Goals, as it is at the heart of sustainable development and is crucial for socio-economic development, energy, and food production, healthy ecosystems and human survival (UN 2018).

Morocco is one of the countries the most threatened by climate change impact (IPCC) and water stress scarcity (Gain et al. 2016). Dam's policy and green morocco plan help the country to overlap issues related to water supply, increase the food security, decrease intern and extern migration, avoid the population centralization in big Cities, reduce social problems such as ignorance and poverty, provide a good life quality, However, it still facing problems, since the stress is still increasing, also the drip irrigation does not assure a strong production growth (Tanouti 2017), (Alonso et al. 2019).

In addition, the pesticide used to eliminate plant pelts help the growth of the agriculture productivity, but in other hand is not aligned with the ecosystem protection notion, the excessive uses of such product, halt the biodiversity and has a harmful sequel on human health, such as the deployment of cancers. The agricultural policy should be oriented toward a biologic production which respects the compromise between human benefice and ecosystems requirement since humankind is a part of the ecosystems and not the Master of It.

Also, Morocco should integrate all dimension of sustainability and combine the economic progress with environment protection, by involving public and semi-public authorities (National office of drinkable water), privates' companies for the elaboration of technical studies, international development institution (World Bank) and the most important invest in the scientific research which help providing advanced tools in terms of water management. For instance, build a national database including all the necessary information about soil, land use and land cover, hydrology…, these data could be introduced in mathematical tools for modeling, the obtaining results serve the decision makers to define the appropriate management

strategies and help ecosystems to build a strong resilience capacity against climate change and natural hazard risks.

Chapter II: Downscaling Global Precipitation Data Using a Machine Learning Algorithm.

1. Introduction

To meet the requirement of precipitation resolution data, many researchers have improved downscaling models. Jia et al., (2011) developed a downscaling model based on the relation between precipitation, Normalized Difference Vegetation Index (NDVI) and elevation, in the Qaidam Basin of Chin. The significant results allow the downscaling of TRMM 3B43 at a fine-scale of 1km using multivariate regression. Fang et al., (2013) improved downscaling accuracy at 1km resolution by the introduction of DEM, humidity, and temperature as environmental factors. Ezzine et al., (2017) enhanced the accuracy of the model based on the Normalized Difference Vegetation Index (NDVI) and Digital Elevation Model (DEM) by adding the distance from the sea to integrate the maritime phenomena. This study enabled to downscale TRMM 3B43 products to a resolution of 1km using stepwise regression. Tsanis et al, (2016) made a great effort to enhance the downscaling accuracy by using a machine learning algorithm based on artificial neural effective works (ANN). This study aims to downscale the TRMM 3B43 product to 1km. Chen et al., (2014) developed a model-based Normalized Difference Vegetation Index (NDVI) and Digital Elevation Model (DEM) based on geographically weighted regression (GWR) to downscale TRMM 3B43 precipitation product at 1km. Similar study was used Normalized Difference Vegetation Index (NDVI) and Digital Elevation Model (DEM) to downscale TRMM 3B43 product at 1 km using a regression model with a residual correction (Zhang & Li, 2018). The downscaling accuracy has been enhanced by (Jing et al, 2017), through developing a model based on Normalized Difference Vegetation Index (NDVI), land surface temperature (LST), and digital elevation model (DEM). This study provides TRRMM product downscaling at 1km using two machine learning algorithms, support vector machine (SVM) and random forests (RF).

This chapter proposes a novel downscaling model, which best accurate precipitation data at a fine scale of 1km. This model is based on Transformed Soil Adjusted Vegetation Index (TSAVI), Digital Elevation Model (DEM), and Distance from the Sea, using a machine learning algorithm.

Precipitation is highly correlated with environmental factors (Jing et al, 2017; Zhang & Li, 2018). The major downscaling models are based mainly on Normalized Difference Vegetation

Index (NDVI) due to its capacity to better accurate precipitation data (Wang et al., 2003.). Indeed, precipitation is a fundamental component of the hydrological cycle. Therefore, precipitation is a limiting factor of soil moisture and vegetation growth. Soil moisture is considered as a significant node that relates precipitation and NDVI (Wang et al., 2003.). In some extent, many studies have demonstrated that NDVI performs a good correlation with precipitation (Chen et al., 2014; l. Duan et al., 2017; Jia et al., 2011; J. Liu et al., 2018; Jing et al, 2017; Y. Zhang & li, 2018). However, NDVI values are influenced by soil (Baret et al., 1991.; Rondeaux et al., 1996).

Soil brightness induces noise into red and near-infrared bands (Rondeaux et al., 1996). Indeed, red and near-infrared are linearly correlated in a way that the intercept and the slope depending on the soil types (Rondeaux et al., 1996). Furthermore, the soil is properties are characterized by its inorganic solids, organic matter, and soil moisture (Rondeaux et al., 1996). The development of remote sensing provides a proper assessment of soil properties dues to its reflectance in the visible and near-infrared spectra (Rondeaux et al., 1996). Therefore, soil line parameters influence the vegetation information in visible and near-infrared bands (Baret et al., 1996; Rondeaux et al., 1996). To sort-out, the soil line parameters the extracting the bottom in red and near-infrared bands is essential. In this context, the Transformed Soil Adjusted Vegetation Index as an improved vegetation index was developed to overcome soil background effects (Baret et al., 1996).

This study aims to improve downscaling models by reducing soil brightness noise by using the Transformed Soil Adjusted Vegetation Index. In this sense, TSAVI, DEM, and distance from the sea were considered as a predictor for desegregating precipitation, using stepwise regression, AIC, and Cp criterion, to evaluate the model error and performance The MSE, MAE, RMSE, and R-Square statistical metrics are used.

2. Methodology

2.1. Study zone

This study was conducted in Morocco (Figure 1). Morocco is in northwestern Africa, between [1.5° -17°] W longitudes and [20.5°-36°] N latitudes. The Kingdom is bathed in the North by the Mediterranean Sea, in the West by the Atlantic Ocean (Ezzine et al., 2017). The country is bordered to the east by Algeria, and to the south and south-east by Mauritania. Morocco covers an area of 710,850 km², included fourteen watersheds, with 25 % of agricultural land (Moumen et al., 2019). Besides, Morocco is surmounted in the West by the Atlas Mountains, in the North

by the Rif, and in the south by a large Sahara. The climate ranges from the Humid to Saharan bioclimatic stage (Ezzine et al., 2017). Furthermore, Morocco is a highly water-stressed country with erratic rainfall and frequent droughts(Africa et al., 2014). Indeed, Morocco receives an amount of rainfall ranging from 100mm to 1200 mm, with an evaporation rate of 80% and an interception rate of 0.6% (Schilling et al., 2020)

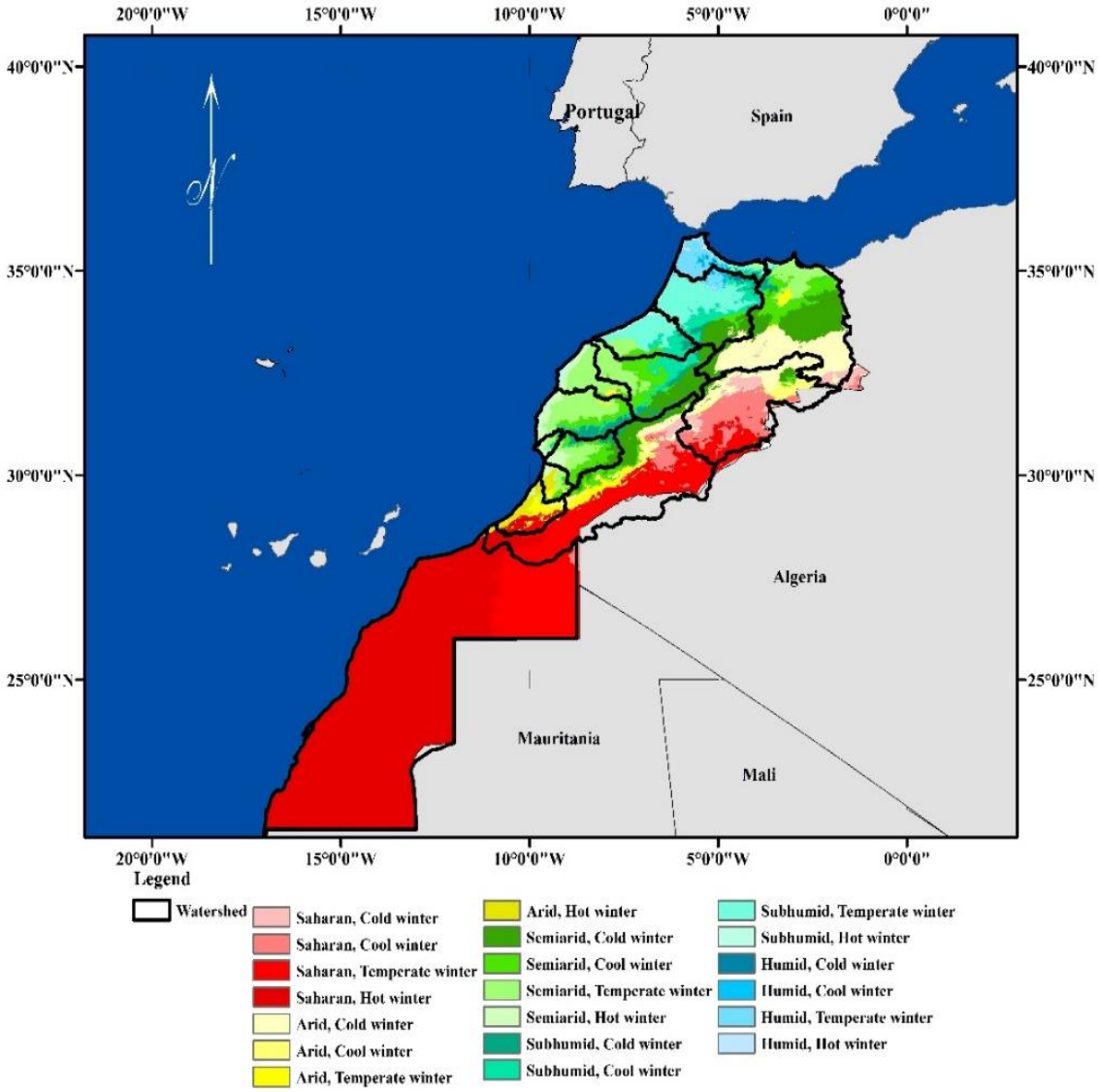


Figure 31: Map of Moroccan sub-basins and bioclimatic stages

2.2. Collection of data

2.2.1. Precipitation data from satellite sensor

The TRMM 3B43 Version 7 is used as precipitation data with a spatial resolution of 0.25 ° × 0.25 °. Over a period of 1999 to 2014.

The bioclimatic map of Morocco was generated using the Emberger quotient (Condés & García-Robredo, 2012; Mokhtari et al., 2013). The latter is calculated using precipitation and

temperature data for a period from 1970 to 2000. The meteorological data has been freely extracted from the worldclim portalhttp://worldclim.org/

Equation 1: Emberger's quotient formula

$$Q = \frac{2000 \times P}{(M + m + 546.4) \times (M - m)} \quad (8)$$

Where: P Annual precipitation (mm), M: Average maxima of the hottest month, m: Average minima of the coldest month

2.2.2. Hydro climatic data

The monthly rainfall data were obtained from the gauge rainfall stations over a 12-year period (1999-2012).

2.2.3. GIS data

- The digital elevation model (DEM) is derived from the Shuttle Radar Topography Mission (SRTM), version 4.1, with a spatial resolution of 30 m. DEM data are available on the portal http://srtm.csi.cgiar.org/.
- Remote sensing images were extracted from the latest generation of the Landsat 8 (OLI) satellite (Mancino et al., 2020). Landsat 8 (OLI) is the 9 Operational Land Imager (OLI) and Thermal Infrared Sensor (TIRS), this satellite sensor is composed from nine bands: band four is red and band five is near infrared (https: // www. usgs.gov/).
- Landsat 8 imagery is used in the Mediterranean region when it comes to providing vegetation indices (Mancino et al., 2020). In addition, Landsat images are available free of charge on the portal https://earthexplorer.usgs.gov/, with a spatial resolution of 30 m. Landsat 8 images from 2010 to 2019 were used in this study to recover bare soil lines and the Adjusted Vegetation Index of Transformed Soil (TSAVI). The rasters for the period 2010-2019 concern the months of May, June, July and August.
- The distance to sea map has been generated referring to the Atlantic and the Mediterranean coastline.

Table 23: Data sets

	Characteristics		
Data	Period	Spatial resolution	Temporary resolution
TRMM 3B43	1999–2012	0.25 °	Monthly
Landsat 8 (OLI)	2010-2019	30 m	-
Hydroclimatic data	1999–2012	1 km	Monthly
DEM (SRTM V4.1)	2008	90 m	-
Distance from sea	2019	1 km	-
Bioclimatic map	2019	1 km	-

2.3. Method

The methodology adopted aims to build a robust model able to best downscale precipitation data using machine learning. The diagram below presents a schematic illustration of the structure and the working of the downscaling model.

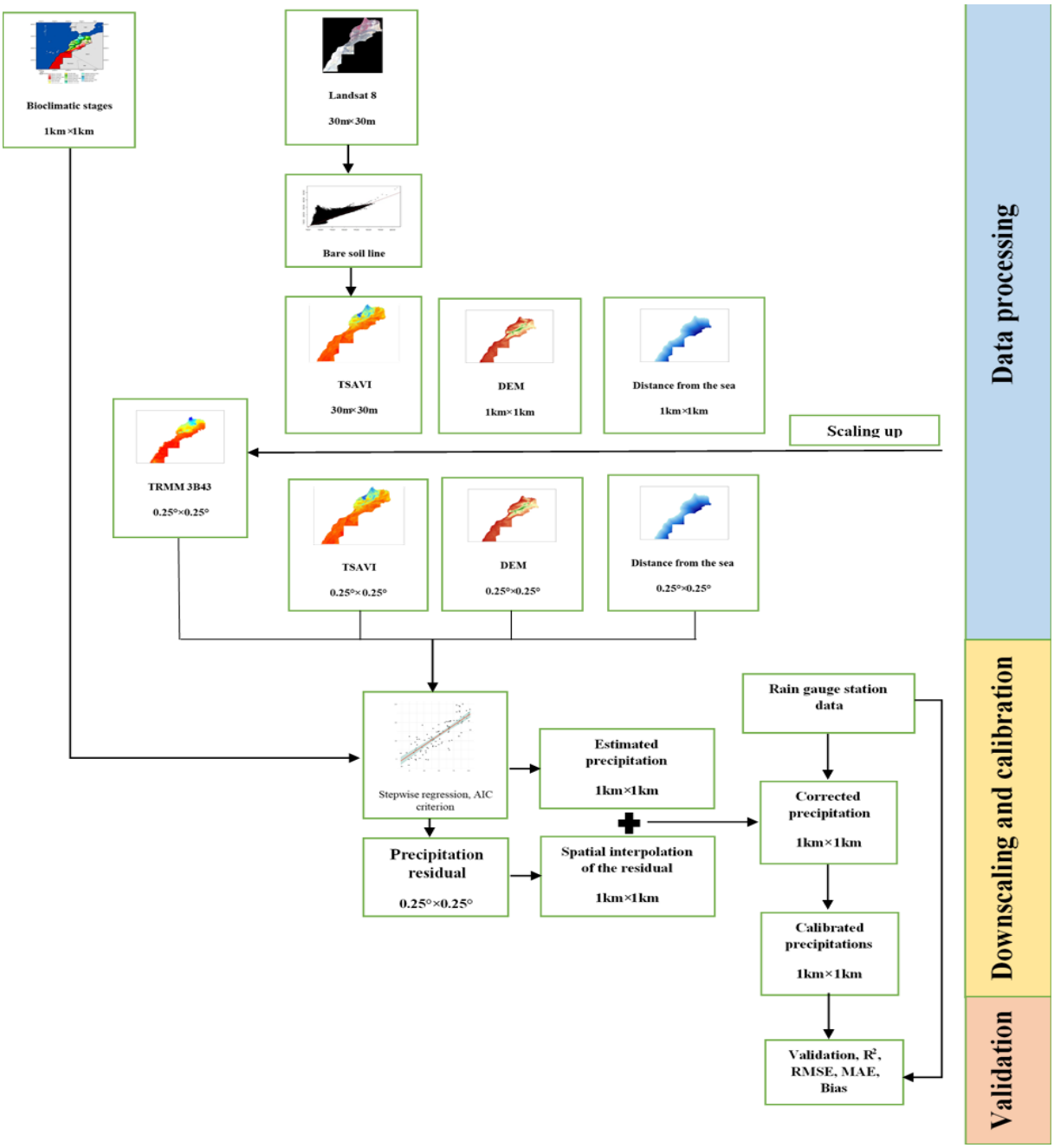


Figure 32: General methodology of the downscaling algorithm

2.3.1. Data preparation

The first step is to calculate the annual precipitation, from the monthly rainfall data TRMM 3B43 over the period 1999-2012. Then, the annual precipitation will be increased to a spatial resolution of 0.25 ° × 0.25 °. In addition, the distance to sea and DEM will also be scaled up to a spatial resolution of 0.25 ° × 0.25 °.

2.3.2. Generation of the adjusted vegetation index of the transformed soil

The TSAVI index is generated from the processing of Landsat 8 images. This step requires the integration of many tools and methods dealing with big data. The reassembly of the images was done via the GIs, in addition to the statistical process via the R software

2.2.3.1. Bare ground line:

Thanks to the development of data science, quantile regression performs better than least squares regression, which has been widely used as a statistical method. Indeed, least squares regression is a parametric model based on assumptions; however, the quantile regression does not form any hypothesis between the distributions of the residuals (Foulds, 1984; Koenker et al., 2007). Quantile regression is effective at extracting lines in two-dimensional scatter plots (Mills et al., 2006; Mills et al., 2009; Xu and Guo, 2013)

In this sense, quantile regression is used to recover the bare soil line. The method was coded in R software and is available in a software package called a quantile raster, which can be downloaded from the R Archive Effective work (CRAN) mirror athttp://www.r-project.org/.

To perform the quantile regression, the tau quantile is set to 0.00001 in order to extract the soil line of variation in the near infrared (NIR) scatter plots versus red. Let us vary the tau step by step, to extract the best effective result with the minimum p-value and the maximum t-value (Ahmadian et al., 2016; Xu & Guo, 2013).

$$\frac{the\ number\ of\ \ points\ below\ or\ on\ the\ bottom\ line}{the\ total\ number\ of\ \ points} \quad (9)$$

The process is applied to 14 watersheds in Morocco

2.2.4. The generation of TSAVI

According to the algorithm presented in the table, the adjusted vegetation index of the transformed soil is generated for the fourteen watersheds of Morocco.

Table 24: The formula for calculating the TSAVI

Vegetation Index	Algorithm	Description	Quote
TSAVI	$\frac{a \times (NIR - a \times RED - b)}{RED + a \times NIR - a \times b + X \times (1 + a^2)}$	a = slope of the Soil Line, b = intercept of the SL, X = 0.08	(Baret and Guyot 1991; Rondeaux, Steven and Baret 1996)

2.2.5. Correlation between products TRMM 3B43 and TSAVI

Least squares regression is used to assess the correlation between the annual precipitation of the product TRMM 3B43 as the dependent variable and TSAVI as the independent variable, over the period 1999-2004. The performance of the correlation is veRified on the basis of R^2.

2.2.6. Correlation between TRMM 3B43 and predictors using machine learning

Machine learning techniques are an important method widely used among data scientists. There are two types of machine learning techniques: supervised and unsupervised learning. In this study, we will apply supervised learning, namely regression. The downscaling model is performed using a stepwise regression based on the Akaike Information Criterion (AIC) and Mallows Cp.

Stepwise regression is a multiple regression method aimed at identifying the best predictors of the fit model. This method attempts to optimize the choice of explanatory variables that predict the dependent variable. The choice of the best explanatory variables is based on various criteria such as F-tests, t-tests, the adjusted R-square, the Akaike information criterion, the Bayesian information criterion and the Mallows Cp indicator (Ormann et al. ., 2018). This criterion seeks to identify a set of independent variables which explains the dependent variable in a significant way (Ormann et al., 2018).

Stepwise regression involves forward and backward selection. On the one hand, the forward selection consists in introducing the variables one by one and keeping the most significant ones with the lowest p-value, until the result is optimal, on the other hand the selection towards the rear is to define all the explanatory variables that are not statistically significant, with the least p-value and reject it thereafter. The stepwise regression aims to best fit a linear regression between the dependent and independent variables, according to the following equation:

$$y = a_0 + a_1 x_1 + a_2 x_2 + ... + a_p x_p + \varepsilon \quad \textbf{(10)}$$

Or: y is a dependent variable, $x_{1 \le j \le p}$: are the independent variables, $a_{1 \le j \le p}$ are the parameters to be estimated, and ε is the intersection or the residue.

To improve model selection in stepwise regression, Akaike's information criterion and Mallows' Cp used in the weighted likelihood methodology for model selection (Agostinelli et al., 2002).

The AIC equation is:

$$AIC = -2 \times \ln(L) + 2 \times k \quad \textbf{(11)}$$

Where: L is the likelihood value and K is the number of estimated parameters.

On the other hand, Mallows's Cp (Taylor & Mallows, 2012) seeks to assess the precision and bias of predictors. They are considered unbiased and accurate estimators of predictors that have a small value close to the number of predictors. (Agostinelli et al., 2002; Lance et al., 2014)

$$C_p = \frac{RSS_p}{MSE_k} + 2 \times p - n \quad \textbf{(12)}$$

Or: RSS_p is the residual sum of squares for the p-variable, MSE_k is the root mean square error for the k-variable, and n is the sample size

The stepwise regression with the AIC and Cp criteria of Mallows was carried out over the period 1999-2004 to identify the best model, after the model is generalized to the entire study period (1999-2014).

2.4. Calibration and validation of precipitation

The group model identified using stepwise regression, were used to downscale precipitation data, with a residual correction. First, we estimate precipitation at a spatial resolution of 0.25°×0.25°. Then we estimate the residual component by generating the difference between the original TRMM 3B43 data and the estimated precipitation. After that, the residual component was downscaled at a spatial resolution of 1km using spatial interpolation. Downscaling precipitation was conducted by using the regression model variables at 1km, which were corrected by adding the residual component.

The calibration of the downscaled data was carried out by using the Geographical Differential Analysis(GDA) calibration method developed by Jehanzeb & Cheema, (2012). GDA method consists of minimizing the difference between the TRMM 3B43 precipitation products and the in-situ rain gauge measurements. Over the period 1999-2014, and for every station gauge, the difference between downscaled precipitation and in situ measurement was generated. Second, the difference was interpolated based on the Distance Weighting algorithm. Finally, we add the geographical difference to the downscaled precipitation at a spatial resolution of 1vkm.

3. Partial conclusion

The objective of this chapter was to describe the methodology approached for the development of the downscaling model. The approach was applied to TRMM 3D43 precipitation data with a spatial resolution of 0.25 ° X 0.254 ° over a period of 1999-2014. The hydro-climatic data used for the calibration are provided by the agencies of the hydraulic basin. The methodology consists in calculating the average annual precipitation from the precipitation data then increasing the spatial resolution, the distance from the input to the sea was calculated from the digital model of the terrain, the adjusted vegetation index (TSAVI) is calculated from the near infrared and red bands of the Landsat8 satellite image, the bare soil lines are extracted from the near infrared versus red scattering diagrams. These parameters were correlated with the TRMM 3D43 precipitation by stepwise regression. The residue generated and subsequently add to the raw rainfall data to correct them.

Chapter III: Hydrological modeling

Test the capacity of the SWAT model to simulate the hydrological behavior of a watershed in a semi-arid climate context; Case study (upstream of Inaouen, Morocco)

1. Introduction

Even if the Inaouene watershed has significant water potential in the eastern part of Morocco, due to its geomorphological location and its karst reservoir, the basin faces a set of problems related to water quality and quantity.

In recent decades devastating floods caused extensive human and material damage, in 1973 a hydroelectric reservoir was built to manage water and mitigate flooding. However, the area still suffers from several problems, which relate to its socio-economic development.

On the other hand, the tributaries of the Inaouen river are exposed to wastewater and marginal discharges. The consequences of such actions are not only limited to the level of the river, they spread and can affect the groundwater, the reservoir (which is mainly used for irrigation), the neighboring area, and on the sanitary and environmental ground.

In addition, the basin has not escaped the impact of global climate change, this current semi-arid climate which has two major phases; dry and wet, the hydrological cycle does not therefore ensure a complete renewal of the water since evaporation and evapotranspiration are limiting factors.

From the perspective of water resources management, this work comes within the framework of hydrological simulation using the SWAT model.

2. The SWAT model

SWAT is a basin-scale continuous-time model that operates on a daily time step and is designed to predict the impact of agriculture on yields of water, sediment, and agricultural chemicals, in basins ungauged slopes. The main components of the model include, hydrology, and soil properties, plant growth, nutrients, pesticides, bacteria and pathogens, and land management, climate data (Gassman et al., 2007). The watershed is divided, on a topographical basis, into spatially related sub-basins and the latter is separated into Unique Hydrologic Response Units (HRUs), incorporating the combination of land cover, soil type and slope. To describe the

physical heterogeneity of the system. The modeled hydrologic components include surface runoff, percolation, lateral flow, groundwater flow, evapotranspiration (ET) and transmission losses. Watershed hydrology simulation with SWAT is divided into land phase and hydrologic cycle routing phase, which controls the amount of water, sediment and nutrients in the main channel of each sub-basin and across. the channel effective works. SWAT estimates the water balance using this formula: Watershed hydrology with SWAT is divided into the land phase and the routing phase of the hydrologic cycle, which controls the amount of water, sediment and nutrients in the main channel of each sub-basin and through the channel effective work. SWAT estimates the water balance using this formula: Watershed hydrology with SWAT is divided into the land phase and the routing phase of the hydrologic cycle, which controls the amount of water, sediment and nutrients in the main channel of each sub-basin and through the channel effective work. SWAT estimates the water balance using this formula:

$$\boldsymbol{SW_t = SW_0 + \sum_{i=1}^{t}(R_i - Q_i - ET_i - P_i - QR_i)} \quad \textbf{(13)}$$

Where SWt is the water content of the soil, SW0 the initial water content of the soil i is the time in days for the simulation period t, and R, Q, ET, P and QR are respectively the daily precipitation, runoff, evapotranspiration, percolation, and return (Neitsch et al. 2011).

Water enters the system as precipitation. The water balance of each HRU in the watershed contains four storage volumes: snow, soil profile (0-2 m), shallow aquifer (2-20 m) and deep aquifer (> 20 m) . The soil profile can contain several layers. Soil-water processes include infiltration, percolation, evaporation, uptake by plants, and lateral flow. Surface runoff is estimated using the SCS curve number or the Green-Ampt infiltration equation. Percolation is modeled with a layered storage routing technique combined with a crack flow model. Potential evaporation can be calculated using Hargreaves' method,

2.1. Spatial discretization of the SWAT model

SWAT uses the D8 algorithm of Jenson and Domingue (1988) for the automatic delimitation of watersheds from the digital elevation model (DEM), the delimitation steps are the same as those used in Arc hydro and HEC GEO HMS; (i) filling of low points, (ii) slope estimation, (iii) determination of flow directions and flow accumulation, (iv) creation of flow matrix, (iv) effective work extraction river.

It is mandatory to choose the threshold number (As) for the initiation of a branch of the hydrographic effective work in order to optimize the number of sub-basins that will be identified in the following steps, the lower this number, the more the hydrographic effective

work. is detailed. The choice depends on the degree of detail sought, a study by Tripathi et al. (2006) highlight significant variations in the simulations of evapotranspiration, percolation and soil water content when the watershed discretization scheme is refined.

To delimit the watershed, it is mandatory to identify the location of the outlet. Algorithm D8 then proceeds from upstream to downstream, including the cells which converge towards the outlet according to the flow direction matrix.

Previous studies have been carried out on the variability of geomorphological properties and highlight the issue of detailed representation and its impact on the end result of the study. Several parameters have an important influence; climatology, geology, pedology land use / land cover distribution and geomorphometric parameters of the watershed (Chaplot 2005; Di Luzio et al. 2005; Hancock 2005; Shrestha et al. 2006; Yair and Raz-Yassif 2004). Then a good DEM resolution is necessary for best results.

The characterization of land use by the SWAT model consists first of all in dividing the land use into different classes, for example, water, forest, bare land, urban areas…., this classification after is matched with the SWAT classification database.

The soil identification is set up using the same steps used for land use, each soil type must be coordinated with the user table in the SWAT database. It is also necessary to define the physical and chemical characteristics of the soil type units, to process the dynamic analysis of the model. According to the Soil Survey Staff, 2001, the general properties of the soil control the amount of water runoff.

The hydrologic model combines the information from the three components noted in what are called the hydrologic response units HRU, each unit is a unique combination between a soil type / Land cover / and slope. This compilation has a unique hydrological behavior with respect to the amount of rain received.

2.2. The hydrological components of the SWAT models

Usually, a model is a simplified representation of a system, using mathematical equations that later differ depending on the scope of the study and the level of detail perceived by the modeler.

In hydrology the models are the representation of the hydrological cycle, and all the processes of interactions between the components evolved in the cycle (earth, atmosphere, groundwater, land cover, etc.), this part presents a description of the different hydrological modules.

represented by SWAT, they rely on the use of equations to simulate hydrologic behavior at the level of each HRU hydrologic response unit.

Figure 33 shows the different components of the hydrological cycle as simulated by the SWAT model, the system is generally divided into major parts; atmospheric components where the process of evaporation and evapotranspiration reproduces, terrestrial component which includes runoff, lateral flow, interception, and subterranean component which groups infiltration, gravity movements of water and percolation.

2.2.1. Atmospheric part :

The estimate of the actual evapotranspiration by the model is based on the calculation of the potential evapotranspiration, the latter as indicated previously in the calculations made. The calculation methods are those proposed by; Taylor, Hargreaves, Penman-Monteith. SWAT adopts the latter's method to estimate ETP, the latter relates the inverse of the latent heat of evaporation of water to the ratio of the slope of the vapor pressure curve to air temperature and the constant which connects absolute humidity and maximum humidity

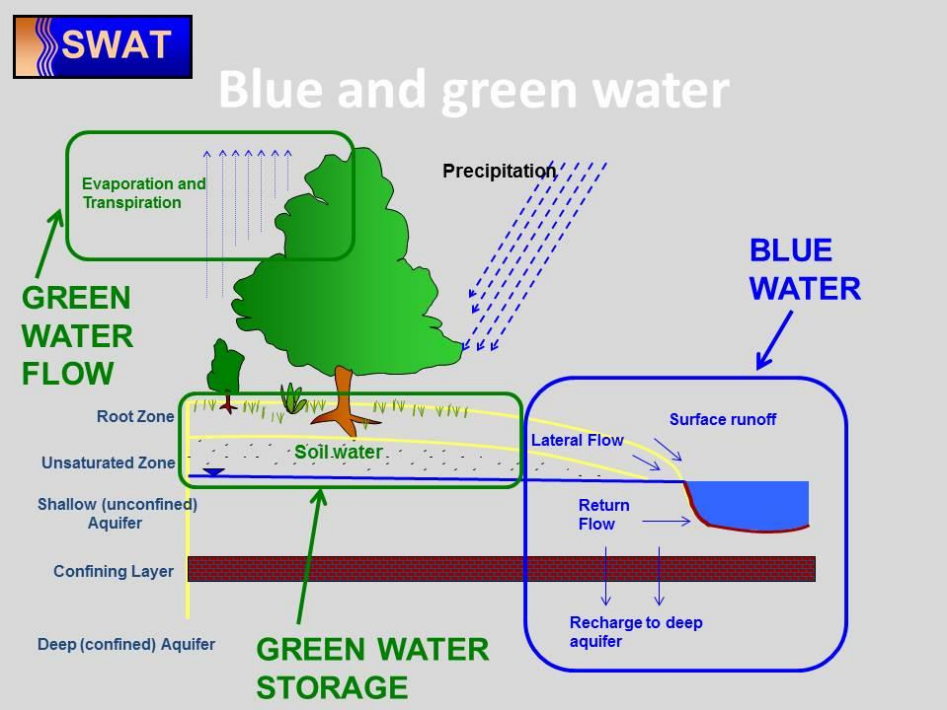


Figure 33:Representation of the hydrological model in the SWAT model

Source: Neitsch & al., 2011

with the difference between the wet bulb temperature and the adiabatic saturation temperature. The whole is multiplied by a set of parameters in the following formula[2]:

$$E_0 = \frac{\Delta \times (R_n - G) + \rho_a C_p \frac{(e_w - e)}{r_a}}{\Delta + \gamma(\frac{r_s}{r_a} + 1)} \quad (14)$$

- Rn: effective radiation
- G: heat flux from the ground
- ρ a: average air density
- cp: specific heat of air
- λ: latent heat of change of state (2450 kJ.kg-1)
- e: vapor pressure at temperature t
- ew: saturated vapor pressure at temperature t
- Δ: the slope of the saturated vapor pressure curve
- ra: aerodynamic resistance
- rs: the resistance of the plant cover
- γ: the psychrometric constant

To do this it is necessary to have the daily temperature and solar radiation data, in the calculation process the model eliminates the evaporation of the water intercepted by the canopy to estimate the transpiration, then adds it to the water. evaporated from the ground.

2.2.2. Land part

The diagram of this component is carried out by the mass preservation equation of the water balance already mentioned at the beginning of the chapter.

2.2.2.1. Interception

Intercepted water means any water stored and trapped in the visible part in the branches of plants or otherwise called the canopy, this quantity of water presents a reserve not to be neglected of water, which contributes to the hydrological cycle in the form of rain intercepted after the end of the rain event. This parameter is directly linked to the density and the phenology of the plant cover, which is dependent on the leaf area index or Leaf Area Index (LAI, m2 m -2), the latter is an important indicator of the exchanges of energy, water and carbon between vegetation and atmosphere, it can be estimated by remote sensing techniques, a study by (Peter

[2] The demonstration and the reference of the formula are met in detail in the chapter DJIKOU, SM, 2006. Calculation of the PENMAN- MONTEITH ETP at different time steps on four sites of the Upper Ouémé Basin.

J. Olsoy & al., 2016), uses a technique of terrestrial laser scanning TLS to estimate this index, which can also be calibrated.

2.2.2.2. Runoff

For the estimation of runoff, the most used method and which was also adopted by this study is the method of Soil conservation service SCS curve number, which makes it possible to determine the quantity of water runoff as a function of the content of water retained by the soil, the latter therefore depends on pedology and land use / plant cover at the same time. The Curve number method was initiated by the soil conservation service in 1964 in the United States, this method was developed and subsequently adapted to other regions of the world.

The runoff has three parts;

- Hortonian runoff: which takes place when the intensity of precipitation exceeds the gravitational force and therefore the infiltration capacity
- Runoff due to soil saturation; The excess water that flows after saturation of the soil and groundwater
- Flows due to the emptying of underground water tables refers to the water that returns to the surface water by the resurgence of water tables

Chow & al ,. 1962 in his book Handbook of Hydrrology, indicates that the Curve Number method is based on two major phenomena identified from the analysis of the IDF Intensity-Duration-Frequency curves. The curves generally take the form of a straight line, the initial accumulation of rain represents the intercepted part, the filling of depressions, all this is represented by the parameter called the initial abstraction, during the rain event, the losses continue in the form of infiltration; it is the current retention, after the end of the precipitations, with the increase of the rains the current retention reaches its maximum, value represented by maximum potential retention.(Chow 1964)

The empirical formula of the SCS-CN model assumes that the ratio between actual retention and maximum potential retention is equal to the ratio between actual runoff and maximum potential runoff, the latter is derived from the difference between precipitation and the initial abstraction:

$$\frac{R}{S} = \frac{Q}{P - I_a} \quad (15)$$

Or;

R = actual retention (mm)

S = potential maximum retention (mm)

Q = accumulated runoff depth (mm)

P = Accumulated rain (mm)

Ia = Initial abstraction (mm)

On the other hand the real retention corresponds to the subtraction of the initial abstract, and of the cumulative runoff from the total of the cumulative precipitation

$$\boldsymbol{R = P - Ia - Q \ (16)}$$

By replacing the term R will have the expression of direct runoff as the following;

$$\boldsymbol{Q = \frac{(P - Ia)^2}{(P - I_a) + S} \ (17)}$$

In 1972 the soil conservation service developed a regression analysis on rainfall and runoff data on a set of small watersheds, with the aim of determining the relationship between the initial abstract and the maximum potential retention as shown in the following figure;

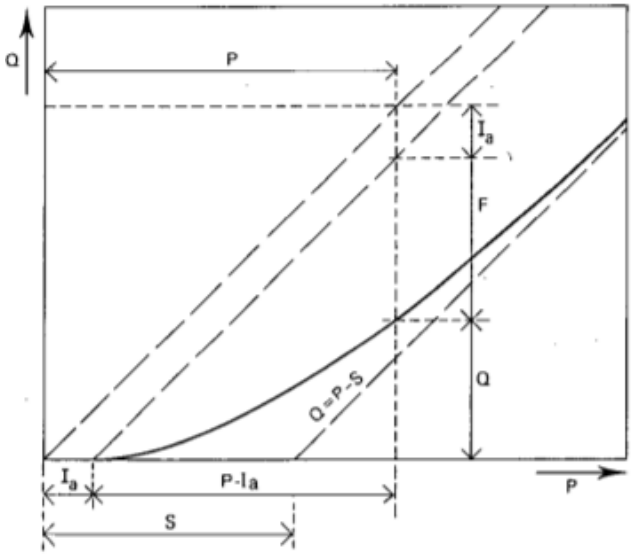


Figure 34: Cumulative runoff curve as a function of cumulative precipitation

Source: Soil Conservation Service, 1972

The results of the study provide an expression of Ia as a function of S like the following, (18)

$$\boldsymbol{Ia = 0.2S}$$

Based on the SCS-CN method, runoff is estimated as a function of precipitation, if the value of the maximum potential retention is available, this value represents the infiltration that takes place after the onset of runoff, and which is controlled by a set of parameters linked to the type

of soil and the nature of the plant cover and land use as well. It is expressed in terms of the Curve Number as follows:

$$CN = \frac{25400}{254+S} \textbf{(19)}$$

The solution of the equation is represented by the following curve (Figure 35), the number of the curve ranges from 0 to 100, since the maximum potential retention is inversely proportional to the number of the curve CN, when S is zero the CN reaches its maximum value 100, runoff matters over infiltration, the reverse is true.

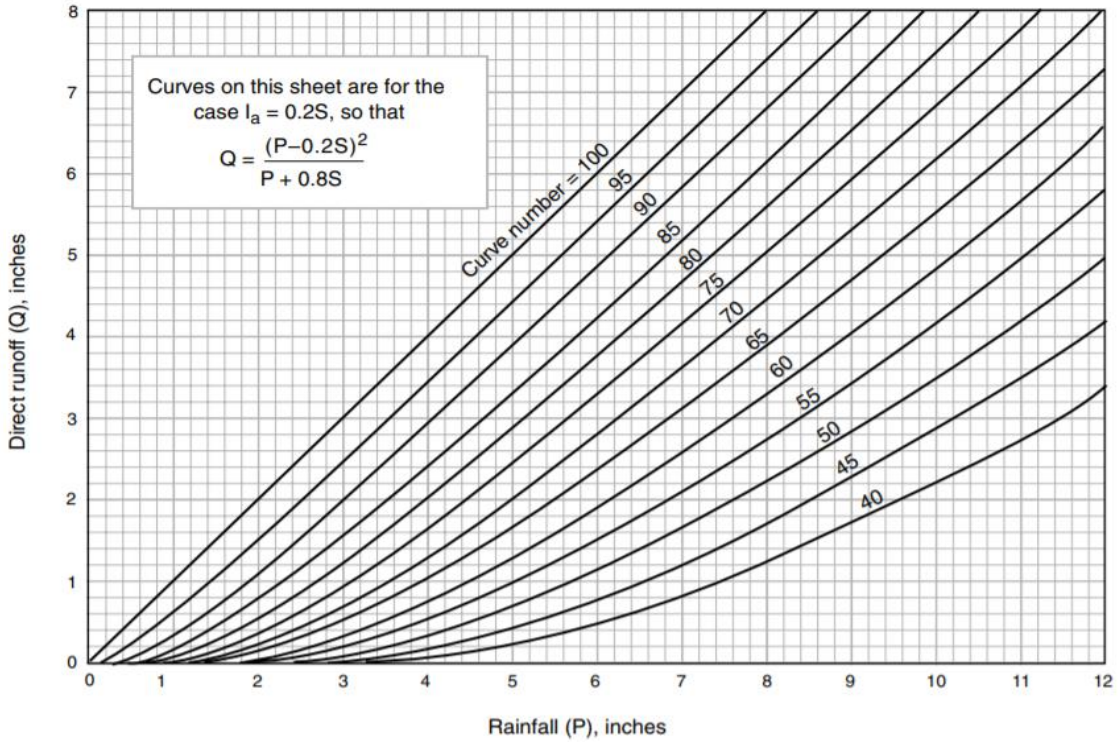


Figure 35: The solution of the runoff equation

Source: Urban Hydrology for Small Watersheds, 1986-chapter 2 page 14

Several factors control CN, such as soil hydrologic groups, initial moisture conditions.

The hydrological groups of the soil: defined by the SCS in four types

Group A: Soils with high infiltration rates even when well wet and a high-water transmission rate. Examples are sands and gravels.

Group B: Soils with moderate infiltration rates when well wetted and moderate water transmission rates. Examples are moderately fine to medium coarse textured soils.

Group C: Soils with low infiltration rates when well wet and low water transmission rate. Examples are soils with a layer that prevents downward movement of water or moderately fine textured soils.

Group D: Soils with very low infiltration rates when completely wet and a very low water transmission rate. For example, clay soils with high swelling potential, soils with permanently high water, soils with a clay plateau or a layer of clay on or near the surface, or shallow soils on the surface. an almost waterproof material.

The tables represent the average value of the CN according to the hydrological groups of the soil, the initial conditions of runoff, urban agriculture, cultivated, other agricultural pastures…, they are investigated in detail in the book of Urban Hydrology for Small Watersheds, 1986 chapter 2.

Note that according to (Neitsch & al., 2011) for each land coupling and land use there are three CNs;

- CN1: dry condition
- CN2: Moderately humid condition
- CN3: Wet condition

2.2.2.3. Concentration time

The time to concentrate and the time it takes for a drop of rain to reach from the farthest part of the watershed outlet to the watershed. The theoretical conception of the formula was evidenced by Mulvaney, using the kinematic wave model to represent the rain runoff on a homogeneous flat plate of roughness k and runoff length L, under a precipitation of intensity constant i, the expression is therefore written as follows (Desbordes M., 1974);

$$t_c = \left(\frac{\mathrm{L}.i^{(1-m)}}{\mathrm{k}}\right) 1/m \quad (20)$$

Where, m is the exponent of the uniform regime flow formula. From this relationship is derived the different empirical relationship for the calculation of tc cited in the bibliography, indeed there are several whose applicability depends on the area of the watershed, the slope and the length of the longest path of thechannel . of water, for example the formula of Turrazza, Ventura, Giandotti.

Usually large-area watersheds have a concentration time greater than 24 hours, so the runoff water does not reach the outlet until after the precipitation has ceased.

2.2.2.4 Peak flow

The peak flow is the maximum flow reached during a rain event, the rational calculation method considers that the maximum flow is attained when all the parts of the catchment area contribute to the flow in a time which corresponds to the time of concentration. The formula is the quotient ratio of the volume that flows in mm of water, the surface of the basin, the intensity of rain for a period which corresponds to the time of concentration or also called peak intensity, by 360 (Montas HJ & al. , 1990)

The flow allows to express the maximum volume of the water flow of a basin, and therefore a determining factor in the generation of floods and floods (combined with other morphometric parameters), also an indicator of the intensity of erosion and sediment input.

2.2.2.4. Snow cover

Precipitation can take place in the form of snow if the temperature reaches the limit of solidification of water molecules. The snow accumulates as long as the temperature does not increase, once increased the limited temperature is exceeded and the water begins to melt again, the retention of the water mass is expressed as following;

$$\boldsymbol{SNO = SNO + R_{day} - E_{sub} - SNO_{melt}} \textbf{ (21)}$$

Or ;

- SNO: is the water content of the snowpack on a given day (mm H2O),
- Rday is the amount of precipitation on a given day (added only if the precipitation is snowy)
- Esub: is the amount of sublimation on a given day (mm H2O)
- SNOmlt: is the amount of sleet on a given day (mm H2O).

According to (Anderson, 1976), The temperature of the snowpack is a function of the average temperature of the preceding days and it varies according to the temperature of the air, the latter

is controlled by a snow temperature offset parameter lsno, the snowpack temperature is therefore expressed as following;

$$\boldsymbol{T_{snow,dn} = T_{snow,dn-1}.(1 - l_{sno}) - \overline{T}_{av} - l_{sno}} \textbf{ (22)}$$

- $\boldsymbol{T_{snow,dn}}$: Is the temperature of the snowpack on a given day (° C),
- $\boldsymbol{T_{snow,dn-1}}$: Snowpack temperature the day before (° C),

- $\boldsymbol{l_{sno}}$:Is the snow temperature shift factor,
- $\boldsymbol{\overline{T}_{av}}$: Is the average air temperature for the current day (° C).

Snowmelt is conceptualized in the SWAT model by a linear equation of the difference between the temperature of the other maximum mean of the snowpack and the threshold temperature of its melt.

$$\boldsymbol{SNO_{mlt} = b_{mlt}.SNO_{cov}\frac{T_{sno}+T_{max}}{2} - T_{mlt}} \textbf{ (23)}$$

- SNOmlt: the amount of melted snow on a given day (mm H2O),
- bmlt: the melting factor for the day (mm H2O / day- ° C),
- Snocov: the fraction of the HRU area covered with snow,
- Tsno: the temperature of the snowpack on a given day (° C),
- Tmx: snow the maximum air temperature on a given day (° C),
- Tmlt: the basic temperature above which the snow melts (° C).

2.2.3. Sub-lateral flow

Between the soil particles, there are pores which can contain liquid or gas, depending on the quantity of the liquid retained in these pores the soil can be considered as saturated or unsaturated. The amount of liquid retained depends on the type and texture of the soil, the bulk density is a parameter which expresses the amount of void in the soil compared to the total volume and is written as follows;

$$\boldsymbol{\rho_b = \frac{M_s}{V_T}} \textbf{ (24)}$$

Or ; is the bulk density of soil expressed in mg / m3, Ms is the mass of the solid part of the soil in mg, and is the total volume of soil in m3, defined as the sum of the volume of air, water and the ground. The relationship between soil porosity and bulk density is expressed as follows;$\rho_b V_T$

$$\boldsymbol{\emptyset_{sol} = 1 - \frac{\rho_b}{\rho_s}} \textbf{ (25)}$$

Where the density of the soil fraction of the soil is a function of the mineralogical composition of the soil in mg / m3, a value of 2.56 mg / m3 is assigned by default to this parameter in the SWAT model.ρ_s

The quantity of water as well as the percolation rate therefore depends on the type of pores and the interconnection between them. The water content of the soil varies between 0 when the soil is unsaturated and the maximum value of when the soil is saturated.$\emptyset_{sol}$

Clay soil has a great retention capacity compared to sandy soil, the interaction between the plant and the useful water reserve in the soil is expressed in the SWAT model by the following relation;

$$\boldsymbol{AWC} \quad = \boldsymbol{FC} \quad - \boldsymbol{WP} \quad \textbf{(26)}$$

Where: AWC is the water reserve in the soil, the water content at the capacity of the field, after 48 draining, WP is the water content at the permanent wilting point, the latter related to the clay content in soil, is expressed as:FC

$$\boldsymbol{WP} \quad = \mathbf{0.4}\frac{\boldsymbol{m_c\rho_b}}{\mathbf{100}} \textbf{(27)}$$

Or ; WP is the water content at the wilting point, mc is the percentage of clay in the soil in%, and it is the bulk density of the soil in mg / m3.ρ_b

2.2.3.1. Percolation

Percolation is the movement of water in layers of soil, confined between the water table and the pedosphere, percolation takes place when the water content exceeds the capacity of the field and the area below is unsaturated, it is calculated by the following formula:

$SW_{ly,excess} = SW_{ly} - FC_{ly}$ yew $SW_{ly} > FC_{ly}$

$SW_{ly,excess} = SW_{ly} - FC_{ly}$ yew $SW_{ly} < FC_{ly}$

With, is the volume of water drained in one day expressed in mm of H2O, is the water contained in the soil layer for one day in mm of H2O, the water content for the field capacity in mm d 'H2O.$SW_{ly,excess} SW_{ly} FC_{ly}$

The amount of water that reaches the lower horizons is an expression as a function of the exponential of the infiltration time, the latter is the ratio of the difference between the amount of water in the saturated soil and the water content of the soil. field capacity in mm of H2O in mm of H2O by the hydraulic conductivity of the soil at saturation in mm / h.(Neitsch et al. 2009)

2.2.3.2. Sub-surface flow

Lateral flow or subsurface flow takes place in soils where hydraulic conductivity is significant in the upper layers of the soil, the layers below are impermeable (Neitsch et al. 2009), the SWAT model conceptualizes this flow by the following equation:

$$Q'_{lat} = \left(Q_{lat} + Q'_{latstor,i-1}\right) * \left(1 - \exp\left(\frac{-1}{TT_{lag}}\right)\right) \textbf{(28)}$$

Or :

- Q_{lat}:The amount of lateral flow that joins the stream in a day mm H2O
- Q'_{lat}: The amount of lateral flow generated by the sub-basin in a day mm H2O
- $Q'_{latstor,i-1}$: The amount of lateral flow stored from the previous days in mm H2O
- TT_{lag}: Lateral flow transfer time in days

SWAT controls lateral flow by four parameters;

SLSOIL: slope length in m

SOL-K: hydraulic conductivity when the soil is saturated in mm / hr

HRU_SLP: The average slope of the watershed in m / m

LAT_TTIME: the transfer time of the lateral flow in days

GDRAIN: Latency time in hours

2.2.4. Underground part:

2.2.4.1. Shallow aquifer

The equation for the water balance of this part is described by;

$$aq_{sh,i} = aq_{sh,i-1} + W_{rchrg,sh} + Q_{gw} - W_{revap} - W_{pump,sh} \textbf{(29)}$$

Or

- $aq_{sh,i}$: Is the amount of water stored in the shallow aquifer on day i (mm H2O),
- $aq_{sh,i-1}$: Is the amount of water stored in the shallow aquifer on day i-1 (mm H2O),
- $W_{rchrg,sh}$: Is the amount of recharge entering the shallow aquifer on day i (mm H2O), Is the groundwater flow, or base flow, into the main channel on day i (mm H2O),Q_{gw}:
- W_{revap} : Is the amount of water moving through the soil zone in response to water deficiencies on day i (mm H2O),

- $W_{pump,sh}$: Is the amount of water pumped out of the shallow aquifer on day i (mm H2O).

2.2.4.2. Deep aquifer

The equation for the water balance of this part is described by;

$$aq_{sh,i} = aq_{sh,i-1} + W_{deep} - W_{pump,sh} \quad (30)$$

- W_{deep}: Is the amount of water percolating from the shallow aquifer into the depth aquifer on day i (mm H2O)
- The other parameters are the same for the saturated zone.

2.3. Routing the model

The spatio-temporal evolution of the flow is described by a mathematical process called routing (Perumal et al, 2007). It estimates the speed of the flow by referring to the time and the distance traveled by the simplification of the Saint-Venant equations, the routing models generally include the mass conservation equations and the dynamic equation.

In the literature there are several routing models, the SWAT platform has two methods:

2.3.1. Muskingum method

This method was implemented in1939 by McCarthy, it is based on the kinematic wave equation equivalent to the differential equation of the volume stored in a system. As defined by Manning's equation[3]the cross section of the flow area is assumed to be directly proportional to the flow rate for a given stub segment. So the storage volume of the prism (one section) can be expressed as a function of the discharge, K. qout, where K is the storage ratio and to the dimension of time, the corner storage volume can be expressed as K X . (qin-qout), where X is a weighting factor that controls the relative importance of inputs and outputs in determining storage in a section. The sum of these terms gives a value for the total storage V(Neitsch et al. 2009)

$$V_{stored} = K.q_{out} + K.X.(q_{in} - q_{out}) \quad (31)$$

[3] The Manning Strickler formula makes it possible to estimate the average speed of a liquid flowing on the free surface, it is the quotient of the hydraulic radius of the section in m, of the hydraulic slope in m / m and of the Strickler coefficient which depends on the roughness of the surface and the sinuosity. https://www.hydrologie.org/MISC/hydr/degoutte/degoutte1.pdf

2.3.2. The variable storage method

This was developed by williams McCarthy in 1969, it differs from the Muskingum method by its consideration of prism storage, it is based on the continuity equation

$$\boldsymbol{V_{in} - V_{out} = \Delta V_{stored}} \textbf{ (32)}$$

Or

- Wine: The input volume during the time step (m3 H2O),
- Vout: The output volume during the time step (m3 H2O),
- Vstored: The change of storage volume per time step (m3 H2O).

2.4. SWAT CUP

SWAT-CUP2, is a program developed by Abbaspour in 2008 which aims to perform sensitivity analysis, calibration and validation of simulations carried out by SWAT using algorithms based on statistical methods such as SUFI2, MCMC, GLUE , and Parasol.

2.4.1. The GLUE method (generalized likelihood uncertainty estimation):

The GLUE method is derived from a shoot of a large number of models distributed with different values of the input parameters, chosen at random by a distribution, in order to compare the simulated values with the observed ones, a range of values of the parameters can be considered as the simulator of the system, if the values assigned to the parameters are not representative and do not characterize the system the probability that they are simulators is zero, the intra-interactions between the parameters do not impact the procedure in its entirety. Simulations with a probability greater than 0 must be taken into account. So the probability must be zero for all the simulations which are dissimilar to the characteristics studied and increase when the similarity increases(Beven and Binley 1992)

So GLUE is based on the use of a subjective likelihood measure which consists of deriving a posterior probability function, which is then used to derive the predictive probability of the output variables. (Abbaspour 2015).

Several probability functions can be used in this context and even modified, by way of example; the probability function of Binley and Beven (1991), Scaled maximum absolute residual, model efficiency or coefficient of determination(Beven and Binley 1992)

GLUE analysis involves three essential steps (Abbaspour 2015):

- The definition of the "generalized likelihood measure",$\boldsymbol{L(\theta_i)}$

- Allocation of the likelihood weight for each parameter,

$$W_i = \frac{L(\theta_i)}{\sum_{k=1}^{N} L(\theta_k)} \quad (33)$$

Where N is the number of sets of behavioral parameters.

- Description of the prediction uncertainty, for the GLUE method the Nash coefficient is well suited for the measurement of the likelihood.

2.4.2. The SUFI-2 method (sequential uncertainty fitting)

The SUFI-2 method is a compilation of the GLUE method (Generalized Like- lihood Uncertainty Estimation), (Beven, 1989, Beven and Binley, 1992) and the gradient approach (Kool and Parker, 1988),(Abbaspour, Johnson and van Genuchten 2004)the procedure is applied to a set of parameters at a time therefore the interactions between them is taken into account. The degrees of uncertainty are quantified by the factor P. The latter designates the probability of obtaining similar or even extreme results in comparison with the data observed by rejecting the hypothesis H1 and accepting the hypothesis H0, a value of P lower at 5% means that the parameter is significant

The 95PPU is calculated at the levels of 2.5% and 97.5% of the cumulative distribution (normal distribution, Figure 36) of an output variable. (Abbaspour et al. 2007)

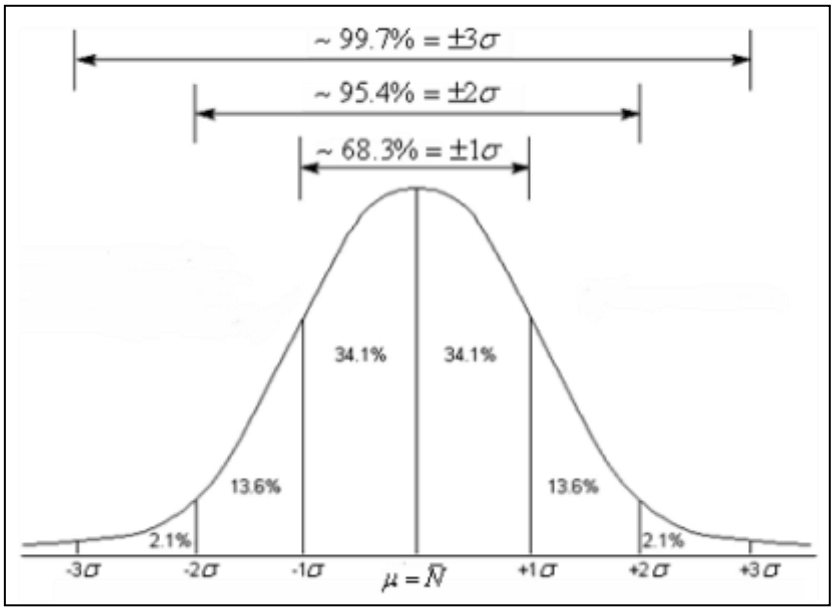


Figure 36: Distribution curve of the normal law

Source: http://unt-ori2.crihan.fr/unspf/2010_Limoges_Vignoles_StatsDescriptives/co/04-3-3%20loi%20normale%20reduite.html

The uncertainty generated in the output parameters encompasses all the uncertainties related to the overall simulation process (uncertainty related to the models, to phenomena that cannot be conceptualized, input data, etc.) (Abbaspour et al. 2007). R^2 is also used to measure the average thickness of the 95 PPU band covering the distribution of the output data, divide by the standard deviation of the measured data.(Abbaspour 2015)

The concept behind the uncertainty analysis of the SUFI-2 algorithm is graphically represented in the publication by Abbaspour et al. 2007 (Figure 37). A single value of an X parameter provides a unique response with the uncertainty of the input, so as the number of input parameters increases, the uncertainty increases

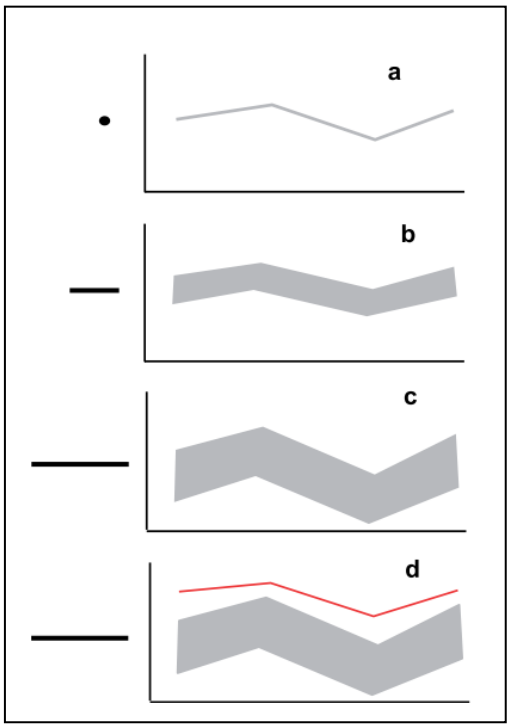


Figure 37: Relation between the uncertainty of the input parameters and the simulated parameters

Source: ABBASPOUR, KC, JOHNSON, CA and VAN GENUCHTEN, MT, 2004. Estimating Uncertain Flow and Transport Parameters Using a Sequential Uncertainty Fitting Procedure. Vadose Zone Journal, vol. 3, no. 4, pp. 1340–1352. ISSN 15391663. DOI 10.2136 / vzj2004.1340.

Therefore, SUFI-2 starts by assuming a large parameter uncertainty (within a physically significant range), so that the measured data initially falls within the 95PPU, goodness-of-fit is theoretically assessed by two factors; The R^2 and the P-factor, the latter is between 0 and 100%, while that of the R-factor is between 0 and infinity. A P-factor of 1 and an R-factor of zero is a simulation that exactly matches the measured data (Abbaspour et al. 2007).

The SWAT CUP platform has other calibration methods like Parasol and MCMC, the detailed description of these methods is provided in the SWAT CUP manual. (Abbaspour 2008)

3. Methodology

For the simulation of the hydrological model, the SWAT model was used, available on https://swat.tamu.edu/, it is added as an extension to the ARC GIS geographic information system software platform.

3.1. Definition of sub-watershed

The first step in hydrological modeling is the delimitation of the sub-watershed from the digital elevation model (Tab 14). The outlet is placed at the entrance to the Idriss Premier dam. The determination of the sub-basins is based on the topography of the watershed, and also the number of climatological stations, the study area has a limited number of stations, therefore the delimitation was made with reference to the hydrographic effective work of the channel. main and secondary water digitized from topographic maps of the study area and introduced by the ARC SWAT model, this step aims to determine the hydrological confluence points, the area and the morphometric characteristic of the area of influence of the climatological station, such as the slope, the longest path of the water effective work,

Table 25: Characteristics of the digital elevation model

Acquisition date	sensor	Spatial resolution	Radiometric resolution
17/10/2017	ASTER Global DEM	30m	16 bits

(Source: http: //earthexplorer.usgs.gov/)

The digital elevation model is required from the NASA site with a WGS84 / EGM96 latitude / longitude Geo-referencing, a Geo-Tiff image format.

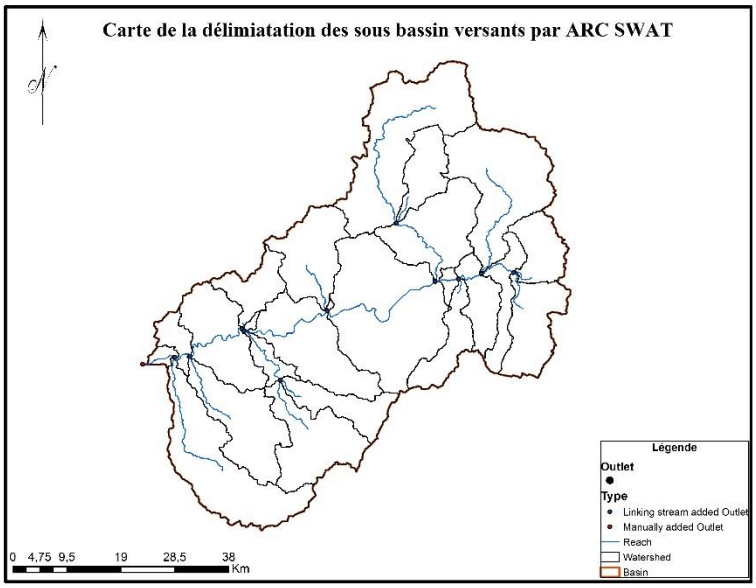


Figure 38: Map of the delimitation of the sub-watersheds by ARC SWAT.

3.2. Hydrological response units (HRU)

The SWAT model subdivides the surface to be modeled into hydrological response unit, they result from the combination between soil types, land cover and slope, a hydrological response unit has a unique combination of only one type of soil, slope, and land use (for example vertisol + urban area + a slope of 10%). HRUs of the same combination have the same behavior with respect to precipitation. The number of HRUs generated is controlled by a threshold which varies from 0 to 100%, a threshold of 0 to consider all the classes, a threshold of 20% for the soil classes neglects all the types of soil whose surface area is smaller at 20% of the entire basin, in the present study a threshold of 20/15/20 [%] for LandUse / Soil / Slope.

3.2.1. The slope map

The percentage of slopes is extracted from the digital elevation model and reclassified by ARC SWAT, 5 classes have been defined.

3.2.2. The soil map

The soil map was digitized from the soil map provided by the Department of Water and Forests of Fez. The physicochemical characteristics of the soil layers are necessary in order to define the fraction of infiltrated, runoff water. For this, the Soil Geographic Survey (ISIRIC) database was used to provide the model with information on the ground. The latter is an automated soil mapping system based on the global compilation of soil profile data and spatial data derived from remote sensing. SoilGrids provides global predictions for soil properties (organic carbon,

bulk density, cation exchange capacity (CEC), pH, soil texture fractions, and coarse fragments) at seven standard depths (0, 5, 15, 30, 60, 100 and 200 cm),

The soil attribute used in this study results from the compilation between the global soil information data and the taxonomy of the soil map provided by the Department of Water and Forests of Fez.

The USLE K factor represents the inherent erodibility of a given soil, and generally ranges from 0.1 (low erodibility) to 0.67 (very erodible), it was estimated from the percentage of sand, silt and soil. organic carbon content. The table shows the USLE K factors (for surface soil layers).

These soils are classified into hydrological soil groups (A, B, C and D) according to the characteristics of the soil in the ISIRIC database. Note that soils in group A have the lowest runoff potential and the highest infiltration rates, while those in group D have the highest runoff potential and lowest infiltration rates.

Hydrological classes, soil texture and hydraulic conductivity are not available on ISRIC, they were determined by SPAW software; Soil-Plant-Air-Water version 6.02.75, developed by the agricultural research service available at[http://hydrolab.arsuda.gov/SPAW/index.htm](Keith E. saxton, 2007). The methodology consists of entering the percentage of sand, silt clay and organic carbon.

All the data collected was linked to the soil map database by joining their attribute tables in order to obtain a table with all the parameters required by the SWAT model (Tab 15)

Table 26: Physico-chemical parameters of the soil and their references

Parameter in the model	MIN_	MAX_	Definition	reference
SUN	n / A	n / A	Soil code	
HYDGRP	0	0	Soil hydrological group	hydrologic soil classification based on soil conservation service (using gis tech march 1988)
SOL_ZMX	0	3500	Maximum rooting depth of the soil profile.	ISRIC
ANION_EXCL	0.01	1	Porosity fraction (empty space) from which anions are excluded.	
SOL_CRK	0	1	Soil crack volume potential.	ISRIC
TEXTURE	0	0	Texture	SPAW model
SOL_Z	0	3500	Depth from the soil surface to the bottom of the layer.	ISRIC
SOL_BD	0.9	2.5	Apparent density wet.	ISRIC
SOL_AWC	0	1	Available water capacity of the soil layer.	ISRIC
SOL_K	0	2000	Saturated hydraulic conductivity.	SPAW model
SOL_CBN	0.05	10	percentage of organic carbon	ISRIC
CLAY	0	100	percentage of marls	ISRIC
SILT	0	100	Percentage of silt	ISRIC
SAND	0	100	percentage of sand	ISRIC
ROCK	0	100	percentage of coarse fragments	ISRIC
SOL_ALB	0	0.25	Albedo	University of Miskolc, Miskolc-Egyetemva´ros, Hungary
USLE_K	0	0.65	USLE erodibility factor	EQUATION

Table 27: Physico-chemical characteristics of the soils in the study area

Type de sol	S5ID	Groupe Hydr	SOL_ZMX	TEXTURE	SOL_Z1	SOL_BD1	SOL_AWC1	SOL_K1	SOL_CBN1	CLAY1	SILT1	SAND1	ROCK1	SOL_ALB1	USLE_K1
Regosol	HS0002	B	803,52	Loam	655,28	1,36	0,13	7,76	2,28	24,49	33,07	42,45	19,59	0,36	0,04
Brunizems	HS0003	B	917,20	Loam	805,42	1,39	0,13	5,93	1,40	25,13	33,24	41,67	16,71	0,36	0,04
Fersiasol	HS0004	C	1234,44	Clay Loam	560,15	1,40	0,12	4,93	1,49	28,40	33,45	38,14	11,84	0,36	0,03
Calcisol	HS0006	B	756,67	Loam	601,58	1,38	0,13	7,04	1,71	24,37	32,69	42,97	18,12	0,36	0,04
Vertisols	HS0009	C	892,35	Loam	595,42	1,41	0,12	6,57	2,00	26,47	34,93	38,63	14,34	0,36	0,04
Brunisol	AI005	B	199,19	Loam	200,00	1,43	0,12	12,95	1,00	24,11	41,65	34,25	16,37	0,36	0,65
Mineral bruts	HS0007	B	834,22	Loam	533,67	1,38	0,13	6,82	1,96	25,46	34,33	40,23	17,74	0,36	0,04
Alternance 2	HS0008	B	908,37	Loam	647,24	1,39	0,13	7,68	1,69	23,57	32,49	43,98	17,12	0,36	0,04
Alternance 3	HS0010	B	948,43	Loam	908,17	1,34	0,13	8,95	2,99	24,48	34,05	41,51	20,50	0,36	0,04
Alternance 4	HS0005	B	809,00	Loam	737,13	1,30	0,13	10,29	3,62	24,63	34,70	40,71	21,97	0,36	0,04
Alternance 1	HS0001	B	892,37	Loam	698,15	1,37	0,13	7,19	2,15	25,04	33,44	41,55	17,86	0,36	0,04

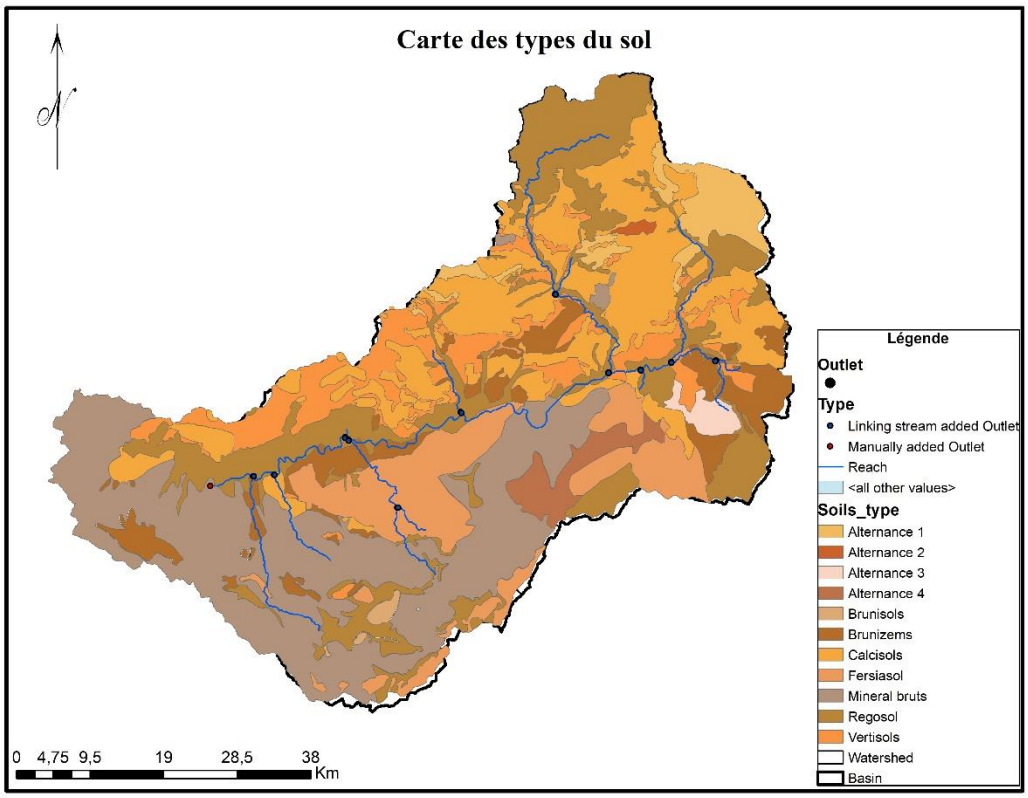


Figure 39: Soil type

3.2.3. Land use

The land use map was extracted from the global coverage map which is a project of the European Space Agency (ESA), it started in 2005 in partnership with the JRC, EEA, FAO, UNEP, GOFC-GOLD and IGBP, the objective of this project is to develop a land use map delivery service. ESA provides land use maps, which cover 2 periods: December 2004 - June 2006 and January - December 2009 from which the map used in this study was obtained. This database has been veRified by the land use map of the Oued Sebou watershed provided by the provincial agriculture directorate (Figure 40), the different types of land use are reclassified according to the database. available in SWAT, in 12 classes (Figure 41),

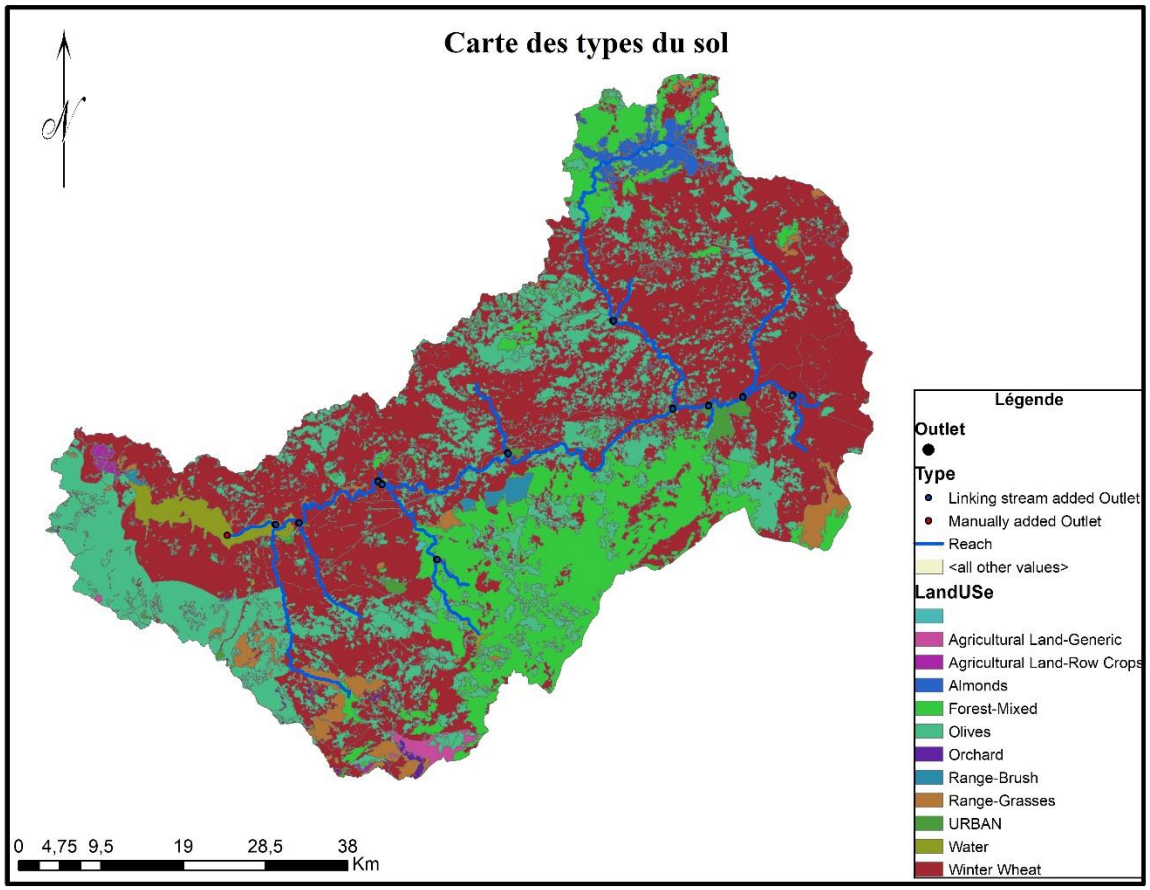


Figure 40: Land use

3.3. Hydro-climatic stations

3.3.1. Climatic station

Two databases were studied, those of real observed data provided by the hydraulic agency of the watersheds in Sebou in Morocco, the second is based on global meteorological data. The Inaouen watershed has about 11 Rain gauge stations, the problem encountered during this stage is the availability of data with a wide spatial and temporal coverage (Tab 17), to include as many stations as possible. used those which have a similar duration taking into account the availability of calibration data, the stations considered are Bab Merzouka , Bab echhoub, idriss premier dam, Boured, Bab ounder, Bni haitem and Zrarda.

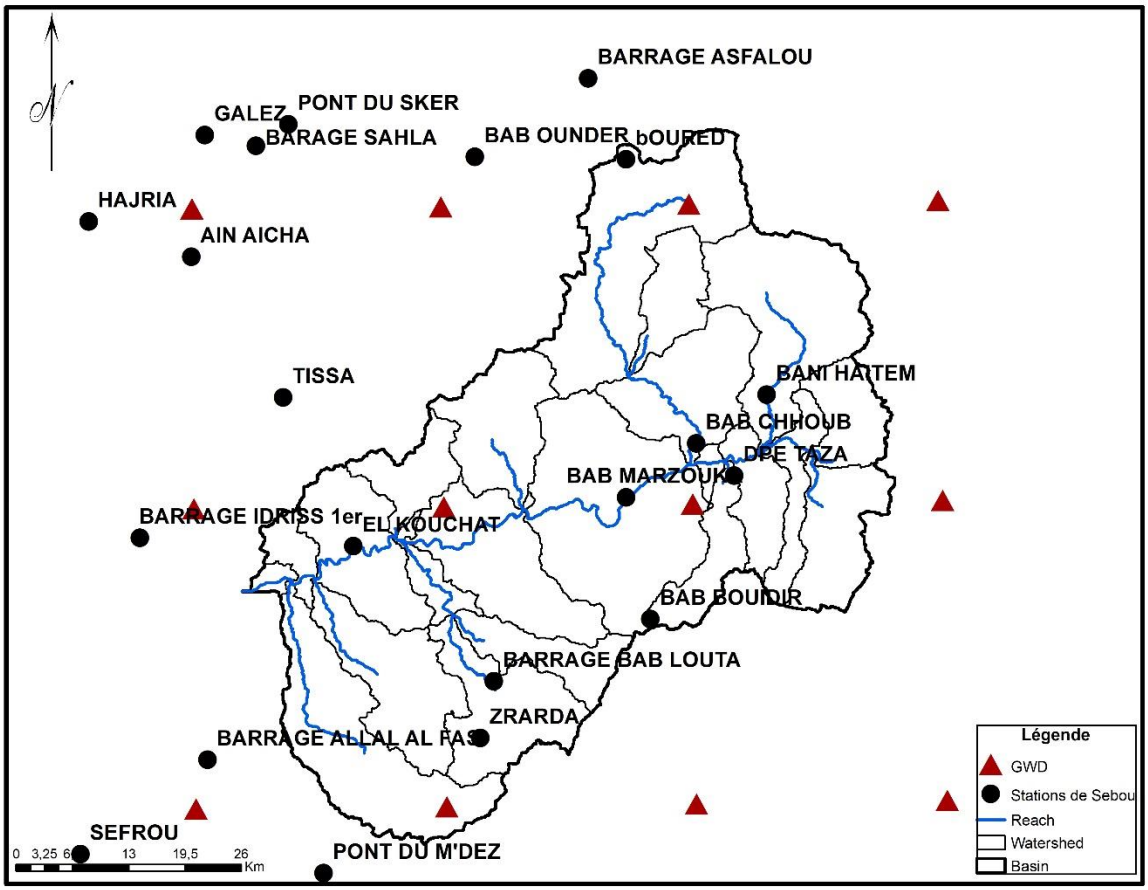


Figure 41: Map of Oued Sebou stations and Global Weather Dtata measurement points.

The methodology consists in introducing the spatial coordinates of the stations used, the SWAT model automatically assigns the station to the epicenter closest to the sub-watershed.

SWAT requires other meteorological data such as relative humidity, temperature, solar radiation, wind speed. For this, we took advantage of testing the reliability of the climate data available in the SWAT platform, from the climate forecasting center CFSR (Climate Forecast System Reanalysis) of the national center for environmental predictions NCEP. The CFSR provides on a global plane, data with a resolution of 30 km (Figure 42), of the atmosphere-ocean-land surface systems, over a period from 1979 to 2014 with a daily time step. Available inhttps://globalweather.tamu.edu/#pubs

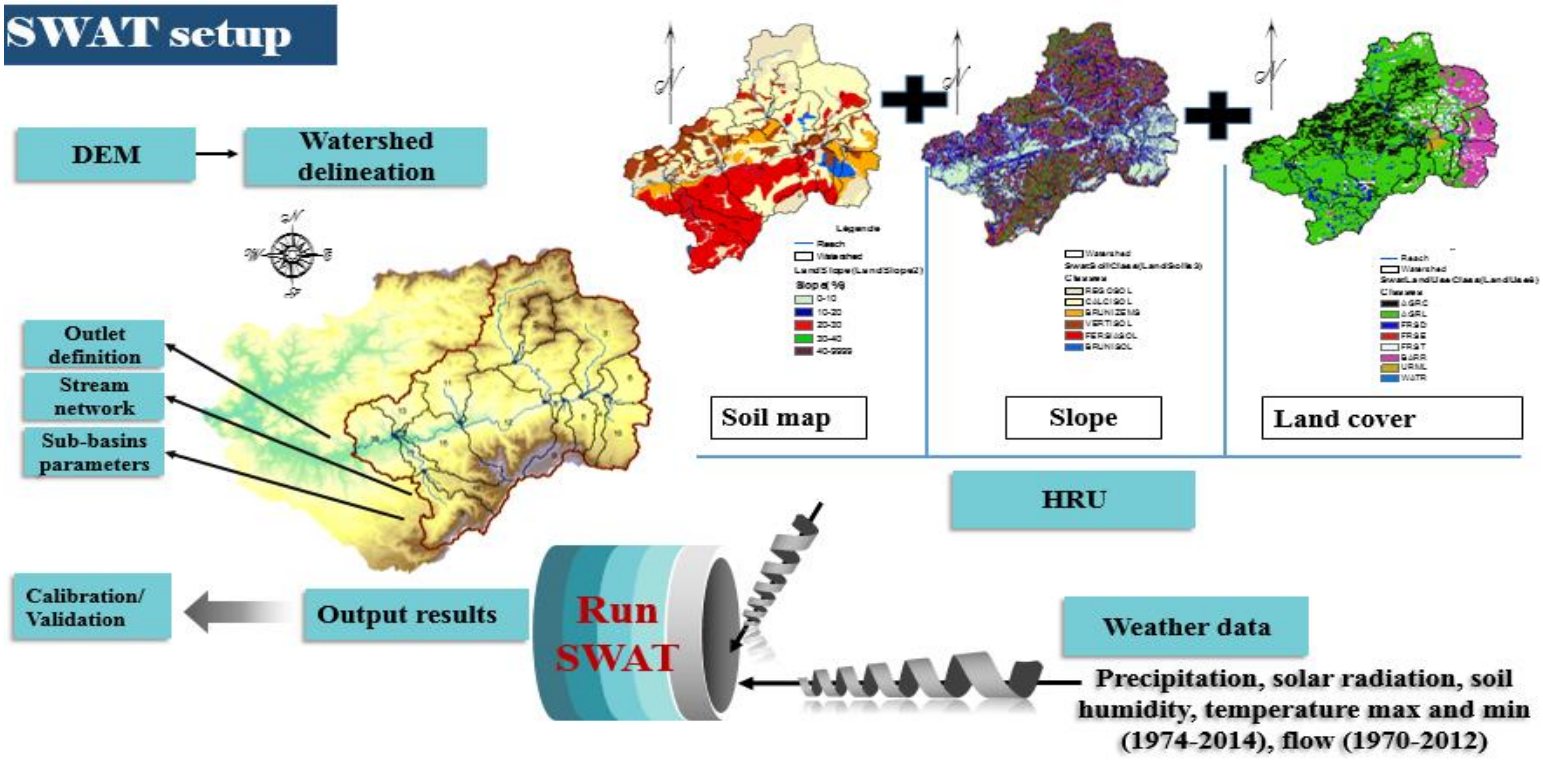
This database has been used previously in hydrological modeling studies by SWAT and show good results (Dile & al ,. 2014) assess the capacity of the CFSR database to make hydrological

predictions, applied to the Nile basin , (Fuka & al., 2013), uses the same database to improve the inputs of the watershed models. Missing data is replaced by the mean calculated by the pcp STAT model and fed into the SWAT model.

Table 28: Coordinates of hydromoetric and pluviometric stations

Station Name	Station type	X	Y	Longitude	Latitude	Rainfall and hydrometric data
BAB MERZOUKA	Hydrometric and pluviometric	615850	400850	-4.14270244	34.20327741	1971-2019 / 1960-2018
BOURED	Hydrometric and pluviometric	615500	440100	-4.14136332	34.55720196	1998-2015
EL KOUCHAT	Hydrometric and pluviometric	583750	394650	-4.49164219	34.15037383	1976-2001
ZRARDA	Hydrometric and pluviometric	598330	373400	-4.33586682	33.95750316	2002-2014
BANI HAITEM	Pluviometric	631900	412500	-3.97298190	34.30489553	1993-2014
BAB CHHOUB	Pluviometric	622470	406250	-4.07534072	34.24942981	1993-2014
BAB LOUTA dam	Pluviometric	599400	379600	-4.32613283	34,011458	2000-2002
BAB BOUIDIR	Pluviometric	617700	386000	-4.12828343	34.06796088	1999-2013
Bage IDRISS 1st	Hydrometric and pluviometric	559700	396000	-4.75239111	34.16416433	1979-2015

Source: Watershed hydraulic agency of Sebou



3.4. Model calibration

The modeling of the hydrological cycle is complex considering the quantity of parameters which control the system as well as the interaction between them. The calibration phase consists of estimating the epistemic parameters that cannot be directly measured, by adjusting the parameters so that the response of the model comes as closely as possible to the observed behavior of the watershed.(Singh et al., 2015).

Two calibration methods are possible, the first is manual and requires a good knowledge of the study area, in this case the quality of the simulation is evaluated by a single visual examination, other evaluation parameters can be calculated. The disadvantage of the latter is the non-adaptability to the complex model. The other method is the automatic calibration implemented by algorithms and systematic programs, the parameters are adjusted by mono or multi objective functions.(Singh et al., 2015).

The over-parameterization of hydrological models is a troublesome factor because the parameters that represent the physical processes can have a different effect on the generation of the flows, therefore the sensitivity analysis is an important step which must precede the calibration to identify the ones. parameters that most influence the outgoing flows.

The literature describes several calibration methods, the Bayesian method, the Kennedy and O'Hagan (KOH) method, the Gaussian GP process, the OBC Optimization-based calibration method, the sequential calibration (Abbaspour et al. 2007)which is adopted in this study since it makes it possible to take into account the physical and morphometric diversity of the basin. The definition of the values of the variation margin has been identified in the work carried out by, (Brihet, 2016), (Brouziyne, 2017) and (Khalid, 2019)

In this study, the sensitivity analysis is carried out by SWAT-CUP for the covering period 1999-2007 at the daily time step for the Bab merzouka station. The margin of the parameters must converge with the real parameters of the basin, those most sensitive are selected thereafter for the calibration.

3.4.1. Calibration

The calibration is carried out on the different components of the hydrological system,

- The parameters that manage the soil-atmosphere interaction, evapotranspiration and interception
- The underground part percolation and infiltration
- And the superficial part (base flow and runoff)

During the first shooting of the model, random values are assigned based on knowledge of the study area and on the literature, then the parameters that most influence the results have been carried out, an iteration of 700 times is carried out then the evaluation parameters are determined, once the range of values is set the process is repeated until satisfactory values of the evaluation criteria are obtained (detailed in section 3.5)

Satisfactory results are those which provide a better performance of the model over the chosen study margin, perfectly represent the real physical parameters, and which can be spatially and temporally transposed. (Singh et al., 2015)

The validation consists in returning the model using the same values of the parameters retained during the calibration over a new period without carrying out any sensitivity analysis or iteration.

3.5. Evaluation criteria

3.5.1. Nash stucliffe

The Nash Stucliffe criterion varies between - ∞ and 1, a Nash coefficient of 1 indicates that the simulated data is 100% correlated with the observed data.

$$NSE = 1 - \left[\frac{\sum_{i=1}^{n}\left(Q\ obs_i - Q\ sim_i\right)^2}{\sum_{i=1}^{n}(Q\ obs_i - \bar{Q}\ obs)^2}\right] \quad (35)$$

With: are the observed flows, are the simulated flows and is the sum of the observed flows, according to the equation the NSE is sensitive to extreme values since the difference is considered squared. $Q\ obsQ\ sim_i\ \bar{Q}\ obs$

(Van Liew and all, 2007) adopt a classification which has been adopted and used by several authors (Durães, 2011), According to this classification, the value NSE = 1 means a perfect fit of the data simulated by the model; ENS> 0.75 (the model is suitable and good); 0.36 <ENS <0.75 model is satisfactory NSE <0.36 model is not satisfactory

3.5.2. The mean absolute error (MAE)

$$\boldsymbol{MAE = 1/N \sum_{i=1}^{N} |Qobs_i - Qsim_i|} \quad \textbf{(36)}$$

MAE measures the difference in the difference between the observed flow rates and the simulated flow rates for N elements.

3.5.3. The root of the mean squared error (RMSE)

$$\boldsymbol{RMSE = \sqrt{1/N \sum_{i=1}^{N} |Qobs_i - Qsim_i|}} \quad \textbf{(37)}$$

In this formula the errors are squared, this parameter is useful when we want to reduce the deviations in the series.

3.5.4. The coefficient of determination R²

The coefficient of determination is the square of the Pearson correlation coefficient, The latter reflects the dispersion of the combination of the observed and simulated data both with respect to the dispersion of each series, this parameter varies between 0 and 1, a value of 0 indicates that the correlation is zero, a value of 1 shows that there is a linear relationship between the observed flows and the simulated flows, but does not mean that the simulation is perfect

$$R^2 = \left(\frac{\sum(Q_{t,obs} - \overline{Q_{obs}})(Q_{t,sim} - \overline{Q_{t,sim}})}{\sqrt{\sum(Q_{t,obs} - \overline{Q_{obs}})^2}\sqrt{\sum(Q_{t,sim} - \overline{Q_{sim}})^2}}\right)^2 \quad (38)$$

3.5.5. Percent bias (PBIAS)

This criterion expresses the bias between the observed and simulated data, and varies between -100% and 100%, a negative value reflects an underestimation of the flows, a positive value reflects an overestimation of the flows, a value of 0 shows that the model is performing.

$$PBIAS = 100 * \frac{\sum(Q_{t,sim} - Q_{t,sim})}{\sum Q_{t,obs}} \quad (39)$$

More details on the model evaluation criteria are available in the publication of (Moriasi et al., 2007a).

4. Partial conclusion

This chapter describes the SWAT model and the different components integrated into the rainfall-runoff modeling process. Hydrological transfer is made up of two major phases, the first is the production of effective rainfall, conceptualized by the water balance equation. The second is the routing phase which includes four sub-parts: water yield, sediment, nutrients, and pesticides.

The followed modeling methodology consists in carrying out a preliminary treatment under the geographic information system, to define the sub-basins, the hydrological response units and to introduce the meteorological databases. After the first simulation the model is transported to SWAT CUP for sensitivity analysis and calibration using the SUFI-2 sequential fit method.

Chapter IV: Deficit Irrigation

This section aims to describe the methodology and the data used to carry out the deficit irrigation estimation.

1. Crop data :

The effective water requirement was calculated, assuming no losses during irrigation (Eq.43). On the other hand, the gross water requirement was calculated, including the excess irrigation water supply (Pomares, 2007) (Eq.45). In addition, the effective rainfall (Pe) (Abdelkhalik et al., 2019) (Eq.44) was estimated based on the rainfall recorded by the Idriss I station, including irrigation water losses. In addition, the irrigation water requirement (IWR) was calculated by the difference between evapotranspiration and effective rainfall (Pe) (Eq.46).

$$ET_c = K_c \times K_r \times ET \quad (43)$$

$$P_e = P \times \eta \quad (44)$$

$$GCR = \frac{ET_c}{E_f} \quad (45)$$

$$IWR = GCR - P_e \quad (46)$$

where ETc is the crop evapotranspiration (mm) which represents the crop water requirement, Kc: crop coefficient, Kr: reduction coefficient, Pe is the effective precipitation, which is the amount of precipitation stored in the soil (mm), P: the recorded rainfall data (mm), ŋ: the percentage of rainfall that peeffective rates the soil, estimated to be 80%, GCR: The gross crop requirement (mm), Ef: the irrigation efficiency of 0.90, IWR: the irrigation water requirement (mm).

Table 29: Monthly harvest coefficient for olive trees (Masmoudi et al., 2004)

harvest coefficient	Month											
	Jan	Feb	March	Apr	May	Jun	Jul	Aug	Seven	Oct	Nov	Dec
Kc	0.50	0.50	0.65	0.60	0.55	0.50	0.45	0.45	0.55	0.60	0.65	0.50

Table 30: The values of the reduction coefficients corresponding to the vegetation cover (Conseil Oleicole International, 1997)

Vegetable cover	Reduction coefficient (Kr)
More than 50%	1.00
40-50%	0.90
35-40%	0.80
30-35%	0.75
Less than 30%	0.70

2. Olive yield

The assessment of the impact of deficit irrigation on crop yields was based on the study conducted by the National Institute of Agronomic Research on Saiss covering the same study area. This later evaluated the behaviour of olive trees with a density of 154 trees/ha under full irrigation and 75% of water requirements. The agro-physiological and biochemical parameters of the olive trees show that no significant difference was recorded between the full irrigation requirement and 75% of the total water requirement in terms of growth and development of the olive tree. Moreover, olive production was hardly affected by water availability, estimated at 0.5 t/ha (INRA, 2019).

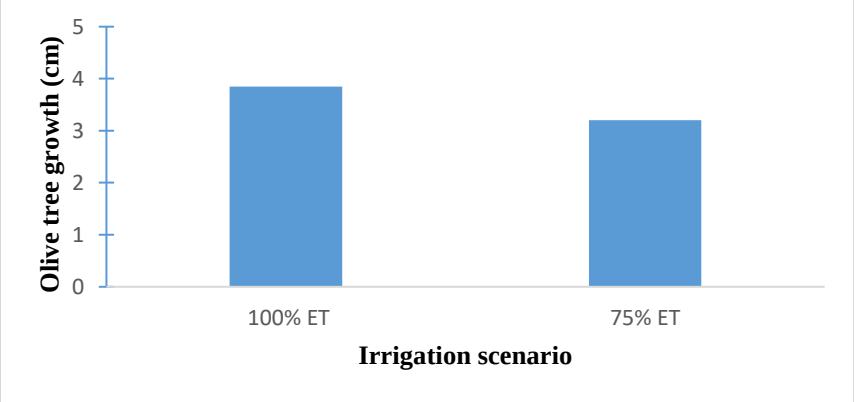


Figure 42: Growth of young olive branches in irrigation scenarios (INRA, 2019)

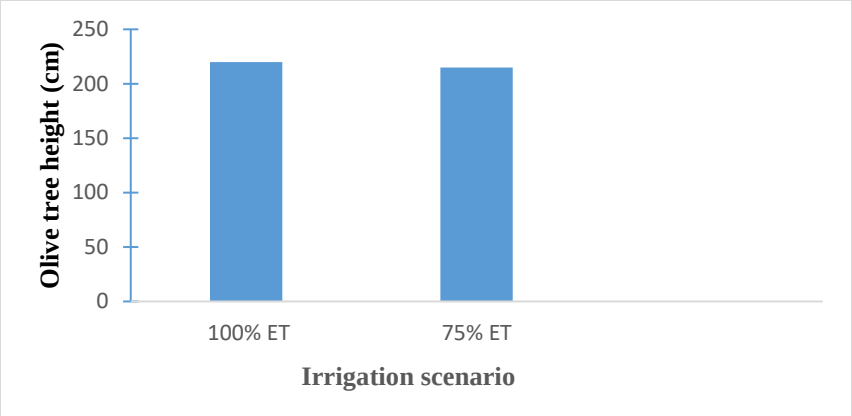


Figure 43: Effect of the irrigation scenario on the height of olive trees (INRA, 2019)

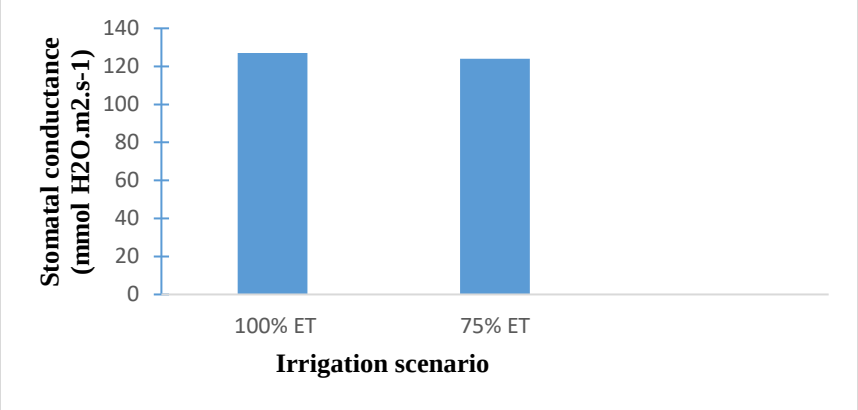


Figure 44: Effect of the irrigation scenario on the conductance of the somatic leaves of olive trees (IN, 2019)

3. Water use efficiency and water productivity

Irrigation water use efficiency (IWUE) was calculated as the ratio of harvested marketable yield (kg/ha) to total water applied (m3 per ha). Economic productivity is defined as the value derived per unit of water used, which indicates the amount of economic output produced per cubic meter of freshwater withdrawn (in Dirham (Dh) per m3). In the Saiss region, average production costs and average margin data are highlighted in Table 23.

Table 31: Average production costs and average margins of olive trees irrigated by drip irrigation in the Saiss region (Source: Regional Directorate of Agriculture of Fès-Meknes)

Average production costs and average margins	
Parameters	Parameters Olive trees irrigated by drip irrigation
Phytosanitary products (DH / ha)	1600
Fertilizer (DH / ha)	1200

Workforce without harvest (dh / ha)	1950
Workforce with harvest (dh / ha)	850
Fuel for irrigation (dh / ha)	2200
Other expenses (dh / ha)	500
Total variable charges (dh / ha)	8300
Yield (t / ha)	6
Fresh (dh / kg)	1.38
Sale price (dh / kg)	3.5
Turnover (dh / ha)	21000
Margin (dh / ha)	12700
Margin (dh / kg)	2.12

4. Partial conclusion

Chapter 3 presents the framework and methodology for assessing the efficiency of deficit irrigation in the region of the Middle Sebou and downstream of Inaouen, the irrigation water requirements is estimated from evapotranspiration and precipitation data.

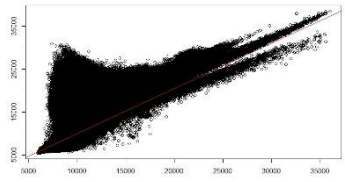
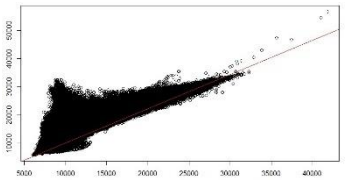
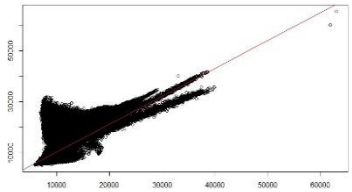
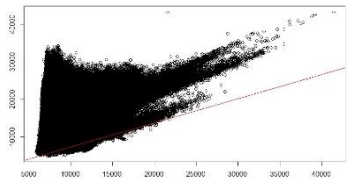
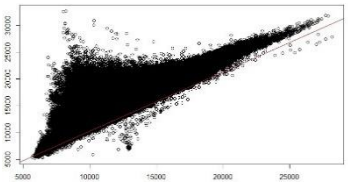
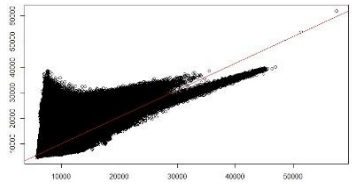
The actual evapotranspiration (AET) was estimated using the Modis Evaporation data over the period 2008-2019 in Google Earth Engine Could-Computing Environment. 2500 ha of olive yields were evaluated with a full drip irrigation system and 75% of the full drip irrigation supply over five years ranged from 2008 to 2019. The Idriss I gauge station was used to calculate crop water requirements for 100% and 75% evapotranspiration. Rainfall data was provided by the watershed hydraulic agency of Sebou for the same period. The evaluation is done by calculating the yield of olive trees and the efficiency of water use.

Part III: Results and discussions

1. Reduction of spatial scale

1.1. Bare ground line

Figure 45 presents the NIR versus RED scatterplots with the extracted soil line, for all Moroccan watersheds. The NIR versus Red scatters plots present some scattered points in low and high Red values, which may impede extracting bares soil line. Using quantile regression, we tried to fit the line with the bottom boundary line, instead of the existence of some sparse points. Especially the case of Tami, which present a high rate of the sparse point below the bottom boundary line. Quantile regression is used in many studies to extract the bare sol line (Ahmadian et al., 2016; Xu & Guo, 2013). According to (Ahmadian et al., 2016; Xu & Guo, 2013), quantile regression shows a better capacity in extracting bare soil line. Furthermore, it shows that the best period of extracting bare soil line is the early green-up season starting from late March to late April, and late senescence season starting from early August to late October (Ahmadian et al., 2016; Xu & Guo, 2013). Table (3) turns –up the slope and the intercept of the extracted bare soil line, based on near-infrared and red scatterplot, using the quantile regression method. The mean bare soil intercept and slope over Morocco are respectively -771.838 and 1.006.

NIR vs R (Deraa)	**NIR vs R (Guelmim-Tiznit)**	**NIR vs R (Ziz-Guir-Gheris)**
		
NIR vs R (Loukous)	NIR vs R (Massa)	NIR vs R (Moulouya)
		
NIR vs R (Oum Er Rabia)	NIR vs R (Safi Eljadia)	NIR vs R (Sahara)

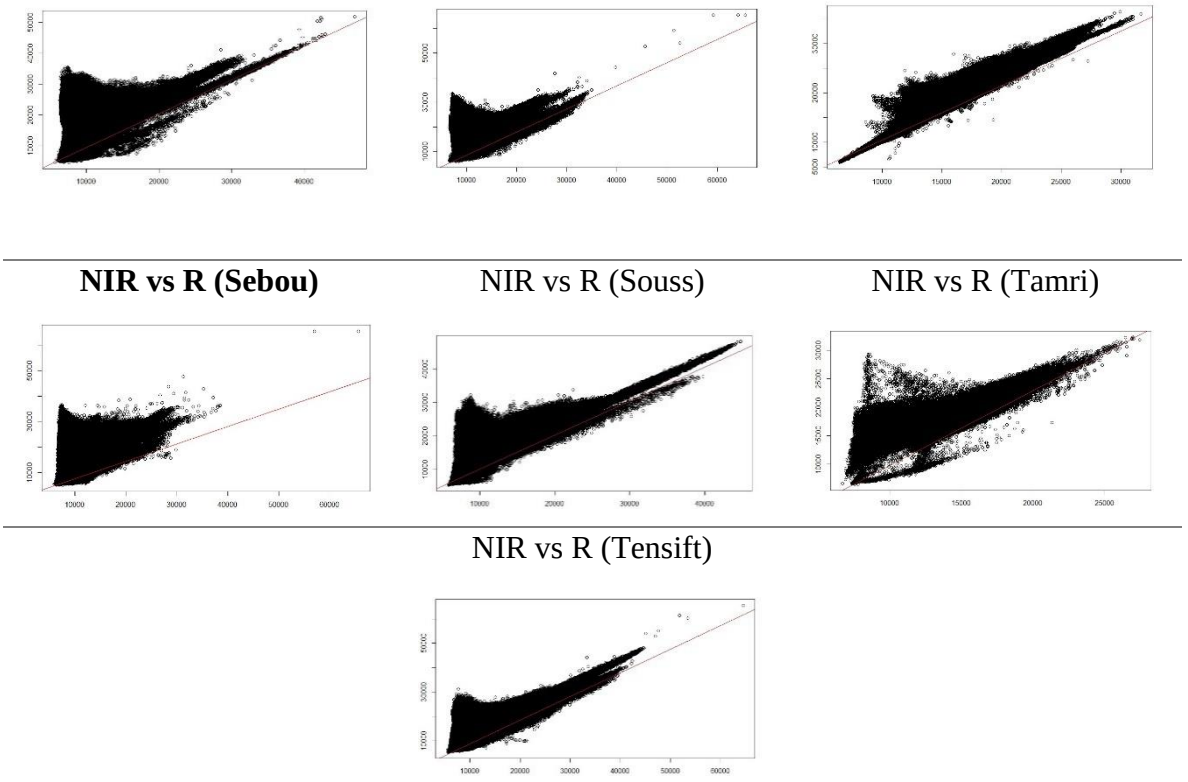


Figure 45: Bare soil line extracted for all Moroccan watersheds, from Landsat 8 OLI images, based on NIR versus red point cloud; using the quantile regression method

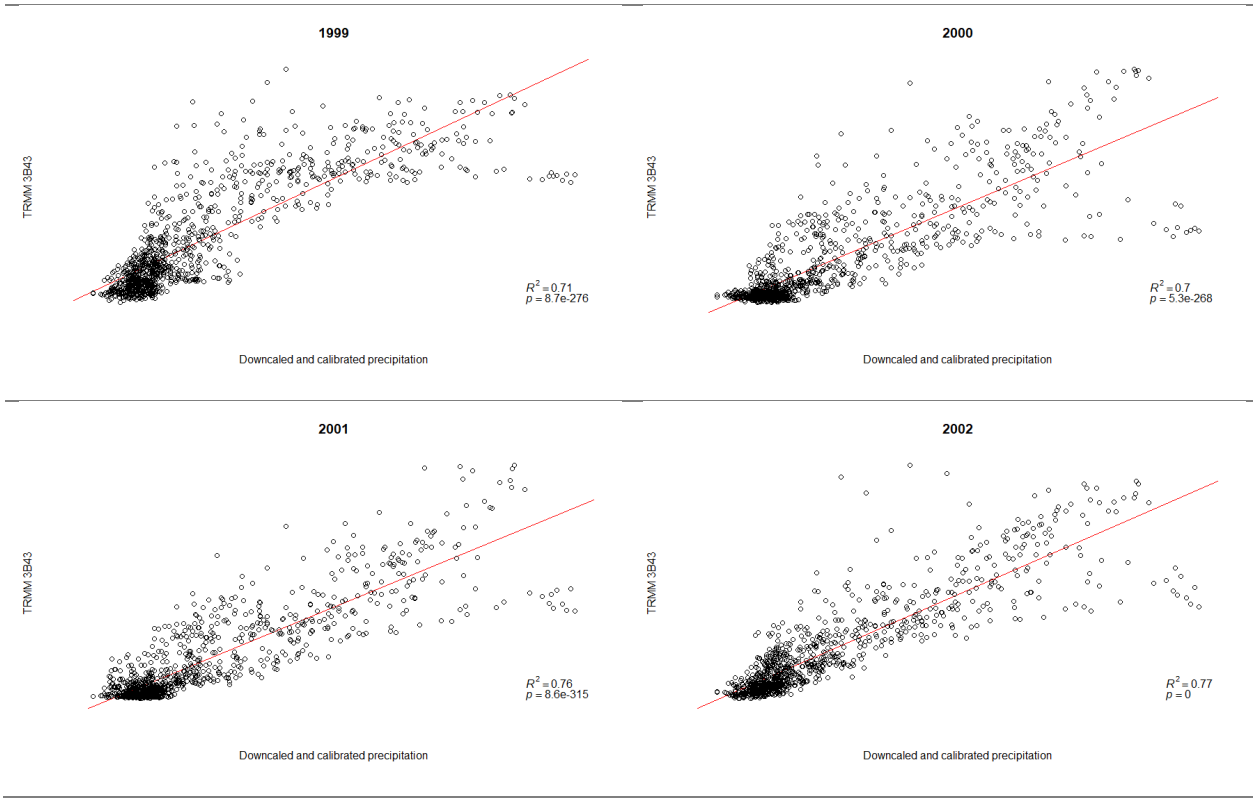
Table 32: Slope and intersection of the line of bare soil extracted from all the watersheds of Morocco, using the quantile regression method

Method	Quantile regression (NIR versus RED)	
Moroccan Watershed	Slope	Intercept
Bouregreg	0.816	-399,329
Deraa	1,053	-546,630
Guelmim-Tiznit	1.215	-1999.385
Loukous	0.645	831,088
Massa	1.102	-767,073
Moulouya	1,048	-488,026
Oum Er Rabia	1,094	-1476.695
Safi Eljadia	0.942	-1010,796

Sahara	1.103	-629,042
Sebou	0.684	735,890
Souss	1.013	-44,562
Tamri	1.313	-3369.862
Tensift	0.971	-1059.236
Ziz-Guir-Gheris	1,092	-582,077

1.2. Correlation between TRMM 3B43 and TSAVI

The correlation between TRMM 3B43 and TSAVI shows a high R^2 with a very significant p value that ranges from 0 to 5.3 × 10-268; therefore, TSAVI is statistically significant in predicting TRMM 3B43 rains. Also, R^2 ranges from 0.7 to 0.88, which shows that the data are very close to the regression line. The results show that TSAVI transmits the greatest variability of TRMM 3B43 products around its mean (Figure 46). The test of the correlation between TRMM 3B43 and TSAVI shows the best fit in comparison with the correlation between TRMM 3B43 and NDVI or NDWI, which has been carried out by several studies (Ezzine, 2017; Nichol & abbas, 2015).



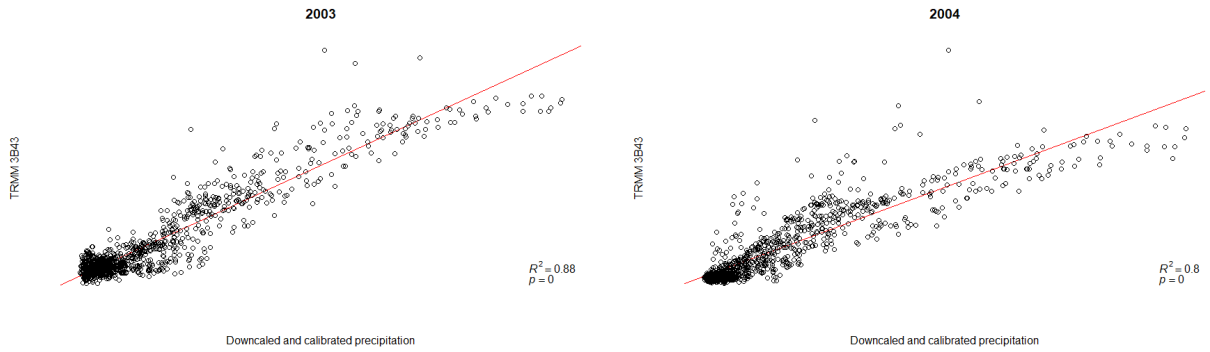


Figure 46: Correlation between TRMM 3B43 and TSAVI precipitation over the period 1999-2004

1.3. Correlation between TRMM 3B43 and predictors using machine learning

TSAVI, sea elevation and distance as independent variables may better explain TRMM precipitation data, than using only TSAVI. In a comparison based on R^2, Figure 46 shows that TSAVI, the elevation and distance of the model from the sea improved the model by an average of 0.17 points. The lower R^2 varies from 0.7 to 0.73 and the high R^2 ranges from 0.88 to 0.89. Figure 47 shows that the average R^2 using TSAVI, the model's elevation and distance from the sea, is 0.77, which is why the model can significantly predict TRMM precipitation. In addition, Figure 48 shows that the range of R^2 over the period 1999-2014 varies from 0.62 to 0.89. In comparison with the reduction models.

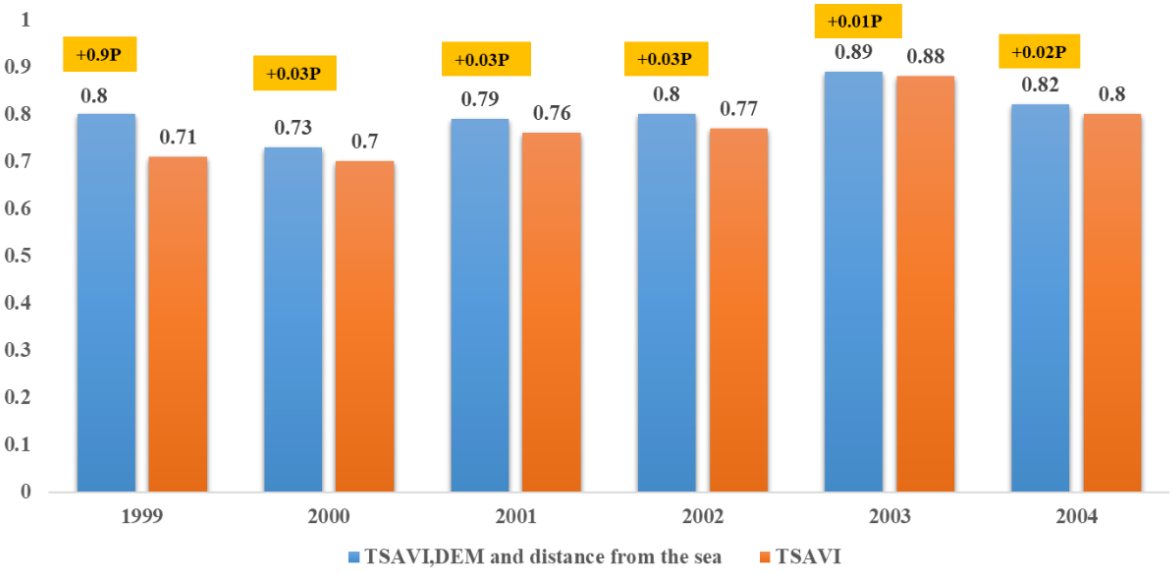


Figure 47: R^2 of the comparison between TRMM versus TSAVI and TRMM versus TSAVI, DEM and distance from the sea, over the period 1999-2014

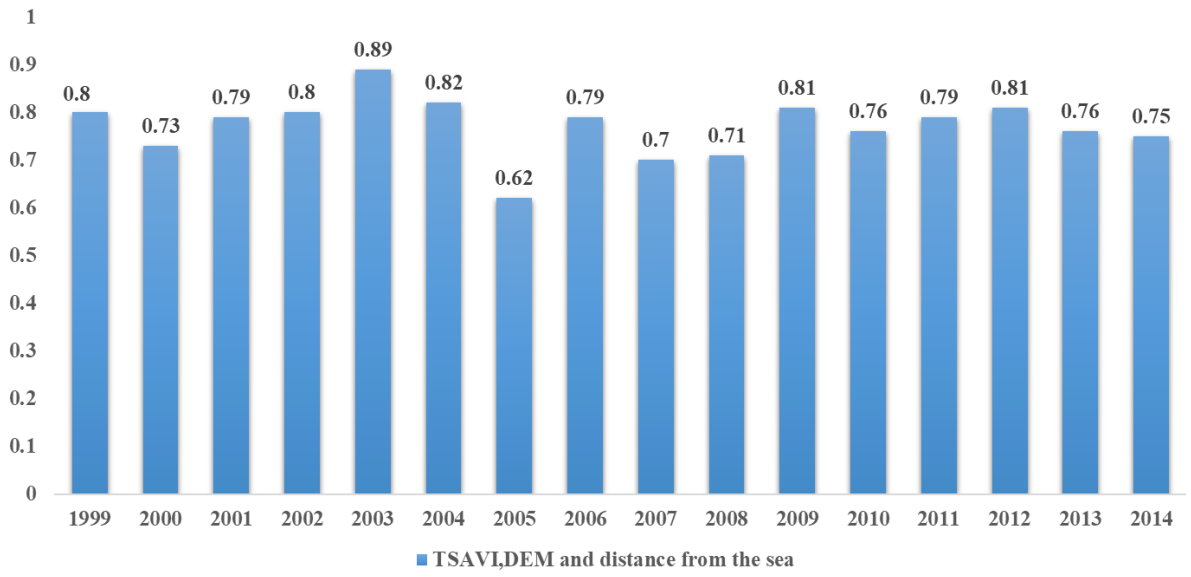


Figure 48: R^2 of the correlation between TRMM precipitation and the independent variables (TSAVI, DEM and distance from the sea; over the period 1999-2014.

Figure 49 shows the accuracy of TSAVI, elevation and distance of the sea model for predicting TRMM precipitation data, using R^2, adjusted R^2, Mallow's Cp and AIC. The model presents a significant R^2, which explains the excellent correlation between TRMM and the independent variables. Moreover, Mallow's Cp is very close to the number of predictors; there for the model that best fits with high precision and low bias.

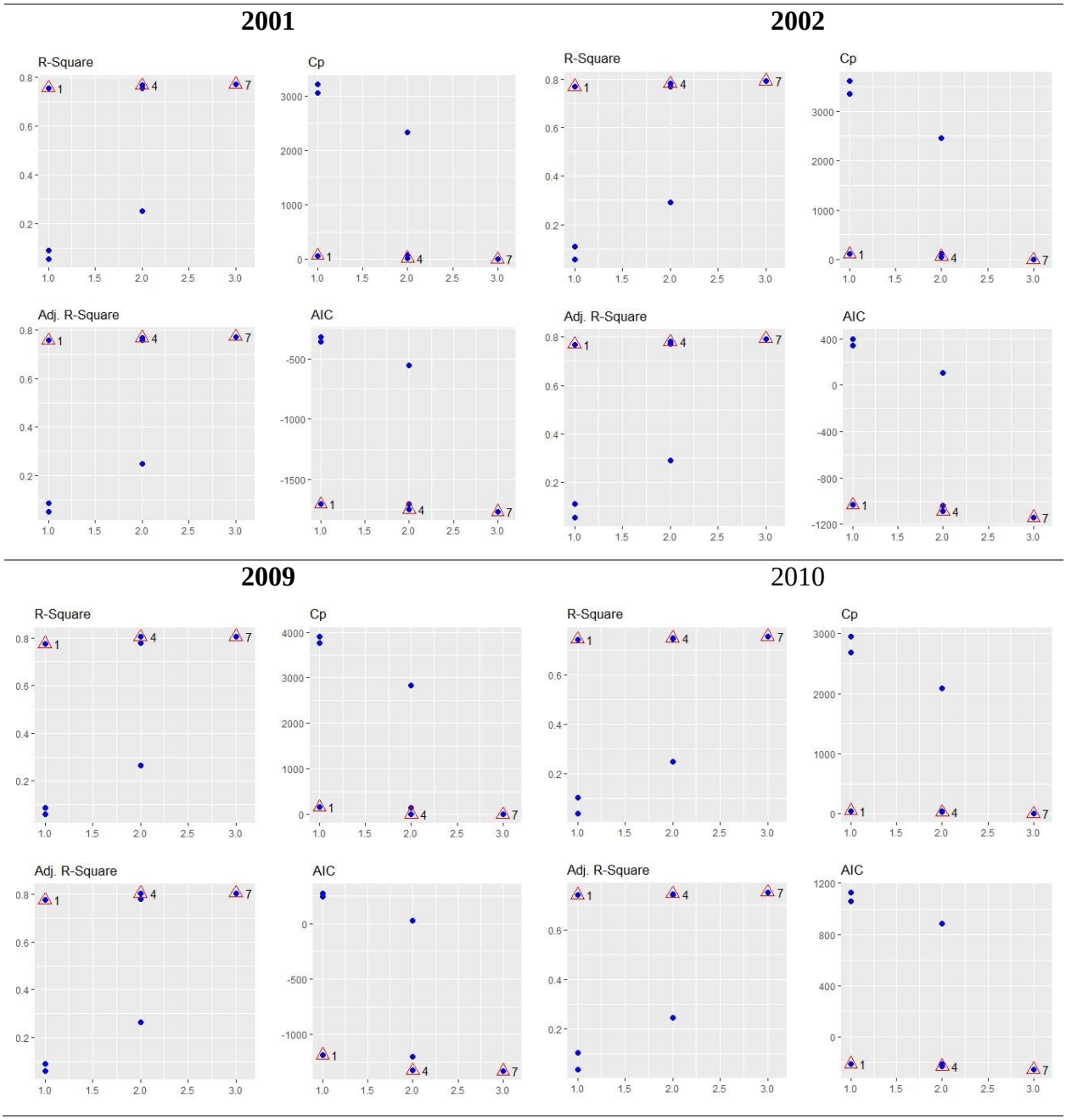


Figure 49: Statistical model precision metrics: R², adjusted R², Cp and AIC; for TRMM vs TSAVI, DEM and sea distance.

1.1. Calibration and Validation

1.1.1. Calibration

Figure 50 shows the spatial distribution of estimated precipitation using TSAVI predictors, elevation and distance from the sea during the reference period 1999-2004. The rainfall is abundant in the North of Morocco and very rare in the South, this is one of the major reasons that make Morocco is under the stress of water scarcity (Moumen et al., 2019).

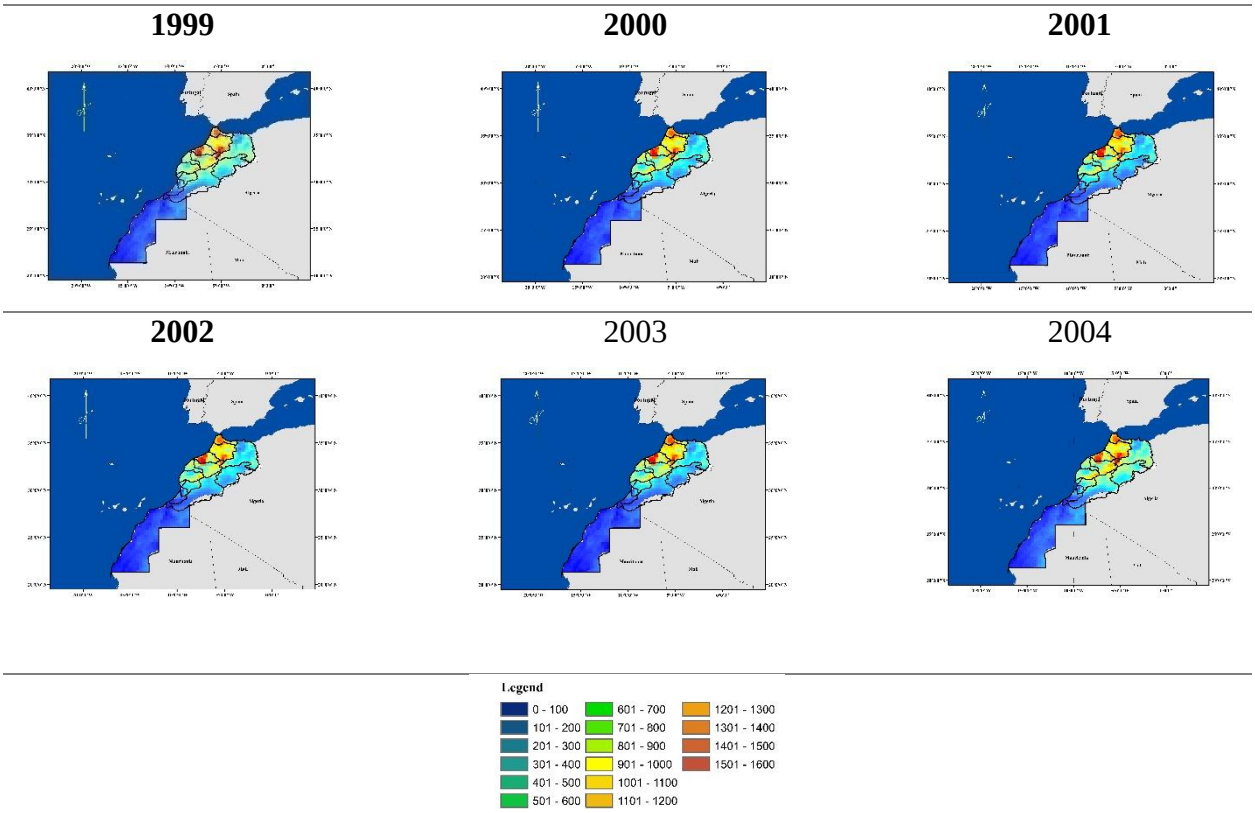
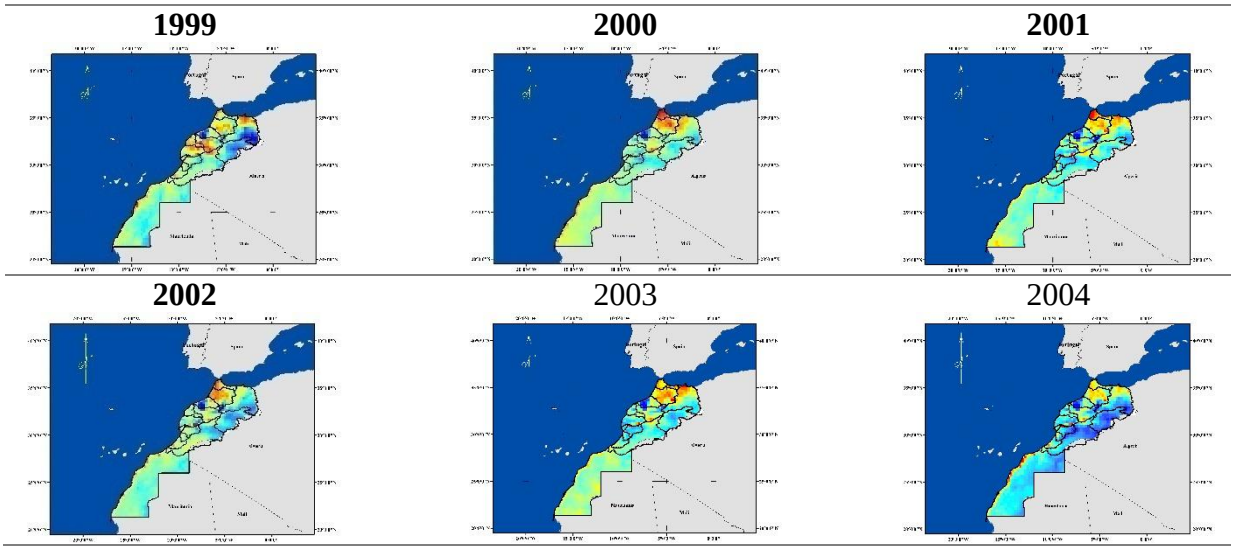


Figure 50: Precipitation estimated using TSAVI, DEM and distance from the sea in a spatial resolution of 0.25 ° × 0.25 °, over the reference period 1999-2004

The spatial distribution of the model error is highlighted in Figure 51. The residual of precipitation that the model could not estimate is used parameter of correction to enhance the model performance. Indeed, positive values indicate the model underestimated TRMM product data. However, negative values indicate that the model overestimates TRMM product data.



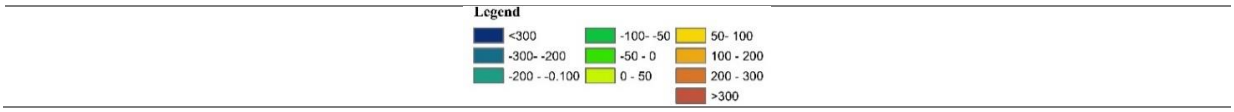


Figure 51: Spatial distribution of the regression residue at a spatial resolution of 1 km × 1 km, over the reference period 1999-2004.

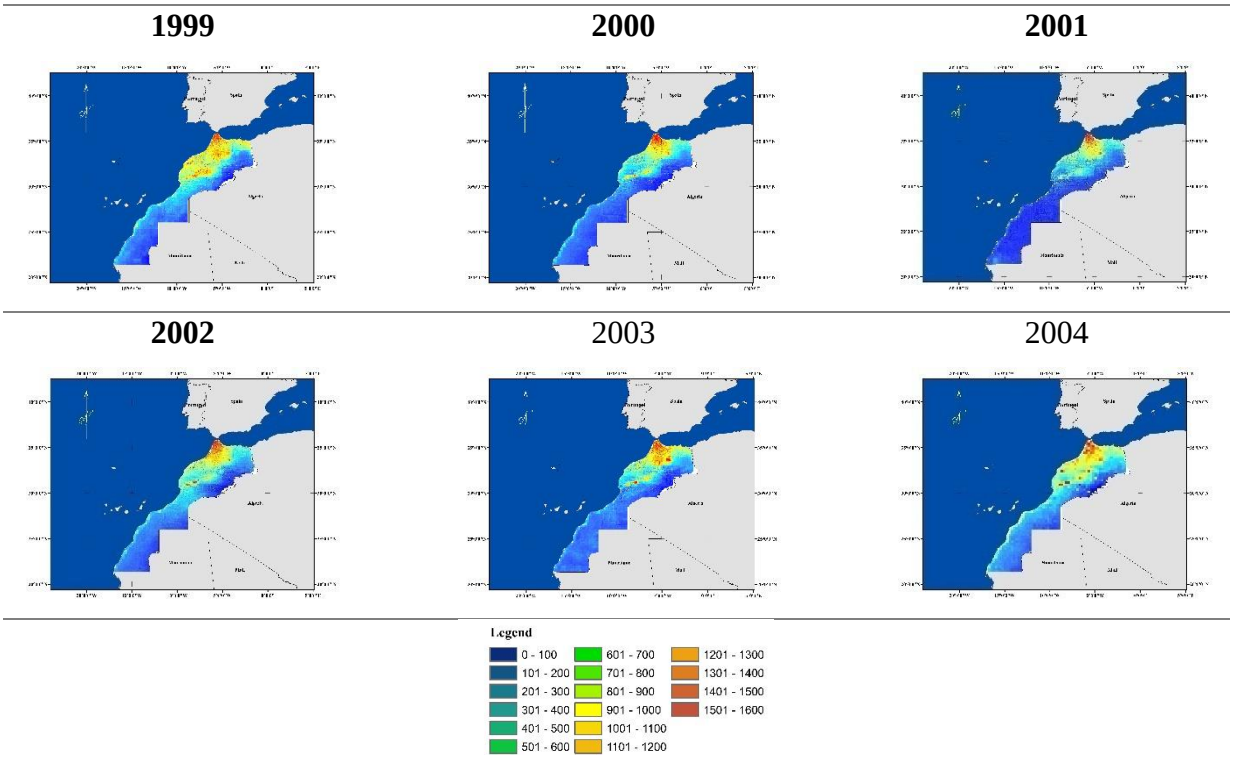


*Figure 52: Precipitation reduced and calibrated to a spatial resolution of 1 km * 1 km, over the reference period 1999-2004*

The reduced and calibrated precipitation using TSAVI, elevation and distance from the sea model shows a significant correlation with the TRMM 3B43 precipitation data. For the reference period, the correlation between TRMM vs reduced and calibrated precipitation presents a high R2, which ranges from 0.85 to 0.91.

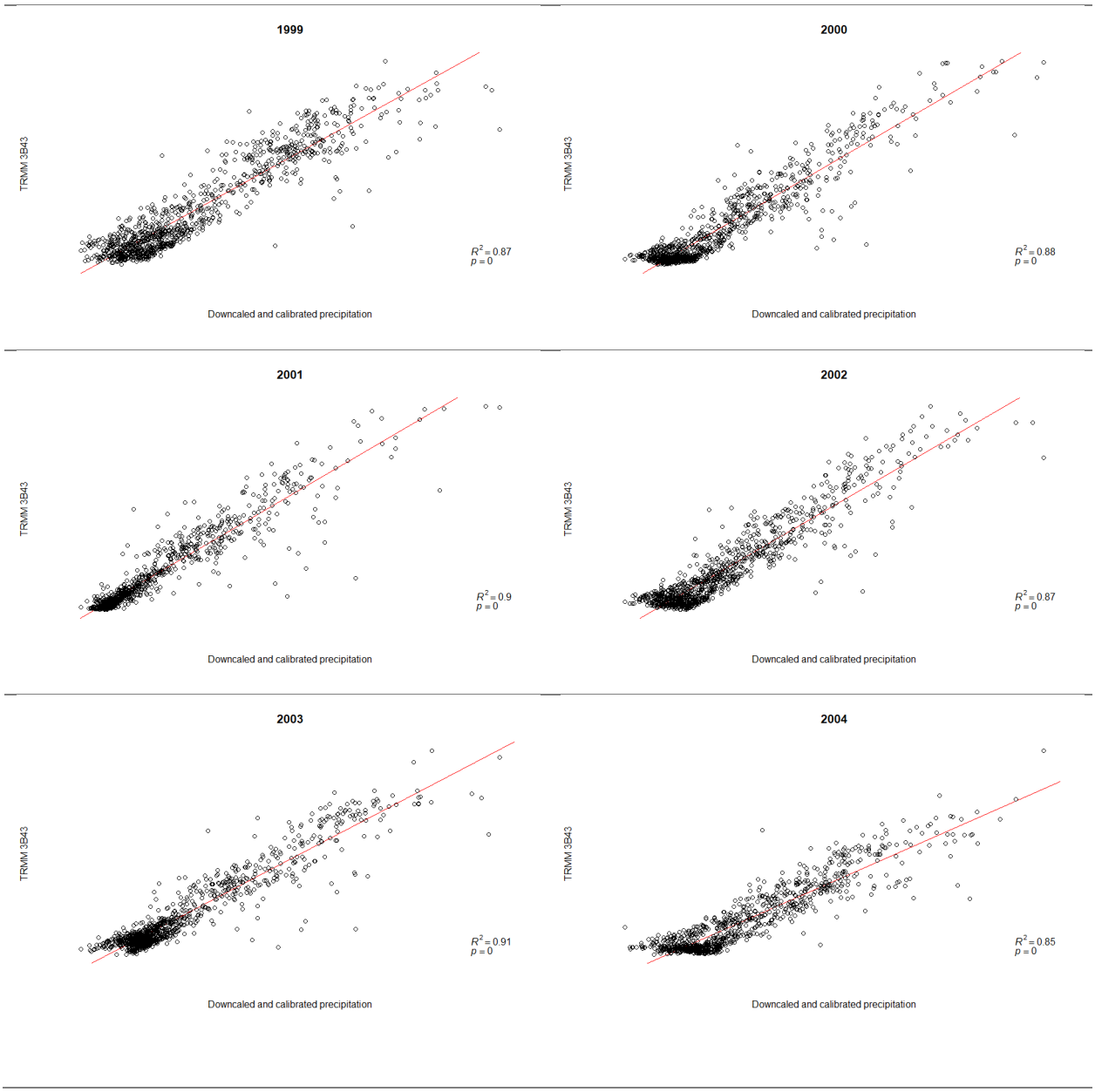


Figure 53: TRMM vs reduced and calibrated precipitation over the reference period 1999-2004

1.1.2. Validation

Ten rain gauges stations were considered for the validation of the model over the period 1999-2004 (The most available data). Table 4 shows that the downscaling model based on TSAVI can fit at a high level the in-situ measurement of precipitation at a spatial resolution of 1km, in comparison to the NDVI based models (Ezzine, 2017; Nichol & Abbas, 2015). Over the period 1999-2004, R2 ranges from 0.83 to 0.99, and bias varied between -0.012 and -0.04. During the same period, RMSE (root mean squared error), and MAE (mean absolute error) shows that the

model performs with a minimum error. RMSE ranges from 15.73 to 47.62, and MAE ranges from 12.65 to 38.94, which indicates that the model has high accuracy in predicting precipitation at a spatial resolution of 1km. The current model was applied over the period 2005-2014, to assess the spatial distribution of the precipitation at 1km over Morocco.

Table 33: Spatial statistical measurements calculated reduced precipitation and validated against in situ measurements of precipitation from rainfall stations

Statistical metrics	1999	2000	2001	2002	2003	2004
R2	0.83	0.96	0.95	0.97	0.99	0.99
RMSE	47.62	46.93	20.05	42.32	15.73	15.92
Bias	-0.12	-0.09	-0.04	-0.07	-0.02	-0.04
MAE	38.94	44.05	15.59	30.49	12.65	13.82

1.1.2.1. Sensitivity to bioclimatic stages

There is a strong correlation between the product TRMM 3B43 and TSAVI for the humid bioclimatic phase. Indeed, table 25 shows a high R^2 value and a significant p-value for the humid bioclimatic stages. The arid and semi-arid bioclimatic stages have an average R^2 of 0.30. In addition, the semi-arid and sub-humid bioclimatic stages display a lower R^2.

The methodology shows its ability to better represent the product TRMM 3B43 at the humid bioclimatic stage compared to the methodology based on NDVI, namely (Ezzine, 2017). In addition, the model based on TSAVI could slightly improve the evaluation of the product TRMM 3B43 at the Saharan bioclimatic stage.

Table 34: Correlation between TRMM 3B43 and TSAVI, for the five bioclimatic stages over the period 1999-2004

Year	Bioclimatic stage	R2	p-value
1999	Humid	0.76	1.7×10-6
	Sub humid	0.36	0.015
	Semiarid	0.11	0.011
	Arid	0.40	9.5×10-14
	Saharan	0.30	1.8×10-11
2000	Humid	0.85	3.2×10-8
	Sub humid	0.16	0.00072
	Semiarid	0.2	7×10-4

	Arid	0.20	3.6×10-6
	Saharan	0.21	4.5×10-8
2001	Humid	0.80	3×10-7
	Sub humid	0.26	1.2×10-5
	Semiarid	0.11	0.012
	Arid	0.32	8.4×10-11
	Saharan	0.41	1.2×10-8
2002	Humid	0.88	7.1×10-9
	Sub humid	0.36	1.7×10-7
	Semiarid	0.15	0.0084
	Arid	0.27	3.9×10-9
	Saharan	0.22	5.8×10-23
2003	Humid	0.82	1.8×10-7
	Sub humid	0.10	0.017
	Semiarid	0.10	0.012
	Arid	0.22	9.9×10-8
	Saharan	0.43	1.4×10-10
2004	Humid	0.83	10-7
	Sub humid	0.12	0.0052
	Semiarid	0.2	0.00069
	Arid	0.37	1.1×10-11
	Saharan	0.27	3.2×10-10

2. Hydrological modeling

The simulation by the SWAT model consists first in the discretization of the spatio-temporal data; delimitation of the watershed, extraction of the hydrographic effective work.

The second step is the superposition of the soil, land cover and slope data for the construction of the hydrological response units.

23 sub-basins were determined and 467 units of HRU hydrological responses with a threshold of 8% for land use, 10% for soil, 9% for soil.

Sou basin	Surface in m²	Reach length in%	Reach slope in%	Reach depth in%	Min elevation	Maximum elevation
1	34041.87	35746.41	0.72	1.34	469.00	727.00
2	8886.51	6147.46	1.17	0.78	469.00	541.00
3	28074.60	26351.23	0.70	1.24	439.00	624.00
4	29503.44	7912.05	0.52	1.26	439.00	480.00
5	65746.89	5655.66	0.32	1.74	421.00	439.00
6	8793.36	4691.47	0.47	0.78	480.00	502.00
7	61050.51	18425.06	0.36	1.69	402.00	469.00
8	75601.35	4587.35	0.41	1.84	402.00	421.00

9	8464.50	3245.07	1.36	0.77	421.00	465.00
10	13532.67	9152.09	1.15	0.93	480.00	585.00
11	15513.12	11337.12	0.93	0.98	281.00	387.00
12	176 857.83	28044.46	0.43	2.59	281.00	402.00
13	7891.83	1382.76	0.65	0.75	239.00	248.00
14	244283.85	599.12	0.33	2.95	237.00	239.00
15	213275.43	20545.13	0.21	2.79	237.00	281.00
16	269017.20	17369.55	0.16	3.06	211.00	239.00
17	320365.53	2225.51	0.13	3.28	202.00	205.00
18	291510.09	4016.47	0.15	3.16	205.00	211.00
19	30544.29	14632.27	1.05	1.28	237.00	391.00
20	9288.27	5709.70	3.64	0.80	391.00	599.00
21	18519.84	16135.91	1.32	1.05	211.00	424.00
22	17591.58	12209.44	1.32	1.03	391.00	552.00
23	28343.52	28591.08	1.41	1.24	205.00	609.00

SWAT has a database of North American soils, so the soils of the Inaouen basin are integrated and reclassified. Regarding land use, a correspondence was assigned to each type of it.

For the temporal discretization the SWAT model is applied with a daily time step over a period of 1998-2014.

1998-1999	1999-2007	2008-2014
Heater	Calibration	Validation

The monthly evapotranspiration balance is estimated by the Thornwaith method, SWAT has three methods for calculating evapotranspiration (see SWAT components section), the only station that has daily temperature data is the Bab Merzouka station, the spatial resolution is low, and the basin does not have any direct measurement station for it, which is why it was derived from the GLOBAL WEATHER database. The temperature will be used to estimate the evapotranspiration, the coefficient that control its rate should be calibrated afterwards to minimize distortion especially in the spring and winter seasons where the precipitation is less than the potential evapotranspiration.

The parameters that control the evapotranspiration in the SWAT model are;

ESCO: Soil evaporation compensation factor, varies between 0.01 and 1, it manages the margin of the water depth in the soil to meet the need for evapotranspiration, by default it takes a value of 0.95, a reduction of this parameter leads to a reduction in the simulated flow since the quantity of extracted water is added during will be low.

EPCO: Plant uptake compensation factor, varies between 0.01 and 1, defines the margin of the water depth in the soil used by plants the default value is 1, an increased value causes the water to decrease in the layers of the soil is therefore the decrease in flow.

CANMAX: maximum canopy storage is the water storage capacity used by the plant cover, varies between 0 and 100, a high value is reflected by a dense plant cover with high storage capacity, water that will be added by interception to the quantity of water run-off.

GW-REVAP: Groundwater "revap" coefficient varies between 0.02 and 2. This parameter is related to the movement of water from the shallow aquifer to the subjacent layers, a high value means water uptake by evatranspiration.

REVAPMIN: Threshold water level in shallow aquifer for revap to occur, varies between 750 mm and 1000 mm, it is the water depth in mm in the shallow aquifer.
The results of the first simulation are mediocre with a negative Nash coefficient, the calibration is carried out at the level of the sub-watershed 15.

2.1. Sensitivity analysis

Abbasapour et al, 2017 propose two calibration approaches under SWAT CUP;

AAT: All at time, this approach consists in making a global sensitivity analysis of all the parameters to be calibrated at the same time by measuring the margin of variability of each one and its impact on the final results, it takes into account the inter- parametric variation, the major drawback of this approach is the tedious simulation procedure; the high number of iterations necessary to estimate the effect of these parameters, moreover the margin of variation of the parameters can exceed the limit of their interval of variation and lead to theoretically erroneous results but practically accpetable.

OAT: Once at time, this approach only one parameter of the user choice, the others are kept fixed, although this approach is simple and requires only a limited number of iterations, it does not consider the interaction between model parameters.

For the current study, the two approaches were adopted following the procedure described in Abbasapour's paper. (Abbaspour et al. 2015). After the simulation of the output variable under ARC SWAT, the file is transported to SWAT CUP, the parameters to be calibrated are chosen by referring to the bibliographic studies already developed and which aim to determine the most

significant parameters, the ranges of variation of each parameter is determined by the OAT approach, subsequently proceed to the AAT approach with number iterations between 200 and 1000, the best simulation is shown after the calculation of the chosen objective function, the new parameter margin of the best antecedent simulation is attributed again to the parameter and a new iteration is launched until satisfactory results are obtained, to finalize it is necessary to carry out again the calibration of each single parameter as indicated in the Abbas guide,(Abbaspour et al. 2015)

By entering the parameters in SWAT CUP, 3 variation modes are available; r consists in multiplying the parameter by (1 + the given values), a: add the values assigned to the value of the parameter, v: replace the old value of the parameter by the new values assigned during calibration.

N° du paramètre	Paramètre	signification	Valeurs Min	Valeurs Max	Valeurs par défaut	Unités
1	v__CH_K2.rte	Effective hydraulic conductivity in main channel alluvium.	-0.01	500	0	[mm/hr]
2	v__ALPHA_BF.gw	Baseflow alpha factor.	0	1	0.048	[days]
3	v__GW_DELAY.gw	Groundwater delay.	0	500	31	[days]
4	v__GWQMN.gw	Threshold depth of water in the shallow aquifer required for return flow to occur.	0	5000	1000	[mm]
5	v__GW_REVAP.gw	Groundwater "revap" coefficient.	0.02	0.2	0.02	na
6	v__SHALLST.gw	Initial depth of water in the shallow aquifer.	0	5000	1000	[mm]
7	v__DEEPST.gw	Initial depth of water in the deep aquifer .	0	10000	2000	[mm]
8	v__GW_REVAP.gw	Groundwater "revap" coefficient.	0.02	0.2	0.02	na
9	v__REVAPMN.gw	Threshold depth of water in the shallow aquifer for "revap" to occur.	0	1000	750	[mm]
10	v__SOL_ZMX.sol	Maximum rooting depth of soil profile.	0	3500	-999	[mm]
11	r__USLE_K().sol	USLE equation soil erodibility (K) factor.	0	0.65	-999	na
12	v__SOL_ALB().sol	Moist soil albedo.	0	0.25	-999	na
13	v_SOL_K	Saturated hydraulic conductivity.	0	2000	-999	[mm/hr]
14	v_SOL_BD	Moist bulk density.	0.9	2.5	-999	[g/cm3]
15	v_SOL_Z	Depth from soil surface to bottom of layer.	0	3500	-999	[mm]
16	v_SOL_AWC	Available water capacity of the soil layer.	0	1	-999	[mm/mm]
17	r__SOL_BD(1).sol	Moist bulk density.	0	3500	-999	[mm]
18	v__ESCO.hru	Soil evaporation compensation factor.	0	1	0.95	na
19	v__LAT_TTIME.hru	Lateral flow travel time.	0	180	0	[days]
20	v__CH_K1.sub	Effective hydraulic conductivity in tributary channel alluvium .	0	300	0	[mm/hr]
21	v__CH_N1.sub	Manning's "n" value for the tributary channels.	0.01	30	0.014	na
22	v__SFTMP.bsn	Snowfall temperature.	-5	5	1	[°C]
23	v__SMTMP.bsn	Snow melt base temperature.	-5	5	0.5	[°C]
24	v__SMFMX.bsn	Maximum melt rate for snow during year (occurs on summer solstice).	0	10	4.5	[mm/(°C day)]
25	v__SMFMN.bsn	Minimum melt rate for snow during the year (occurs on winter solstice).	0	10	4.5	[mm/(°C day)]
26	v__SNOCOVMX.bsn	Minimum snow water content that corresponds to 100% snow cover.	0	500	1	[mm]
27	v__EPCO.bsn	Plant uptake compensation factor.	0	1	0.95	na
28	v_ESCO.bsn	Soil evaporation compensation factor.	0	1	0.95	na
29	v__SURLAG.bsn	Surface runoff lag time.	1	24	4	[days]
30	v__USLE_P.mgt	USLE equation support practice	0	1	1	na
31	v__LAI_INIT.mgt	Initial leaf area index	0	8	0	na
32	r__CN2.mgt	SCS runoff curve number for moisture condition 2	35	98	-999	na

2.2. CFSR database

Climate data from CFSR are widely used to simulate the hydrological system in watersheds with limited input values, in different regions of the world. (Tomy and Sumam 2016) assess the quality of CFSR data in SWAT simulation of the Karuvannur basin, the results show that it is preferable to use actually measured data, in their absence not to exceed 3 stations. (Kessete, Moges and Steenhuis 2019) claim that CFSR data must be statistically corrected before being used, the study they conducted on the Nile watershed. Another study shows that the quality of validation of the model process by the observed data is better than the CFSR model(Mararakanye, Le Roux and Franke 2020). On the other hand, the studies carried out by this database and applied to the Moroccan watersheds show satisfactory results (Brihet et al, 2016; Fadil et al.,) On the Beht basin, the results were mediocre (Mimich, 2019).

The obtained simulation result for the Innaoune watershed using this database shows as well a unsatisfactory result, the Nash coefficient ranges between -0.28 and -.012.

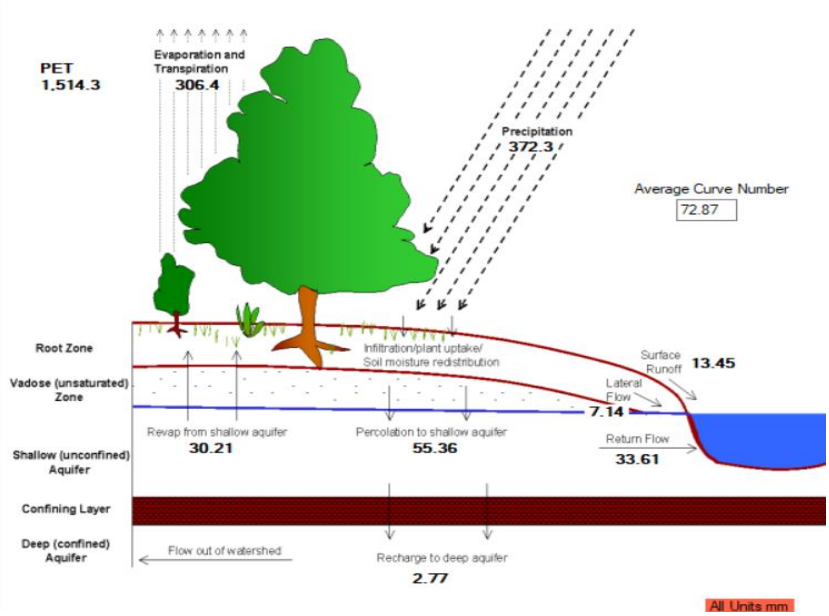


Figure 54: Water balance obtained by the SWAT model using the CFSR database

Month	Average Precipitation in mm	Snow cover in (mm)	Surf Q (mm)	Lat in (mm)	Water intake in (mm)	AND in (mm)	Sed intake in (mm)	PET in (mm)
1	42	0.64	1.74	1.08	8.1	24.55	0.11	47.27
2	49.65	2.53	3.52	1.05	11.73	27.65	0.2	53.29
3	43.41	0	2.17	1.1	12.82	44.99	0.18	99.83
4	37.88	0	0.66	0.7	8.56	45	0.03	122.01
5	28.4	0	0.29	0.51	4.68	49.61	0.02	167.23
6	12.87	0	0.05	0.27	1.28	28.15	0	201.72
7	2.32	0	0	0.13	0.39	9.2	0	242.01
8	6.9	0	0.01	0.09	0.28	6.17	0	217.7
9	18.97	0	0	0.17	0.3	15.24	0	153.22
10	26.82	0	0.15	0.3	0.56	16.11	0	107.76
11	63.88	0	3.7	0.78	4.68	19.26	0.17	58.31
12	38.95	0.65	1.14	0.96	3.61	20.31	0.03	43.68
Sum	372.05	3.82	13.43	7.14	56.99	306.24	0.74	1514.03

The average annual precipitation of the Inaouen watershed calculated from the observed data is in the order of 597 mm, the one calculated by the CFRS data is in the order of 372 mm, it is almost halved, which explains the major difference between the simulated flow rates.

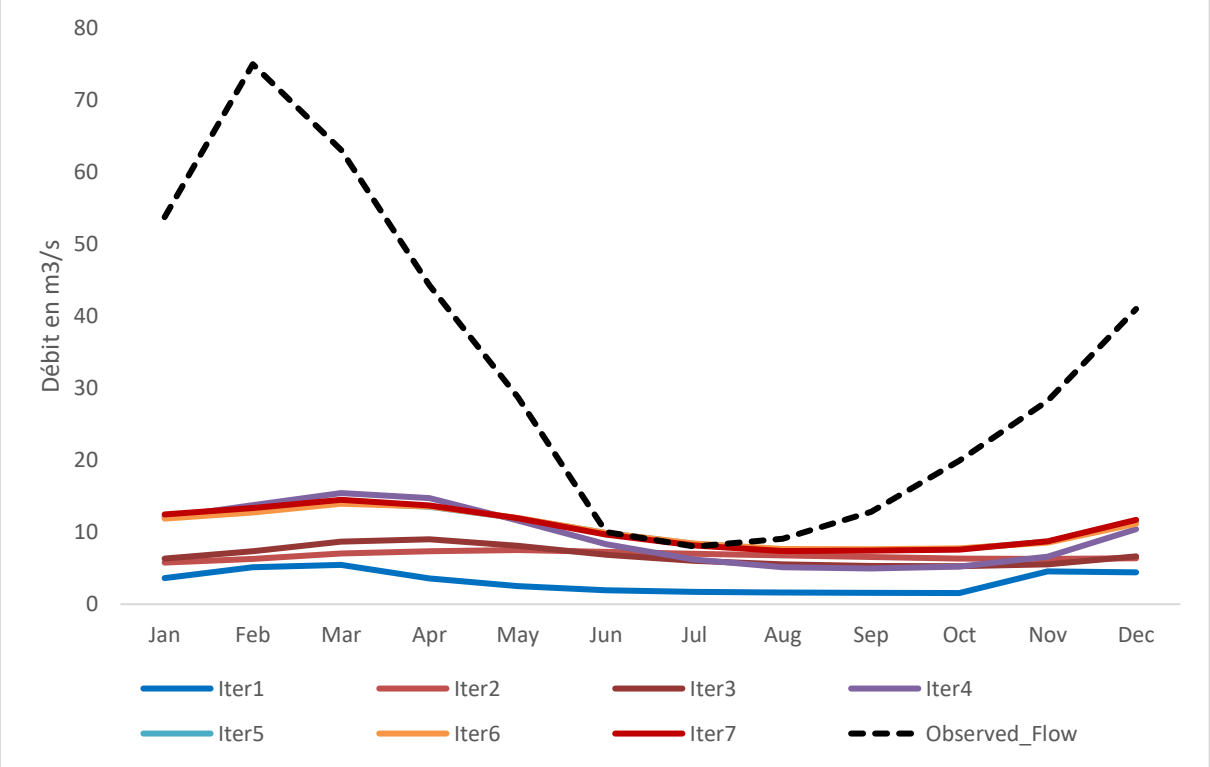


Figure 55: graph of a comparison between the observed average monthly flows and that obtained by the different iterations using the CFSR database

2.3. Simulation using observed data

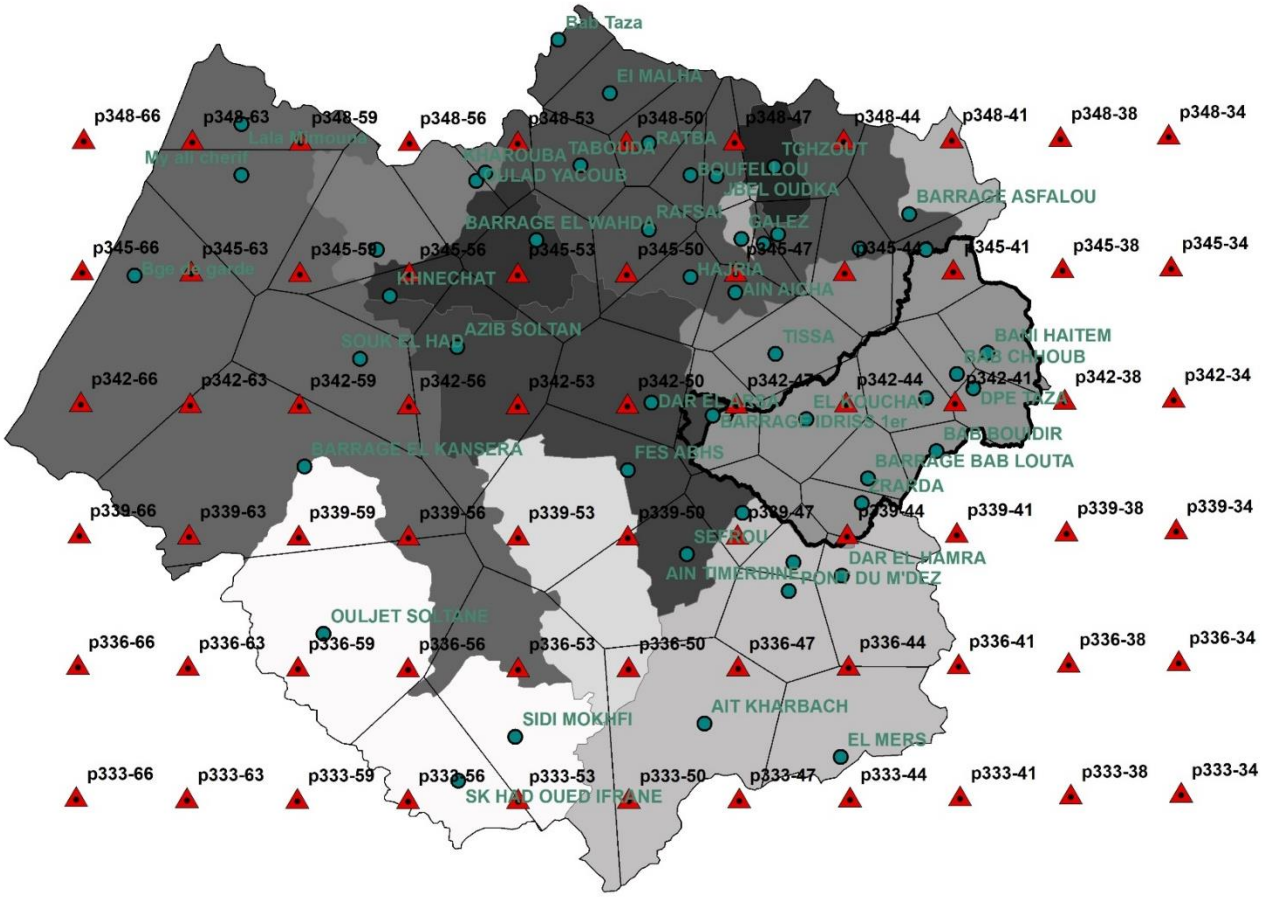


Figure 56: Location of stations in the CFSR database and data observed in the Sebou watershed

The first step is to determine 4 stations from the CFSR database that surround the observed stations used, as shown in the following table;

Observed Station	CFSR stations
Bab Merzouka	P342-44, P342-41, P339-41, P339-44
Idriss Premier	P342-44, P342-47, P339-44, P339-47
Zrarda	P342-44, P342-41, P339-41, P339-44
Bni Haitem	P345-41, P345-38, P342-41, P342-38

2.4. Simulation results with observed data

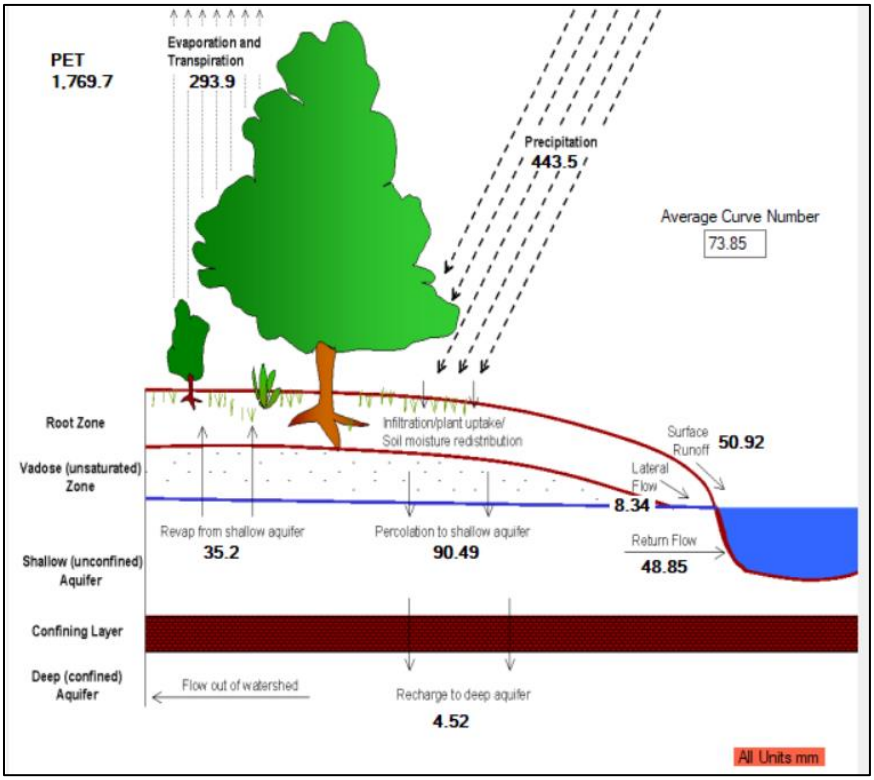


Figure 57: The initial water balance of the Inaouen watershed

This figure shows the initial water balance for the Inaouen catchment, compared to the water balance generated by using the CSRF database there is a clear increase in the amount of lateral flow by around 27 mm, so the recharge of the shallow and deep aquifer is almost double.

2.5. Sensitivity analysis

2.5.1. AAT approach

We used the same parameters simulated with the CFSR data, with successive iterations of 50, 100, 200, 500, 700 on SWAT CUP using the SUFI 2 algorithm, the most sensitive parameters were selected for OAT calibration.

Table 35: Parameter values obtained by the different iterations of the AAT approach

	P-Factor	R-Factor	R^2	NS	BR^2	MSE	SSQR	PBIAS	KGE	RSR	MNS	Min-sim	StdDev-Sim
Iteration 01	0.2	1.64	0.01	-0.43	0.0002	3.10E + 02	2.50E + 02	-214.8	-1.43	1.2	-1.51	11.5	5.03
Iteration 02	0.29	1.94	0	-0.24	0.0001	2.70E + 02	2.30E + 02	-147	-0.88	1.11	-1.03	8.67	4.19
Iteration 03	0.97	1.07	-1	-0.06	-1	2.30E + 02	2.30E + 02	-100	-1	1.03	0.2	0	0
Iteration 04	0.69	0.94	0	-0.44	0	3.20E + 02	2.40E + 02	-217	-1.45	1.2	-1.48	11.13	5.91
Iteration 05	0.96	0.96	0	-0.36	0.0001	3.00E + 02	2.30E + 02	-185	-1.18	1.17	-1.27	10	5.26

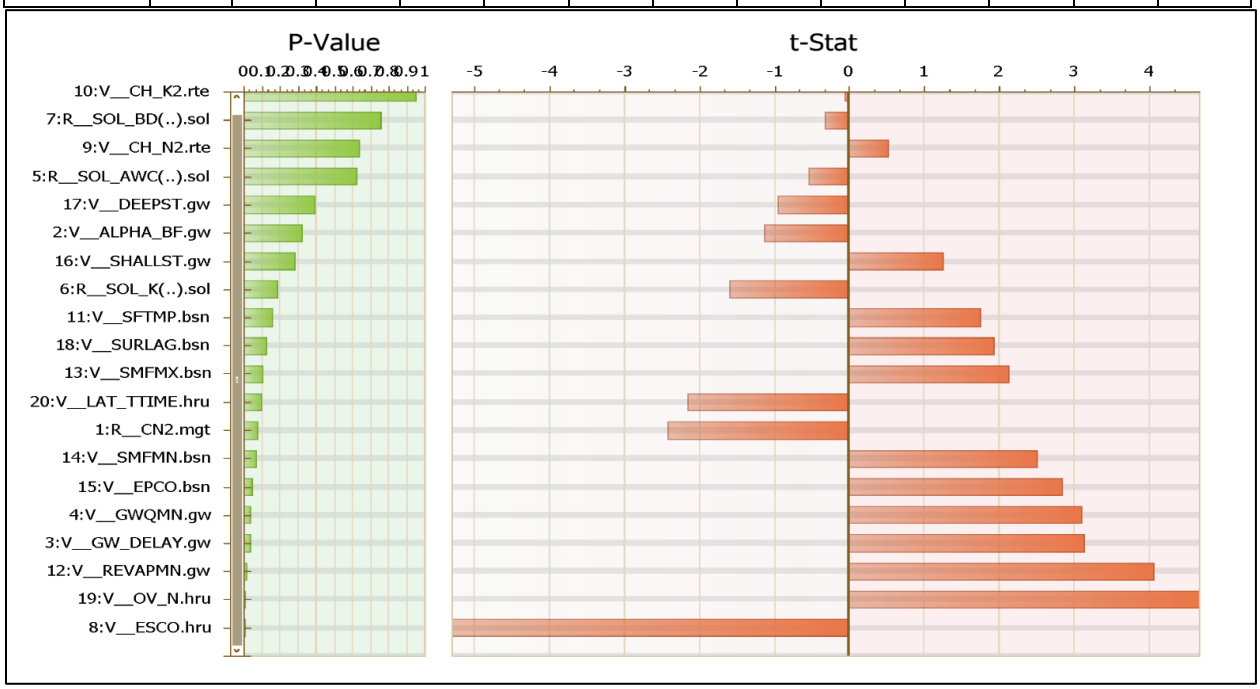


Figure 58: Results of the sensitivity analysis

The figure shows the hierarchy of the different parameters according to the p-value and the t-stat, the significant parameter is the one with the lowest p-value and the highest t-stat. In the case of the Inaouen catchment, the REVAPMN parameter has a great influence.

- Initials runoff SCS curve number for moisture condition 2 (CN2),
- Groundwater "revap" coefficient (GW_REVAP),
- Threshold depth of water in the shallow aquifer required for return flow to occur (GWQMN),
- Threshold depth of water in the shallow aquifer for "revap" to occur (REVAPMN),

- Baseflow alpha factor for deep aquifer (ALPHA_BF),
- Manning value for the main channel (CH_K2),
- Soil evaporation compensation factor (ESCO),
- Plant uptake compensation factor (EPCO)
- Manning's “n” value for land flow (OV_N)

2.5.2. One at time simulation

The calibration period considered for this approach is 1/1 / 1998-31 / until 12/2007 with one year for the warmup, each parameter was evaluated separately by 20 iterations. As already indicated, the choice of parameters depends on the results of the study previously carried out as well as the results of the overall sensitivity analysis.

According to the first simulation, the Inaouen is too sensitive to the parameter related to the groundwater.

The GW-REVAP parameter which varies between 0.02 and 0.2 controls the capillary movement of water from the deep-water table to the upper layers, the closer its value to 0.2 the greater the capillary movement and therefore the evapotranspiration is high.

REVAPMN manage the threshold of water movement from the surface aquifer to the unsaturated zone, movement is only possible if the height of the water in the aquifer in mm is greater than or equal to that already fixed. The parameter varies between 0.1 and 500, if for example the height of the water in the surface water table is 250 mm, the upward movement is only possible for a value of REVAP equal to or greater than 250 mm.

GWQMN determines the height of the water required to initiate the base flow.

GW_DELAY defines the time necessary for water to move from the root zone of the shallow aquifer to transform into base flow (percolation time), it varies from 0 to 500 days.

The surface runoff coefficient governs the runoff as a function of the concentration time. The water reaches the point furthest from the watershed within a time specified by the concentration time, if the drained area is large as in the case of the Inaouen watershed, the time in which the water arrives at the outlet exceeds one day, the SWAT model considers the water that does not reach the outlet as a temporal reservoir governed by the SURLAG parameter which controls the fraction of water

to be released to reach the outlet in a day. If its value is high, the fraction of water flowing will also be high, which will lead to an increase in the flow rate.

Evapotranspiration is controlled by the plant and soil evapotranspiration compensation factors EPCO and ESCO, these two parameters control the amount of water evapotranspirated and depend on the soil depth and the density of the vegetation cover.

CN2: the parameter of the curve number strongly influences the outflow, an increase in the parameter leads to a reduction in the surface flow, according to the lithological map of the basin the Rif part is dominated by clays and therefore a high flow.

CH_K2 or hydraulic conductivity of the bottom of the watershed, this parameter is linked to the routing of the watershed notably influences the flood hydrograph.

2.6. Calibration

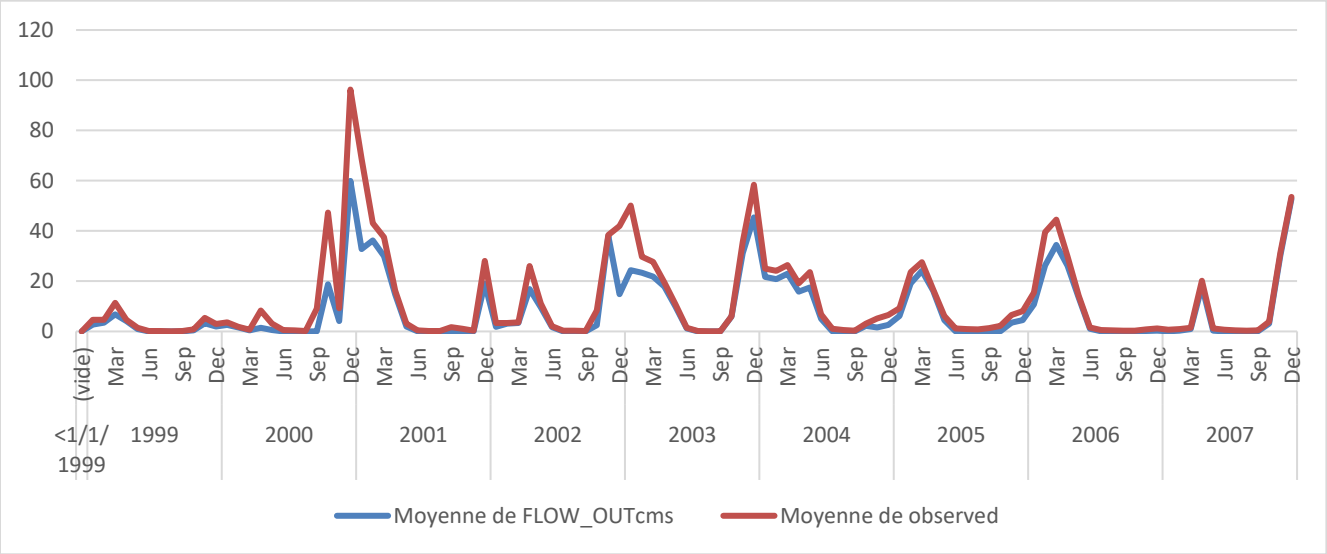


Figure 59: Comparison between observed and simulated flow rates for the 1999-2007 calibration period

The hydrograph shows the variation of the flows grouped in monthly averages as a function of time. The blue curve represents the observed flows, red the simulated ones. Visual examination indicates that the model reproduces the general appearance of the flow variation as well as the seasonal irregularities. Note that the model overestimates the outflows which can be explained by the distorted distribution of the rain, especially the infiltration water in the karst areas and the evapotranspired part.

The initial model shows negative Nash results and underestimates the observed flows.

2.7. Model validation

The validation step consists of running a new simulation using the parameters retained during the calibration and introducing them to the model using new data series, in this case the considered validation period ranges from 01/01/2008 until 07/31/2014.

According to the Moriasi evaluation criteria (Tab. 25) the results of the model validation are not satisfactory. The peaks are underestimated by the model, especially for the year 2010 which experienced significant amounts of precipitation.

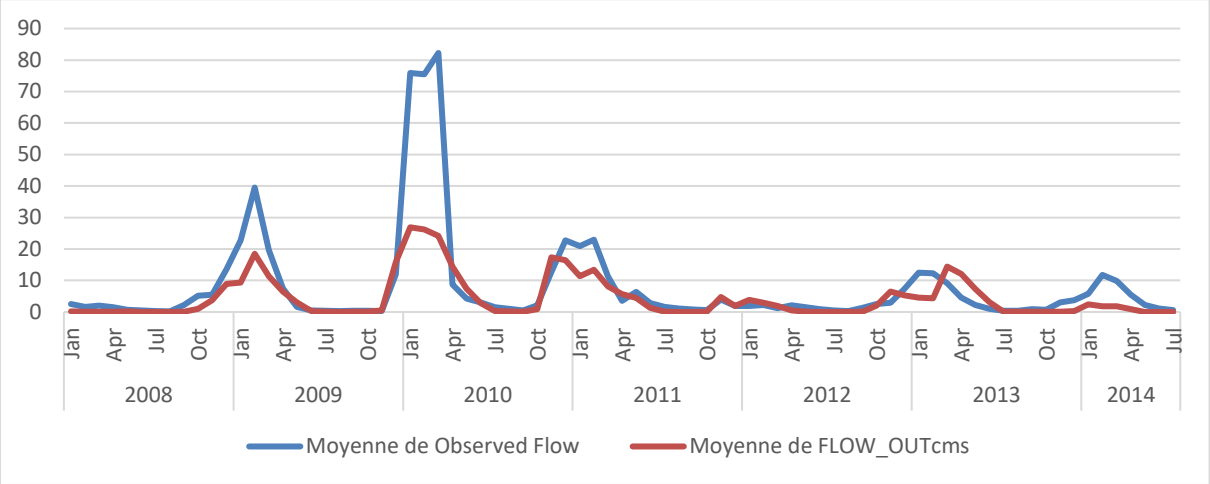


Figure 60: Comparison between observed and simulated flows for the 2008-2014 validation period

Table 36: Evaluation criteria of the simulation

	NSE	PBIAS	RMSE Standard	RSR
Calibration	0.53	16.4	4	0.68
Validation	0.49	30	27.56	0.79

2.8. Discussion

The SWAT model was performed on the Inaouen watershed. Two climatic data bases were tested, the first is the CFSR data base, the second comes from the observed stations.

The physical conceptualization of the watershed is made through the DEM of the land, the soil map and the land use map as well as their metadata, indicating the properties of the land. The calibration and the validation of the model are carried out by the observed flows of the Bab Merzouka station over the periods going from 1998-2007 for the calibration and from 2008-2014 for the validation.

The results of the first simulation using the CFSR database are not satisfactory, the latter underestimates the rainfall observed, and therefore the outflows were low. A correction must be made before their use, especially for pools with contrasting climate.(Kessete, Moges and Steenhuis 2019) Propose a methodology for correcting these data, it consists in projecting the CFSR stations with the stations of the observed data, by using linear scale, the grid which indicates the strongest correlation coefficient is selected for the correction of the Bias .

The model was run again using the same soil and land cover databases, with observed precipitation data. The first simulation shows an improved results compared to the previous one (a Nash of 0.43 without calibration). The default simulation is transferred to SWAT CUP to process the sensitivity analysis by both AAT and OAT approaches.

The parameters that most impact the outputs are (CN2), (GW_REVAP), (GWQMN), (REVAPMN), (ALPHA_BF), (CH_K2), (ESCO), (EPCO) and (OV_N). The sensitivity of the model to these parameters confirms the results of certain studies already carried out (Abdelhamid Fadil1 et al., 2011), (White and Chaubey, 2005), (Yassine Bouslihim et al., 2016).

Iterations of 10, 50, 100, 500 and 700 have been processed, the parameters of the best simulation are retained for validation.

The methodologies used for the representation of the land part as well as the routing of the model are; Soil Conservation Services SCS and the Muskingum method.

The hydrograph shows that the model reproduces the general pattern of flow variation. But sometimes it underestimates the observed flows, for example in the calibration period the maximum simulated flow in 03/09/2010 with a value of 883 m3/s, while it reaches 1000m3/s fot observed flow. According to a study, which tested the model's ability to simulate water patterns, SWAT tended to under-predict in dry soil conditions (Mapfumo et al., 2011). High peak flows can be explained by HORTONIAN precipitation. When the precipitation intensity exceeds the infiltration capacity. Thus, the model underestimates the flow especially for drought periods, which may be due to a faulty estimation of the base flows. And the fraction of water added to the stream by the resurgence of karst formations. The abundance of olive cultivation and agricultural activities in the central and southern part of the catchment (see land use map), implies an intensive

abstraction of water from the Taza aquifer as well as private irrigation water contributing to the base flow.

In general, the correlation between observed and simulated daily flows is quite acceptable, according to (Van Liew et all, 2007). However, the results could be improved by reducing the uncertainties.

In general, the correlation between observed and simulated daily flows is well established, according to (Van Liew et all, 2007). However, the results could be improved by reducing the uncertainties.

These are due to conceptual simplifications (e.g. number of SCS curves method for flow distribution), processes occurring in the catchment but not included by the program (e.g. water erosion), processes included in the program, but their occurrence in the catchment is unknown to the modeler or unexplainable due to data limitations (e.g. dams and reservoirs, water transfers, agricultural management affecting water flow) and the quality of the input data (Abbaspour et al. , 2015).

Altitude is a factor that should not be neglected. The number of stations used for the modeling does not cover the altitudinal variation of the study area, especially as the parameter varies widely from upstream to downstream, so the inhomogeneity of the allocation of hydrological and hydrometric stations is reflected by the suboptimal performance of the model.

3. Deficit Irrigation

3.1. Evapotranspiration :

Figure 61 shows the monthly evapotranspiration data retrieved from MODISA16, using Google Earth Engine, over the period 2008-2019, in the Middle Sebou and Inaouen Downstream. The temporal variation of the evapotranspiration along each year is evident, mostly when we compare the rainy months against the driest ones. The peak evapotranspiration data are observed during the rainy months, especially March, April, and May. However, the minimum evapotranspiration values are observed during the driest months, July and August. During the period ranging from 2008 to 2019, the highest evapotranspiration was observed in March 2017 with 904.47 mm. However, the minimum evapotranspiration value was observed in July 2016, with 25.24 mm. The mean value of evapotranspiration during the same period is 220 mm, with a standard deviation of

167.38. The variation of evapotranspiration values from March to May is not significant because the precipitation from January to April keeps the soil moisture content. During the period ranging from August to December, vegetation presents the lowest evapotranspiration values, due to the highest fractions of the available energy used as sensible heat fluxes (H) (Antônio et al., 2013; Yang et al., 2016). Evapotranspiration is strongly correlated with surface soil moisture (Kurc & Small, 2004). In arid and semiarid regions, the evapotranspiration is limited by soil moisture (Rodriguez-Iturbe, 2000). (Shen et al., 2017) found that transpiration is high where the climate is more humid, and there is a great canopy. Moreover, (Shen et al., 2017) shows that the peak of evapotranspiration retrieved by MODIS sensor, over in Australian Semi-Arid and Arid Basins, occurred in January to May. Hence, under dry conditions, the vegetation closes its stomata, limiting its transpiration and photosynthesis. The same result was found by (Antônio et al., 2013).

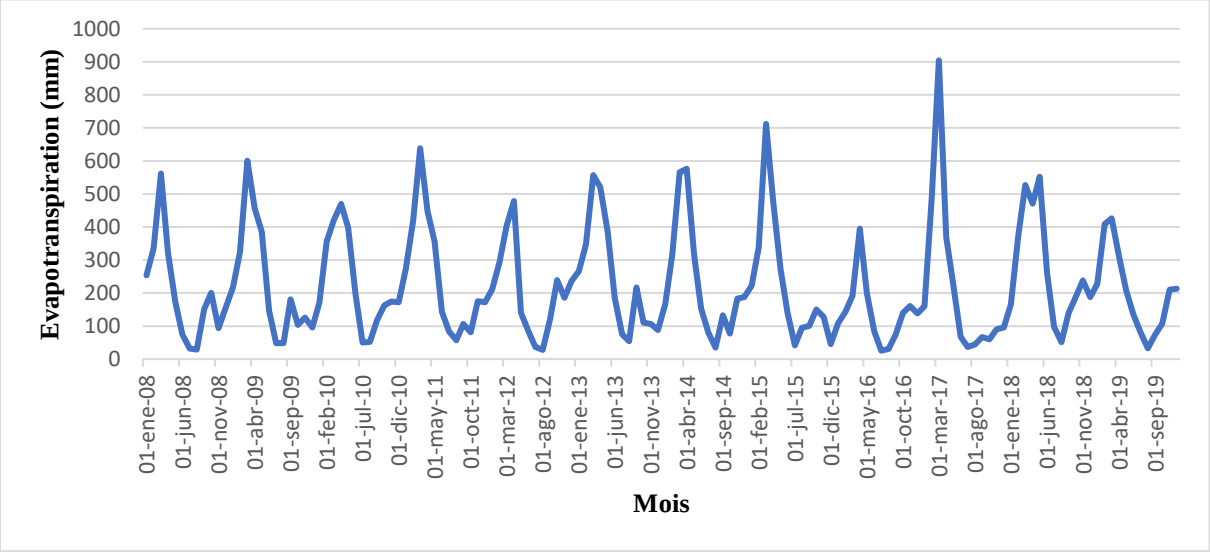


Figure 61: Monthly evapotranspiration derived from MODISA16 over the period 2008-2019

3.2. Irrigation deficit:

Figure 62 points out the variety of gross water requirement per hectare over the period 2008-2019. The visual examination of Fig 6 shows that the peak of the gross water requirement per hectare is observed during the rainy months, especially March, April, and May. The minimum gross water requirement values are observed during the driest months, especially in July and August. During the period ranging from 2008 to 2019, the highest gross water requirement was observed in March 2017 with 457.3 mm. However, the minimum gross water requirement value was observed in July 2016, with 8.9 mm. The mean value of gross water requirement during the same period is 97.1

mm, with a standard deviation of 81.91. Fig 7 presents the variation of the irrigation water crop requirement per hectare over the period 2008-2019. As expected, the peak of the irrigation water crop requirement per hectare is observed during the rainy months, especially March, April, and May. The minimum irrigation water crop requirement values are observed during the driest months, especially in July and August. The highest irrigation water crop requirement was observed in March 2017 with 440.5 mm. However, the graph shows there are months were the rainfall covers more than the gross water requirement, with an observed maximum surplus of 162.4 mm, in October 2018. Covering the gross water requirement through rainfall provides enough water storage in the olive trees' root zones, which can maintain their continuous vegetative developments. The fact that the rainfall covers more than the gross water requirement in some months can urge the decision-makers or the farmers to firstly not irrigation during these months and to think about rainfall harvesting, to overcome crop water requirement during the drought periods.

Furthermore, the mean value of gross water requirement during the same period is 65.4 mm, with a standard deviation of 78.66. The visual examination of Fig 8 shows that deficit irrigation could reduce the irrigation water requirement, especially during April, Jun, July, August, September, October, and November. During the period ranged from 2008 to 2019 the highest irrigation water requirement, for the 2500 ha, under deficit irrigation was observed in March 2017 with 11 million m3 per month, the graph shows there is some months were the rainfall covers more than the gross water requirement, with an observed maximum surplus of 5.2 million m3 per month, in October 2018. The mean value of irrigation water requirement under deficit irrigation during the same period is 1.2 million m3 per month, with a standard deviation of 2. Fig 9 presents the amount of water-saving over the period ranging from 2008 to 2019. Applying deficit irrigation can afford water saving up to 0.4 million m3 per month, with an annual average of five million m3. The water-saving based on deficit irrigation, conducted over the current study goes hand on hand with previous studies, which recommended deficit irrigation (Abdelkhalik et al., 2019; Anabela Fernandes-Silva et al., 2018; Chai et al., 2016; El Jaouhari et al., 2018; Fereres & Soriano, 2007; Mandal et al., 2020; Marra et al., 2016; Ozer et al., 2020; Sabri et al., 2017; Tinoco et al., 2016; Wahba, 2017).

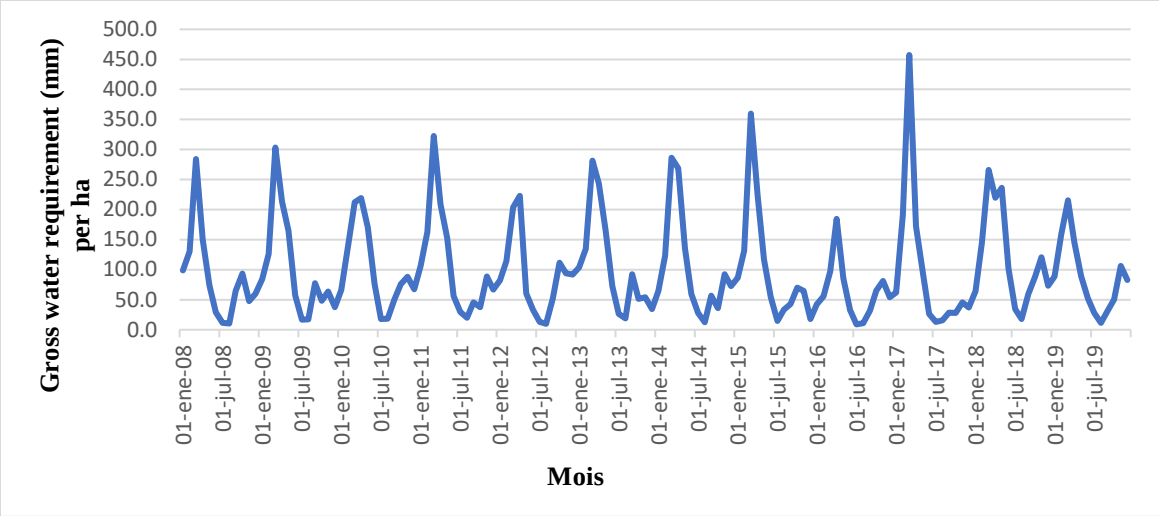


Figure 62: Gross water requirements (mm) per ha, over the period 2008-2019

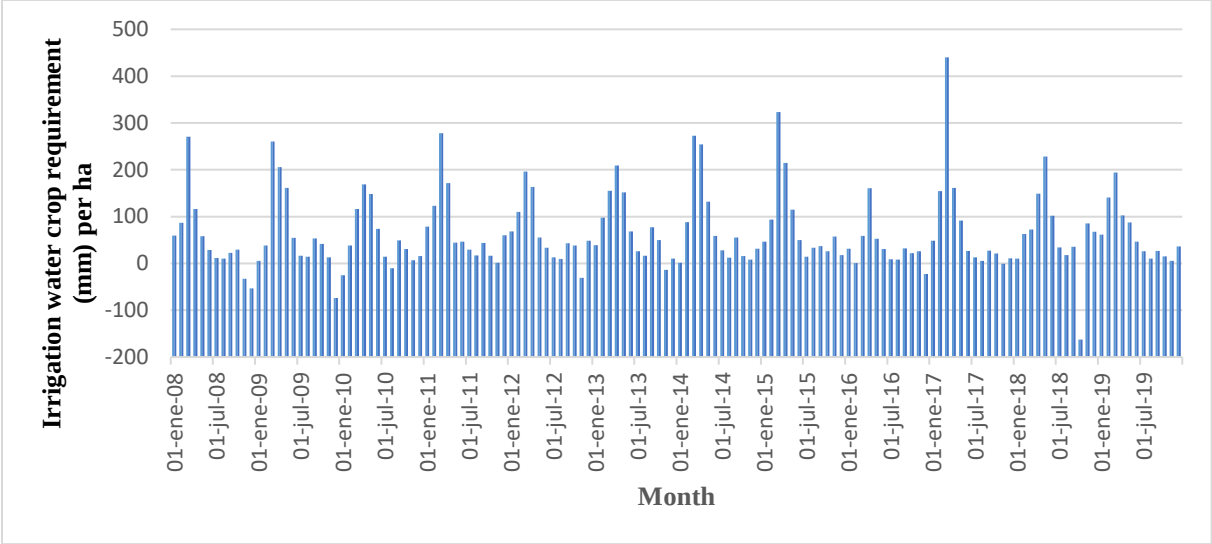


Figure 63:Irrigation water requirements (mm) per ha, over the period 2008-2019

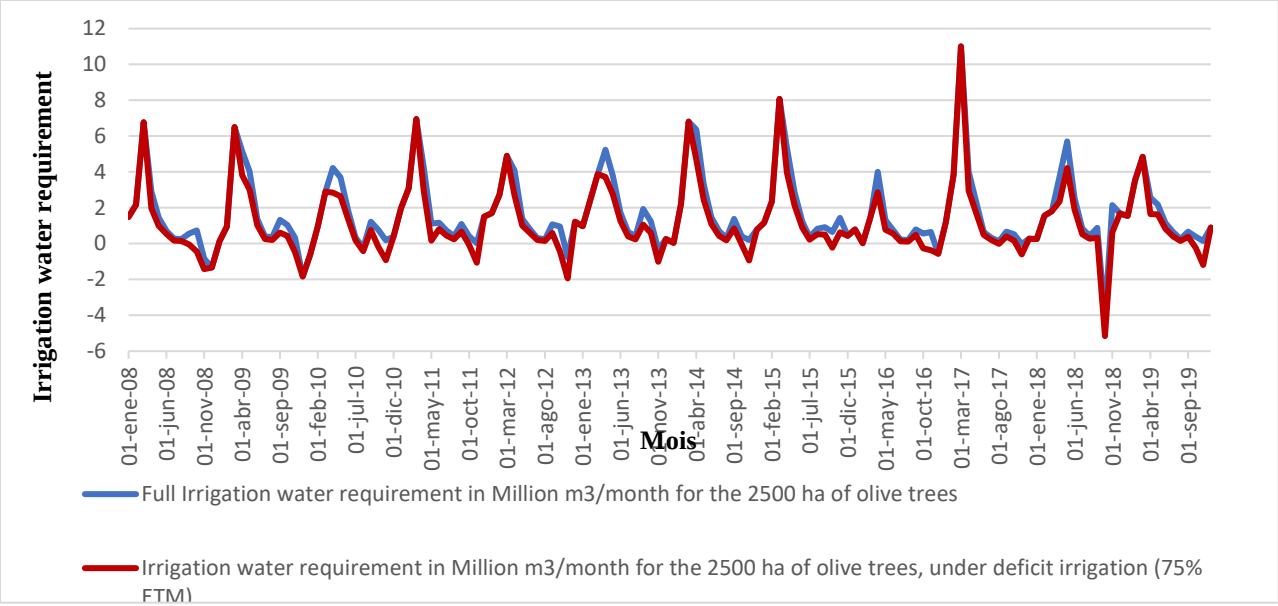


Figure 64: Variation in irrigation water requirements in the event of complete irrigation and irrigation deficit, over the period 2008-2019

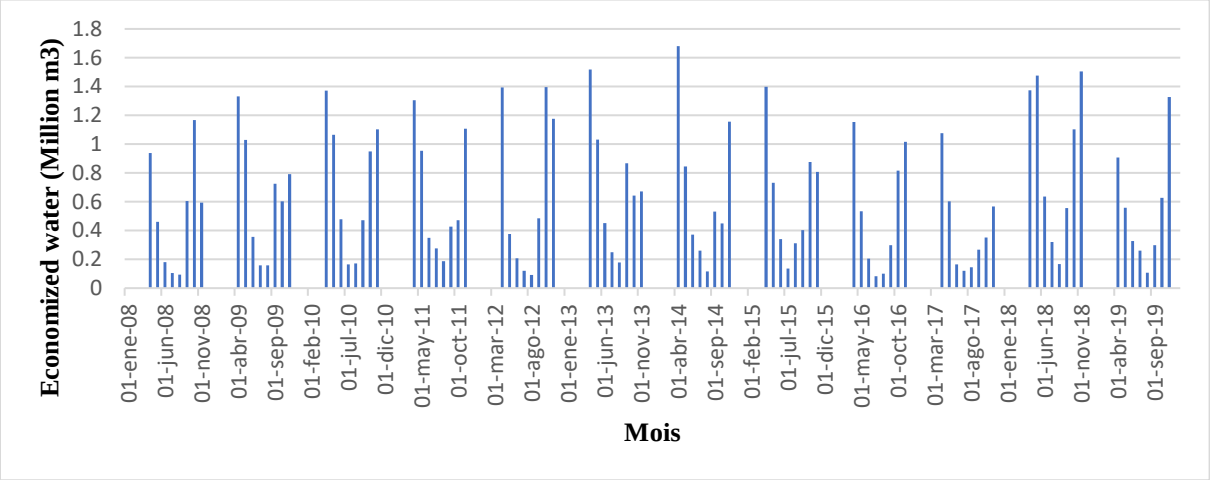


Figure 65: Water saved thanks to the deficit irrigation applied over the period 2008-2019

3.3. Water use efficiency and water productivity

Figure 66 shows the annual variation in water use efficiency per hectare over the period 2008-2019 with full irrigation supply and deficit irrigation. Visual examination shows that the peak water use efficiency per hectare for complete irrigation and deficit irrigation is 1.46 kg / m3 and 2.28 kg / m3, respectively. However, the minimum water use efficiency values per hectare for the two scenarios are 0.58 kg / m3 and 0.63 kg / m3. The average value of water use efficiency per

hectare is 0.81 kg / m3 and 1.06 kg / m3, which is a standard deviation of 0.24 and 0.46. As expected, deficit irrigation can improve water use efficiency by an average of 0,

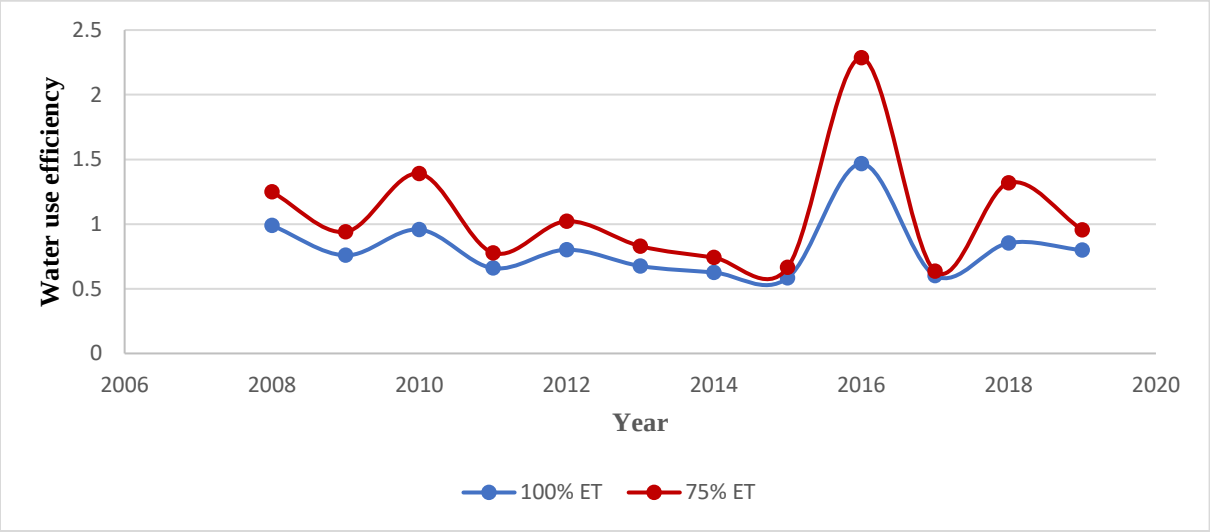


Figure 66: Water use efficiency under full irrigation supply and deficit irrigation, over the period 2008-2019

Figure 67 shows the annual variation in water productivity per hectare over the period 2008-2019 with complete irrigation and irrigation deficit. The peak water productivity per hectare for complete irrigation and deficit irrigation is respectively 3.10 Dh / m3 and 4.84 Dh / m3. However, the minimum values of water productivity per hectare for the two scenarios are 1.23 Dh / m3 and 1.34 Dh / m3. The average values are 1.72 Dh / m3 and 2.26 Dh / m3, with a standard deviation of 0.52 and 0.97. As expected, deficit irrigation can improve water productivity by an average of 0.54 Dh / m3.

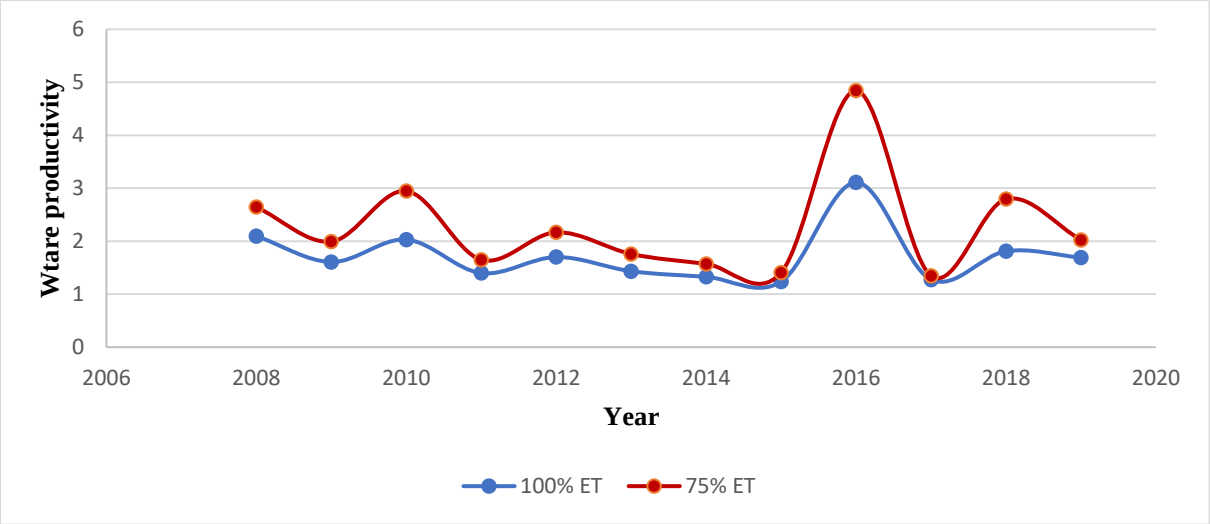


Figure 67: Water productivity under full irrigation supply and deficit irrigation, over the period 2008-2019

General conclusion

The study offers a comprehensive approach to address the problems associated with water scarcity. The main problem faced is the acquisition of data, the gauging stations observed do not provide a high spatio-temporal coverage, the satellite provides a wide range of data in several areas (climatic data, data on water quality. ..), therefore the problem to be solved is the spatial resolution and the correction of the biases. The downscaling method has been used successfully - in several studies - to generate data at better resolution. Once the climate data has been generated, it could be used to carry out studies (modeling of precipitation, forecasting future changes, etc.), and to define strategies for the management of

In the first part of this study a new model of precipitation reduction was developed, considering the bioclimatic zoning. The downscaling model is based on TSAVI, DEM and distance from the sea. The study was carried out on Morocco. In this part the product TRMM 3B43 1999-2014 was used. The evaluation of the relationship between the model components and the TRMM 3B43 product is performed using a stepwise regression based on the AIC criterion and the Mallows Cp indicator, as a machine learning technique. The results show a significant correlation between the products TRMM 3B43 and TSAVI with an R^2 ranging from 0.7 to 0.88. The other environmental factors, namely the DEM and the distance from the sea, improved the performance of the model.

In addition, the Adjusted Vegetation Index on transformed soil (TSAVI) improved the downscaling model on the Humid and Saharan bioclimatic stages due to its ability to reduce soil luminosity with an average R^2 of 0, respectively, 82 and 0.30. The statistical parameters RMSE, MAE and bias show that the reduced and calibrated precipitation corresponds better to the precipitation data measured in situ.

The second part is focused on hydrological modeling to test the applicability of the SWAT model on the Inaouen basin and also to understand its hydrological functioning to make future predictions.

In this study, the distributed SWAT model was applied to the Inaouene watershed, to test its ability to simulate large-scale hydrological behavior. The DEM, land use, soil maps were introduced under ARC SWAT to conceptualize the morphometric parameters of the basin. One year was used for the model warm up, the calibration was carried out over a period of 8 years, 4 was used for the

validation. The simulation results are not very satisfactory, this can be explained by the presence of karsts which constitute a temporary reservoir contributing to the supply of the water yield, calibration problems can also be due to the quality of the observed flows.

The third part proposes an approach to overcome the consequent problems of climate change, it is subdivided into two sub-parts; the first is focused on the extraction of monthly evaporation data from MODIS16A2 under Google Earth Engine (GEE), data used in the second part of the study, which aims to assess the efficiency of deficit irrigation on a plot of 2,500 olive trees. This theoretical study is applied to the downstream perimeter of Middle Sebou and Inaouen.

The irrigation water requirement was estimated between the evapotranspiration and adequate rainfall (Pe). The assumption was the ability of the deficit irrigation to economize water and provide a good crop in term of quality and quality.

The study first deal with the problem of data acquisition, the evapotranspiration parameters is mandatory for carrying it out, the problem encountered with this data is the absence of the monitoring station that provide temperature, and even if available the spatial and temporal resolution are low, the processing of MODIS data under the Google Earth Engine provides the required data. The obtained results show that under deficit irrigation condition 17% of the total used water could be saved, and then reduce the water irrigation supply by an average of 5Mm3, a slight decrease in olive production was noted and estimated as 0.5t/ha. The obtained result is aligned with the previous studies. For instance (Liu et al., 2013), assessed the crop water requirement and discuss the suitable irrigation system for two different regions; Tibet and China, the results claim that sustainable irrigation systems may be more successful to deal with water deficit drawbacks, another study was processed by (Zhou et al., 2018), it aims to compare two irrigation system; sprinkler and drip irrigation on a potatoes yield, the results underline that the drip irrigation provides a significant result in term of water-saving comparing to sprinkler irrigation which moreover causes the nitrate leaching and re-introduces the agriculture process in nexus; pollutants generator- damaged sector. Other study was carried out on the same, it aims to evaluate the agro-physiological response of potato in the plain of Sais (Morocco), the used methodology consisted of implementing an experimental plot and apply three irrigation regimes the 100%, the 75% and the 50% of crop evapotranspiration, the obtained results claimed that the

best agronomic water use efficiency was recorded for irrigated treatments at 75% of Etc (El Bergui et al., 2020).

Theoretically the obtaining result are satisfactory, however, to transpose the paradigm to practice, and guarantee a successful deficit irrigation, a good knowledge of the physiologic characteristic of the crop and the soil texture is required. Every type of crop has a defined needed amount of water, the available water of a plant refers to a difference between water content at field capacity and water content at permanent wilting point which is the minimum amount of water that a plant requires to wilt, then if the provided water is below this value the plant loss turgidity and wilt. Concerning the soil, in a sandy soil most of percolated water is infiltrated, and the loam soil generally dispose of a greater water capacity due to its texture. Then, to adopt the DI as a global strategy an inventory of the suitable crops to DI should be established, according the to the Food and Agriculture Organization (FAO, 1979), crops that are less sensitive to the DI are those with a short growing season with high tolerance to drought. The application of the technic on crops that need a humid condition and high-water amount during all the growth cycle maybe less to not suitable for it.

The current study goes together with the Moroccan generation Green Plan of water-saving. The deficit irrigation is a good alternative to enhance irrigation water efficiency considering the hydrologic conditions, especially evapotranspiration. In economic terms, the result shows that with deficit irrigation, the decision-maker, or the farmer could save about 5 million m3 per year, which is a boost to the global economy if the method is transposed and applied to other Moroccan regions.

Futures perspectives.

The present study comes within the framework of the management of water resources. The results obtained can be used by decision makers to define appropriate management strategies. They can also be considered as a support for the national strategy for sustainable development (SNDD). The latter reflects the fundamental visions for the construction of a new model of society, the economic, social, and environmental leveling, the establishment of the foundations as well as the constitutional reforms and the operationalization of sustainable development. However, other aspect must be investigated to improve the quality of the proposed approach:

- The integration in the model of the contribution of irrigation part in the total water yield.
- Investigation of the water quality and make a coupled qualitative and quantitative model
- The development of soil and land use maps with good resolution to both update existing data and improve the quality of the model
- Integration of climate scenarios and variation in land use to make future predictions.
- Develop other downscaling models adapted to the Moroccan climatic context by integrating other indicators to reduce errors.
- Carry out a practical evaluation of the efficiency of the deficit irrigation and transpose the methodology to other regions.
- In terms of water security, the country still has to address the problems of water scarcity, it should integrate all dimensions of sustainability and combine economic progress with environmental protection, involving public and semi-public authorities (National Drinking Water Office), private companies for the elaboration of technical studies, the international development institution (World Bank) and the most important investments in scientific research that contribute to provide advanced tools in terms of water management. As well as designing the concept of sustainable cities.

References

Abbaspour, k.c., JOHNSON, C.A. and VAN GENUCHTEN, M.T., 2004. Estimating Uncertain Flow and Transport Parameters Using a Sequential Uncertainty Fitting Procedure. Vadose Zone Journal, vol. 3, no. 4, pp. 1340–1352. ISSN 15391663. DOI 10.2136/vzj2004.1340.

Abbaspour, k.c., 2008. SWAT Calibration and Uncertainty Programs.

Abbaspour, k.c., yang, j., maximov, i., siber, r., bogner, k., mieleitner, j., zobrist, j. And srinivasan, r., 2007. Modelling hydrology and water quality in the pre-alpine/alpine Thur watershed using SWAT. Journal of Hydrology, vol. 333, no. 2–4, pp. 413–430. ISSN 00221694. DOI 10.1016/j.jhydrol.2006.09.014.

Abbaspour, k.c., rouholahnejad, e., vaghefi, s., srinivasan, r., yang, H. and KLØVE, B., 2015. A continental-scale hydrology and water quality model for Europe : Calibration and uncertainty of a high-resolution large-scale SWAT model. Journal of Hydrology [en línea], vol. 524, pp. 733–752. ISSN 0022-1694. DOI 10.1016/j.jhydrol.2015.03.027. Disponible en: http://dx.doi.org/10.1016/j.jhydrol.2015.03.027.

Abbaspoura K.C. Srinivasanb R. Yanga H. &Kløved B. (2015). A continental-scale hydrology and water quality model for Europe: Calibration and uncertainty of a high-resolution large-scale SWAT mode. Journal of hydrology page 733-752

Abbaspour, k.c., 2015. SWAT - CUP SWAT Calibration and Uncertainty Programs, A User Manual. Eawag Aquatic Research. S.l.

Abdelhamid Fadil, Hassan Rhinane, Abdelhadi Kaoukaya, Youness Kharchaf, Omar Alami & Bachir. (2011). Hydrologic Modeling of the Bouregreg Watershed (Morocco) Using GIS And SWAT Model, Journal of Geographic Information System, 2011, 3, 279-289 doi:10.4236/jgis.2011.34024

Abdelkhalik, A., Pascual, B., Nájera, I., Baixauli, C., & Pascual-Seva, N. (2019). Deficit irrigation as a sustainable practice in improving irrigation water use efficiency in cauliflower under Mediterranean conditions. *Agronomy*, *9*(11). https://doi.org/10.3390/agronomy9110732

Abdulrazzak, M., Elfeki, A., Kamis, A., Kassab, M., Chaabani, A., & Noor, K. (2019). Flash flood risk assessment in urban arid environment : case study of Taibah and Islamic universities ' campuses , Medina , Kingdom of Saudi Arabia. Geomatics, Natural Hazards and Risk, 10(1), 780–796. https://doi.org/10.1080/19475705.2018.1545705

Africa, North, Royaume Maroc, Implementing Mitigation, and Of Water Scarcity. 2014. "Drought Management in Morocco."

Ahmadian, N., Demattê, J. A. M., Xu, D., Borg, E., & Zölitz, R. (2016). A New Concept of Soil Line Retrieval from Landsat 8 Images for Estimating Plant Biophysical Parameters. Remote Sensing Article. https://doi.org/10.3390/rs8090738

Agostinelli, C. (2002). Robust model selection in regression via weighted likelihood methodology. 56, 289–300.

Aguilar, A. L., Flores, H., Crespo, G., Marín, M. I., Campos, I., & Calera, A. (2018). Performance assessment of MOD16 in evapotranspiration evaluation in Northwestern Mexico. *Water (Switzerland)*, *10*(7). https://doi.org/10.3390/w10070901

Akaike, H. (1974). A New Look at the Statistical Model Identification. 19, 716–723.
Aksebi, Najib. 2012. “Une Nouvelle Stratégie Pour l ’ Agriculture Marocaine : Le « Plan Maroc Vert ».” NEW MEDIT: 12–24.
A. Laamari, M. Boughlala, A. Herzenni, M. Karrou and A. Bahri. “Chapter 7: Water Policies in Morocco – Current Situation and Future Perspectives 101.” : 101–17
Alcamo, J., P. Döll, F. Kaspar, and S. Siebert (1997), Global change and global scenarios of water use and availability: An application of Water- GAP 1.0, Rep. A9701, Cent. for Environ. Syst. Res., Univ. of Kassel, Kassel, Germany.) www.usf.uni kassel.de/usf/archiv/dokumente/projekte/ watergap.teill.pdf
Alcamo J, Henrichs T and Rsch T 2000 World water in 2025-global modeling and scenario analysis for the world commission on water for the 21st centuryKassel World Water Series 2 Kassel, Germany, Center for Environmental Systems Research, University of Kassel www.usf.uni-kassel.de/usf/archiv/ dokumente/kwws/kwws.2.pdf
Alcamo, J., P. Döll, T. Henrichs, F. Kaspar, B. Lehner, T. Rösch, and S. Siebert (2003b), Global estimation of water withdrawals and availability under current and “business as usual” conditions, Hydrol. Sci. J., 48, 339–348, doi:10.1623/hysj.48.3.339.45278
Alonso, A et al. 2019. “Comparative Assessment of Irrigation Systems ’ Performance : Case Study in the Tri Ff a Agricultural District , NE Morocco.” Agricultural Water Management 212(August 2018): 338–48. https://doi.org/10.1016/j.agwat.2018.08.033.
Anabela Fernandes-Silva, M. O., Anabela Fernandes-Silva, M. O., & Ferreira, T. A. P. and I. (2018). Deficit Irrigation in Mediterranean Fruit Trees Deficit Irrigation in Mediterranean Fruit Trees and and Grapevines: Water Stress Indicators and Crop Grapevines: Water Stress Indicators and Crop Responses. *IntechOpen*, 13. https://doi.org/http://dx.doi.org/10.5772/57353
Analysis, Crosscutting. 6 Transboundary Waters Systems – Status and Trends Crosscutting Analysis.
Arnold, J. G., R. Srinivasan, R. S. Muttiah, and J. R. &Williams. (1998). Large Area Hydrologic Modeling and Assessment Part I: Model Development. Journal of the American Water Resources Association 34: 73-89
Antônio, A. H., Scherer-Warren, M., Hernandez, F. B. T., Andrade, R. G., & Leivas, J. F. (2013). Large-scale water productivity assessments with MODIS images in a changing semi-arid environment: A brazilian case study. *Remote Sensing*, *5*(11), 5783–5804. https://doi.org/10.3390/rs5115783.
Arkin, F. R. (1980). On the Relationship between Satellite-Observed Cloud Cover and Precipitation.
Arkin, P. A. (1979). The Relationship between Fractional Coverage of High Cloud and Rainfall Accumulations during GATE over the B-Scale Array.
Arriens, van Beek and Lincklaen. 2014. “Water Security: Putting the Concept into Practice.” Background Paper No. 20, Global Water Partnership Technical Committee (TEC), Stockholm.
Auajjar J. & Boulegue J. (1999) : Les minéralisations Pb-Zn (Cu) Ba du district du Tazekka (Taza, Maroc oriental), chronique de la recherche minière, N° 536-537, p.121-135.
Azin khalid (INRA d’agadir), Soudi Brahim (IAV). “Compostage et Bio Méthanisation Pour La Valorisation Agronomique et Énérgitique Des Déchets Agricoles Organiques Dans Le Sous

Massa." http://www.agri-mag.com/2017/06/compostage-et-bio-methanisation-souss-massa/.
Banque mondiale. (2012). Morocco Natural Hazards Probabilistic Risk Analysis and National Strategy Development.
Banque mondiale. (2007). "Making the Most of Scarcity: Accountability for Better Water Management Results in the Middle East and North Africa." MENA Development Report. World Bank, Washington, DC
Banque mondiale (2013). Renforcement de la résilience du Maroc : apports pour une stratégie de gestion intégrée des risques.
Baret, F., & Guyot, G. (1991). Potentials and Limits of Vegetation Indices for LAI and APAR Assessment. 173, 161–173.
Baret, F., Guyot, G., & Major, D. J. (1989). Tsavi: a vegetation index which minimizes soil brightness effects. 2, 1355–1358.
Base, C. D. E., Modelisation, D. E. L. A., & Et, H. (2013). Compétitivité économique du maroc.
Bedient, P. B. and W. C.& Huber. (2012) "Hydrology and Floodplain Analysis", 5th Ed. Prentice-Hall Publishing Co., Upper Saddle River, NJ, February 2012, 800 page textbook.
Belay, H., Ayalew, S., & Hailu, D. (2020). Journal of Hydrology : Regional Studies Hydrological performance evaluation of multiple satellite precipitation products in the upper Blue Nile basin , Ethiopia. Journal of Hydrology: Regional Studies, 27(August 2018), 100664. https://doi.org/10.1016/j.ejrh.2020.100664

Benouniche, M., Kuper, M., & Hammani, A. (2014). Mener le goutte à goutte à l'économie d'eau: ambition réaliste ou poursuite d'une chimère? *Alternatives Rurales*, (2), 1–12.

Benouniche, M., Kuper, M., Hammani, A., & Boesveld, H. (2014). Making the user visible: analysing irrigation practices and farmers' logic to explain actual drip irrigation performance. *Irrigation Science*, *32*(6), 405–420. https://doi.org/10.1007/s00271-014-0438-0

Berbel, J., Gutiérrez-Martín, C., Rodríguez-Díaz, J. A., Camacho, E., & Montesinos, P. (2014). Literature Review on Rebound Effect of Water Saving Measures and Analysis of a Spanish Case Study. *Water Resources Management*, *29*(3), 663–678. https://doi.org/10.1007/s11269-014-0839-0

Berterreche, L., Champredonde, R., & Dartus, D. (2008). Etude de la génération de crues rapides par la confrontation de deux logiciels.
Boschung, A. Nauels, Y. Xia, V. Bex and P.M. Midgley (eds.)]. Cambridge University Press, Cambridge, United Kingdom and New York, NY, USA
Bouslihim Y., Kacimi I., Brirhet .H, Khatati M., Rochdi A., El Amrani N., Pazza, Miftah A., Yaslo Z. (2016). Hydrologic Modeling Using SWAT and GIS, Application to Subwatershed Bab-Merzouka (Sebou, Morocco), Journal of Geographic Information System, pages 8, 20-27.
http://www.scirp.org/journal/jgis http://dx.doi.org/10.4236/jgis.2016.81002
Brienen, S., Rust, H. W., Sauter, T., Themeßl, M., Venema, V. K. C., & Chun, K. P. (2010). Precipitation downscaling under climate change : recent developments to bridge the gap between dynamical models and the end user. 2009, 1–34. https://doi.org/10.1029/2009RG000314.1.
Brirhet H., (2016). 'Intégration des modèles globaux et distribués dans la modélisation hydrologique du bassin versant d'Issan, région de Souss.', PhDThesis, Thèse de Doctorat, Université Sidi Mohamed Ben ABDELLAH, Fes

Burt, C. M. (2004). Rapid field evaluation of drip and microspray distribution uniformity. *Irrigation and Drainage Systems*, *18*(4), 275–297. https://doi.org/10.1007/s10795-004-2751-x

Campos-Taberner, M., Moreno-Martínez, Á., García-Haro, F. J., Camps-Valls, G., Robinson, N. P., Kattge, J., & Running, S. W. (2018). Global estimation of biophysical variables from Google Earth Engine platform. *Remote Sensing*, *10*(8), 1–17. https://doi.org/10.3390/rs10081167

Card, Dallas. 2005. "The Case of Privatization in Cochabamba, Bolivia Prepared for Julia Sagebien INTD 5003 Water Wars: The Case of Privatization in Cochabamba, Bolivia." http://my2.ewb.ca/site_media/static/attachments/group_topics_grouptopic/15584/Bolivian Water War.pdf.

Chai, Q., Gan, Y., Zhao, C., Xu, H. L., Waskom, R. M., Niu, Y., & Siddique, K. H. M. (2016). Regulated deficit irrigation for crop production under drought stress. A review. *Agronomy for Sustainable Development*, *36*(1), 1–21. https://doi.org/10.1007/s13593-015-0338-6

Chen, F., & Li, X. (2016). Evaluation of IMERG and TRMM 3B43 Monthly Precipitation Products over Mainland China. 1–18. https://doi.org/10.3390/rs8060472

Chen, F., Liu, Y., Liu, Q., & Li, X. (2014). International Journal of Remote Spatial downscaling of TRMM 3B43 precipitation considering spatial heterogeneity. August, 37–41. https://doi.org/10.1080/01431161.2014.902550

Chokkavarapu, N., & Ravibabu, V. (2019). Comparative study of GCMs , RCMs , downscaling and hydrological models : a review toward future climate change impact estimation. SN Applied Sciences, 1(12), 1–15. https://doi.org/10.1007/s42452-019-1764-x

Ciabatta, L., Brocca, L., Massari, C., Moramarco, T., Gabellani, S., Puca, S., & Wagner, W. (2016). International Journal of Applied Earth Observation and Geoinformation Rainfall-runoff modelling by using SM2RAIN-derived and state-of-the-art satellite rainfall products over Italy. International Journal of Applied Earth Observations and Geoinformation, 48, 163–173. https://doi.org/10.1016/j.jag.2015.10.004

Colo G. (1961): Contribution à l'étude du Jurassique du Middle Atlas septentrional. Notes et Mém. Serv. Géol. Maroc, n° 139, 226 pp.

Cook, Christina, and Karen Bakker. 2012. "Water Security: Debating an Emerging Paradigm." Global Environmental Change 22(1): 94–102. http://dx.doi.org/10.1016/j.gloenvcha.2011.10.011.

Condés, S., & García-robredo, F. (2012). Forest Ecology and Management An empirical mixed model to quantify climate influence on the growth of Pinus halepensis Mill . stands in South-Eastern Spain. 284, 59–68. https://doi.org/10.1016/j.foreco.2012.07.030

DARA. (2012). DARA and the Climate Vulnerable Forum, Climate vulnerability monitor 2nd edition. In A guide to the cold calculus of a hot plaeffective .

Darand, M., Amanollahi, J., & Zandkarimi, S. (2017). Evaluation of the performance of TRMM Multi-satellite Precipitation Analysis (TMPA) estimation over Iran. Atmospheric Research. https://doi.org/10.1016/j.atmosres.2017.02.011

David R. Maidment, (1992). Handbook of hydrology McGraw-Hill

Douglas E M, Githui F, Mtafya A, Green P, Glidden S and Vörösmarty C J 2006 Characterizing water scarcity in Africa at different scales J. Environ. Manage. 10 1–10 "Dahir N°1-16-113 Du 6 Kaada 1437 Portant Promulgation de La Loi N°36-15 Relative à l'eau." 2016.

Duan, L., Fan, K., Li, W., & Liu, T. (2017). Spatial downscaling algorithm of TRMM

precipitation based on multiple high-resolution satellite data for Inner Mongolia , China. 2001.

Duan, Z., & Bastiaanssen, W. G. M. (2013). Remote Sensing of Environment First results from Version 7 TRMM 3B43 precipitation product in combination with a new downscaling – calibration procedure. Remote Sensing of Environment, 131, 1–13. https://doi.org/10.1016/j.rse.2012.12.002

Durães MF., Mello CR. & Naghettini M. (2011). Applicability of the SWAT model for hydrologic simulation in Paraopeba River Basin, MG. Cerne. Lavras 17: 481-488

El Bergui, O., Abouabdillah, A., Bouabid, R., El Jaouhari, N., Brouziyne, Y., & Bourioug, M. (2020). Agro-physiological response of potato to 'sustainable' deficit irrigation in the plain of Saïs, Morocco. *E3S Web of Conferences*, *183*, 1–10. https://doi.org/10.1051/e3sconf/202018303001

El Jaouhari, N., Abouabdillah, A., Bouabid, R., Bourioug, M., Aleya, L., & Chaoui, M. (2018). Assessment of sustainable deficit irrigation in a Moroccan apple orchard as a climate change adaptation strategy. *Science of the Total Environment*, *642*(June), 574–581. https://doi.org/10.1016/j.scitotenv.2018.06.108

El, Khalid, and Ghomari Directeur. 2016. "La Politique et Les Bienfaits Des Barrages Au Maroc."

Elhassnaoui, I., Moumen, Z., Serrari, I., Bouziane, A., Ouazar, D., & Hasnaoui, M. I. (2019). Generation of synthetic design storm hyetograph and hydrologic modeling under HEC HMS for Ziz watershed. International Journal of Innovative Technology and Exploring Engineering, 8(10), 3308–3319. https://doi.org/10.35940/ijitee.J1214.0881019

Essery, C. I., & Wblcock, D. N. (1991). The variation in rainfall catch from standard UK Meteorological Office raingauges: a twelve year case study.

Ezzine, H., Bouziane, A., Ouazar, D., & Hasnaoui, M. D. (2017). Downscaling of Open Coarse Precipitation Data through Spatial and Statistical Analysis , Integrating NDVI , NDWI , Elevation , and Distance from Sea. 2017.

Faure-Muret A. & Choubert G. (1971) : Note au sujet des nappes de charriage desTemsamane (Rif oriental, Maroc). C.R Acad. Sc. Paris, France, t.272, ser. D . P. 2657. 2660.

Falkenmark M, Kijne J W, Taron B, Murdoch G, Sivakumar M V K and Craswell E 1997 Meeting water requirements of an expanding world population [and discussion] Phil. Trans. R. Soc. B 352 929–36

Falkenmark, M. 2001. "The Greatest Water Problem: The Inability to Link Environmental Security, Water Security and Food Security." International Journal of Water Resources Development 17(4): 539–54.

Fang, J., Du, J., Xu, W., Shi, P., Li, M., & Ming, X. (2013). Advances in Water Resources Spatial downscaling of TRMM precipitation data based on the orographical effect and meteorological conditions in a mountainous area. Advances in water resources, 61, 42–50. https://doi.org/10.1016/j.advwatres.2013.08.011

Feng, Aiqing et al. 2018. "Assessing the Inundation Risk Resulting from Extreme Water Levels under Sea-Level Rise: A Case Study of Rongcheng, China." Geomatics, Natural Hazards and Risk 9(1): 456–70. https://doi.org/10.1080/19475705.2018.1447026.

FAO. (1998). Chapter 7 - ETc - Dual crop coefficient (Kc = Kcb + Ke).

Fereres, E., & Soriano, M. A. (2007). Deficit irrigation for reducing agricultural water use.

Journal of Experimental Botany, *58*(2), 147–159. https://doi.org/10.1093/jxb/erl165

Frija, I., Frija, A., Marlet, S., Leghrissi, H., Faysse, N., & Meriem, C. (2016). Gestion de l'usage d'une nappe par un groupement d'agriculteurs : l'expérience de Bsissi Oued El Akarit en Tunisie. *Alternatives Rurales*, (October), 12.

Foulds, L. R. (1984). Linear Programming and Extensions 1.1.

Fowler, H. J., & Ekstr, M. (2009). Multi-model ensemble estimates of climate change impacts on UK seasonal precipitation extremes. 416(January), 385–416. https://doi.org/10.1002/joc

Gain, Animesh K, Carlo Giupponi, and Yoshihide Wada. 2016. "Measuring Global Water Security towards Sustainable Development Goals Measuring Global Water Security towards Sustainable Development Goals."

Gassman, P. W., Reyes, M. R., Green, C. H., & Arnold, J. G.(2007) The soil and water assessment tool: Historical development, applications, and future research directions, Trans. ASABE, 50, 1211–1250

Giuseppe Mancino, Agostino Ferrara, A. P. and A. N. (2020). Landsat 7 (ETM +) Derived Vegetation Indices in a Mediterranean Environment. 8.

Global Nexus. 2017. "Morocco's Water Security : Productivity, Efficiency, Integrity."

Goal, Sustainable Development, and Synthesis Report. 2018. Sustainable Development Goal 6 Synthesis Report on Water and Sanitation 2018.

G. NAUMANN, P. BARBOSA, H.CARRAO, A.SINGLETON, A. J. V. (2012). Monitoring Drought Conditions and Their Uncertainties in Africa Using TRMM Data. 1867–1874. https://doi.org/10.1175/JAMC-D-12-0113.1

Gregg, W. W., & Casey, N. W. (2004). Global and regional evaluation of the SeaWiFS chlorophyll data set. 93, 463–479. https://doi.org/10.1016/j.rse.2003.12.012

Grey, David, and Claudia W. Sadoff. 2007. "Sink or Swim? Water Security for Growth and Development." Water Policy 9(6): 545–71.

Guofeng, Z., Dahe, Q., Yuanfeng, L., Fenli, C., & Pengfei, H. (2016). Accuracy of TRMM precipitation data in the southwest monsoon region of China. https://doi.org/10.1007/s00704-016-1791-0

Gutjahr, O. (2013). Comparing precipitation bias correction methods for high-resolution regional climate simulations using COSMO-CLM Effects on extreme values and climate change signal. 2012. https://doi.org/10.1007/s00704-013-0834-z

He, M., Kimball, J. S., Maeffective a, M. P., Maxwell, B. D., Moreno, A., Beguería, S., & Wu, X. (2018). Regional crop gross primary productivity and yield estimation using fused landsat-MODIS data. *Remote Sensing*, *10*(3). https://doi.org/10.3390/rs10030372

Hengl, T., Mendes de Jesus, J., Heuvelink, G. B. M., Ruiperez Gonzalez, M., Kilibarda, M., Blagotić, A.& Kempen, B. (2017). SoilGrids250m: Global gridded soil information based on machine learning. PLOS ONE, 12(2), e0169748. https://doi.org/10.1371/journal.pone.0169748

Hoepffner C. (1989) : L'évolution structurale hercynienne de la meseta marocaine orientale. Essai de mise au point. Notes Memo. Serv. Geol. Maroc, 355, 229-238.

Immerzeel, W. W., Rutten, M. M., & Droogers, P. (2009). Remote Sensing of Environment Spatial downscaling of TRMM precipitation using vegetative response on the Iberian Peninsula. Remote Sensing of Environment, 113(2), 362–370. https://doi.org/10.1016/j.rse.2008.10.004

IPCC 2007, Summary for Policymakers, in Climate Change 2007: Impacts, Adaptation and

Vulnerability. Contribution of Working Group II to the Fourth Assessment Report of the Intergovernmental Panel on Climate Change, Cambridge University Press, Cambridge, UK, p. 17. Available at: (https://www.ipcc.ch/report/ar4/wg2/)

IPCC, 2013: Summary for Policymakers. In: Climate Change 2013: The Physical Science Basis. Contribution of Working Group I to the Fifth Assessment Report of the Intergovernmental Panel on Climate Change [Stocker, T.F., D. Qin, G.-K. Plattner, M. Tignor, S.K. Allen, J.

IPCC, 2014: climate Change 2014: Synthesis Report. Contribution of working Groups I, II and III to the Fifth Assessment Report of the intergovernmental Panel on Climate change [Core writing Team, R.K. Pachauri and L.A Meyer (eds.)]. IPCC, Geneva, Switzerland, 151 pp. Available at: (http://www.ipcc.ch/report/ar5/syr/)

INRA. (2019). Rapport d'Activité. International, C. O. (1997). *Encyclopedie mondiale de l'olivier*. Conseil Oleicole International.

Institute of Industrial Science, The University of Tokyo, 4-6-1 Komaba, Meguro-Ku, Tokyo 153-8505, Japan. 2Japan Science and Technology Agency, 4-1-8 Honcho, Kawaguchi- Shi, Saitama 332-0012, Japan. 3Frontier Research Center for Global Change, Japan Agence.

Irvem, A., & Ozbuldu, M. (2019). Evaluation of Satellite and Reanalysis Precipitation Products Using GIS for All Basins in Turkey. 2019.

Ivana Kottasova. Frederik Pleitgen and Laura Smith-Spark, CNN. "Floods Bring Misery to Central Europe." 2013.

Jamal, P., Stitou, E., Messari, E., Dridri, P. A., Abdel, P., Chaouni, A., … Fès, F. S. T. (2012). UFR : Chimie de l ' Environnement Discipline : Géologie Présentée par J amal Naoura N aoura.

Jehanzeb, M., & Cheema, M. (2012). International Journal of Remote Local calibration of remotely sensed rainfall from the TRMM satellite for different periods and spatial scales in the Indus Basin. November, 37–41.

Jerome, Sara. 2015. "A Brief History Of Water Conflict."

Julie Bosman, Julie Turkewitz and Timothy Williams. "In the Midwest, Relentless Floods Dredge Up 'Shadow' of 1993." 2019

Jia, S., Zhu, W., Aifeng, L., & Yan, T. (2011). Remote Sensing of Environment A statistical spatial downscaling algorithm of TRMM precipitation based on NDVI and DEM in the Qaidam Basin of China. Remote Sensing of Environment, 115(12), 3069–3079. https://doi.org/10.1016/j.rse.2011.06.009

J. Wang, P. M. R. & K. P. P. (2003). International Journal of Remote Sensing Temporal responses of NDVI to precipitation and temperature in the central Great Plains , USA. March 2013, 37–41.

Khaddor, I. (2016). Simulation numérique des écoulements à surface libre du bassin versant de Mghogha en Middle de SIG, Télédétection, HEC-HMS et HEC-RAS: Études des protections contre les inondations dans la ville de Tanger, nord de Maroc. UNIVERSITE ABDELMALEK ESSAADI FACULTE DES SCIENCES et TECHNIQUES TANGER.

Kannan, N., Santhi, C., White, M. J., Mehan, S., Jeffrey, G., & Gassman, P. W. (2019). Some Challenges in Hydrologic Model Calibration for Large-Scale Studies : A Case Study of SWAT Model Application to Mississippi-Atchafalaya River Basin, 1–23. https://doi.org/10.3390/hydrology6010017

Karaska, M. A., Huguenin, R. L., Beacham, J. L., Wang, M., Jensen, J. R., & Kaufmann, R. S. (2004). AVIRIS Measurements of Chlorophyll , Suspended Minerals , Dissolved Organic Carbon , and Turbidity in the Neuse River , North Carolina. 70(1), 125–133.

Kidd, C. (2001). Satellite rainfall climatology : a review. 1066, 1041–1066.
Kidd, C., & Levizzani, V. (2011). Status of satellite precipitation retrievals. 1109–1116. https://doi.org/10.5194/hess-15-1109-2011
Kim, J. P., Jung, I. W., Park, K. W., Yoon, S. K., & Lee, D. (2016). Hydrological Utility and Uncertainty of Multi-Satellite Precipitation Products in the Mountainous Region of South Korea. https://doi.org/10.3390/rs8070608
Klepper O and van Drecht G 1998 WARiBaS, water assessment on a river basin scale; a computer program for calculating water demand and water satisfaction on a catchment basin level for global-scale analysis of water stress Report 402001009 National Institute of Public Health and the Environment (RIVM)

KESSETE, N., MOGES, M.A. and STEENHUIS, T.S., 2019. *Evaluating the applicability and scalability of bias corrected CFSR climate data for hydrological modeling in upper Blue Nile basin, Ethiopia* [en línea]. S.l.: Elsevier Inc. ISBN 9780128159989. Disponible en: http://dx.doi.org/10.1016/B978-0-12-815998-9.00002-6.
Koenker, R., Bassett, G., & Jan, N. (2007). Regression Quantiles. 46(1), 33–50.
Kro, S., & Law, R. J. (2005). Sensing the sea. 23(5). https://doi.org/10.1016/j.tibtech.2005.03.004

Kumar, L., & Mutanga, O. (2018). Google Earth Engine applications since inception: Usage, trends, and potential. *Remote Sensing*, *10*(10), 1–15. https://doi.org/10.3390/rs10101509

Kurc, S. A., & Small, E. E. (2004). Dynamics of evapotranspiration in semiarid grassland and shrubland ecosystems during the summer monsoon season, central New Mexico. *Water Resources Research*, *40*(9), 1–15. https://doi.org/10.1029/2004WR003068

LABIDI, Aya. 2016. "Le Compost et Ses Bienfaits Biologiques. http://www.agrimaroc.ma/le-compost-et-ses-bienfaits-biologiques/.
Lance, B. C. E. (2014). Mallows ' Cp Statistic I. 1–2.

Laville E., Piqué A., Amrhar M. & Charroud M. (2004) : A restatement of the Mesozoic

Atlasic Rifting (Morocco). Journal of African Earth Sci., 38, 145-153.

Lautze J and Manthrithilake H 2012 Water security: old concepts, new package, what value? Nat. Resour. Forum 36 76–87
Luzio, M. Di, Srinivasan, R., & Arnold, J. G. (2003). INTEGRATION OF WATERSHED TOOLS AND SWAT MODEL INTO BASINS 1, 38(4), 1127–1141.
Likens, R. P.,ed.,(1981) Annual Book of ASTM Standards, part19, Soil and Rocks, Building stones, pp.509-514

Levidow, L., Zaccaria, D., Maia, R., Vivas, E., Todorovic, M., & Scardigno, A. (2014). Improving water-efficient irrigation: Prospects and difficulties of innovative practices. *Agricultural Water Management*, *146*, 84–94. https://doi.org/10.1016/j.agwat.2014.07.012

Liu, Z. fei, Yao, Z. jun, Yu, C. qun, & Zhong, Z. ming. (2013). Assessing Crop Water Demand and Deficit for the Growth of Spring Highland Barley in Tibet, China. *Journal of Integrative Agriculture*, *12*(3), 541–551. https://doi.org/10.1016/S2095-3119(13)60255-5

Liu, J., Zhang, W., & Nie, N. (2018). Spatial Downscaling of TRMM Precipitation Data Using an Optimal Subset Regression Model with NDVI and Terrain Factors in the Yarlung Zangbo River Basin , China. 2018.

Liu, P., Di, L., Du, Q., & Wang, L. (2018). Remote Sensing Big Data : Theory , Methods and Applications. 2016–2019. https://doi.org/10.3390/rs10050711

Lopez-Gunn, E., Zorrilla, P., Prieto, F., & Llamas, M. R. (2012). Lost in translation? Water efficiency in Spanish agriculture. *Agricultural Water Management*, *108*(May), 83–95. https://doi.org/10.1016/j.agwat.2012.01.005

Lundqvist, J., de Fraiture, C., & Molden, D. (2008). Saving Water: From Field to Fork Curbing Losses and Wastage in the Food Chain. SIWI Policy Brief. SIWI, 2008. *Stockholm International Water Institute*, 36.

Maidment, D. R. (1993). - Handbook of hydrology (Vol. 9780070, p. 397323). New York: McGraw-Hill.

Mallows, C. L. (1973). Technometrics Some Comments on C p. April 2013, 37–41.

Mandal, S., Vema, V. K., Kurian, C., & Sudheer, K. P. (2020). Improving the crop productivity in rainfed areas with water harvesting structures and deficit irrigation strategies. *Journal of Hydrology*, *586*, 124818. https://doi.org/10.1016/j.jhydrol.2020.124818

Mapfumo, E., D. S. Chanasyk, and W. D.& Willms. (2004). Simulating daily soil water under foothills fescue grazing with the Soil and Water Assessment Tool model (Alberta, Canada). Hydrol. Process. 18(3): 2787-2800

Marra, F. P., Marino, G., Marchese, A., & Caruso, T. (2016). Effects of different irrigation regimes on a super-high-density olive grove cv. "Arbequina": vegetative growth, productivity and polyphenol content of the oil. *Irrigation Science*, *34*(4), 313–325. https://doi.org/10.1007/s00271-016-0505-9

Masmoudi, C., Masmoudi, M. M., & Ben Mechlia, N. (2004). Irrigation De L'Olivier :Cas Des Jeunes Plantations Intensive. *Revue Ezzaitouna*, *10*(1 et 2), 37–51.

Mehta, A. V, Yang, S., Group, M. S., & Springs, C. (2008). Advances in Geosciences Precipitation climatology over Mediterranean Basin from ten years of TRMM measurements. 87–91.

Meyer, V., & Schwarze, R. (2019). The Economics and Management of Flood Risk in Germany. Volker Meyer and Reimund Schwarze, 473–495.

Milewski, A., Elkadiri, R., & Durham, M. (2015). Assessment and Comparison of TMPA Satellite Precipitation Products in Varying Climatic and Topographic Regimes in Morocco. 5697–5717. https://doi.org/10.3390/rs70505697

Mills, A., Fey, M., Donaldson, J., Todd, S., & Theron, L. (2009). Soil infiltrability as a driver of plant cover and species richness in the semi-arid Karoo , South Africa. 321–332. https://doi.org/10.1007/s11104-009-9904-5

Mills, A. J. (2006). Unravelling the effects of soil properties on water infiltration : segmented quantile regression on a large data set from arid south-west Africa. 783–797.

Ministère Délègue Auprès Du Ministre De L'énergie, Des Mines, D. L. E. D. L. C. D. L. (2014). Chapitre I : Les changements climatiques au Maroc 15.

Ministry of Agriculture and Maritime Fisheries. 2016. "STRATEGIE DU PLAN MAROC VERT : ENVIRONNEMENT ECONOMIQUE ET SOCIAL DU SECTEUR AGRICOLE."

Miller, E. Willard; Miller & Ruby M.(1992). water quality and availability. ABC-CLIO santa Barbara, California, Denever, Colorado. Oxford, England

Mohamed E., & Peter W., (2017). Independent Consultants Mediterranean Environmental

Technical Assistance Program, evaluation of METAP.
Mokhtari, N., Mrabet, R., Lebailly, P., & Bock, L. (2013). Spatialisation des bioclimats , de l ' aridité et des étages de végétation du Maroc. 50–66.

Molle, F., & Sanchis-Ibor, C. (2019). *Irrigation Policies in the Mediterranean: Trends and Challenges*. *Global Issues in Water Policy* (Vol. 22). https://doi.org/10.1007/978-3-030-03698-0_10

Molle, F., & Tanouti, O. (2017). La micro-irrigation et les ressources en eau au Maroc : un coûteux malentendu. *Alternatives Rurales*, *5*(5), 18.

Mondal, P., Jain, M., Defries, R. S., Galford, G. L., & Small, C. (2014). Sensitivity of crop cover to climate variability : Insights from two Indian agro-ecoregions. Journal of Environmental Management. https://doi.org/10.1016/j.jenvman.2014.02.026
Moumen, Z. (2019). Test the Capacity of SWAT Model to Simulate the Hydrological Behavior of Watershed in Semi-Arid Climate Hydrologic Modeling Using SWAT. https://doi.org/10.4018/978-1-5225-9771-1.ch008
Moumen, Z., El, N., El, A., Tvaronavičienė, M., Moumen, Z., El, N., El, A., Tvaronavičienė, M., & Water, A. L. (2019). Water security and sustainable development. HAL Id : hal-02342701.

Mutanga, O., & Kumar, L. (2019). Google earth engine applications. *Remote Sensing*, *11*(5), 11–14. https://doi.org/10.3390/rs11050591

Najja, S., Zad, M., Zulkafli, Z., & Muharram, F. M. (2018). Satellite Rainfall (TRMM 3B42-V7) Performance Assessment and Adjustment over Pahang River. 1–24. https://doi.org/10.3390/rs10030388
Nichol, J. E., & Abbas, S. (2015). Science of the Total Environment Integration of remote sensing datasets for local scale assessment and prediction of drought. Science of the Total Environment, The, 505, 503–507. https://doi.org/10.1016/j.scitotenv.2014.09.099
Neitsch, S. L., Arnold, J. G., Kiniry, J. R., and Williams, J. R. (2011): Soil and Water Assessment Tool Theoretical Documentation Version 2009, Grassland, Soil and Water Research Laboratory, Agricultural ResearchService and Blackland Research Center, Texas Agricultural Experiment Station, College Station, Texas.
Ntem, Benito, and Lough Melvin. "Table of Transboundary River Basins and Countries." : 211–15.
Oki T, Agata Y, Kanae S, Saruhashi T, Yang D and Musiake K 2001 Global assessment of current water resources using total runoff-integrating pathways Hydrol. Sci. J. 46 983–95
Oki, T. 2006. "Global Hydrological Cycles and World Water." Science (August): 1068–73. http://research.bpcrc.osu.edu/hydro/publications/OkiKanae_GlobalHydro_Science.pdf.

Ozer, H., Coban, F., Sahin, U., & Ors, S. (2020). Response of black cumin (Nigella sativa L.) to deficit irrigation in a semi-arid region: Growth, yield, quality, and water productivity. *Industrial Crops and Products*, *144*(December 2019), 112048. https://doi.org/10.1016/j.indcrop.2019.112048
Ormann, C. A. F. D., Alabrese, J. U. M. C., Rroita, G. U. G. U., Atechou, E. L. M., & Ahn, V. O. B. (2018). Model averaging in ecology : a review of Bayesian , information-theoretic , and tactical approaches for predictive inference. 0(0), 1–20. https://doi.org/10.1002/ecm.1309

Parente, L., & Ferreira, L. (2018). Assessing the spatial and occupation dynamics of the Brazilian pasturelands based on the automated classification of MODIS images from 2000

to 2016. *Remote Sensing*, *10*(4). https://doi.org/10.3390/rs10040606

Pascual-Seva, N., San Bautista, A., López-Galarza, S., Maroto, J. V., & Pascual, B. (2016). Response of drip-irrigated chufa (Cyperus esculentus L. var. sativus Boeck.) to different planting configurations: Yield and irrigation water-use efficiency. *Agricultural Water Management*, *170*, 140–147. https://doi.org/10.1016/j.agwat.2016.01.021

Perry, C., Steduto, P., Allen, R. G., & Burt, C. M. (2009). Increasing productivity in irrigated agriculture: Agronomic constraints and hydrological realities. *Agricultural Water Management*, *96*(11), 1517–1524. https://doi.org/10.1016/j.agwat.2009.05.005

Paredes-trejo, F., Barbosa, H., & Santos, C. A. C. (2019). Evaluation of the Performance of SM2RAIN-Derived Rainfall Products over Brazil. 1–28.

Park, N. (2013). Spatial Downscaling of TRMM Precipitation Using Geostatistics and Fine Scale Environmental Variables. 2013.

Peck, L. (1974). Measurements. I(4), 857–863.

PERRIN, C., SAMIE, R., & HENDRICKX. 2009. "Les Outils Du Projet : Modélisation Hydrologique et Représentation Des Usages. Journée de Restitution Du Projet." EDF (Toulouse) Cemagref,.

Pierre, U., Doctorale, E., Naturelles, R., & Moussa, M. R. (2009). Quels apports hydrologiques pour les modèles hydrauliques ? Vers un modèle intégré de simulation des crues.

Piqué A., Soulaimani A., Hoepffner C., Bouabdelli M., Laville E., Amrhar M. & Chalouan A. (2007). Géologie du Maroc. Ed. Géode, collection Terre et Patrimoine, série manuels, p.178- 210.

Pomares, F. G. (2007). La fertilización y la fertirrigación, programas de nutrición, influencia sobre la programación. *Actas de Horticultura*, *50*, 133–143.

Poortinga, A., Clinton, N., Saah, D., Cutter, P., Chishtie, F., Markert, K. N., … Towashiraporn, P. (2018). An operational before-after-control-impact (BACI) designed platform for vegetation monitoring at plaeffective ary scale. *Remote Sensing*, *10*(5). https://doi.org/10.3390/rs10050760

Postel, S., Polak, P., Gonzales, F., & Keller, J. (2001). Drip irrigation for small farmers: A new initiative to alleviate hunger and poverty. *Water International*, *26*(1), 3–13. https://doi.org/10.1080/02508060108686882

Raven P.H., Raven, L.R. Berg, D.M. (2009). Hassenzahl. Environnement, Boeck Université.

Raskin P, Gleick P, Kirshen P, Pontius G and Strzepek K 1997 Water Futures: Assessment of Long-range Patterns and Prospects (Stockholm: Stockholm Environment Institute)

Razouk, R. (2016). Irrigation de l'olivier : de bonnes pratiques pour chaque système de production. Par Dr Rachid RAZOUK, INRA – Meknès | INRA Meknès Magazine.

Rodda, J C, & Smith, S. W. (1986). Technical note the significance of the systematic error in rainfall measurement for assessing wet deposition. 20, 1059–1064.

Rodda, John C, & Dixon, H. (2011). Rainfall measurement revisited. 1842, 131–136. https://doi.org/10.1002/wea.1884

Rodriguez-Iturbe, I. (2000). Ecohydrology: A hydrologic perspective of climate-soil-vegetation dynamics. *Water Resources Research*, *36*(1), 3–9. https://doi.org/10.1029/1999WR900210

Rondeaux, G., Steven, M., & Baret, F. (1996). Optimization of Soil-Adjusted Vegetation Indices.

107(August 1994), 95–107.
Sabaoui A. (1998) : Rôle des inversions dans l'évolution méso-cénozoiques du Middle Atlas septentrional (Maroc). L'exemple de la transversale ElManzel-Ribat, ElKhayr-Bou Iblane. Thèse d'état, Univ. Mohamed V. Rabat, 432p.

Sabri, A., Bouaziz, A., Hammani, A., Kuper, M., Douaik, A., & Badraoui, M. (2017). Effet de l'irrigation déficitaire contrôlée sur la croissance et le développement foliaire du palmier dattier (Phoenix dactylifera L.). *Cahiers Agricultures*, *26*(5), 1–11. https://doi.org/10.1051/cagri/2017033

Schilling, J., Hertig, E., Tramblay, Y., & Scheffran, J. (2020). Climate change vulnerability , water resources and social implications in North Africa.

Schneider, U., Becker, A., Finger, P., Meyer-christoffer, A., Ziese, M., & Rudolf, B. (2014). GPCC ' s new land surface precipitation climatology based on quality-controlled in situ data and its role in quantifying the global water cycle. 15–40. https://doi.org/10.1007/s00704-013-0860-x

Schwaller, M. R., & Morris, K. R. (2011). A Ground Validation Effective work for the Global Precipitation Measurement Mission. Gcos 2006, 301–320. https://doi.org/10.1175/2010JTECHA1403.1

Sciences, G. E., County, B., Branch, H. S., Sciences, G. E., & County, B. (2007). Multitemporal Analysis of TRMM-Based Satellite Precipitation Products for Land. 1165–1183. https://doi.org/10.1175/2007JHM859.1

Sese-Minguez, S., Boesveld, H., Asins-Velis, S., van der Kooij, S., & Maroulis, J. (2017). Transformations accompanying a shift from surface to drip irrigation in the Cànyoles Watershed, Valencia, Spain. *Water Alternatives*, *10*(1), 81–99.

Segond, M., Wheater, H. S., & Onof, C. (2007). The significance of spatial rainfall representation for flood runoff estimation : A numerical evaluation based on the Lee catchment , UK. 116–131. https://doi.org/10.1016/j.jhydrol.2007.09.040

Shaodan Chen, Liping Zhang, D. S. and J. C., & State. (2019). Spatial Downscaling of Tropical Rainfall Measuring Mission (TRMM) Annual and Monthly Precipitation Data over the Middle and Lower Reaches of the Yangtze River Basin , China. https://doi.org/10.3390/w11030568

Shrestha S, Aihara Y, Bhattarai AP. 2018. "Development of an Objective Water Security Index and Assessment of Its Association with Quality of Life in Urban Areas of Developing Countries. SSM Popul Health." SSM Popul Health 6: 276–285.

Shen, H., Leblanc, M., Frappart, F., Seoane, L., O'Grady, D., Olioso, A., & Tweed, S. (2017). A comparative study of GRACE with continental evapotranspiration estimates in Australian semi-arid and arid basins: Sensitivity to climate variability and extremes. *Water (Switzerland)*, *9*(9), 1–19. https://doi.org/10.3390/w9090614

Silva, E., & Lopes, S. (2017). Validation of Satellite Rainfall Products over a Mountainous Watershed in a Humid Subtropical Climate Region of Brazil. https://doi.org/10.3390/rs9121240

Smith, G. (2018). Step away from stepwise. Journal of Big Data. https://doi.org/10.1186/s40537-018-0143-6

Srinivasan, R., & J. G. Arnold. (1994). Integration of a basin-scale water quality model with GIS. Water Resour. Bull. 30(3): 453-462 The Royal Institute for Strategic Studies, M.

(2014). ANTICIPATION ET GESTION DES RISQUES D ' EVENEMENTS CLIMATI QUES EXTREMES ET DE CATASTROPHES NATURELLES AU MAROC Rapport de synthèse.

Srinivasan, V., M. Konar, and M. Sivapalan. 2017. "A Dynamic Framework for Water Security." Water Security 1: 12–20. http://dx.doi.org/10.1016/j.wasec.2017.03.001.

SONG YANG, E. A. S. (2008). Convective – Stratiform Precipitation Variability at Seasonal Scale from 8 Yr of TRMM Observations : Implications for Multiple Modes of Diurnal Variability. July 1987. https://doi.org/10.1175/2008JCLI2096.1

Spring, S., & Peck, E. L. (1980). Robert E . Norton Memorial Lecture. 61(8), 894–902.

Tanouti, Oumaima. 2017. "Squaring the Circle : Agricultural Intensification vs . Water Conservation in Morocco." 192: 170–79.

Tang, G., Ma, Y., Long, D., Zhong, L., & Hong, Y. (2016). Evaluation of GPM Day-1 IMERG and TMPA Version-7 legacy products over Mainland China at multiple spatiotemporal scales. JOURNAL OF HYDROLOGY, 533, 152–167. https://doi.org/10.1016/j.jhydrol.2015.12.008

Tang, L., Tian, Y., Yan, F., & Habib, E. (2015). An improved procedure for the validation of satellite-based precipitation estimates. Atmospheric Research. https://doi.org/10.1016/j.atmosres.2014.12.016

Thematic, Waters et al. "WATERS THEMATIC PRIORITY AREA PRACTICES in Transboundary Water."

Thiemig, V., Rojas, R., Zambrano-bigiarini, M., & Roo, A. De. (2013). Hydrological evaluation of satellite-based rainfall estimates over the Volta and Baro-Akobo Basin. Journal of Hydrology, 499, 324–338. https://doi.org/10.1016/j.jhydrol.2013.07.012

Tinoco, V., Willems, P., Wyseure, G., & Cisneros, F. (2016). Evaluation of reservoir operation strategies for irrigation in the Macul Basin, Ecuador. *Journal of Hydrology: Regional Studies*, *5*, 213–225. https://doi.org/10.1016/j.ejrh.2015.12.063

Tsanis, D. D. A. I. K. (2016). Comparison of multiple linear regression and artificial neural effective work models for downscaling TRMM precipitation products using MODIS data. Environmental Earth Sciences. https://doi.org/10.1007/s12665-016-5883-z

Tuo, Y., Duan, Z., Disse, M., & Chiogna, G. (2016). Science of the Total Environment Evaluation of precipitation input for SWAT modeling in Alpine catchment : A case study in the Adige river basin (Italy). Science of the Total Environment, The, 573, 66–82. https://doi.org/10.1016/j.scitotenv.2016.08.034

UN-Water. (2013). Water Security & the Global Water Agenda: A UN-Water Analytical Brief. In Citeseer. Retrieved from http://www.unwater.org/publications/publications detail/en/c/197890/%5Cnhttp://citeseerx.ist.psu.edu/viewdoc/download?doi=10.1.1.360.9258&rep=rep1&type=pdf

UN [united Nations]. (2015). The 2030 Agenda for Sustainable Development, A/RES/70/1. 16301(October), 13–14

Van Liew MW, Veith TL, Bosch DD, Arnold JG (2007) Suitability of SWAT for the Conservation effects assessment project: A comparison on USDA – ARS watersheds. Journal of Hydrologic Engineering 12: 173-189.18

Villalobos, F. J., Testi, L., & Fereres, E. (2016). Principles of Agronomy for Sustainable Agriculture. *Principles of Agronomy for Sustainable Agriculture*.

https://doi.org/10.1007/978-3-319-46116-8

Viviana Maggioni, Patrick C. Meyers, M. D. R. (2016). American meteorological. https://doi.org/10.1175/JHM-D-15-0190.1

Vörösmarty, C. J., P. Green, J. Salisbury, and R. B. Lammers (2000), Global water resources: Vulnerability from climate change and population growth, Science, 289, 284–288, doi:10.1126/science.289.5477.284

Vörösmarty C J et al 2010 Global threats to human water security and river biodiversity Nature 467 555–61

Wahba, M. A. S. (2017). Assessment of Options for the Sustainable Use of Agricultural Drainage Water For Irrigation in Egypt by Simulation Modelling. *Irrigation and Drainage*, *66*(1), 118–128. https://doi.org/10.1002/ird.2029

Wang, G., Yang, H., Wang, L., Xu, Z., & Xue, B. (2014). Using the SWAT model to assess impacts of land use changes on runoff generation in headwaters, 1042(December 2012), 1032–1042. https://doi.org/10.1002/hyp.9645

Wang, W., Lu, H., Yang, D., Sothea, K., Jiao, Y., & Gao, B. (2016). Modelling Hydrologic Processes in the Mekong River Basin Using a Distributed Model Driven by Satellite Precipitation and Rain Gauge Observations. 1–19. https://doi.org/10.1371/journal.pone.0152229

Ward, R. C., and M. Robinson,(1990). Principales of hydrology, McGraw-Hill, London.

Wenlong Jing, Pengyan Zhang, H. J. and X. Z. (2017). Reconstructing Satellite-Based Monthly Precipitation over Northeast China Using Machine Learning Algorithms. https://doi.org/10.3390/rs9080781

White K. L., & Chaubey I. (2005). "Sensitivity Analysis, Cali-bration, and Validations for a Multisite and Multivariable SWAT Model," Journal of the American Water Resources Association, Vol. 41, No. 5, pp. 1077-1089. doi:10.1111/j.1752-1688.2005.tb03786.x

Winchell M., Srinivasan R., Di Luzio M., & Arnold J. (2009). "ArcSWAT 2.3.4 Interface for SWAT2005: User's Guide, Version September 2009," Texas Agricultural Experi-ment Station and Agricultural Research Service- US De-partment of Agriculture

Wheater, H. S. (2017). Modelling hydrological processes in arid and semi-arid areas. R a i n fa l l - ru n o f f m o d e l l i n g. 2000, 1–20.

World Bank. 2012. Water quality management Morocco, prepared Mediterranean Environmental Technical Assistance Program., Washington, D.C.

Xue, C., Song, W., Qin, L., Dong, Q., & Wen, X. (2015). International Journal of Applied Earth Observation and Geoinformation A spatiotemporal mining framework for abnormal association patterns in marine environments with a time series of remote sensing images. International Journal of Applied Earth Observations and Geoinformation, 38, 105–114. https://doi.org/10.1016/j.jag.2014.12.009

Xu, D., & Guo, X. (2013). A Study of Soil Line Simulation from Landsat Images. 1, 4533–4550. https://doi.org/10.3390/rs5094533

Yang, Z., Zhang, Q., & Hao, X. (2016). Evapotranspiration Trend and Its Relationship with Precipitation over the Loess Plateau during the Last Three Decades. *Advances in Meteorology*, *2016*. https://doi.org/10.1155/2016/6809749

Yuan, F., Zhang, L., Wah, K., Win, W., Ren, L., & Zhao, C. (2017). Assessment of GPM and TRMM Multi-Satellite Precipitation Products in Streamflow Simulations in a Data-Sparse Mountainous Watershed in Myanmar. https://doi.org/10.3390/rs9030302

Zhang, T., Li, B., Yuan, Y., Gao, X., Sun, Q., & Xu, L. (2018). Remote Sensing of Environment Spatial downscaling of TRMM precipitation data considering the impacts of macro-geographical factors and local elevation in the Three-River Headwaters Region. Remote Sensing of Environment, 215(May), 109–127. https://doi.org/10.1016/j.rse.2018.06.004

Zhang, Y., & Li, Y. (2018). Fine-Resolution Precipitation Mapping in a Mountainous Watershed : Geostatistical Downscaling of TRMM Products Based on Environmental Variables. 1–27. https://doi.org/10.3390/rs10010119

Zhao, H., Yang, B., Yang, S., & Huang, Y. (2017). NU SC Institute of Environment and Sustainable Development in Agriculture , Chinese Academy of. Atmospheric Research. https://doi.org/10.1016/j.atmosres.2017.11.005

Zheng, X. (2015). International Journal of Remote A methodological approach for spatial downscaling of TRMM precipitation data in North China. January, 37–41. https://doi.org/10.1080/01431161.2014.995275

Zhou, Z., Guo, B., Su, Y., Chen, Z., & Wang, J. (2020). Multidimensional evaluation of the TRMM 3B43V7 satellite-based precipitation product in mainland China from 1998 – 2016. 1–24. https://doi.org/10.7717/peerj.8615

Zhou, F., Xu, Y., Chen, Y., Xu, C., Gao, Y., & Du, J. (2013). Hydrological response to urbanization at different spatio-temporal scales simulated by coupling of CLUE-S and the SWAT model in the Yangtze River Delta region, *485*, 113–125. https://doi.org/10.1016/j.jhydrol.2012.12.040

Zhou, Z., Plauborg, F., Parsons, D., & Andersen, M. N. (2018). Potato canopy growth, yield and soil water dynamics under different irrigation systems. Agricultural Water Management, 202(January), 9–18. https://doi.org/10.1016/j.agwat.2018.02.009

Annexes

Annex 1: Descriptive statistics of Bab Merzouka station

Results for Decades = 1980

Variable	Season	Total Count	Mean	StDev	Variance	CoefVar	Minimum	Q1	Median
Relative humidity	Fall	30	0,5489	0,1126	0,0127	20,51	0,3780	0,4466	0,5340
	Spring	30	0,5965	0,0879	0,0077	14,74	0,4198	0,5305	0,5835
	Summer	30	0,3639	0,0601	0,0036	16,52	0,2441	0,3213	0,3605
	Winter	30	0,7036	0,0767	0,0059	10,90	0,5592	0,6635	0,7050
Mean Temperature	Fall	30	18,960	4,923	24,233	25,96	11,907	14,226	18,348
	Spring	30	14,854	3,004	9,023	20,22	10,403	12,781	14,723
	Summer	30	26,668	2,504	6,272	9,39	20,892	24,548	27,190
	Winter	30	9,193	1,322	1,748	14,38	6,763	8,336	9,057
Precipitation	Fall	30	48,00	46,91	2200,15	97,72	0,00	4,00	33,00
	Spring	30	61,24	47,41	2248,03	77,42	1,00	19,50	46,50
	Summer	30	3,433	5,270	27,771	153,49	0,000	0,000	0,500
	Winter	30	73,1	61,4	3765,0	83,97	9,0	31,0	49,0

Variable	Season	Q3	Maximum	IQR
Relative humidity	Fall	0,6553	0,7406	0,2088
	Spring	0,6841	0,7543	0,1536
	Summer	0,4149	0,4797	0,0936
	Winter	0,7669	0,8270	0,1034
Mean Temperature	Fall	24,195	26,166	9,969
	Spring	17,755	22,157	4,974
	Summer	28,667	30,532	4,119
	Winter	10,099	12,594	1,764
Precipitation	Fall	75,00	154,00	71,00
	Spring	105,10	168,00	85,60
	Summer	6,000	22,000	6,000
	Winter	111,5	268,0	80,5

Results for Decades = 1990

Variable	Season	Total Count	Mean	StDev	Variance	CoefVar	Minimum	Q1	Median
Relative humidity	Fall	30	0,5559	0,0926	0,0086	16,66	0,4141	0,4792	0,5466
	Spring	30	0,5757	0,0981	0,0096	17,05	0,4053	0,4907	0,5818
	Summer	30	0,3485	0,0685	0,0047	19,66	0,2253	0,2964	0,3391
	Winter	30	0,6891	0,1049	0,0110	15,22	0,5119	0,5820	0,7001
Mean Temperature	Fall	30	17,802	4,287	18,378	24,08	10,539	13,851	17,743
	Spring	30	15,161	3,045	9,275	20,09	10,140	12,780	14,659
	Summer	30	26,640	2,865	8,209	10,76	17,774	24,920	27,186
	Winter	30	9,453	1,608	2,586	17,01	7,180	8,309	9,260
Precipitation	Fall	30	38,83	33,29	1108,35	85,73	2,00	17,00	30,00
	Spring	30	63,00	53,54	2866,69	84,99	5,00	27,00	41,50
	Summer	30	5,67	11,53	132,85	203,40	0,00	1,00	3,00
	Winter	30	72,1	66,4	4414,8	92,11	2,0	22,0	55,0

Variable	Season	Q3	Maximum	IQR
Relative humidity	Fall	0,6156	0,8121	0,1363
	Spring	0,6298	0,8080	0,1392
	Summer	0,3825	0,5619	0,0861
	Winter	0,7822	0,8537	0,2003
Mean Temperature	Fall	20,951	24,789	7,100
	Spring	17,120	21,594	4,340
	Summer	28,729	31,131	3,809
	Winter	10,581	14,073	2,272

Precipitation	Fall	56,00	137,00	39,00
	Spring	82,75	201,00	55,75
	Summer	6,00	63,00	5,00
	Winter	97,5	283,0	75,5

Results for Decades = 2000

Variable	Season	Total Count	Mean	StDev	Variance	CoefVar	Minimum	Q1
Relative humidity	Fall	29	0,5504	0,1156	0,0134	21,00	0,3589	0,4432
	Spring	30	0,5562	0,0967	0,0094	17,38	0,3934	0,4650
	Summer	30	0,31481	0,04591	0,00211	14,58	0,23128	0,27914
	Winter	29	0,6968	0,1198	0,0143	17,19	0,3844	0,6334
Mean Temperature	Fall	29	18,322	4,850	23,522	26,47	9,152	13,006
	Spring	30	15,660	3,094	9,575	19,76	11,525	13,022
	Summer	30	27,590	1,825	3,330	6,61	23,156	26,092
	Winter	29	9,347	1,927	3,712	20,61	6,186	7,971
Precipitation	Fall	29	53,90	51,39	2640,81	95,35	0,00	12,00
	Spring	30	48,26	38,39	1473,74	79,55	0,00	20,00
	Summer	30	0,467	1,042	1,085	223,21	0,000	0,000
	Winter	29	69,7	55,6	3086,9	79,72	0,0	27,5

Variable	Season	Median	Q3	Maximum	IQR
Relative humidity	Fall	0,5260	0,6458	0,7915	0,2026
	Spring	0,5372	0,6438	0,7433	0,1788
	Summer	0,30970	0,35468	0,42368	0,07554
	Winter	0,7024	0,7855	0,8819	0,1521
Mean Temperature	Fall	19,466	22,863	24,828	9,857
	Spring	14,976	17,977	22,140	4,955
	Summer	28,170	28,974	30,103	2,882
	Winter	8,926	10,801	13,790	2,829
Precipitation	Fall	31,00	88,00	177,00	76,00
	Spring	36,00	68,00	164,00	48,00
	Summer	0,000	0,250	4,000	0,250
	Winter	57,0	110,5	193,0	83,0

Results for Decades = 2010

Variable	Season	Total Count	Mean	StDev	Variance	CoefVar	Minimum	Q1	Median
Relative humidity	Fall	13	0,5464	0,1444	0,0208	26,42	0,3973	0,4180	0,4716
	Spring	15	0,6528	0,1347	0,0182	20,64	0,4089	0,5622	0,6661
	Summer	14	0,3276	0,0620	0,0038	18,93	0,2272	0,2708	0,3314
	Winter	15	0,7754	0,0723	0,0052	9,32	0,6232	0,7349	0,7940
Mean Temperature	Fall	13	19,60	5,28	27,91	26,95	11,61	14,35	20,77
	Spring	15	16,26	4,03	16,21	24,75	11,59	12,08	15,80
	Summer	14	28,473	3,003	9,016	10,55	22,108	26,639	29,166
	Winter	15	9,646	0,890	0,792	9,22	7,828	9,035	9,467
Precipitation	Fall	13	82,5	89,3	7981,9	108,29	0,0	11,0	46,0
	Spring	15	86,3	104,8	10989,1	121,42	2,0	21,0	48,0
	Summer	14	4,00	7,23	52,31	180,81	0,00	0,00	0,50
	Winter	15	82,1	66,4	4413,9	80,96	11,0	31,0	61,0

Variable	Season	Q3	Maximum	IQR
Relative humidity	Fall	0,6791	0,8129	0,2611
	Spring	0,7341	0,8941	0,1719
	Summer	0,3751	0,4314	0,1043
	Winter	0,8190	0,8835	0,0840
Mean Temperature	Fall	25,03	26,05	10,68
	Spring	18,78	23,30	6,70
	Summer	30,920	31,742	4,281
	Winter	10,500	10,818	1,466

Precipitation	Fall	138,8	280,0	127,8
	Spring	81,0	334,0	60,0
	Summer	5,25	24,00	5,25
	Winter	109,0	228,0	78,0

Annex2: Descrptive statistics of Idriss first station

Results for Decades = 1980

Variable	Season	Total Count	Mean	StDev	Variance	CoefVar	Minimum	Q1	Median
Relative humidity	Fall	30	0,4821	0,1193	0,0142	24,76	0,2968	0,3834	0,4558
	Spring	30	0,5763	0,0897	0,0081	15,57	0,3924	0,4983	0,5726
	Summer	30	0,3367	0,0629	0,0040	18,68	0,2130	0,2792	0,3422
	Winter	30	0,6610	0,0918	0,0084	13,89	0,4875	0,6054	0,6805
Mean Temperature	Fall	30	21,761	5,081	25,814	23,35	14,700	17,066	21,118
	Spring	30	16,517	3,181	10,119	19,26	11,637	14,133	16,158
	Summer	30	28,654	2,715	7,369	9,47	22,088	26,617	29,356
	Winter	30	11,377	1,593	2,536	14,00	8,675	10,069	11,327
Precipitation	Fall	30	36,58	38,60	1489,83	105,51	0,00	1,02	23,95
	Spring	30	44,82	31,30	979,55	69,83	0,00	24,10	39,65
	Summer	30	2,723	4,852	23,546	178,18	0,000	0,000	0,450
	Winter	30	48,30	35,86	1286,27	74,26	0,00	16,55	45,65

Variable	Season	Q3	Maximum	IQR
Relative humidity	Fall	0,5963	0,6724	0,2130
	Spring	0,6598	0,7429	0,1615
	Summer	0,3801	0,4719	0,1009
	Winter	0,7254	0,8046	0,1200
Mean Temperature	Fall	26,607	29,606	9,541
	Spring	18,729	24,048	4,596
	Summer	30,764	33,172	4,147
	Winter	12,650	14,674	2,581
Precipitation	Fall	64,20	113,00	63,17
	Spring	59,50	116,50	35,40
	Summer	2,725	17,100	2,725
	Winter	61,60	130,80	45,05

Results for Decades = 1990

Variable	Season	Total Count	Mean	StDev	Variance	CoefVar	Minimum	Q1	Median
Relative humidity	Fall	30	0,5028	0,0938	0,0088	18,65	0,3470	0,4372	0,5042
	Spring	30	0,5379	0,0959	0,0092	17,84	0,3661	0,4579	0,5548
	Summer	30	0,3235	0,0747	0,0056	23,10	0,2090	0,2776	0,3030
	Winter	30	0,6456	0,1026	0,0105	15,89	0,4746	0,5540	0,6559
Mean Temperature	Fall	30	20,237	4,355	18,964	21,52	12,928	16,022	20,626
	Spring	30	17,243	3,082	9,499	17,87	11,684	14,560	17,073
	Summer	30	28,571	3,061	9,368	10,71	18,822	26,967	29,595
	Winter	30	11,754	1,746	3,048	14,85	8,870	10,481	11,576
Precipitation	Fall	30	27,93	26,96	726,89	96,54	0,00	10,40	20,45
	Spring	30	35,18	24,89	619,46	70,74	0,00	13,20	31,80
	Summer	30	3,85	8,93	79,74	231,95	0,00	0,00	0,00
	Winter	30	45,39	47,34	2240,68	104,29	0,00	8,65	30,15

Variable	Season	Q3	Maximum	IQR
Relative humidity	Fall	0,5650	0,7305	0,1277
	Spring	0,5826	0,7869	0,1247
	Summer	0,3502	0,5769	0,0726
	Winter	0,7540	0,7869	0,2000
Mean Temperature	Fall	23,652	27,576	7,630
	Spring	19,349	23,779	4,790
	Summer	30,912	32,759	3,945
	Winter	12,567	15,609	2,086
Precipitation	Fall	33,70	112,20	23,30
	Spring	62,07	77,50	48,87
	Summer	4,08	43,40	4,08
	Winter	86,47	192,30	77,82

Results for Decades = 2000

Variable	Season	Total Count	Mean	StDev	Variance	CoefVar	Minimum	Q1
Relative humidity	Fall	29	0,4899	0,1070	0,0114	21,83	0,3101	0,3953
	Spring	30	0,5361	0,0945	0,0089	17,62	0,3635	0,4506
	Summer	30	0,29595	0,04601	0,00212	15,55	0,21790	0,25880

	Winter	29	0,6433	0,1183	0,0140	18,39	0,3492	0,5671
Mean Temperature	Fall	29	20,832	4,723	22,304	22,67	12,121	15,898
	Spring	30	17,423	3,286	10,800	18,86	13,030	14,990
	Summer	30	29,418	1,779	3,165	6,05	24,924	28,532
	Winter	29	11,692	2,054	4,219	17,57	8,206	10,136
Precipitation	Fall	29	42,25	39,21	1537,16	92,80	1,10	10,63
	Spring	30	33,69	28,05	787,05	83,28	0,00	15,85
	Summer	30	1,700	1,850	3,421	108,82	0,000	0,000
	Winter	29	48,76	37,01	1370,00	75,91	0,00	21,85

Variable	Season	Median	Q3	Maximum	IQR
Relative humidity	Fall	0,4686	0,5878	0,7013	0,1925
	Spring	0,5447	0,6192	0,6998	0,1686
	Summer	0,28738	0,32525	0,40022	0,06646
	Winter	0,6465	0,7474	0,8411	0,1802
Mean Temperature	Fall	21,838	25,128	27,430	9,230
	Spring	16,784	19,843	24,131	4,854
	Summer	29,762	30,916	31,956	2,384
	Winter	11,566	12,786	16,397	2,650
Precipitation	Fall	33,40	68,10	154,90	57,47
	Spring	28,91	43,99	119,50	28,14
	Summer	0,800	3,150	5,400	3,150
	Winter	37,70	74,00	141,70	52,15

Results for Decades = 2010

Variable	Season	Total Count	Mean	StDev	Variance	CoefVar	Minimum	Q1	Median
Relative humidity	Fall	13	0,5924	0,1510	0,0228	25,49	0,3736	0,4842	0,5476
	Spring	15	0,6837	0,1220	0,0149	17,85	0,4585	0,5993	0,7055
	Summer	14	0,4034	0,0765	0,0058	18,96	0,2519	0,3458	0,4294
	Winter	15	0,8080	0,0668	0,0045	8,26	0,6791	0,7410	0,8458
Mean Temperature	Fall	13	20,13	4,88	23,84	24,26	13,67	14,52	20,32
	Spring	15	16,822	3,641	13,254	21,64	12,037	13,569	17,356
	Summer	14	27,870	3,003	9,016	10,77	23,416	25,521	28,106
	Winter	15	10,486	1,430	2,043	13,63	8,083	9,558	10,012

Precipitation	Fall	13	58,3	49,9	2487,9	85,54	1,5	9,4	56,3
	Spring	15	54,9	48,9	2387,4	89,04	4,4	9,2	46,9
	Summer	14	5,06	9,31	86,60	183,99	0,00	0,00	2,83
	Winter	15	72,6	46,8	2194,4	64,50	5,5	34,0	64,1

Variable	**Season**	**Q3**	**Maximum**	**IQR**
Relative humidity	Fall	0,6823	0,8943	0,1981
	Spring	0,7812	0,8917	0,1819
	Summer	0,4510	0,5160	0,1052
	Winter	0,8570	0,8736	0,1160
Mean Temperature	Fall	25,18	26,94	10,65
	Spring	19,140	22,917	5,571
	Summer	30,413	32,804	4,892
	Winter	10,868	13,227	1,310
Precipitation	Fall	101,0	156,0	91,6
	Spring	74,7	158,0	65,5
	Summer	4,51	35,50	4,51
	Winter	114,8	142,1	80,8

Abstract

In the realm of Climate change, population growth, industrialization, water is resources are under high pressure. To help manager and decision makers to adopt the appropriate land management strategies, the grasping of the hydrological behavior and quantification of water yield are paramount. In this cradle the main objective of the presented thesis is to provides an integrated approach to tackle water drawbacks.

The methodology adopted consists of improving downscaling models by reducing soil brightness noise using the Transformed Soil Adjusted Vegetation Index, TSAVI, DEM, and distance from the sea. The second part aims to test the ability of the distributed model SWAT (Soil & water Assessment Tool) to simulate and reproduce the hydrological behavior of Inaouen watershed, SWAT was performed on a daily time step from 1999 to 2007 for calibration and 2008 to 2014 for validation. The model accuracy was evaluated by measuring the Nash-Sutcliffe coefficient and R^2, RMSE, MAE, et PBIAS. The last part aims to estimate the evapotranspiration using Modis Evapotranspiration Product and assess the productivity of 2500 ha of the olive crop under deficit irrigation condition.

The result exhibits that the Transformed Soil Adjusted Vegetation Index (TSAVI) enhanced the downscaling model over the Humid and Saharan bioclimatic stages due to its capacity to reduce the soil brightness with an R^2 ranging between 0.30 and 0.82. Concerning the hydrological modeling the obtained resulted when using the CFSR database are not satisfactory, the model is enhanced when using the observed climatic data for calibration but still need to be improved. This could be explained by the inadequacy of the parameters that represent the groundwater transfers (**REVAP, GWQMN**, **GW_REVAP**, **and REVAPMN**) to Inaouen basin. The last part result's shows that 0.75 of full irrigation could save water irrigation by 17% by reducing water irrigation supply by an average of 5Mm3.

This study highlights the importance of Geographic Information Systems, hydrological modelling, and remote sensing in addressing water issues. The methodology used could be transposed to other regions facing the same problems.

Keywords: ISRIC database, Distributed model, Hydrologic Response Unit, Spatial downscaling, TSAVI, Deficit irrigation, SWAT, CFSR, hydrologic modeling, Water security, Sustainable development, Water management.